UniSR

**UNIVERSITA' VITA-SALUTE SAN RAFFAELE**

**CORSO DI DOTTORATO DI RICERCA INTERNAZIONALE IN MEDICINA MOLECOLARE**

**CURRICULUM IN: Cellular and Molecular Biology (CMB)**

# The inhibition of the HMGB1/CXCL12/CXCR4 axis in inflammation-related cancers: a structural and functional study

DoS: Dr. Giovanna Musco

Second Supervisor: Prof. Dr. Michael Sattler

Tesi di DOTTORATO di RICERCA di Malisa Vittoria Mantonico matr. 017142

Ciclo di dottorato XXXVI

SSD BIO/13 – Biologia Applicata

Anno Accademico 2022/2023

# CONSULTAZIONE TESI DI DOTTORATO DI RICERCA

Il/la sottoscritto/I          MALISA VITTORIA MANTONICO

Matricola / *registration number*     017142

nat_ a/ *born at*          FULDA, GERMANY

il/*on*               15/04/1992

autore della tesi di Dottorato di ricerca dal titolo / *author of the PhD Thesis titled*

THE INHIBITION OF THE HMGB1/CXCL12/CXCR4 AXIS
IN INFLAMMATION-RELATED CANCERS: A STRUCTURAL
AND FUNCTIONAL STUDY

☒AUTORIZZA la Consultazione della tesi / AUTHORIZES *the public release of the thesis*

☐ NON AUTORIZZA la Consultazione della tesi per ...... mesi /DOES NOT AUTHORIZE *the public release of the thesis for ...... months*

a partire dalla data di conseguimento del titolo e precisamente / *from the PhD thesis date, specifically*

Dal / *from*   ....../....../......     Al / *to*   ....../....../......

Poiché /*because*:

☐ l'intera ricerca o parti di essa sono potenzialmente soggette a brevettabilità/ *The whole project or part of it might be subject to patentability;*

☐ ci sono parti di tesi che sono già state sottoposte a un editore o sono in attesa di pubblicazione/ *Parts of the thesis have been or are being submitted to a publisher or are in press;*

☐ la tesi è finanziata da enti esterni che vantano dei diritti su di esse e sulla loro pubblicazione/ *the thesis project is financed by external bodies that have rights over it and on its publication.*

Si rende noto che parti della tesi sono indisponibili in relazione all'utilizzo di dati tutelati da segreto industriale **(da lasciare solo se applicabile)** /*Please Note: some parts of the thesis are not available in relation to the norm of the use of information protected by trade secret* **(To leave only if relevant)**

E' fatto divieto di riprodurre, in tutto o in parte, quanto in essa contenuto / *Copyright the contents of the thesis in whole or in part is forbidden*

Data /Date  08/03/2024          Firma /Signature  Malisa Vla Mantonico

# Declaration of Authorship

This thesis has been:

- composed by myself and has not been used in any previous application for a degree. Throughout the text I use 'I' and 'We' interchangeably.

- has been written accoding to the editing guidelines approved by the University.

The presented work, performed by myself, Malisa Vittoria Mantonico, in partial fulfilment to obtain the PhD degree at Vita-Salute San Raffaele University, Milan (Italy), has been published with me as first author (Mantonico et al., 2024). Chapters 2-7 contain results (including figures and data), discussion as well as materials and methods that were adapted from Mantonico et al., 2024. All the results presented here were obtained by myself, except for:

1 **Nuclear Magnetic Resonance** experiments were performed together with former technician **Giacomo Quilici**, Biomolecular NMR Laboratory, Division of Genetics and Cell Biology, IRCCS Ospedale San Raffaele, Milan, Italy.

2 **Isothermal Titration Calorimetry** measurements were performed and analysed by myself in collaboration with **Dr. Tim Schulte**, Institute of Molecular and Translational Cardiology, IRCCS Policlinico San Donato, Milan, Italy and **Prof. Dr. Stefano Ricagno**, Institute of Molecular and Translational Cardiology, IRCCS Policlinico San Donato, Milan, Italy and Department of Biosciences, Università degli Studi di Milano, Milan, Italy.

3 **Small Angle X-ray** experiments were performed and analysed by **Dr. Gabriele Giachin**, department of Chemical Sciences (DiSC), University of Padua, 35131, Padova, Italy.

4 **Microscale Thermophoresis** were performed and analysed by **Dr. Chiara Zucchelli**, Biomolecular NMR Laboratory, Division of Genetics and Cell Biology, IRCCS Ospedale San Raffaele, Milan, Italy.

5 **Proximity Ligation Assays** on cells were performed and analysed by **Liam Sean Colley**, HMGBiotech S.r.l., 20133 Milan, Italy and School of Medicine and Surgery, Università Milano-Bicocca, 20126 Milan, Italy and **Dr. Massimo Crippa**, Chromatin Dynamics Unit, Division of Genetics and Cell Biology, IRCCS Ospedale San Raffaele, Milan, Italy.

6 The final **Structural Model** representation was created by **Dr. Michela Ghitti**, Biomolecular NMR Laboratory, Division of Genetics and Cell Biology, IRCCS Ospedale San Raffaele, Milan, Italy.

All sources of information are acknowledged by means of reference.

*Acknowledgements*

The present work performed by myself, Malisa Vittoria Mantonico, in partial fulfilment of the requirements for obtaining the PhD degree at Vita-Salute San Raffaele University, Milan, Italy.

First of all, I would like to thank Dr. Giovanna Musco for offering me the opportunity to pursue a PhD in her laboratory and for being my mentor. I really learned from her what scientific reasoning means and how to apply my scientific knowledge for problem solving in general. She has definitely shaped me as a researcher.

Another very central figure to me is Dr. Michela Ghitti, who has taught me how to prepare presentation, helped me with any scientific problems and has read and corrected my work throughout the PhD. She has really elevated my work and think that she is a great scientific mentor! I thank as well Dr. Chiara Zucchelli, who was always available for any questions and help regarding my laboratory work, posters and presentations. Moreover, she always had great suggestions, when I got stuck with some issues.

Thanks to my collaborators Dr. Tim Schulte and Prof. Dr. Stefano Ricagno and to the technical help of Dr. Luca Broggini, I learned how to utilize biophysical calorimetry assays. I enjoyed a lot the scientific meeting and exchange with collaborators Liam Colley and Dr. Massimo Grippa! It was really nice to see the biological aspect of my studies. I would like to thank Luca Mollica for the insightful discussions about HMGB1 and NMR!

The time during my PhD was accompanied with a lot of fun moments with Anne Nielsen, Maryam Omrani, Arash Ghodousi, Chiara Menegazzi, Irene Franco, Daniel Spies, Federico Ballabio, Chantal Fabris and Alejandra Carriles, Valeria Mannella, Camilla Carmeno! I would like to thank in particular Marco della Torre and Anne Nielsen for the support during the 3rd PhD year!

Finally, my life partner Emanuele Ciardulli who supported me throughout this journey and my extended family (parents, in-laws, Fausto Ciardulli, Roberto and Kiko Mantonico) made it possible to pursue this PhD.

I hope that one day I can show this work to my daughter. I hope that one day she will understand the importance people's support in achieving great goals in life! I really think that I was lucky to have found amazing people around me. THANK YOU ALL FOR ELEVATING ME!

I would like to thank to the Italian Association for Cancer Research (FIRC-AIRC), that granted me with a research fellowship.

*Abstract*

**BACKGROUND:** Over the last decade, studies in the chemokine biology field revealed remarkable complexity of the chemokine interactome. The discovery of chemokine heteromers and their ability to enhance or dampen the functional responses of their cognate receptors led to new therapeutic opportunities to manipulate the chemokine system in a sophisticated manner. Chemokine CXCL12 forms with fully reduced (fr) alarmin HMGB1 a physiologically relevant heterocomplex (CXCL12•frHMGB1) that synergically promotes the inflammatory response elicited by the G-protein coupled receptor CXCR4. The functional synergism of the heterocomplex has been linked to inflammatory diseases, in particular rheumatoid arthritis, and to inflammation-related cancers, such as malignant mesothelioma. Targeting therefore CXCL12•frHMGB1 to treat inflammatory disorders and possibly cancer by dampening CXCR4 hyperactivity and surface retention might be a promising therapeutic strategy. However, the molecular details of heterocomplexation were still elusive, as they lack the information of an experimentally validated structure. Moreover, HMGB1 belongs to the class of intrinsically disordered proteins displaying a high degree of flexibility, whose interaction sites and binding modes are difficult to predict by current artificial intelligence tools.

**AIM:** The aim of this work is therefore to obtain an experimentally validated atomic-resolution model of CXCL12•frHMGB1 in solution

**RESULTS:** We show by an integrated structural approach (NMR, ITC, MST, AUC, SAXS) that CXCL12 and frHMGB1 form an ensemble of dynamic interconvertible heterocomplexes and unravel biologically relevant binding sites of CXCL12•frHMGB1. Herein, we uncover an unexpected role of the acidic intrinsically disordered region (IDR) of HMGB1 in complex formation with CXCL12 and furthermore in binding to CXCR4 on the cell surface. The heteromeric binding interface involves both the HMG tandem domains and acidic IDR of frHMGB1 in recognizing the dimerization surface of CXCL12. Importantly, the acidic IDR of HMGB1 remains structurally disordered in complex establishing dynamic contacts between HMGB1's structured domains, linker and CXCL12. The result of this dynamic interplay is that CXCL12•frHMGB1 cannot be represented by a single structure but by an ensemble of heterocomplexes. Unlike previous assumptions, we demonstrated experimentally that one CXCL12 molecule binds to frHMGB1 in a 1:1 ratio and that CXCL12 is able to discriminate the redox state of HMGB1 by binding preferentially to BoxA of frHMGB1. Like many chemokine interactions, the dissociation constant of hetero-association is in the low-micromolar range and mainly charge-driven with the acidic IDR recruiting CXCL12 via long-range electrostatic interactions favouring thereby the recognition process.

**CONCLUSION:** On this basis, CXCL12•frHMGB1 is a *fuzzy* protein complex, which by definition is an ensemble of complexes that are formed due to retained structural disorder of flexible regions. The CXCL12-HMGB1 interaction diverges from the classical rigid heterophilic chemokines dimerization. Pharmacological inhibition of *fuzzy* interaction sites of CXCL12•frHMGB1 may pave the way for the treatment against inflammatory conditions and malignancies.

# List of Abbreviations

*A*

**ACK** **A**typical **c**hemo**k**ines

**Ac-pep** **A**cidic tail **pep**tide synthetic

**Ac-pep$_{rec}$** **A**cidic tail **pep**tide **rec**ombinant

**Akt or PKB** **P**rotein **k**inase **B**

**ALL** **A**cute **l**ymphocytic **l**eukemia

**AML** **A**cute **m**yeoloma **l**eukemia

**AUC** **A**nalytical **u**ltra**c**entrifugation

*B*

**BBB** **B**lood-**b**rain **b**arrier

*C*

**cAMP** **C**yclic **a**denosine **m**ono-**p**hosphate

**C-motif** **C**ysteine motif

**CCL** **CC** motif chemokine **l**igand

**CCR** **CC** motif chemokine **r**eceptor

**CDK** **C**yclin-**d**ependent **k**inase

**CRD** **C**arbohydrate **r**ecognition **d**omain

**Cryo-EM** **Cryo**-**E**lectron**m**icroscopy

**CSP** **C**hemical **s**hift **p**erturbation

**CXCL** **CXC** motif chemokine **l**igand

**CXCL12** **CXC** chemokine **l**igand **12**

**CXCL12-LM** **CXC** chemokine **l**igand **12** - **l**ocked **m**onomer

**CXCL12-LD** **CXC** chemokine **l**igand **12** - **l**ocked **d**imer

**CXCR** **CXC** motif chemokine **r**eceptor

**CXCR4** **CXC** chemokine **r**eceptor **4**

*D*

**DAG** **Dia**cyl**g**lycerol

**DAMP** **D**anger **A**ssociated **M**olecular **P**attern

**DFL** **Dif**lunisa**l**

**D$_{max}$** **max**imal particle **d**istance

**dsHMGB1** **Di**sulphide **H**igh **M**obility **G**roup **B**ox **1**

*E*

**ECL** **E**xtra**c**ellular **l**oops

| | |
|---|---|
| **EOM** | **E**nsemble **o**ptimization **m**ethod |
| **ERK** | **E**xtracellular-signal-**r**egulated kinase |
| *G* | |
| **GAG** | **G**lycos**a**mino**g**lycan |
| **Gal** | Ga(lactoside-binding)lectins = **Gal**ectins |
| **GPCR** | **G** **P**rotein **C**oupled **R**eceptor |
| **GRK** | **G**-protein coupled **r**eceptor **k**inase |
| *F* | |
| **Fc** | **F**ragment **c**rystallizable |
| **FID** | **F**ree **i**nduction **d**ecay |
| **frHMGB1** | **F**ully **r**educed **H**igh **M**obility **G**roup **B**ox **1** |
| *H* | |
| **HGF** | **H**epatocyte **g**rowth **f**actor |
| **HMGB1** | **H**igh **M**obility **G**roup **B**ox **1** |
| **HMGB1-TL** | HMGB1 **t**ail-**l**ess |
| **HSQC** | **H**eteronuclear **s**ingle **q**uantum **c**oherence |
| *I* | |
| **IC$_{50}$** | Half-maximal **i**nhibitory **c**oncentration |
| **IDR** | **I**ntrinsically **d**isordered **r**egion |
| **IP3** | **I**nositol tri**p**hosphate |
| **ITC** | **I**sothermal **t**itration **c**alorimetry |
| *J* | |
| **JAK/STAT** | **Ja**nus **k**inase/**s**ignal **t**ransducers and **a**ctivators of **t**ranscription |
| *K* | |
| **K$_A$** | Association constant |
| **K$_D$** | Dissociation constant |
| *M* | |
| **MCA** | 5,5'-**m**ethylenedi-2,3-**c**resotic **a**cid |
| **MD** | **M**olecular **d**ynamics |
| **MST** | **M**icro**s**cale **t**hermophoresis |
| **MS-SV-AUC** | **M**ulti-**s**ignal SV-AUC |
| **MW** | **M**olecular **w**eight |
| *N* | |
| **NMR** | **N**uclear **M**agnetic **R**esonance |
| *P* | |
| **P** | **P**opulation |
| **PAM** | **P**amoic **a**cid |
| **PAP** | 3' phosphoadenosine-5'phosphate |
| **PAPS** | 3' phosphoadenosine-5'phosphosulphate |
| **PCNSL** | **P**rimary **c**entral **n**ervous **s**ystem **l**ymphoma |
| **PDB** | **P**rotein **D**ata **B**ank |

| | |
|---|---|
| **PDF** | **P**air **d**istance distribution **f**unction |
| **PI3K** | **P**hosphatidyl**i**nositol 3-**k**inase |
| **PLA** | **P**roximity **l**igation **a**ssay |
| **PLC** | **P**hospholipase **C** |
| *R* | |
| **RAGE** | **R**eceptor for **a**dvanced **g**lycation **e**nd products |
| **RF** | **R**adio**f**requency |
| **Rg** | **R**adius of **g**yration |
| *S* | |
| **SAXS** | **S**mall **a**ngle **X**-ray **s**cattering |
| **SDF1** | **S**tromal **c**ell **d**erived **f**actor-**1** |
| **SDS PAGE** | **S**odium **d**odecyl **s**ulphate **p**oly**a**crylamide **g**el **e**lectrophoresis |
| **SEC** | **S**ize **e**xclusion **c**hromatography |
| **SE-AUC** | **S**edimentation **e**quilibrium - **A**nalytical **u**ltra**c**entrifugation |
| **SV-AUC** | **S**edimentation **v**elocity - **A**nalytical **u**ltra**c**entrifugation |
| *T* | |
| **TCS** | **T**ransferred **c**ross-**s**aturation |
| **TLR4** | **T**oll-**l**ike **r**eceptor **4** |
| **TM** | **T**rans**m**embrane domains |
| *V* | |
| **VS** | **V**irtual **s**creening |
| *X* | |
| **XCL** | **XC** motif chemokine **l**igand |
| **XCR** | **XC** motif chemokine **r**eceptor |

# Contents

# List of Figures

# List of Tables

# Chapter 1

# Introduction and Aim of Thesis

## 1.1   Chemokines and their cognate G-protein coupled receptors

Chemokines play a fundamental role in the physio-pathological response mechanisms of the innate and adaptive immune system by orchestrating cell recruitment, trafficking and activity (Charo and Ransohoff, 2006a). As they serve as primary guidance cues for controlled leukocyte trafficking (Baggiolini, 1998), their involvement in inflammatory diseases (Premack and Schall, 1996), such as atherosclerosis (Zernecke and Weber, 2014) and HIV infection (Cocchi et al., 1996), has been deeply investigated in in-vitro and in-vivo studies. Chemokine activity has a dual role in suppressing and supporting tumorigenesis and metastasis formation (Balkwill, 2003, Rollins, 2006, Mantovani et al., 2008, Allavena et al., 2011). However, its involvement in dictating the tumour fate in the microenvironment is still at its infancy and an important matter of study.

The chemokine system (Figure 1.1) is characterized by a set of almost 50 ligands, which engage in a promiscuous fashion with a panel of more than 20 chemokine receptors (Bachelerie et al., 2014a, Murphy et al., 2000). Chemokines belong to the largest family of 8-10 kilodalton small, homeostatic cytokines exhibiting chemotactic functions through their cognate receptors (Blanchet et al., 2012). The canonical chemokine receptor, also known as G-protein coupled receptor (GPCR), consists of 7 transmembrane domains joined by extracellular loops, linked to a heterotrimeric G protein. The unconventional chemokine receptor is G-protein independent and operates as a scavenger to create chemokine gradients for chemotaxis (Gether, 2000). The chemokine interactome (Figure 1.1), modulates the GPCR signalling by engaging ligands and their receptors in homo- and hetero-association reactions (Mellado et al., 2001). Some of these associations depend on other molecules, such as cell surface glycosaminoglycans (GAGs) (Proudfoot et al., 2003). The activation of chemokine receptors occurs through proteolytic cleavage of the N-terminus of their agonists after entering the receptor transmembrane domains (TMs). This truncation leads in most cases to the diminished function of the agonist or to complete antagonism (Clark-Lewis et al., 1991).
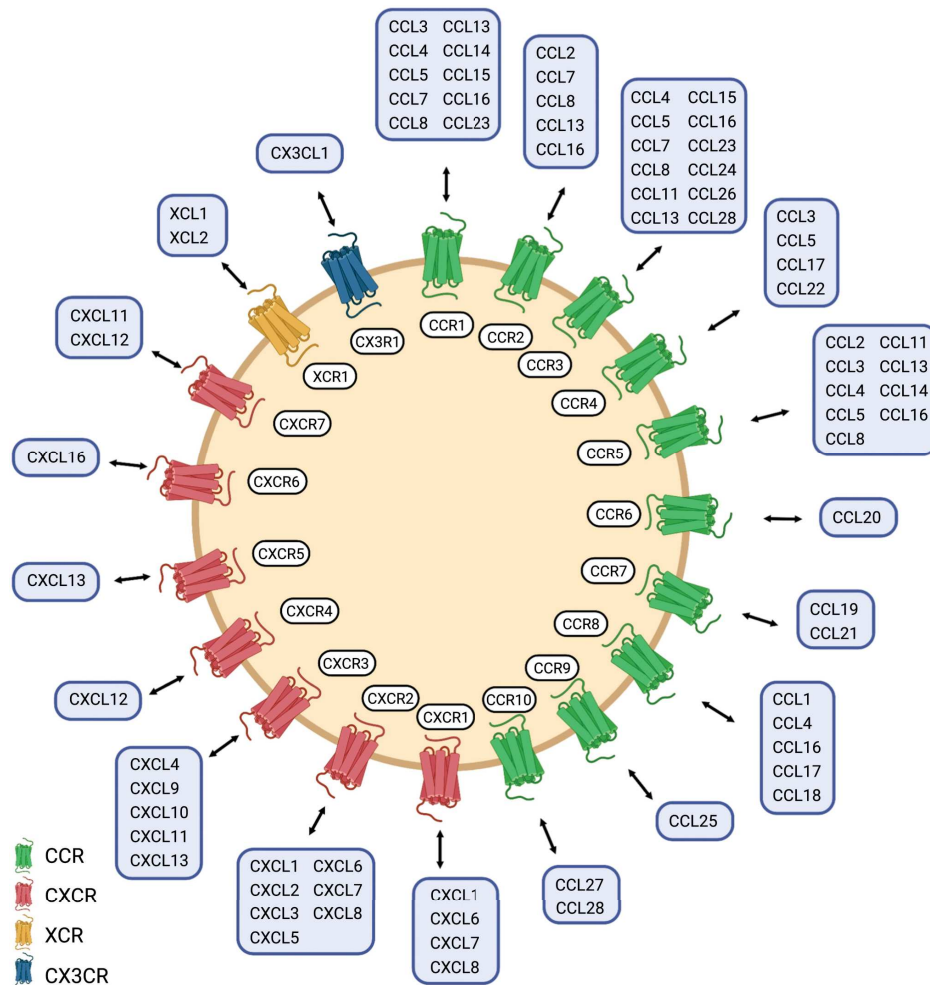
**Figure 1.1:** *The chemokine interactome.* *Scheme of chemokine-chemokine receptor interaction network, figure reused with permission from Elsevier (license no. 5724760858023), from (Märkl et al., 2022). The different chemokine receptor types are represented in different colors: CCR (green), CXCR (red), XCR (orange), or CX3CR (blue). The cognate chemokine ligands are listed in the light blue boxes. Abbreviations: CCL, CC motif chemokine ligand; CCR, CC motif chemokine receptor; CXCL, CXC motif chemokine ligand; CXCR, CXC motif chemokine receptor; XCL, XC motif chemokine ligand; XCR, XC motif chemokine receptor.*

Structurally, chemokines share a conserved cysteine motif (C-motif) that categorizes them into C, CC, CXC or CX3C type ligands with "X" representing the residue spacing between the cysteines (Clark-Lewis et al., 1991), as shown in Figure 1.2 A, B. These form disulphide bonds that stabilize the typical chemokine fold composed of a flexible N-terminus, a three-stranded antiparallel β-sheet, short loops, a $3_{10}$ helix and a C-terminal α-helix, as depicted in the schematic representation in Figure 1.2 A. Despite the variable sequence identity (20% to 90%), this folding is highly conserved among the major families of CC and CXC chemokines (Rajagopalan and Rajarathnam, 2006). The structural integrity of chemokines is therefore essential for receptor binding and activation.

2
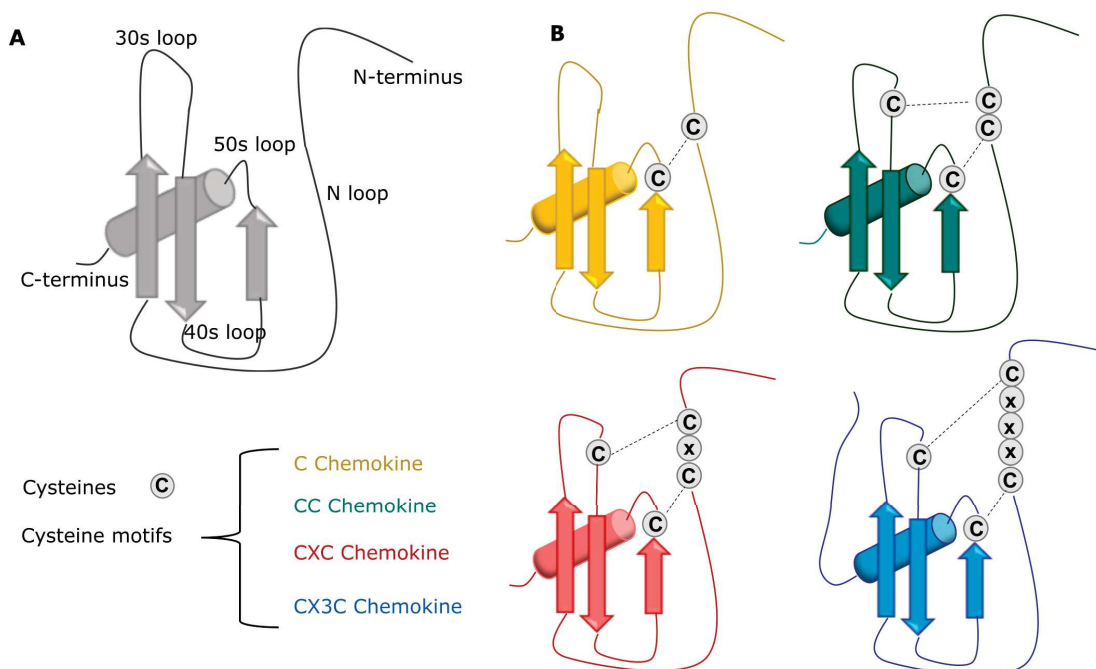
**Figure 1.2:** *Chemokine classification*. *Chemokines are categorized according to the conserved cysteine motifs. (A) Conserved structure architecture of chemokines. (B) Schematic representation of chemokine structures categorized based on cysteine motifs in C (yellow), CC (green), CXC (red) and CX3C (blue) chemokines.*

## 1.2 Chemokine homo-associations and receptor activation

Chemokine homo-associations emerged as a physiological process in regulating the downstream signalling. Homo- as well as hetero-associations typically occur amongst CC and CXC chemokines due to energetically favoured binding interfaces formed between their respective monomers. These arrangements can appear as dimers, trimers, tetramers and as complexes of higher order.

The CC-type dimers align their N-termini to form a two-stranded antiparallel β-sheet, which gives them an elongated and dumbbell shape, as shown in Figure 1.3 A. The CXC chemokines instead dimerize by arranging their first $\beta_1$-strand to form a central antiparallel β-sheet compost of six strands, which results in a globular shape (Figure 1.3 B) (Miller and Mayo, 2017). Exceptions of the typical CC- and CXC-type dimer conformation are CCL20 and CCL7 that form CXC-type dimers, XCL1 that adopts a β-sandwich-type structure (Clore and Gronenborn, 1995 , Meunier et al., 1997) and CXCL12, CCL2 and CCL27 that can exist in both conformations (Hoover et al., 2002, Lubkowski et al., 1997, Jansma et al., 2010).

Homoassociations of chemokines are considered to be weak interactions with apparent dissociation constants ($K_D$) values in the micromolar range (Murphy et al., 2010, Chen and Mayo, 1991, Mayo, 1991). Nonetheless, chemokine oligomerization has been demonstrated to be
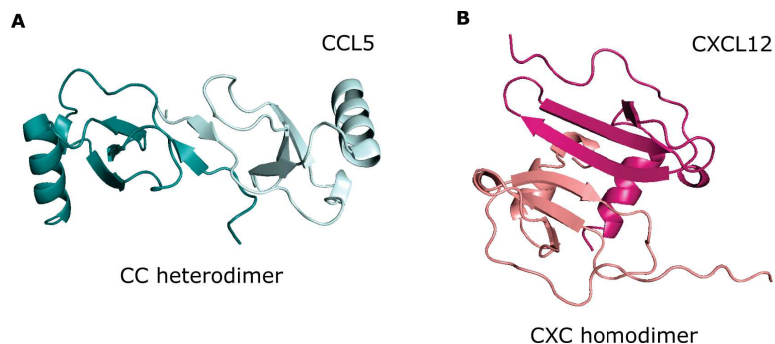
**Figure 1.3:** ***Structures of CC and CXC chemokine homodimers.*** *Structures of homodimers of (A) CCL5 (PDB code: 2L9H) and (B) CXCL12 (PDB code: 1QG7).*

relevant for leukocyte recruitment in vivo (Mellado et al., 2001). Although the binding affinities in-vitro are low, chemokine self-assembly in-vivo may be enhanced through changes in the chemical environment determined by pH, solution ions and presence of specific modulatory ligands, such as glycosamicoglycans (GAGs) (Figure 1.4) (Yang et al., 1994, Veldkamp, 2005). The interactions between GAGs and chemokines are of electrostatic nature and comprise arginine, lysine or histidine that form the basic ("B") signature of chemokines in general. Binding affinities depend on GAG composition and length and chemokine oligomeric state (Brown et al., 2017a). Chemokine homodimers usually bind stronger to GAG ligands compared to their monomers (Lortat-Jacob, Grosdidier, and Imberty, 2002, Sawant et al., 2016, Ziarek et al., 2017a). However, self-assembly of chemokines independently from GAG binding has been identified as a general mechanism to generate concentration gradients for inducing chemotaxis and other signalling processes.

The general accepted mechanism of GPCR signalling activated by chemokines is shown in Figure 1.4. The signal transduction is initiated by conformational rearrangements in the TM region of the GPCR upon ligand-binding. The heterotrimeric G-protein at the receptor dissociates into different G$\alpha$ isoforms and into the G$\beta\gamma$ dimer. The G$\alpha$ isoforms and the G$\beta\gamma$ subunits induce differential signalling by triggering the formation of second-messenger effectors, such as cyclic adenosine mono-phoste (cAMP), inositol triphosphate (IP3) and diacylglycerol (DAG). This in turn stimulates the release of intracellular calcium and activation of multiple kinase cascades, which results in the activation of the final cellular responses. Despite the high variability and promiscuity of the chemokine interactome, the receptor responses appear to be very specific in their final functional outcome. Chemokine oligomerization represents only one mechanism by which selectivity for specific downstream events is achieved.
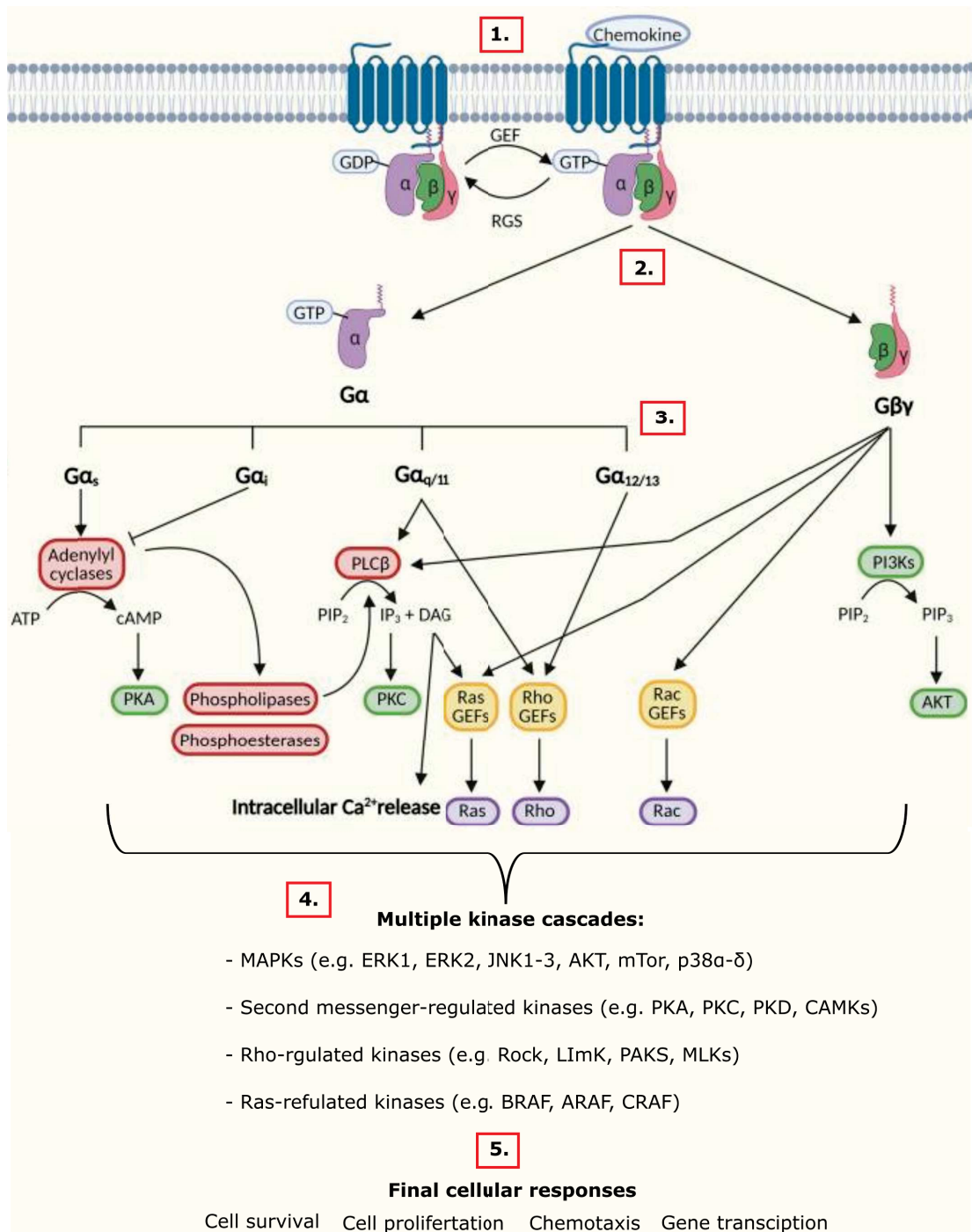
**Figure 1.4:** *G protein-dependent signalling.* *Figure reused according to the Creative Commons Attribution License 4.0 (CC BY) terms and adapted from Lai and Mueller, 2021. Schematic diagram of the chemokine receptor signalling pathways upon activation. (1.) G protein activation upon chemokine binding. The exchange of guanosine diphosphate (GDP) to guanosine triphosphate (GTP) leads to the dissociation of the GTP-bound $G_\alpha$ unit from the $G_{\beta\gamma}$ dimers. (2.-3.) $G\alpha$ proteins are divided intro for different isoforms. The $G\alpha$ isoforms and the $G_{\beta\gamma}$ subunits induce differential signalling involving intracellular calcium mobilization, stimulation or inhibition of cAMP production and activation of second messengers (Ras, Rho and Rac). (4.) Second messengers trigger multiple kinase cascades contributing to the final signalling responses (5.): chemotaxis, survival, proliferation and gene transcription.*

Agonists of GPCRs can trigger a broad range of signalling pathways. While full agonists activate the entire G protein repertoire and arrestin axis equally (Figure 1.5 A), biased agonists stimulate only a subset preferring one signal transducer over another (e.g. β-arrestin vs. G protein, as shown in Figure 1.5 B) (Drury et al., 2011a). Other ligands act as antagonists by blocking the entire receptor activity. Some chemokine oligomers are biased agonists. Structural studies elucidating the functional aspect of biased agonism of GPCRs offer the potential for the development of more targeted therapeutics with less side effects.
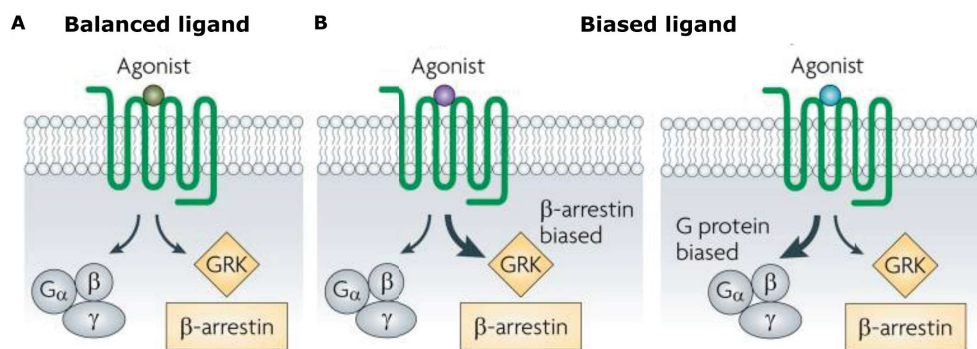


**Figure 1.5:** *__Biased chemokine receptor signalling__. Figure reused with permission from Springer Nature (license no. 5732391098431) and adapted from Rajagopal et al., 2010a. (A) Balanced signalling: Ligand-binding leads to activation of both G-protein dependent and β-arrestin signalling equally. (B) Biased ligand agonism: Either G-protein signalling or β-arrestin signalling are triggered respectively by a biased agonist.*

## 1.3   Chemokine heterocomplexes

The chemokine biology is evidently more complex than the simple ligand-receptor interaction. Chemokines can antagonize or synergize their cognate receptors with other chemokines by forming heterocomplexes. Despite belonging to different chemokine classes, certain CC and CXC chemokines can indeed associate non-covalently. The term "*hetero-*" refers hereby to chemokine oligomers, mostly dimers, that are formed by monomeric units belonging to different C-motif chemokine classes.

Chemokine heterocomplexes can magnify the functional responses with respect to their single components (Cecchinato et al., 2016a). Besides heterocomplexation on a single receptor, synergism and cooperativity can also occur through simultaneous or sequential triggering of multiple receptors (Proudfoot and Uguccioni, 2016, De Buck et al., 2017. Synergism provoked by chemokine heterocomplexes has been described as a crucial mechanism in regulating inflammatory conditions (Marshall and Ballante, 2017, Duan et al., 2017a). Koenen

et al., 2009 provided a striking evidence of functional synergism mediated by chemokine-based heterodimers in inflammatory diseases in-vivo. They showed that atherosclerosis in hyperlipidemic mice was associated with enhanced monocyte recruitment mediated by the CCL5•CXCL4 complex, as peptides disrupting the heterocomplex inhibited monocyte migration and reduced the disease progression. Other chemokine heterocomplexes associated with functional synergism are for instance CXCL4 and CXCL8, which induce enhanced CXCL12-elicited migration of bone marrow-derived B-cells (Paoletti et al., 2005), as well as CCL19, which triggers augmented leukocyte migration upon heterocomplexation (Kuscher et al., 2009). Besides synergism, chemokine heteromers have also shown inhibitory effects. For example, CXCL12-induced chemotaxis of B cells is inhibited by the addition of CCR5 agonists, such as CCL4, implying heterocomplexation as the source of the inhibitory activity (Honczarenko et al., 2002).

The list of chemokine heterodimers increases and over 200 were identified with modulatory functions in the chemokine system (Blanchet, Weber, and Hundelshausen, 2023). The trend of chemokine heteromer pairs is increasing and extending to structurally diverse chemokines, termed as atypical chemokines (ACKs). ACKs comprise small (8–25 kDa) chemo-kines that lack the classifying N-terminal cysteine residues. Like chemokines, they bind to chemokine receptors with high affinity and elicit chemotactic cell migration (Kapurniotu, Gokce, and Bernhagen, 2019). Macrophage migration-inhibitory factor (MIF) is an ACK that binds to chemokine receptors CXCR2 and CXCR4 to promote atherogenic leukocyte recruitment (Brandhofer et al., 2022). MIF forms with platelet chemokine CXCL4L1 a heterocomplex with inhibitory effects on MIF-elicited chemotaxis and thrombus formation (Brandhofer et al., 2022).

To summarize, chemokine heteromers amplify or attenuate chemokine responses of the corresponding receptors to modulate the chemokine system. Accumulating evidence from in vitro and in vivo experiments elucidate the functional role of synergism and antagonism exerted by chemokine heterocomplexes in inflammatory and oncological situations. Thus, targeting heterophilic chemokine-chemokine interactions appears to be a promising approach for the development of novel anti-inflammatory and anti-cancer drugs.

**Table 1.1:** ***Examples of chemokine receptor modulators.*** *Chemokines exerting antagonistic and synergistic activities on chemokine receptors. Table reproduced from Cecchinato et al., 2023.*

| Activity | Receptor | Modulator | Reference |
|---|---|---|---|
| Antagonism | CCR1 | CCL4 | Chou et al., 2002 |
| | | CCL26 | Petkovic et al., 2004a |
| | CCR2 | CCL2 | Gong et al., 1997 |
| | | CCL11 | Ogilvie et al., 2001 |
| | CCR3 | CCL18 | Loetscher et al., 2001, Fulkerson et al., 2004, Nibbs et al., 2000 |
| | | CXCL9 | |
| | | CXCL10 | |
| | | CXCL11 | |
| | CCR5 | CCL7 | Blanpain et al., 1999 |
| | | CCL26 | Petkovic et al., 2004a |
| | | CCL11 | Petkovic et al., 2004b |
| Synergism | CCR2 | CCL19 | Kuscher et al., 2009 |
| | | CCL21 | |
| | CCR4 | CXCL10 | Sebastiani et al., 2005 |
| | CCR5 | CXCL4 | Von Hundelshausen et al., 2005 |
| | CCR7 | CXCL13 | Paoletti et al., 2005 |
| | CXCR3 | CXCL12 | Krug et al., 2002, Vanbervliet et al., 2003 |
| | CXCR4 | CXCL9 | Venetz et al., 2010 |
| | | HNP1 | Alard et al., 2015 |
| | | Galectins | Eckardt et al., 2020a |
| | | HMGB1 | Schiraldi et al., 2012, Cecchinato et al., 2018 |

# 1.4 Chemokine CXCL12

Stromal cell derived factor-1 (SDF1) is a prototypical C-X-C chemokine (9-16 kDa) exerting essential homeostatic processes during embryogenesis, hematopoiesis, angiogenesis and inflammation (Wisler et al., 2014, Nagasawa et al., 1996, Juarez, Bendall, and Bradstock, 2004). The name originates from its first isolation as a pure protein from bone marrow stromal cells (Tachibana et al., 1998). SDF1, also referred to as CXCL12, is the only CXC chemokine that exists in humans in six different isoforms ($\alpha$ to $\phi$, Figure 1.6, A) as a result of differential RNA splicing. The alpha and beta isoforms of CXCL12 are the most abundantly expressed isoforms in liver, pancreas and spleen (Tashiro et al., 1993, Yu et al., 2006a). Besides the abundance and availability of CXCL12 molecules in cell, evolutionary pressure led to high sequence identity (e.g. 99% amino acid sequence identity between human and mouse) and exceptional homology amongst CXCL12 orthologs to retain the essential chemotactic function (Hersh et
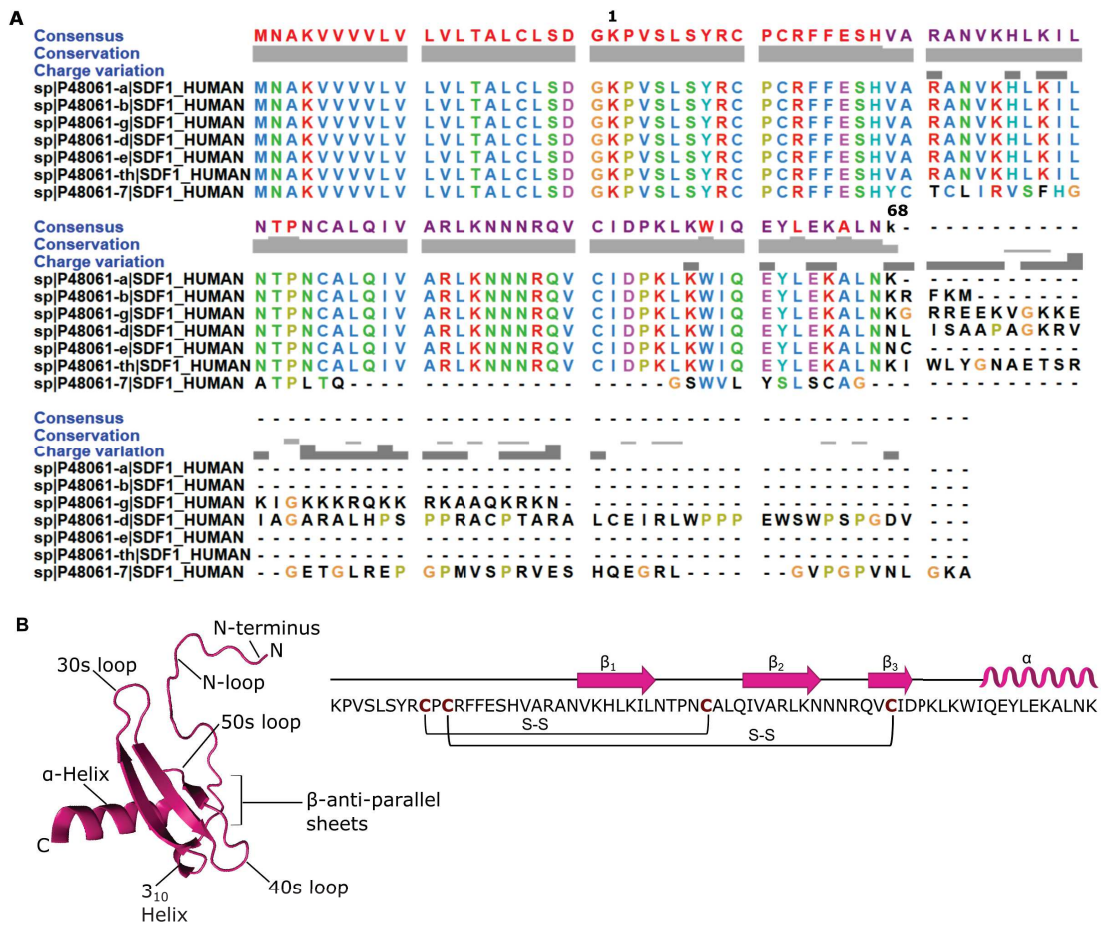
**Figure 1.6:** *Protein sequence of CXCL12 isoforms, also referred to as SDF-1, and the molecular structure of CXCL12-alpha.* *(A) Multiple sequence alignment of human CXCL12 isoforms using COBALT: constraint-based alignment tool for multiple protein sequences (Papadopoulos and Agarwala, 2007). Protein sequences of CXCL12, named as sp | Uniprot code -isoform | SDF-1_ HUMAN, are listed in the following order: SDF-1-alpha$_{1-68}$ (P48061-2), SDF-1-beta$_{1-72}$ (P48061-1), hSDF-1gamma (P48061-3), hSDF-1delta (P48061-4), hSDFepsilon (P48061-5), hSDFtheta (P48061-6), SDF-7 (P48061-7). The first 21 amino acid residues belong to the signal peptide sequence of CXCL12. The numbering starts with the first residue of CXCL12 involved in CXCR4 activation. (B) Structure and amino acid sequence of CXCL12-alpha (PDB code: 2kee).*

al., 2018).

Thus, CXCL12 shows the key features of the typical chemokine fold (Figure 1.6 B). It comprises 68 amino acid residues and is composed of an unstructured N-terminus (aa 1–8), long flexible loop (N-loop), three-stranded β-sheet joined by loops (30s, 40s and 50s), a 3$_{10}$ helix, followed by a C-terminal α-helix (Dealwis et al., 1998a). The three-dimensional structure of CXCL12 was determined by NMR spectroscopy (Yu et al., 2006b, Crump et al., 1997) and X-ray diffraction (Murphy et al., 2007). Mutagenesis studies of CXCL12 revealed that residues of the N-terminus including the N-loop and β-sheet are implicated in binding to CXCR4 and

thus critical for the CXCR4-mediated signalling ( Yu et al., 2006b, Crump et al., 1997, Dealwis et al., 1998a, Doranz et al., 1999). CXCL12 mediates cell motility, proliferation and survival through its canonical and non-canonical receptors CXCR4 and CXCR7, also known as ACKR3 ( Berger, Murphy, and Farber, 1999, Ratajczak et al., 2006, Rajagopal et al., 2010a, Sun et al., 2010). Figure 1.7 represents some of the key pathways involved in the CXCL12-induced signal transduction of CXCR4 and CXCR7. Binding of CXCL12 engages the N-terminus and extracellular loops (ECLs) of CXCR4 and induces thereafter conformational rearrangements in the receptor transmembrane domain (TM) region (Brelot et al., 2000, Zhou et al., 2001, Kobilka, 2007, Weis and Kobilka, 2008, Goldsmith and Dhanasekaran, 2007). This initiates the dissociation of the CXCR4-bound trimeric G-protein [56] leading to the subsequent release of the G$\alpha$ and G$\beta\gamma$ subunits, which in turn trigger intracellular Ca$^{2+}$ flux and the activation of the PI3K/Akt, PLC, and ERK1/2 pathways (Vlahakis et al., 2002, Ganju et al., 1998). This results in gene transcription, cell migration, proliferation and survival (Proost et al., 1999). CXCR4 oligomerization can also activate the G-protein independent Janus kinase/signal transducers and activators of transcription (JAK/STAT) pathway (Christopherson, Hangoc, and Broxmeyer, 2002). Termination of the signal transduction occurs through G-protein receptor kinase (GRK) phosphorylation and CXCL12 binding to CXCR7, which initiate the internalization of phosphorylated CXCR4 by $\beta$-arrestin (Rajagopal et al., 2010a). Doing so, CXCL12 signalling reduces the receptor levels in CXCR4-expressing tissues through the scavenger receptor CXCR7.
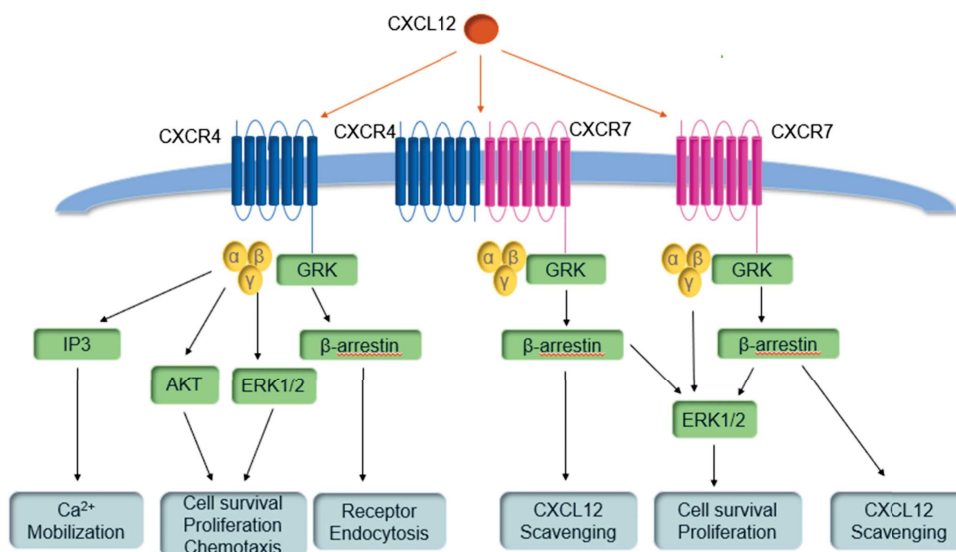


**Figure 1.7:** *CXCL12-CXCR4/CXCR7 signaling pathway*. *Figure reused according to the Creative Commons Attribution (CC By) license terms, from Lounsbury, 2020. CXCL12 binding activates CXCR4 through G protein dissociation and GRKs. This subsequently triggers intracellular Ca$^{2+}$ release and the activation of PI3K, AKt, ERK1/2 pathways which result in cell survival, proliferation and chemotaxis. GRKs primarily induce the recruitment of $\beta$-arrestin leading to CXCR4 internalization. CXCR7 could induce $\beta$-arrestin independently or through CXCR4/CXCR7 heterodimer, resulting in MAPK activation and CXCL12 scavenging.*

The evolutionary conservation of the structure and function of CXCL12 in addition to its functionally relevant truncated analogs (Ohnishi et al., 2000, Veldkamp et al., 2008 ) underscores the importance of its diverse regulatory activities through CXCR4 and CXCR7 in cell. Indeed, structural, functional and computational work (Zhou et al., 2001, Kawatkar et al., 2011, Xu et al., 2013, Ziarek et al., 2017a, Stephens et al., 2020a) aim to elucidate several molecular mechanisms that explain the CXCL12/CXCR4/CXCR7 activity (Santagata et al., 2021) with the focus on CXCL12 and CXCR4, one of the most extensively studied modulators related to cancer development (Shi, Riese, and Shen, 2020). Such mechanisms include homo-and hetero-associations of CXCL12 and/or CXCR4 and CXCR7. Therapeutic intervention involves targeting the canonical CXCL12/CXCR4 axis with pharmacological agents to treat different cancers over the past years (Wang et al., 2020). With the prospect of designing new therapeutic drugs with higher efficacy, structural information about the CXCL12-CXCR4 interaction that triggers disease-relevant pathways is fundamental, but requires a deeper understanding of the homo- and hetero-assembly of both ligand and receptor.

## 1.5   The CXCL12-CXCR4 Interaction

Both high concentrations of CXCL12 and upregulated CXCR4 activity are associated with tumour development and cancer progression as a result of aberrant cell trafficking (Su et al., 2005, Wagner et al., 2009, Wang et al., 2014). Current therapeutic strategies consist of identifying agents that target either CXCL12 or CXCR4 or that interfere with the CXCL12•CXCR4 complex to inhibit CXCR4-mediated tumorigenesis driven by hyperactivity. To discover therapeutic molecules capable of interfering with interactions that resolve the pathological outcome in the CXCL12/CXCR4 axis, a deep understanding of the CXCL12-CXCR4 interaction at atomistic level is fundamental. For this purpose, structural studies aim to shed light on the functional activity of the CXCL12/CXCR4 by investigating the underlying interactions.

Matthew P. Crump et. al. (Crump et al., 1997) solved the structure of CXCL12 by NMR and identified the receptor binding sites of CXCL12 by measuring binding affinities and immobilized calcium levels between sequentially truncated N-terminal constructs of CXCL12 and CXCR4-expressing cells. They discovered that the first residues of the N-terminus of CXCL12 established an important contact with CXCR4 with Lys-1 ($K_1$) and Pro-2 ($P_2$) being directly involved in receptor activation. The receptor binding site comprising residues 12–17 of the N-terminal loop of CXCL12 is referred to as RFFESH motif. Based on these findings, a mechanistic model for complex formation between CXCL12 and CXCR4 has been postulated describing two independent binding events (Figure 1.8 A-C). The first contact is established by the RFFESH motif of CXCL12 binding to the N-terminus of CXCR4 (Figure 1.8 B), followed by the entrance of the N-terminus of CXCL12 in the TM region of CXCR4 triggering its activation with $K_1P$ residues of CXCL12 (Figure 1.8 C).
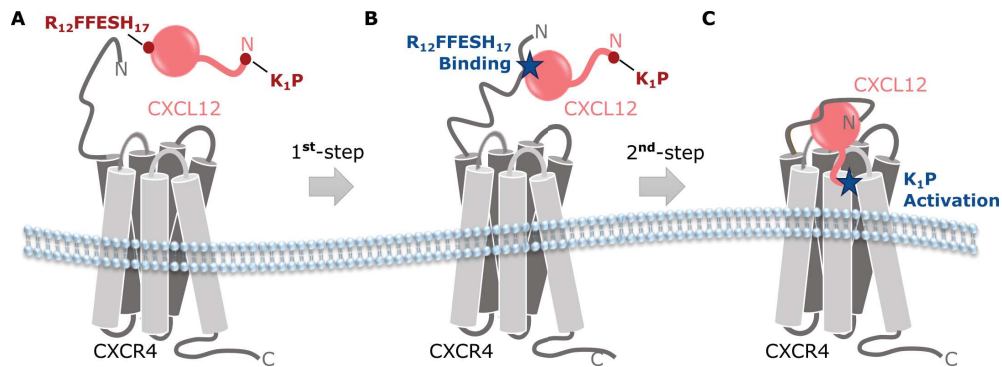
**Figure 1.8:** *CXCL12-CXCR4 two binding site mechanism.* *(A) Two binding regions of CXCL12 comprising residues RFFESH and KP are important for binding and activating CXCR4. (B) 1st step: the first contact is established by the RFFESH motif of CXCL12 with the extracellular N-terminal domain of CXCR4. (C) 2nd step: the first two residues of CXCL12 (KP) activate CXCR4 upon binding to the transmembrane region.*

Veldkamp et al., 2006 demonstrated that sulphation of the N-terminal tyrosines of CXCR4 is important for binding to CXCL12 in NMR titrations of CXCL12 with tyrosine-sulphated peptide corresponding to the CXCR4 N-terminus (Figure 1.9 A, B). The sulfonation pattern at tyrosine (Y) positions Y-7, Y-12 and Y-21 (sY7, sY12, sY21) increased binding affinity and site specificity on CXCL12. In particular, the sulphation of Y-21 (sY21) contributed the most to the affinity and specificity for CXCL12 and to its dimerization suggesting sulphation as an important driver for the CXCL12-CXCR4 recognition process (Veldkamp et al., 2006, Farzan et al., 2002).
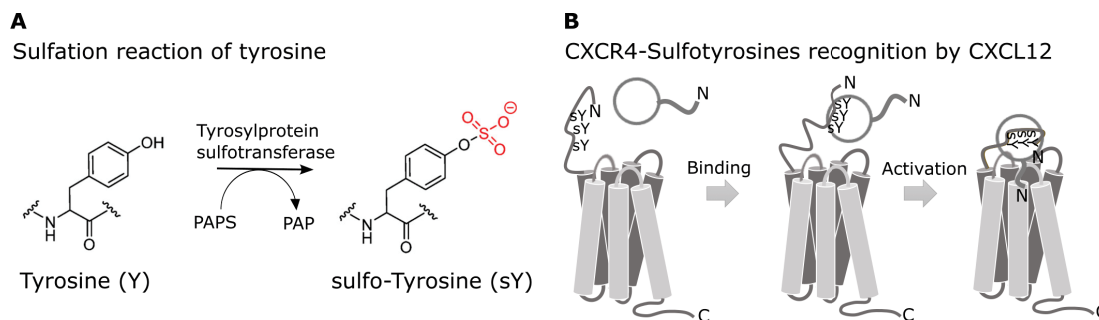


**Figure 1.9:** *Sulphation of tyrosines of CXCR4 important for CXCL12 recognition.* *(A) Chemical reaction of tyrosine sulphation. (B) Sulfotyrosines of CXCR4 N-terminus recognized by CXCL12. Abbreviations: PAPS = 3' phosphoadenosine-5'-phosphosulphate, PAP=3' phosphoadenosine-5'-phosphate.*

Veldkamp et al., 2008 and Ziarek et al., 2013a furthermore revealed crucial binding modes of CXCL12 involving the initial part of CXCR4 based on NMR titrations of a 38-mer peptide resembling the CXCR4-N-terminus, also referred to as p38, into generated monomeric and dimeric variants of CXCL12 (Figure 1.10 A and B). The utilized monomeric and dimeric mutants of CXCL12, termed by the authors as "locked" monomer (LM) and "locked" dimer (LD), were engineered with disulphide bonds at specific positions to stabilize the monomeric conformation of CXCL12 and to connect covalently two CXCL12 molecules, respectively. As
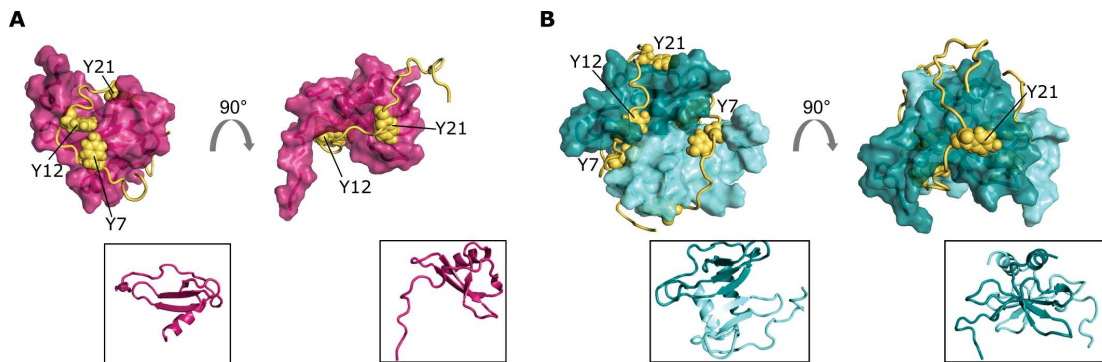
**Figure 1.10:** *Binding of CXCR4 N-terminal peptide involves different binding region of CXCL12 monomer and dimer. CXCR4 N-terminal domain peptide (p38) in yellow bound to (A) CXCL12-LM (PDB code: 2n55) and (B) CXCL12-LD (PDB code: 2k04). CXCL12-LM and CXCL12-LD are shown in surface representation coloured in magenta and cyan/teal, respectively. Tyrosine residues are represented as spheres to highlight the different binding sites of p38 to CXCL12 oligomers. Insets show the orientation of CXCL12-LM and CXCL12-LD in cartoon representation.*

illustrated in Figure 1.10 (A, B), p38 binds to CXCL12-LM and CXCL12-LD at different regions suggesting different binding mechanisms between CXCR4 and CXCL12 oligomers. To be specific, p38 "wraps" around CXCL12-LM (PDB code: 2n55) crossing the three stranded anti-parallel β-sheet region, whereas in CXCL12-LD (PDB code: 2k04) it is displaced and touches different areas. Given the importance of Y21 of p38 in recognizing CXCL12, the authors inspected the binding pocket of Y21 in the structures of p38 bound to CXCL12-LM and CXCL12-LD. Of note, Y21 established hydrophobic contacts with residues V18, R47 and V49 of CXCL12-LD, whereas with CXCL12-LM the hydrophobic contacts appear to be primarily satisfied by V49 and E15. Interestingly, Veldkamp et al., 2008 showed that p38 promoted CXCL12 dimerization by fluorescence polarization measurements and deduced from the appearance of NMR spectra the presence of a stable 2:2 symmetric CXCL12:p38 complex, as illustrated in Figure 1.10 B. The NMR structure of CXCL12-LM bound to p38 (Figure 1.10 A) was solved later by Ziarek et al., 2017a and used for modelling the entire CXCL12•CXCR4 complex in a 1:1 ligand:receptor ratio (shown later).

Overall, these findings indicate that post-translational modifications, in this case tyrosine-sulphation of the N-terminus of CXCR4, is crucial for the recognition process and that the N-terminal domain of CXCR4 establishes distinct interaction contacts for CXCL12 monomer and dimer may dictate the oligomer selectivity for CXCL12 implying another layer of signalling regulation. Although these data are compatible with the two-step binding model, However, the lack of evidence that the interactions between CXCL12 and the N-terminal fragment of CXCR4, reported in the NMR study, would correspond to the binding of CXCL12 to the entire CXCR4 remains to be clarified. The analogous problem was found for the HIV-1 interaction with receptor CCR5, presented by Cormier et al., 2001, who demonstrated that the binding of HIV-1 gp120 to CCR5 is different when gp120 binds to an N-terminal sulfopeptide of CCR5 and the entire CCR5 (Cormier et al., 2001). Thus, the structural basis for the CXCL12–CXCR4

interaction remains obscure.

Groundbreaking findings emerged from advances in the application of NMR spectroscopy to larger protein complexes by enabling the binding analysis of CXCL12 to full-length CXCR4 (Kofuku et al., 2009a). Methyl-based transferred cross-saturation (TCS) NMR experiments unveiled a more extensive interaction surface of CXCL12 engaging with CXCR4 compared to mutational studies in the past. The binding site spread over the whole chemokine including the $\beta_1$-strand (V23, L26, and I28), the $\beta_3$-sheet (L29, V39, and V49), and the 50-s loop (L55) in addition to the N-terminus (V3 and L5). The question of the exact stoichiometry of the CXCL12•CXCR4 complex has been re-considered and addressed by several studies to build a structural model.

Several computational models aid to describe the CXCL12-CXCR4 interactions in agreement with the experimental and functional data. The ones reported here shed light on the critical role of residues of CXCL12 and CXCR4 in binding and signalling (Ziarek et al., 2017a, Stephens et al., 2020a). These models have been validated through experimental and computational means by others (Tamamis and Floudas, 2014, Wang et al., 2020. The established in-silico structures of the CXCL12•CXCR4 complex show CXCL12 buried with the N-terminus in the transmembrane region of CXCR4 in a 1:1 complex (Figure 1.11 A and B, 1:2 stoichiometry not shown). Both models highlight the dominance of electrostatic interactions between CXCL12 and CXCR4 residues (Figure 1.11 C, D) but display the highest dissimilarity in the flexible N-terminal domain of CXCR4 in binding to CXCL12 (Figure 1.11 A and B, coloured in cyan). Model 1 was obtained from docking the NMR solution structure of CXCL12-LM bound to p38 (PDB code: 2n55) into the crystal structure of CXCR4 (PDB code: 3odu) (Ziarek et al., 2017a). It shows the N-terminus of CXCR4 and the $\beta_1$-strand of CXCL12-LM forming a parallel-stranded $\beta$-sheet arrangement as an interaction surface mimicking the dimerization interface of CXCL12. As mentioned before, CXCL12-LD binds differently to p38 in a 2:2 ratio suggesting a entire 2:2 ligand•receptor complex Veldkamp et al., 2008. The hybrid Model 1 has been supported by another computational derived CXCL12-CXCR4 model (Tamamis and Floudas, 2014) describing identifying key regions of CXCL12 and CXCR4 that are mainly of electrostatic nature, but interestingly points out that the N-terminal domain of CXCR4 displays the highest flexibility in binding to CXCL12.

Model 2 results from a combination of structure-guided mutagenesis of CXCR4 with computational modelling to propose an experimental validated CXCL12•CXCR4 complex model (Stephens et al., 2020a). It elucidates the initial signal transduction of CXCR4 upon CXCL12 binding. The N-terminal domain of CXCR4 "wraps around" one CXCL12 molecule binding thereby the $3_{10}$ and the C-terminal $\alpha$ helix of CXCL12. In this pose, the $\beta_1$-strand of CXCL12 forms with the distal N-terminal residues 1-MEGISI(sY7) of CXCR4 an anti-parallel $\beta$-sheet occupying the dimerization surface of CXCL12. The model as well suggests intermolecular interactions mediated by electrostatic contacts (Figure 1.11 D). Despite the similarity between the

**A** Model 1: NMR hybrid model

CXCL12

N-terminus
CXCR4

CXCR4

**B** Model 2: Mutagenesis based model

CXCL12

N-terminus
CXCR4

CXCR4

**C** Electrostatic surface representation of model 1

**D** Electrostatic surface representation of model 2
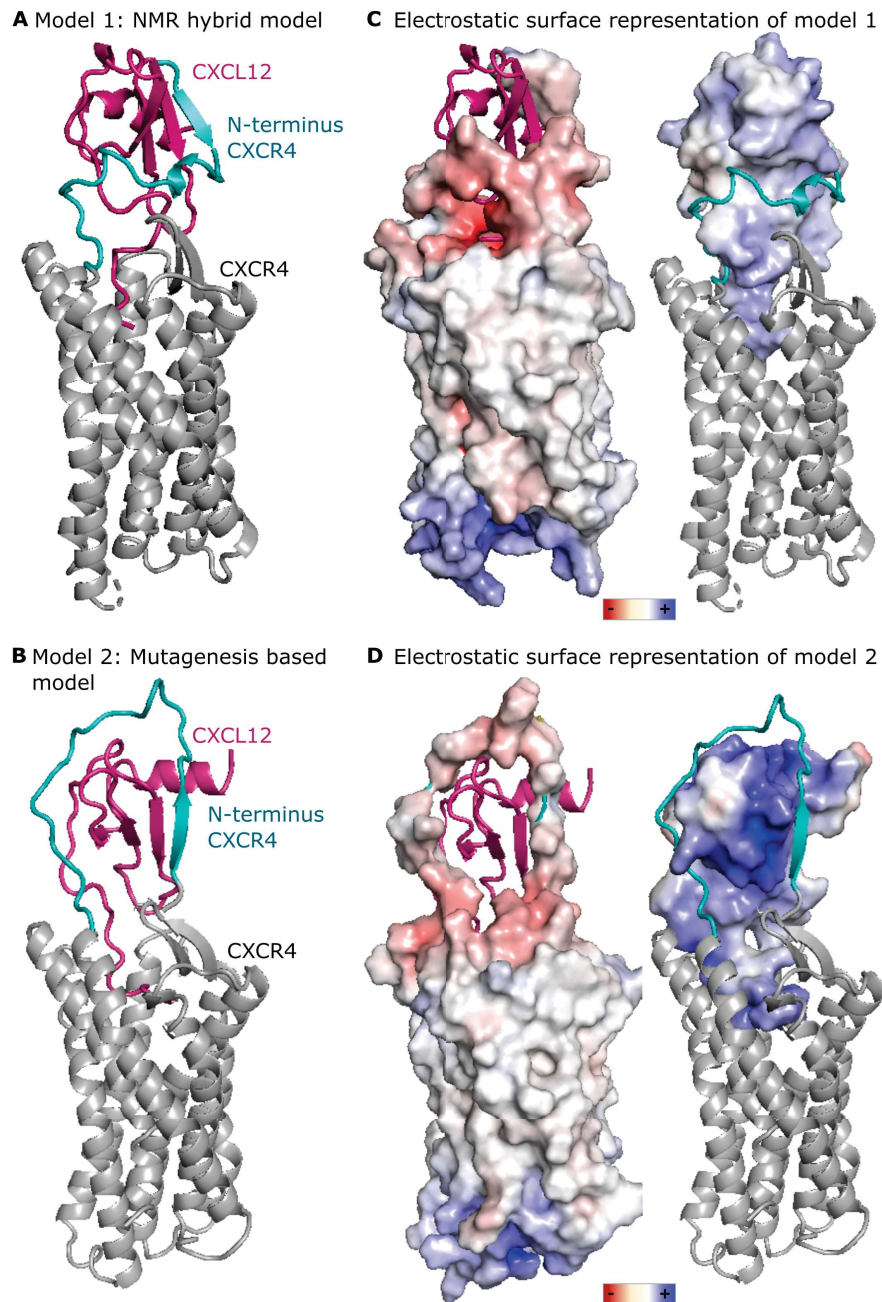
**Figure 1.11:** *Structural models of the CXCL12•CXCR4 complex.* *Models of the CXCL12•CXCR4 complex obtained from (A) docking of CXCL12-LM:p38 in CXCR4 (Model 1) by Ziarek et al.,* *2017a* *and (B) Homology modelling combined with charge swap mutagenesis data (Model 2) by Stephens et al.,* *2020a*. *Electrostatic surface representation of CXCR4 (left) and CXCL12 (right) of (C) Model 1 and (D) Model 2.*

two models, the different orientation β-sheet arrangement is a structural-relevant difference. However, the anti-parallel alignment is supported by experimental evidence from charge-swap

mutagenesis (Stephens et al., 2020a). Other models describe the CXCL12-CXCR4 interaction as a 1:2 ligand-receptor complex considering CXCR4 homodimerization (not shown).

A weak point of both representative models of the CXCL12•CXCR4 complex is the undescribed activation state of CXCR4, as they are build on the X-ray structure of the inactive CXCR4 conformation (PDB code: 3odu). Recent cryo-electronmicroscopy (cryo-EM) studies show CXCL12 monomer bound to the active CXCR4 conformation including parts or the entire G-protein (Liu et al., 2023, Saotome et al., 2024). In addition, atomic-level molecular dynamics (MD) simulations were also used to describe the structural activation of CXCR4 with Gi protein and internal water distribution upon binding to CXCL12 (Figure 1.12, Wang et al., 2020). All structural representations show the conformational activation of CXCR4 involving the displacement of the TM-6 helix. Despite the progress in the structure determination of the CXCL12•CXCR4 complex, the role of the flexible N-terminal domain of CXCR4 in binding to CXCL12 is still an open question, but an important matter to understand the dynamics of ligand selection in the extracellular environment.



Initial state      Intermediate state      Active state
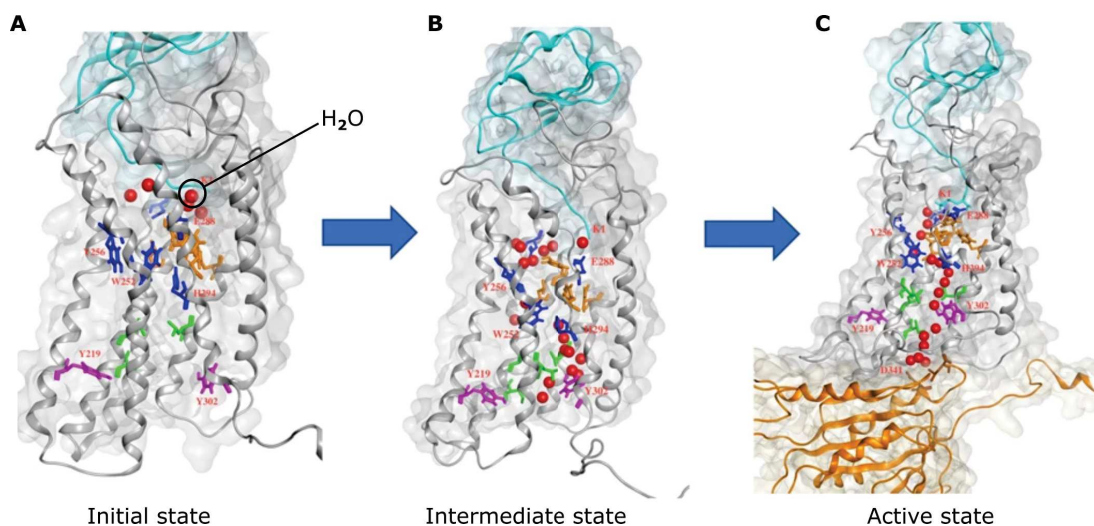
**Figure 1.12:** ***MD simulation of Internal water formation in the CXCL12-CXCR4 complex with empty G$_\alpha$i-protein.*** *Figure reused according to Creative Commons Attribution (CC BY) license terms from Chang et al., 2020. Water molecules represented as red spheres move along the CXCR4 TM region. The side chains illustrated as sticks of the hydrophobic layer 1 (HL1) and 2 (HL2) are colored in orange and green. (A) Initial state of agonist CXCL12 bound to receptor CXCR4. (B) Intermediate state of CXCL12 bound to CXCR4 after 1.8 $\mu$s MD simulations. (C) Active state of CXCL12-bound CXCR4 in complex with G$\alpha$i-protein after 1.0 $\mu$s MD simulations.*

In light of the emerging structural information, the two-site model, although useful, appears to be an oversimplification of the chemokine-receptor recognition. Future studies involve the integration of different techniques to determine the structure of the flexible regions of the CXCL12•CXCR4 complex.

## 1.6   Drug discovery targeting the CXCL12/CXCR4 axis

An increasing number of studies have attributed an oncogenic role to the dysregulation in the CXCL12/CXCR4 axis caused by elevated levels of CXCL12 and overexpression of CXCR4 nourishing the lingering activities of tumour formation, growth, survival and metastasis (Su et al., 2005, Wagner et al., 2009, Wang et al., 2014). The CXCL12/CXCR4 signalling is therefore a promising target in the discovery of anti-cancer drugs.

Hyperactivity and overexpression of CXCR4 negates the efficacy of cytotoxic chemotherapy due to enhanced survival signalling and rehoming of the leukemia cells to the protective bone marrow. For instance, treatment resistance in acute myeoloma leukemia (AML) after chemotherapy has been linked to CXCR4 upregulation (Sison et al., 2014, Chopra and Bohlander, 2019). CXCR4 antagonists in the form of small molecules and peptides (Figure 1.13) sensitized successfully leukemia cells to chemotherapy (Zhao et al., 2022). The small molecule AMD3100 (Plerixafor) reduced cytotoxic protection mediated by overexpressed surface CXCR4 (Flomenberg, 2005). The agent AMD3100 was approved in 2008 by the FDA for short-term treatment of Hodgkin's lymphoma and multiple myeloma and is considered to be anti-metastatic agents in many cancer types involving CXCR4 (Wang et al., 2020, Li et al., 2018, LIAO et al., 2015, Kioi et al., 2010). Peptide T140 and its analogs, e.g. 4F-benzoyl-TN14016, are inhibitors of CXCR4-mediated migration of human breast cancer in-vivo and leukemia (Tamamura et al., 2003). Other therapeutic approaches are still at pre-clinical stage and include the application of other CXCR4-binding ligands, such as drug carriers with CXCR4-antibodies to facilitate pharmacologic delivery (Engl et al., 2006, Kuhne et al., 2013) or CXCR4 gene silencing by siRNAs (Abedini et al., 2012).
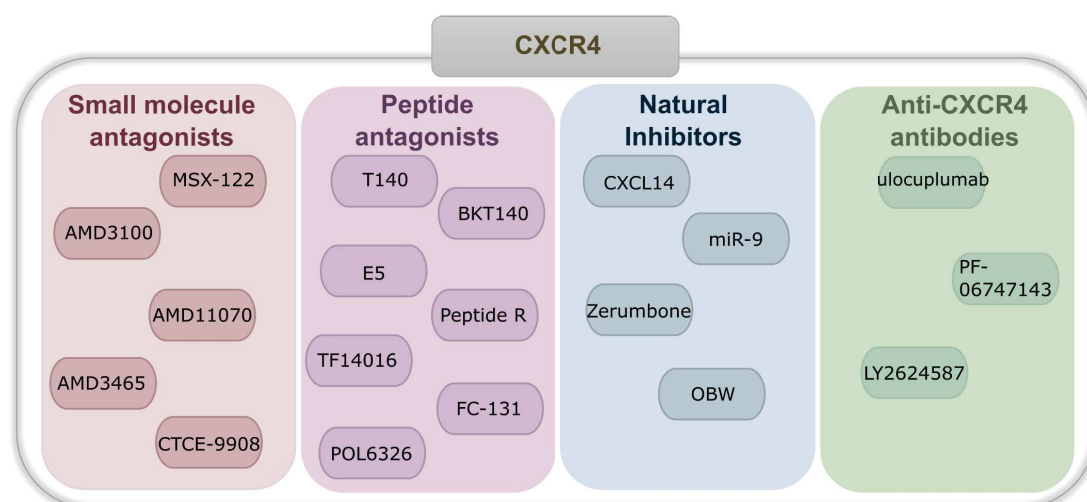


**Figure 1.13: *Therapeutic targeting the CXCL12/CXCR4/CXCR7 signalling axis.*** *Therapeutic strategies target CXCR4 with antagonists: small molecules, peptides, natural inhibitors and anti-CXCR4 antibodies.*

However, given the large tissue distribution of CXCR4, the risk of developing side effects from general and prolonged CXCR4 inhibition, as observed for instance with chronic AMD3100 treatment in acute leukemia, has spread concerns. A potential problem with CXCR4 antagonists is their effect on persistent cell mobilization. Patients may experience an increase in leukocytes (leukocytosis) or a decrease in platelets circulating in the blood (thrombocytopenia). The size of the spleen may increase after long-term administration of CXCR4 antagonists, which can result in spleen rupture and cause death (Karpova et al., 2017). Moreover, improvements in efficiency of current CXCR4 antagonists are marginal and efforts in designing metastatic inhibitors with reduced side effects has been proven challenging and less promising for reaching the clinical stage.

The potential adverse effects and the slow progress in optimizing CXCR4 antagonists led to alternative strategies to interfere with CXCR4-guided metastatic homing. Such approaches involve targeting CXCL12, as it activates multiple tumorigenic signalling pathways of CXCR4. Although chemokines have been considered to be "undruggable", the discovery of the pharmacological agent chalcone as CXCL12 binder and consequently CXCR4 inhibitor has demonstrated that chemokines are viable targets for drug design (Hachet-Haas et al., 2008). Chalcone (Figure 1.14 A) and its analogs enabled the consideration of new therapeutic approaches in targeting CXCL12. However, no structural information about chalcone binding to CXCL12 has been revealed. The first structure-guided approach on CXCL12 has been later adopted by Veldkamp et al., 2010 who identified compound ZINC310454 (ZINC database) that inhibited efficiently CXCR4-mediated calcium response by targeting CXCL12 at the binding pocket of sulfotyrosine 21 (sY21) of p38 (Figure 1.14 B). Optimized in-silico fragment-based method by J. Ziarek et al., 2013 provided ZINC210454 derivates with improved binding affinity in terms of lower dissociation constant (Figure 1.14 C) and half-maximal inhibitory concentration ($IC_{50}$) confirming that the sY21 binding site of CXCL12 is critical for the CXCL12-CXCR4 interaction (Veldkamp et al., 2006). Other optimized small molecules (Smith et al., 2014, Smith et al., 2016) as well as peptides have been discovered that bind to the CXCL12:p38 binding interface with inhibitory effects. Peptides inhibited the proliferation of cell lines of AML and acute lymphocytic leukemia (ALL) by stimulating apoptosis (Pillozzi et al., 2018a). The obtained compound, a 17-mer peptide derived from the N-terminal CXCR4 domain, and a small drug-like molecule represent good scaffolds for further fragment optimization to assemble novel drugs assembly. Another peptide antagonist of CXCL12, named as W4, displayed potent anti-metastasis agent that inhibits CXCL12-induced cell migration in CXCR4-positive breast cancer and leukemia cells (Duan et al., 2017a). In terms of binding affinity, peptide W4 binds to ligand CXCL12 with a $K_D$ value of 57 nM better than AMD3100.

**A** Chalcone

$K_D$ = 150 +/- 50 nM
$IC_{50}$ = 800 μM
R= H

**B** ZINC310454

$K_D$ = 64 +/- 15 nM
$IC_{50}$ = 800 μM

**C** Fragment-based optimization of ZINC310454

$K_D$ = 24 +/- 28 μM

$IC_{50}$ = 11 +/- 24 μM
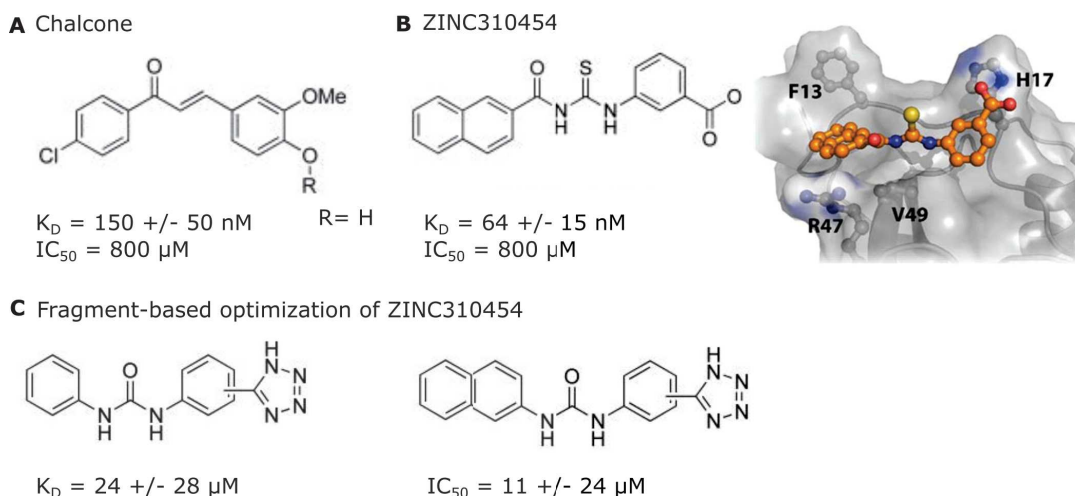
**Figure 1.14:** *CXCL12 inhibitors. Figure adapted according to Creative Commons Attribution (CC BY 4.0) license terms from J. Ziarek et al., 2013. (A) Chalcone. (B) ZINC310454 molecule obtained by structure-based drug discovery of CXCL12. (C) Optimized molecules based on scaffold structure (B).*

Despite the promising results, peptide antagonists for CXCL12 have been rarely published, but may represent another therapeutic option to patients for treating a variety of diseases, including cancer, inflammation, and cardiovascular diseases.

The reason for the scarce success of current therapeutic agents has been attributed to the redundancy of the chemokine system and calls for more specific modulators of the chemokine system. For more targeted drug design elucidation of the chemokine interaction network is therefore crucial. Structural information about CXCL12 and CXCR4 oligomerization are therefore fundamental to understand the regulation of the CXCR4-mediated signalling cascade (Xue et al., 2017).

## 1.7 CXCL12 homodimerization

Accumulating evidence provide a novel mechanism, by which CXCL12 dictates divergent receptor signalling. CXCL12 exits pre-dominantly as monomer or dimer that establish different binding contacts to CXCR4. Consequently, different bound CXCR4 conformations are triggered by monomeric and dimeric CXCL12 that selectively activate distinct signalling pathways.

Under physiological conditions, secreted CXCL12 exists as a mixture of both forms (Ray et al., 2012a). In fact, structure determination by NMR spectroscopy and X-ray diffraction at different experimental conditions show CXCL12 as a monomer and a dimer, respectively (Figure 1.15 A, Dealwis et al., 1998a, Ohnishi et al., 2000, Baryshnikova and Sykes, 2006). The adopted conformation by monomer and dimer CXCL12 is different, which is evident by the different tilt angle between the $\beta_1$ strand and $\alpha$ helix (Figure 1.15 B). The monomeric conformation is favoured at small tilt angles ($< 90°$) with respect to the dimer conformation ($\approx 90°$).
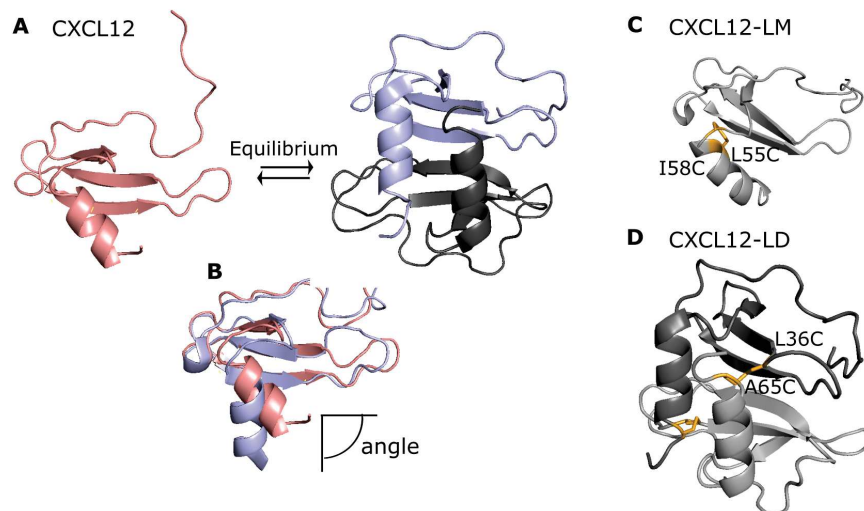
**Figure 1.15:** ***Structures of monomeric and dimeric CXCL12 and CXCL12-LM.*** *(A) Structures of CXCL12 monomer (PDB code: 2sdf) and CXCL12 dimer (PDB code: 1qg7). (B) Superimposition of CXCL12 monomer with one CXCL12 molecule of CXCL12 dimer structure to highlight the conformational differences: The spatial angle between the $\beta_1$-strand and C-terminal $\alpha$-helix form different angles, close to 90° favours the dimeric conformation. (C) Structure of CXCL12-LM (PDB code: 2n55). Disulphide bridge between engineered cysteines at position L55 and I58 of CXCL12-LM stabilize the monomeric conformation by preventing $\beta_1$-strand and C-terminal $\alpha$-helix to assume angles close to 90°. (D) Structure of CXCL12-LD (PDB code: 2K01). Two disulphide bridges link two CXCL12 monomers at L36C and A65C, respectively.*

Interestingly, Veldkamp et al., 2008 discovered that both states exist in a dynamic equilibrium and demonstrated that solution properties (pH, counterions and GAG molecules) affected CXCL12 dimerization (Veldkamp, 2005). CXCL12 dimer is formed at basic pH and requires stabilizing counterions, such as phosphate, sulphate, or citrate. The dimerization of CXCL12 is furthermore favoured in the presence of heparin (Veldkamp, 2005, Ziarek et al., 2013a) suggesting a functional role of the dimer under the influence of GAGs. Moreover, they show that the protonation state of His25, clustered with other basic amino acids (V23-KHLKI-L29) on the $\beta_1$-strand, governs the CXCL12 monomer–dimer equilibrium. Nonetheless, chemokines exist predominantly as monomers at low nanomolar concentrations, as they mediate migration and calcium mobilization. Indeed, the CXCL12-H25R variant stabilizing the monomeric state triggered the mobilization of calcium, cell migration and $\beta$-arrestin recruitment, as expected for the agonistic activities of CXCL12 monomer (Drury et al., 2011b). Since that variant was still prone to dimerization, constitutively monomeric CXCL12-LM (Figure 1.15 C) with engineered disulphide bonds at position L55C and I58C reproduced the balanced G protein–dependent and $\beta$-arrestin–dependent responses associated with normal CXCR4 signalling (Ziarek et al., 2017a). Despite the evidence of CXCL12 dimers in mammalian cells (Ray et al., 2012a), the concern that dimerization was an artifact of high concentrations in in-vitro studies remained. The generated CXCL12-LD (Figure 1.15 D) containing two CXCL12 molecules cross-linked with disulphide bonds at positions L36C and A65C activated the calcium flux but inhibited cell

migration and recruitment of β-arrestin (Drury et al., 2011b). Both CXCL12-LM (Ziarek et al., 2017a, Ziarek et al., 2013a) and CXCL12-LD (Veldkamp et al., 2008) were utilized to dissect CXCR4-mediated chemotaxis and calcium mobilization in-vitro confirming the selective activation through the two oligomeric forms of CXCL12. The hint that dimeric CXCL12 may act as partial antagonist stem from experiments showing prevented metastasis of colonic carcinomas upon CXCL12 administration suggesting the formation of CXCL12 dimer as possible inhibitor (Drury et al., 2011b). Indeed, CXCL12-LD inhibited implantation of lung metastasis of melanoma cells more effectively than AMD3100 and blocked pulmonary tumour growth (Takekoshi et al., 2012).

Based on this evidence, CXCL12 dimer may be used as an inhibitor to attenuate the chemoattractant activities elicited by CXCL12 monomer. Hence, agents driving the equilibrium towards the dimeric state of CXCL12, such as heparin, or the adiministration of CXCL12 to favour the formation of CXCL12 dimer are considered therapeutic approaches. The latter goes along with the administration of cytokines as biological therapeutic agents used to treat against cancer, autoimmune diseases and viral infections (Silva and Lobo, 2020). However, the stability and poor bioavailability of cytokines led to different strategies in developing stable protein agents with improved pharmacokinetic properties and less adverse effects. The design of macrocyclic peptides emerged as an appealing approach in protein therapeutics (Kapurniotu and Bernhagen, 2023). Sakai et al., 2023 designed lasso-grafted peptides with improved pharmacokinetics and blood-brain-barrier (BBB) penetration as cytokine mimics for the human receptor tyrosine kinase MET. They developed a surrogate agonist of MET to exploit its mechanism of organ homeostasis and tissue repair for therapeutic purposes. Met dimerizes upon activation by its ligand hepatocyte growth factor (HGF) that displays therapeutic efficacy in preclinical models (Sakai, Aoki, and Matsumoto, 2015). The grafted macrocyclic-peptide inserts into the loop regions of fragment crystallizable regions that serve as host scaffolds and preserve the HGF-micking agonistic properties of the macrocyclic peptide. As a result, the HGF-mimicking agonist displayed extended life-time and BBB penetration (Sakai et al., 2023). Another potential therapeutic approach involves targeting of chemokine•chemokine heterocomplexes.

## 1.8 CXCL12 heterocomplexes

Chemokine CXCL12 forms molecular hybrids with CXCL4 and CXCL9 exhibiting antagonistic and synergistic activities, respectively. While the first acts as an antagonist of CXCL12-elicited chemotaxis of breast cancer cells providing therefore a therapeutic opportunity (Nguyen et al., 2022), the latter promotes CXCL12-mediated recruitment of tumour-infiltrating lymphocytes and malignant B cells in primary central nervous system lymphoma (PCNSL) (Venetz et al., 2010). Structural studies elucidating the mechanism by which the CXCL12 heteromers induce immune responses that favour or suppress tumorigenesis in the microenvironment are encouraged to advance the field.

Besides CXC chemokine partners, CXCL12 engages also with other molecular effectors, such as inflammatory mediator ga(lactoside-binding)lectin-3 (Gal-3). Like some chemokines, Gal-3, is upregulated during inflammation and therefore extensively studied in inflammatory diseases. Under inflammation, metalloproteinases cleave the N-terminal region of Gal-3, resulting in free Gal-3 carbohydrate recognition domain (CRD) (Ochieng et al., 1994). In this state, Gal-3 binds to CXCL12 targeting the $\beta_1$ strand that represents a hub for multiple interactions with GAGs and chemokines for homo- and hetero-assembly. The interaction surface of CXCL12 upon binding to Gal-3 is similar to the one of CXCL12 homodimer and in part coincides with the receptor binding site and the GAG binding site (Hundelshausen et al., 2021). The authors discard therefore a hypothetical complex composed of CXCL12, Gal-3, GAG and CXCR4 but suggest an equilibrium of the individual interactions in which the components come together in close proximity.
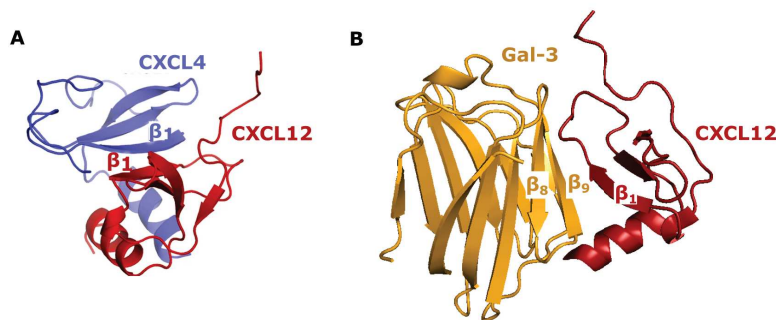


**Figure 1.16:** *CXCL12 heterocomplexes. Panel A adapted in accordance with the terms of the Creative Commons Attribution (CC BY) license from Nguyen et al., 2022. (A) Structural model of the CXCL4•CXCL12 heterodimer. The CXCL4 and CXCL12 monomer are coloured in blue and in red with labelled $\beta_1$ strands forming the intermonomer interface. (B) Alignment of Gal-3 structure (PDB code: 1a3k) and CXCL12 (PDB code: 3gv3 ) to represent the heterodimer, whose structural model was published by Eckardt et al., 2020b.*

Gal3 is not the only inflammatory mediator capable of forming a heterocomplex with CXCL12. Another candidate is the extracellular High Mobility Group Box 1 (HMGB1) that belongs to the class of alarmins or Danger Associated Molecular Patterns (DAMPs). The next sections will provide a detailed background about the CXCL12•HMGB1 heterocomplex and HMGB1, the protagonists of our structural and functional studies.

### 1.8.1 CXCL12 heterodimerization with High Mobility Group Box 1

In addition to heteromeric interactions across the CC- and CXC-chemokine class borders, the discovery of molecular hybrids between chemokines and other effector molecules, such as galectins (Hundelshausen et al., 2021), GAGs (Veldkamp, 2005, Brown et al., 2017a) and inflammatory mediators (Cecchinato et al., 2023, Schiraldi et al., 2012), has expanded the complexity within the chemokine-receptor network to capitalize on specificity, redundancy, and

functional selectivity. Like chemokine-chemokine heterodimers, alarmins modulate the receptor axis in a similar, but peculiar fashion to achieve a specific functional outcome to resolve the inflammation. Since the CXCL12/CXCR4 axis has proven to be a difficult target, with both disease-promoting and protective properties, chemokine-alarmin heterodimers appear to be alternative targets to develop therapeutic treatments of inflammatory disorders and cancer.

In recent years, the alarmin HMGB1, an endogenous Danger Associated Molecular Pattern (DAMP) molecule released upon injury, has been shown to form a heterocomplex with CXCL12 that induces enhanced CXCR4 signalling (Schiraldi et al., 2012). On one side, the CXCL12•HMGB1 heterocomplex promotes tissue regeneration and repair (Tirone et al., 2018, Bianchi et al., 2017), on the other side the heterodimer favours the inflammatory state in active rheumatoid arthritis (Cecchinato et al., 2018) and appears to support the tumorigenic activities of CXCR4. Compared to CXCL12 alone, the CXCL12•HMGB1 heterodimer is more efficient mediating cell migration without inducing CXCR4 internalization in-vitro and in-vivo. In addition, the heterodimer has a potentiating effect on ERK activation and calcium rise (Cecchinato et al., 2016a). The synergism results from the activation of both G protein and β-arrestins-mediated signalling pathways to sustain chemotaxis and β-arrestin2 dependent retention of CXCR4 on the cell surface (D'Agostino et al., 2020). The heterocomplex acts therefore as a balanced agonist of CXCR4 with the difference that the β-arrestin isoforms 1 and 2 are triggered differently, when CXCL12 alone or the heterocomplex is bound to CXCR4 (D'Agostino et al., 2020). This suggests the recruitment of different molecules determining the activation of CXCR4 downstream axis. The association of CXCR4's hyperactivity and surface preservation with complex formation between CXCL12 and HMGB1 suggests a pro-tumorigenic activity of the heterocomplex, especially in the context of inflammation-related cancers (Guo et al., 2016). Extracellular HMGB1 binds to specific partners and receptors in a redox-dependent manner. It was shown that CXCL12•HMGB1 is formed, when HMGB1's conserved cysteines are fully reduced to thiols (Schiraldi et al., 2012). However, the structural information about the chemokine•alarmin heterocomplex is scarce leading to a limited comprehension of its synergistic mechanism as well as redox-selectivity of CXCL12 in binding to HMGB1. One hypothesis behind the potentiating effect of the heterocomplex is that frHMGB1 operates as a cargo of two CXCL12 molecules that activate a pair of CXCR4 receptors promoting thereby CXCR4 dimerization (Figure 1.17 A and B, Fassi et al., 2019). However, the structural illustration does not take into account how CXCL12 for example could discriminate the different redox forms of HMGB1. Moreover, it is not clear, whether the heterocomplex induces different conformational changes of CXCR4 homodimers compared to CXCL12, which could explain the differential receptor signalling including phosphorylation patterns and recruitment of additional molecules. Tumour cells may benefit from the synergism of CXCL12•frHMGB1 in sustaining the hyperactivity of CXCR4. In this sense, we describe the heterocomplex as a pathological one.
Thus, given the pathological role of the CXCL12•frHMGB1 in inflammatory disorders and possibly also in cancer, targeting of the heterocomplex appears to be an appealing strategy in dampening oncogenesis mediated by CXCR4. In fact, the identification of Diflunisal (DFL,
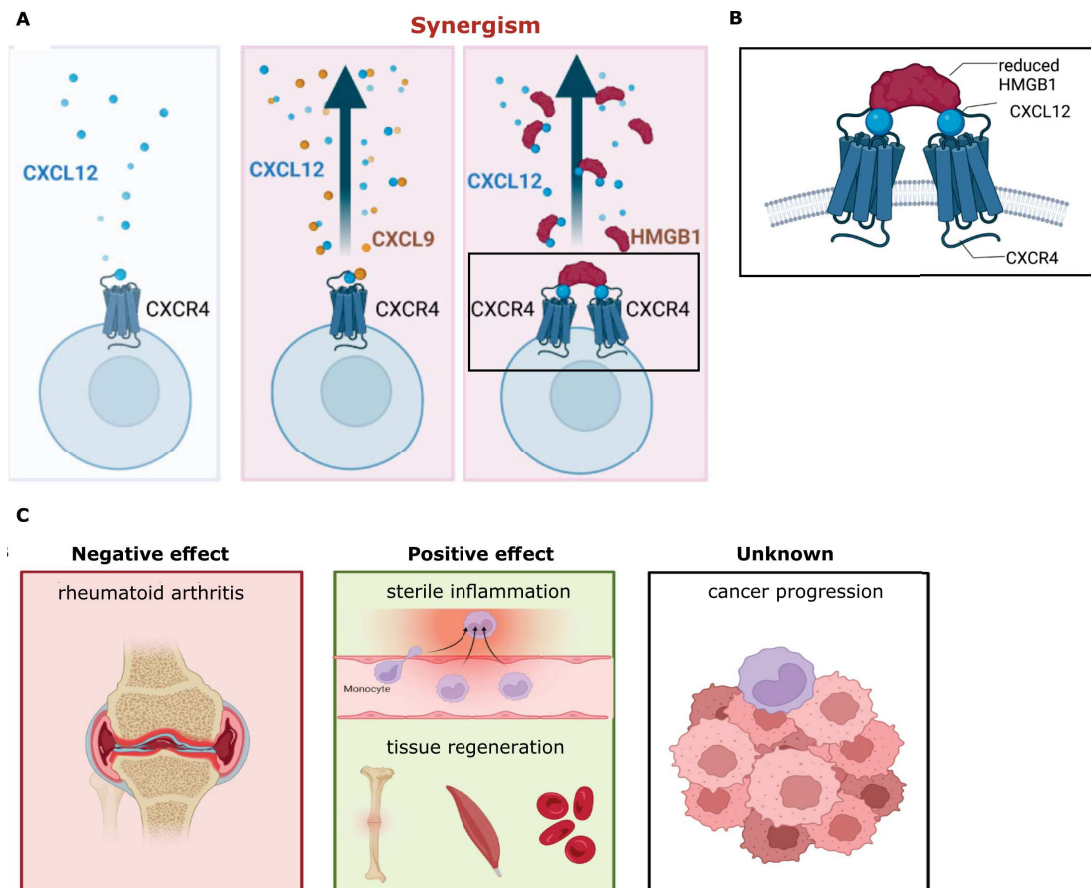
**Figure 1.17:** *The CXCL12•HMGB1 heterocomplex. Figure adapted in agreement with the terms of the Creative Commons Attribution License (CC BY) from Cecchinato et al., 2023. (A) Depiction of functional synergism by CXCL12 heteromers. CXCL12•CXCL9 and CXCL12•frHMGB1 trigger enhanced signalling through CXCR4. (B) Representation of the CXCL12 • HMGB1 heterocomplex that may explain the synergism. (C) The functional activity of the CXCL12•frHMGB1 heterocomplex in rheumatoid arithritis, tissue regeneration and possible effect on cancer.*

Figure 1.18), an aspirin-like anti-inflammatory drug, exhibited potent inhibition of the CXCR4-mediated chemotaxis by targeting the CXCL12•frHMGB1 heterocomplex (De Leo et al., 2019). Structural validation by NMR spectroscopy and biophysical assays reveal that DFL binds directly both HMGB1 and CXCL12 and is capable of disrupting the CXCL12•frHMGB1 heterodimer when added in stoichiometric excess (De Leo et al., 2019). Diflunisal represents therefore the first molecular probe that targets the CXCL12•frHMGB1 heterocomplex. Glycyrrhizin, a previously known HMGB1 inhibitor, has been later found to bind also CXCL12 and to inhibit similarly to DFL inflammatory cell migration in vivo (Mollica et al., 2007). Pamoic acid (PAM, Figure 1.18), a salicylate commonly used in drug formulations, has been identified in-vitro as another CXCL12•frHMGB1 dependent chemotaxis inhibitor (De Leo et al., 2022). Importantly, PAM delivered by aerosol in vivo to mice with P. aeruginosa infection

24

shows no toxicity in the airways and can ameliorate neutrophilic inflammation and lung damage (De Leo et al., 2022). Virtual screening (VS) delivered 5,5'-methylenedi-2,3-cresotic acid (MCA, Figure 1.18 C) as best small molecule inhibitor of in vitro chemotaxis mediated by the CXCL12•frHMGB1 complex with an with the half maximal inhibitory concentration (IC$_{50}$) value in the sub-nanomolar range (De Leo et al., 2022). Moreover, recent computational dockings identified the first peptide (HBP08) binding HMGB1 and selectively inhibiting the cell migration mediated by the CXCL12•frHMGB1 heterocomplex with an IC$_{50}$ value of 50 $\mu$M and highest affinity (K$_D$ of $0.8 \pm 0.4\mu$M) (Sgrignani et al., 2021).



Diflunisal (DFL)          Pamoic acid (PAM)          5,5-Methylenedi-2,3- cresotic acid (MCA)
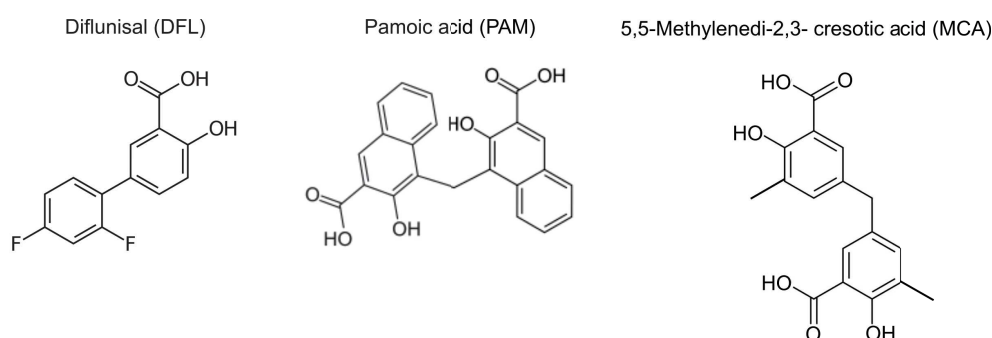
**Figure 1.18:** *Small molecule inhibitors of the CXCL12 • HMGB1 heterocomplex. Chemical structures of (A) Diflunisal (DFL), (B) Pamoic acid (PAM) and (C) 5'5-Methylenedi-3,4-cresotic acid (MCA).*

Collectively, these results show that pharmacological agents interfering with the CXCL12•HMGB1 complex inhibit efficiently CXCR4-induced chemotaxis in-vitro. Thus, targeting the heterophilic binding surface of CXCL12 and HMGB1 has proven to be a promising strategy for the identification and design of novel drug candidates to treat severe chronic inflammatory conditions. However, the development of optimized protein-protein interaction antagonists, either peptidomimetics or small organic molecules, is hampered by the fact that the three-dimensional structure of the CXCL12•frHMGB1 complex is unknown. Current high-resolution descriptions of this interaction are still elusive, thus making structure-based drug discovery extremely challenging. So far, researchers coped with this problem by targeting the isolated component of the heterocomplex. Research, including the present study, seeks to establish a structurally validated model of the CXCL12•frHMGB1 complex through experimental means. This work will therefore facilitate and advance the design of more potent and effective pharmacological drugs by providing an experimental template of the CXCL12•frHMGB1 complex for rational design. However, numerous obstacles, both at the structural and technical levels, arise when examining the complicated nature of CXCL12 and frHMGB1.

## 1.8.2 High Mobility Group Box 1 (HMGB1)

HMGB1 belongs to the group of nuclear chaperones and alarmins capable of performing multitasking activities based on its cellular location: inside the nucleus, it acts as a DNA modulator

and repair molecule; in the cytosol or mitochondria, it modulates autophagy and apoptosis; on the cell surface of neurons, it promotes axon sprouting and neurite outgrowth (Vénéreau, Ceriotti, and Bianchi, 2015). Stressed cells and malign tumours release HMGB1 in massive amounts to the extracellular milieu, where it activates different receptors depending on the redox-state of its highly conserved cysteine residues C23, C45 and C106. The cysteines can be either fully reduced to thiols or completely oxidized to sulphonyl groups or the intermediate stage is, when the cysteines C23 and C45 form an intramolecular disulphide bond. The functionally active redox states of HMGB1 are the all-thiol and disulphide form. The latter is formed under oxidative conditions. Fully reduced HMGB1 (frHMGB1) triggers the receptor for advanced glycation end products (RAGE) to stimulate autophagy and CXCL12 secretion, while the disulphide HMGB1 (dsHMGB1) promotes the production of inflammatory cytokines and chemokines via Toll-like receptor 4 (TLR4) (Yu et al., 2006c). Both forms are not mutually exclusive and can interconvert depending on the presence of reactive oxygen species (ROS) and oxidizing condition in the extracellular milieu. Both processes of HMGB1-signalling appear to be sequentially during the development of inflammation and its resolution. It is therefore not trivial to assess a beneficial or detrimental role to HMGB1's redox forms, as they are produced at the biological needs of the cell. frHMGB1 binds to CXCL12 and exerts chemoattractant activities through CXCR4, while dsHMGB1 loses the ability to engage with CXCL12 to stimulate CXCR4-mediated chemotaxis (Venereau et al., 2013a,Venereau et al., 2012). Instead, dsHMGB1 interacts with the lymphocyte antigen (Xu et al., 2011) (MD2)-TLR4 complex and stimulates activation of NF-kB, inducing the secretion of multiple proinflammatory cytokines and chemokines (Yu et al., 2006c). The oxidizing environment eventually induces the latest stage of oxidation of HMGB1 to the sulphonyl form, which no longer promotes chemoattractant and proinflammatory activities. dsHMGB1 binds to TLR4 and leads to malignant transformation by generating chronic inflammation. From this aspect, HMGB1 is a typical oncogene, however, it can also exert anti-tumor function via the immune system through immunogenic cell death (ICD)(Galluzzi et al., 2017). Extracellular HMGB1 is implicated in many tasks as DAMP molecule and fine-tunes its functions through redox-selective binding to different receptors and interaction partners in a highly sensitive manner.

Structurally, HMGB1 is a 215-amino acid protein that contains three main functional domains: two L-shaped DNA binding tandem domains HMG-Box A (aa 9–79) and HMG-Box B (aa 89-163) joined by a basic linker and an intrinsically disordered C-terminal region (aa 186–215) composed of consecutive aspartic and glutamic acid (D/E) repeats. Box A contains a pair of cysteines (Cys23 and Cys45), that can form a disulfide bond under oxidative conditions, while Box B has only one unpaired cysteine (Cys106) (Li et al., 2004, Najima et al., 2005, Knapp et al., 2004a, Thomas and Travers, 2001). As mentioned before, the redox state of HMGB1's conserved cysteines determine its function as chemoattractant or inflammaotry cytokine with frHMGB1 and dsHMGB1 displaying specific binding regions for interaction partners to undergo chemotaxis or cytokine-inducing activities, respectively (Janko et al., 2014). The schematic representation in Figure 1.20 illustrates the diverse biological activities of HMGB1's functional domains. Focusing on the extracellular activities, binding of Box B domain is responsible for

**High Mobility Group Box 1 (HMGB1)**
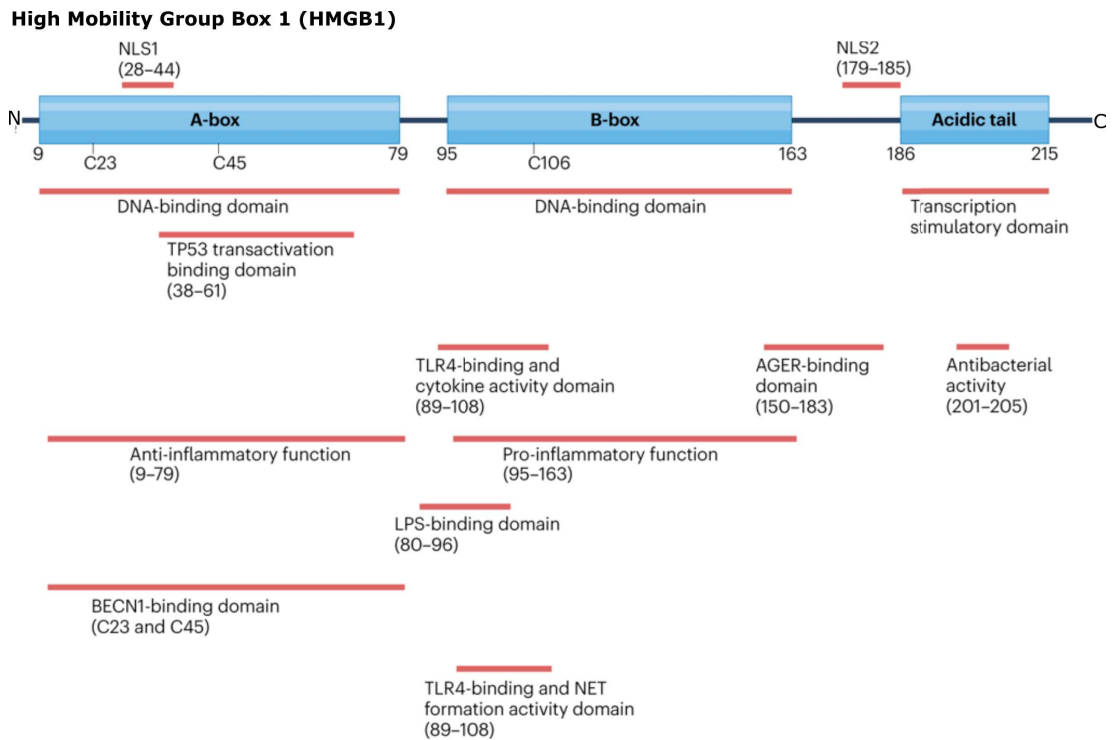
**Figure 1.19:** *Schematic representation of functional domains of human High Mobility Group Box 1 (HMGB1). Figure reused and adapted in agreement with the terms of the Creative Commons Attribution License (CC BY) from Tang et al., 2023. HMGB1 is mainly composed of two DNA-binding domains (BoxA and BoxB) and a negatively charged C terminus (acidic tail). HMGB1 contains three redox-sensitive cysteine residues (C23, C45 and C106). Depending on its subcellular location, HMGB1 can act as DNA chaperone in the nucleus maintaining chromosme structure and function or in the extracellular environment operating as a damage-associated molecular pattern or danger signal under conditions of stress to mediate immune responses by interacting with various receptors and binding partners.*

the inflammatory state presenting specific recognition sites for receptors TLR4 (aa 150-183) and RAGE (aa 150 and 183) (Li et al., 2003), whereas Box A works as an antagonist of Box B (Tang et al., 2010). The N-terminus of HMGB1 (6–12 aa) binds to heparin, which reduces the affinity of HMGB1 for its receptors inhibiting thereby the proinflammatory activity (Li et al., 2015, Ling et al., 2011). Importantly, the anti-bacterial action of HMGB1 is mediated by the C-terminal acidic region (aa 201-205), the reason for which it is difficult to obtain decent amounts of recombinant HMGB1 from E-coli expression systems (Gong et al., 2009).

HMGB1 contains intrinsically disordered regions (IDRs), the interdomain linker and acidic C-terminus composed of aspartate (D) or glutamate (E) residues. IDRs in general represent a large fraction of the proteome across species. Although they lack a defined three-dimensional structure, they still have functional abilities. The biological relevance of IDRs was first described in gene-regulatory proteins, some of which contain negatively charged D/E repeats similar to the acidic C-terminal segment of HMGB1 (Ueshima, Nagata, and Okuwaki, 2017, Watson, Stott, and Thomas, 2007, Wiebe, Nowling, and Rizzino, 2003). In fact, the acidic IDR

of HMGB1 plays a central role in the nucleolar function, in which it regulates DNA-binding to the basic charged HMG boxes through charge shielding (Ueda et al., 2004, Wang et al., 2007). As a result, HMGB1 does not adopt a single structure but an ensemble of interconvertible conformations, in which the binding mode of the acidic IDR to the HMG boxes can vary in degrees from a bound to a free state. Herein, the conformational space of HMGB1 is restricted to a closed and open conformation, in which the acidic IDR is bound to the HMG domains like a sandwich or completely free floating outside the HMG boxes, respectively (Figure 1.20) (Stott et al., 2010).
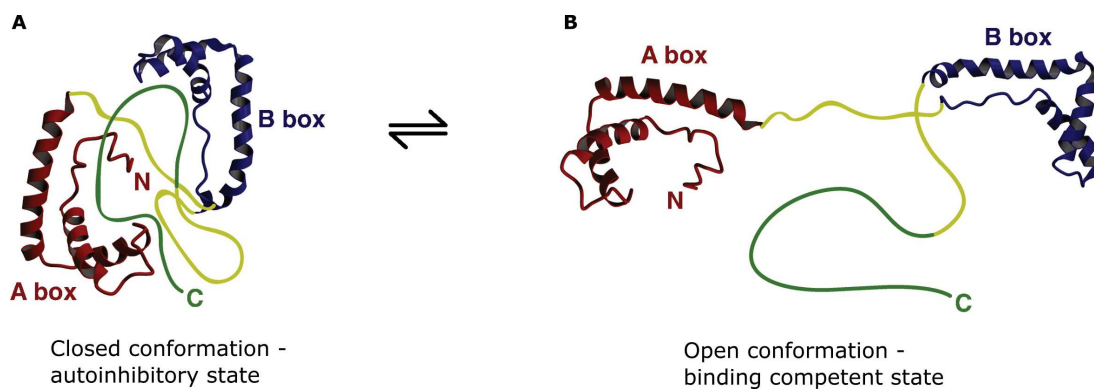


**Figure 1.20:** *Conformational space of HMGB1 between closed collapsed and open state.* *Figure resused according to the Creative Commons Attribution License (CC BY) from source Stott et al., 2010.* *(A) Closed collapsed state of HMGB1 inhibits binding of other charged molecules, in particular DNA, to the basic charged HMG tandem domains (autoinhibition state). (C) The open conformation is the uninhibited state of HMGB1 able to bind DNA at BoxA and BoxB and the acidic IDR free to interact with other binding partners.*

The low sequence variability of the acidic IDR renders its binding unspecific, transient and charge driven offering thereby many binding opportunities for HMGB1. These typical IDR characteristics can be retained to a certain degree in complex with other interaction partners, a phenomenon defined as *fuzzy*. The term *fuzzy* stems from the *fuzzy logic* of variables assuming values between true (=1) and false (=0) defining in this case a spectrum of structural disorder from entirely folded to unfolded in protein complexes (Tompa and Fuxreiter, 2008). The acidic IDR creates in HMGB1 a large number of microstates by means of intramolecular interactions with linker and DNA-binding domains and can be in this sense categorized as fuzzy. Fuzzy regions usually drive the formation of biomolecular condensates, which are membrane-less assemblies comprising proteins or nucleic acids mediated through phase separation. Recent studies show that disease -associated mutations replacing the acidic IDR of HMGB1 with positively charged residues alter the phase separation of HMGB1 leading to promoted partitioning of HMGB1 in the nucleus (Mensah et al., 2023). The acidic IDR plays therefore a central role in the regulating liquid-liquid phase separation of HMGB1 in the cell and consequently its function. In the light of emerging studies acknowledging the structural multiplicity of proteins caused by IDRs, HMGB1 represents a prototypical example of a *fuzzy* protein. The molecular interactions generated by HMGB1's acidic IDR elucidate the complexity

of DNA-binding regulation, but are poorly investigated in the context of complex formation with other ligands, such as CXCL12. The current model of the CXCL12•frHMGB1 heterocomplex describes the heterophilic interactions as well-defined, ordinary protein-protein binding interfaces involving exclusively the structured domains of frHMGB1 (Fassi et al., 2019). According to the proposed model, the heterocomplex consists of two CXCL12 monomers binding to the concave pockets of Box A and B, respectively to activate two CXCR4 molecules (Cecchinato et al., 2023). This scenario implies that the enhanced cell migration and retention of CXCR4 on the cell surface results from HMGB1 offering two CXCL12 monomers to a CXCR4 homodimer. However, this model proposes an oversimplified version of interaction that is based on CXCL12-binding to the individual structured domains and does not comply with the multivalent, redox-selective interferences of HMGB1 and omits the monomer/dimer specific binding of CXCL12 to CXCR4. Thus, interaction studies by NMR showing CXCL12-binding to Box A and Box B separately (Schiraldi et al., 2012) are not sufficient to provide a comprehensive picture that includes the fuzzy interactions of HMGB1. Instead, more biophysical techniques are necessary to shed light on the functional complexity of CXCL12 and HMGB1 from a structural perspective. In conclusion, the current heterodimer model bypasses the structural complexity and conformational dynamics of HMGB1 by neglecting the influence of its IDRs, in particular the acidic C-terminal tail. Thus, the model of the heterocomplex may oversimplify the mechanism of synergism, as it lacks functional relevant interactions between HMGB1's IDRs and CXCL12 driving hetero-association and binding to CXCR4.

## 1.9   Aim of thesis

The synergistic actions mediated by the CXCL12•HMGB1 heterodimer trigger pro-inflammatory and tumorigenic activities through exclusively CXCR4. The HMGB1/CXCL12/CXCR4 axis is thus a valuable target for the development of selective anti-inflammatory and anti-cancer compounds.

**The overarching aim of this thesis is to provide a three-dimensional atomistic model of the CXCL12•frHMGB1 complex to overcome simplistic descriptions of this physio-pathologically relevant heterocomplex.** We consider the inherent dynamics of extracellular HMGB1 due to its intrinsically disordered acidic C-terminus to be important for complex formation with CXCL12, the reason for which we include the acidic IDR in our structural studies. Importantly, we investigate the heterodimer binding surface and stoichiometry by taken into account the two oligomeric states of CXCL12. In combination with structural analysis, we aim to demonstrate the importance of the HMGB1 acidic IDR in mediating CXCL12 binding to CXCR4 on a cellular level.

We thus adopted a dissecting approach using a tail-less HMGB1 analog with truncated acidic IDR (HMGB1-TL), a synthetic and recombinant acidic IDR peptide (Ac-pep and Ac-pep$_{rec}$) and HMGB1 full length (Figure 1.21) to study the interactions with CXCL12 including its monomeric form. In our work, we utilized CXCL12-LM (Figure 1.15 C and Figure 1.21 A) to discriminate heterophilic interactions of CXCL12 with conformational changes in the structural studies. We chose this mutant, since it is effective in stabilizing the monomeric state of CXCL12. The disulphide bond of variant L55C I58C keeps CXCL12 monomer in a closed conformation, where the dimerization along the $\beta_1$ sheet and $\alpha$-helix with another monomer is prevented through steric blockade. The characterization of the heteromeric interactions between CXCL12 and HMGB1 poses technical challenges as well. The application of crystallographic-based methods is limited to static ligand-receptor complexes and require proteins that primarily consist of structured and ordered domains producing sufficient electron density. Thus, X-ray diffraction cannot be utilized to determine the structure of the CXCL12•HMGB1 heterodimer, as the disordered regions of HMGB1 hamper its crystallization and the small size of the heterodimer does not generate detectable electron density to give interpretable Cryo-electron microscopy maps. We adopted therefore an integrative structural approach that consists of a set of in-solution methods to describe the heteromeric interaction in terms of binding interface, affinity, size, stoichiometry and shape. We utilized chemical shift perturbations of two-dimensional Nuclear Magnetic Resonance (NMR) experiments to map the interaction surface on CXCL12 and HMGB1, respectively and estimate binding affinities by Isothermal titration calorimetry (ITC) and microscale thermophoresis (MST). We combine analytical ultracentrifugation (AUC) – sedimentation experiments with Small Angle X-ray scattering (SAXS) to determine the complex stoichiometry, size and shape. NMR driven computational dockings in combination with SAXS analysis are utilized to generate a low-resolution three-dimensional structures of the

CXCL12•HMGB1 heterodimer. The output of the structural studies is validated in cellular assays to demonstrate the validity of our model by including the receptor CXCR4. In collaboration with the research group of Prof. Marco Bianchi, proximity ligation assays (PLA) on AB1 mesothelioma cells overexpressing CXCR4 are utilized to detect interactions involving CXCL12, HMGB1 and CXCR4.

Overall, results emerging from this thesis are expected to represent an important step forward in the characterization of heterophilic chemokine interactions. This work provides novel insights into heterophilic chemokine interactions by introducing fuzzy interactions of atypical chemokines. The adopted approaches elucidate the manifestation of fuzziness in chemokine heterocomplexes and paves a new avenue for therapeutic targeting of fuzzy interactions.
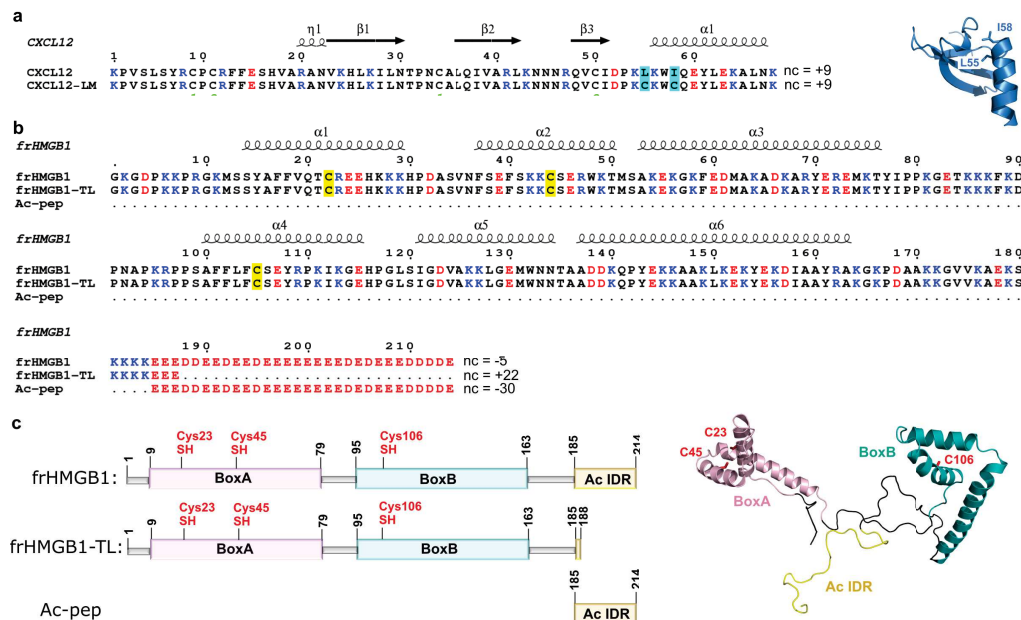


**Figure 1.21:** *Strategy to dissect the heterophilic interactions between CXCL12 and functional domains of HMGB1. Figure reused according to the Creative Commons Attribution License (CC By 4.0) terms, from Mantonico et al., 2024. Sequence alignment performed with ENDscript server (Robert and Gouet, 2014) and structure of (A) CXCL12 and CXCL12-LM and of (B) HMGB1, HMGB1-TL and Ac-pep. (C) Schematic representation of domains and redox sensitive cysteine residues with the structure of full-length frHMGB1.*

# Chapter 2

# The CXCL12-HMGB1 Binding Interface studied by NMR

## 2.1 Introduction

Chemokine CXCL12 and the fully-reduced (fr) HMGB1 form a heterocomplex that elicits synergistic signalling through CXCR4. The unavailable experimental structure of the heterocomplex led to an oversimplified depiction of its three-dimensional atomic structure, as the underlying heterophilic interactions of the complex lack the structural information of HMGB1's IDRs. Previous examination of the CXCL12•frHMGB1 binding interface by NMR solely relies on chemical shift mappings of CXCL12 and the single domains BoxA and BoxB of HMGB1 (Schiraldi et al., 2012). However, several studies demonstrated that the acidic IDR of HMGB1 has a functional role both in the nucleus and extracellular environment, where it operates as a DNA-binding modulator to the basic charged HMG boxes (Cato et al., 2008) and exerts anti-bacterial activity (Gong et al., 2009), respectively. On a structural level, the acidic IDR undergoes multivalent interactions with the interdomain linker and HMG tandem domains generating thereby multiple coexisting dynamic conformations of HMGB1 (Stott et al., 2010). Therefore, the resulting structural multiplicity of HMGB1 challenges the traditional lock-key principle in the context of hetero-association with other binding partners, as it can form multiple heterocomplexes instead of a unique heterodimer (Sharma et al., 2015). The "fuzzy" nature of frHMGB1 has to be addressed in the heterophilic interactions with CXCL12 with appropriate approaches in applying NMR spectroscopy.

We opted for a dissecting strategy to characterize the binding between CXCL12 and the different functional domains of full-length frHMGB1 by NMR titration experiments (Figure 1.21). We use the synthetic and recombinant acidic IDR peptide (Ac-pep and Ac-pep$_{rec}$) and tailless HMGB1 construct devoid of the acidic IDR (frHMGB1-TL) in comparative NMR titrations of full-length frHMGB1 with CXCL12 and "locked" monomeric CXCL12-LM. We utilize NMR titration experiments that generally serve to obtain the interaction surface of the protein upon ligand-binding, as ligand-interaction induces spectral perturbations of the protein's amino acid resonance frequencies. We acquire a Heteronuclear Single Quantum Coherence (HSQC) spectrum that correlates proton ($^1$H) and nitrogen ($^{15}$N) atoms of the protein's peptide bonds

as a finger print spectrum of the protein, where each peak corresponds to an amino acid residue of the protein. At each titration point, a $^1$H-$^{15}$N HSQC spectrum of the protein is recorded to analyse spectral perturbations in terms of peak displacement and intensity reduction upon ligand-binding. The requirement for acquiring a 2D $^1$H-$^{15}$N HSQC spectrum of the protein are NMR-active nuclei. While protons are naturally in abundance NMR-active, nitrogen atoms need to be enriched with $^{15}$N isotope to be detected by NMR. The quantification of peak displacement, termed as chemical shift perturbation (CSP), and intensity change as the ratio of intensities of protein bound (I) and protein free ($I_0$), allows for inspecting the key regions of the protein involved in ligand binding. We performed NMR titrations on $^{15}$N enriched CXCL12 and CXCL12-LM with added amounts of Ac-peps, frHMGB1-TL or frHMGB1 and vice versa to describe the binding interface of the CXCL12•frHMGB1 heterocomplex. Residues exhibiting spectral perturbations greater than the average (AVG) +/- standard deviation (SD) are involved in binding and mapped on the structures.

## 2.2   Results

### 2.2.1   The HMGB1 acidic IDR takes part in the formation of the HMGB1-CXCL12 heterocomplex

***Titrations of*** $^{15}$***N CXCL12 and*** $^{15}$***N CXCL12-LM with Ac-pep, frHMGB1-TL, frHMGB1***

As CXCL12 presents basic charged areas, we expected that electrostatic interactions between the acidic IDR and CXCL12 are important in complex formation with frHMGB1. In fact, the titration of Ac-pep to $^{15}$N CXCL12 induced a drastic change of the corresponding $^1$H-$^{15}$N HSQC spectrum (Figure 2.1 A), displaying substantial chemical shift perturbations (CSPs, in the 0.2-0.6 ppm range) and intensity reduction over all the peaks of $^{15}$N CXCL12 (Figure 2.1 A-C). Peaks exhibited extensive line-broadening or disappeared beyond the detection of sub-stoichiometric added amounts of Ac-pep, but reappeared at 1:1 stoichiometry (Figure 2.2 A). The dissociation constant ($K_D$) determined via line-shape analysis using software TITAN (Waudby et al., 2016) was in the sub-micromolar range ($K_D = 0.2 \pm 0.1\,\mu$M), as shown in Figure 2.2 B. CXCL12 residues with the highest CSPs were R12, H17, V18, R20, V23, K24, H25, A40, R41, N45, W47, L66, N67 (Figure 2.1 B). Of note, the amide resonances of V23, K24, and H25, L66, N67 are located on the homodimerization interface of CXCL12 (Figure 1.15). Besides direct ligand-binding, peak perturbations of NMR-HSQC spectra may also arise from structural changes upon binding (allosteric effects), conformational rearrangements as well as oligomerization. CXCL12 is known to homodimerize, therefore spectral perturbations at the known dimerization surface of CXCL12 might stem also from changes in the monomer-dimer equilibrium of CXCL12 (Veldkamp, 2005).
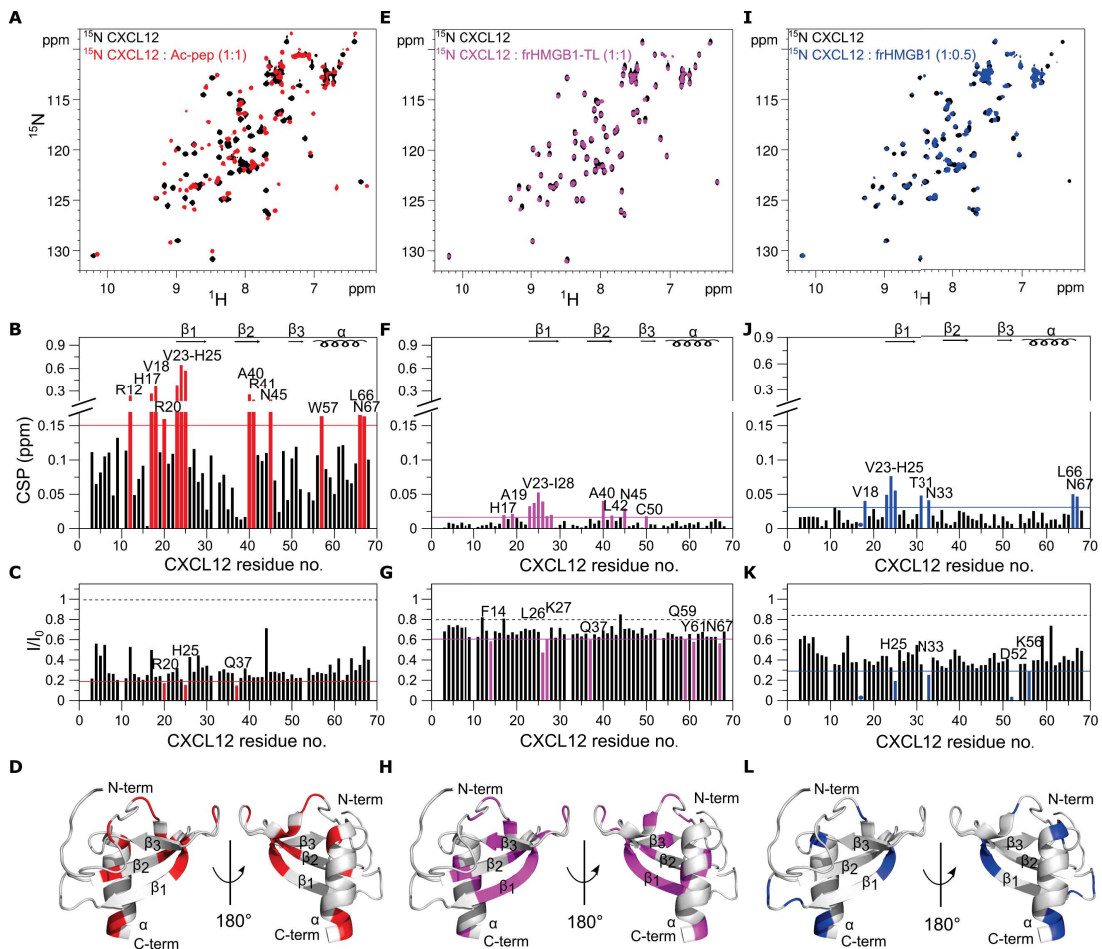
**Figure 2.1:** *HMGB1's acidic IDR and tandem domains target the dimerization surface of CXCL12.*
*(A, E, I) Superposition of HSQC spectra of CXCL12 free (0.1 mM, black) and CXCL12 bound to Ac-pep (red), frHMGB1-TL (magenta), HMGB1 (blue). Bar plots show CSP and $I/I_0$ ratio of CXCL12 upon binding to Ac-pep (B and C), frHMGB1-TL (F and G), frHMGB1 (J and K); highlighted and labelled are CXCL12 residues exhibiting* CSP > AVG + SD$_{corr}$ *and* $I/I_0$ < AVG − SD *beyond the continuous line, dashed black line in bar plots of $I_0$ ratio indicates the peak intensity decrease due to the titration dilution effect. Dots in the CSP plots represent disappearing residues. Interaction surface mapping on the structure of CXCL12, represented as grey cartoon (PDB code: 2kee) upon binding to (D) Ac-pep (red areas), (H) frHMGB1-TL (magenta areas), (L) frHMGB1 (blue areas).*

Thus, to simplify spectral analysis and to distinguish CSPs due to direct interactions with Ac-pep from those related to changes in the CXCL12 oligomerization state, CXCL12-LM was utilized in NMR titrations (Ziarek et al., 2013b). The spectral perturbations of CXCL12-LM upon Ac-pep addition were similar to those observed with wild type CXCL12, in terms of peak broadening (K$_D$ = 0.2 ± 0.1 μM as measured by software TITAN) and CSPs (Figure 2.3 A-C). The highest CSPs stem from residues V23, K24, H25, suggesting that in fact the N-terminal part of the first β$_1$-strand is a direct interaction surface of Ac-pep. Increasing ionic strength to 150 mM led to exacerbated line broadening for the wild-type protein. One possible explanation may be the emerging effect of the dimer-monomer equilibrium favoured towards the dimeric
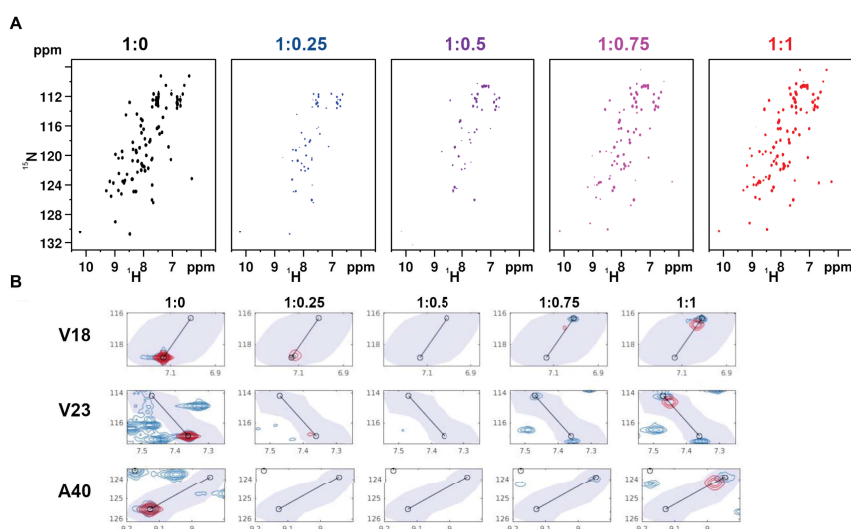
**Figure 2.2:** *Estimation of binding affinity of acidic IDR to CXCL12 by NMR lined shape analysis. (A) HSQC spectra of CXCL12 (0.1 mM, black) at different Ac-pep titration points (colored from blue to red). (B) Line shape analysis of V18, V23 and A40 residues of free and bound CXCL12 to estimate $K_D$ of Ac-pep binding.*

species of CXCL12 at higher ionic strengths.

The $K_D$ estimation from line-shape analysis was hampered due to the low spectral quality of CXCL12. It was possible to estimate a $K_D$ of $\approx 9$ $\mu$M (TITAN) at 150 mM NaCl for CXCL12-LM upon binding to Ac-pep, as the line-broadening effect of CXCL12-LM upon titration with Ac-pep was less pronounced. NMR titrations of $^{15}$N CXCL12 and $^{15}$N CXCL12-LM with Ac-pep demonstrate direct binding of HMGB1's acidic IDR to CXCL12. Conversely, the addition of frHMGB1-TL to both $^{15}$N CXCL12 (Figure 2.1 E-G) and $^{15}$N CXCL12-LM (Figure 2.3 E-G) induced minor CSPs (in the 0.02-0.06 ppm range). Small peak displacement is typically observed for chemokine heterocomplexation and are indicative for interactions occurring in the intermediate exchange regime on the NMR chemical shift timescale (Eckardt et al., 2020a). The highest displacement and peak intensity reduction are mainly localized on the dimerization surface of CXCL12 and CXCL12-LM upon binding to frHMGB1-TL (Figure 2.1 E-H; Figure 2.3 E-H). Interestingly, residues mostly affected by the interaction with HMGB1-TL in part coincided with the ones affected by Ac-pep (V23-H25, A40, N45), implying that both the acidic IDR and the HMG tandem domain are potentially able to engage the same CXCL12 surface. Comparison of CSP profiles of $^{15}$N CXCL12 and $^{15}$N CXCL12-LM upon addition of either Ac-pep and HMGB1-TL with the one obtained from titrations with full-length frHMGB1 were all similar, with residues located on the $\beta_1$-strand and on the $\alpha$-helix displaying the highest CSPs (Figure 2.1 B, F, J; Figure 2.3 B, F, J). However, the CSPs induced by full-length frHMGB1 were
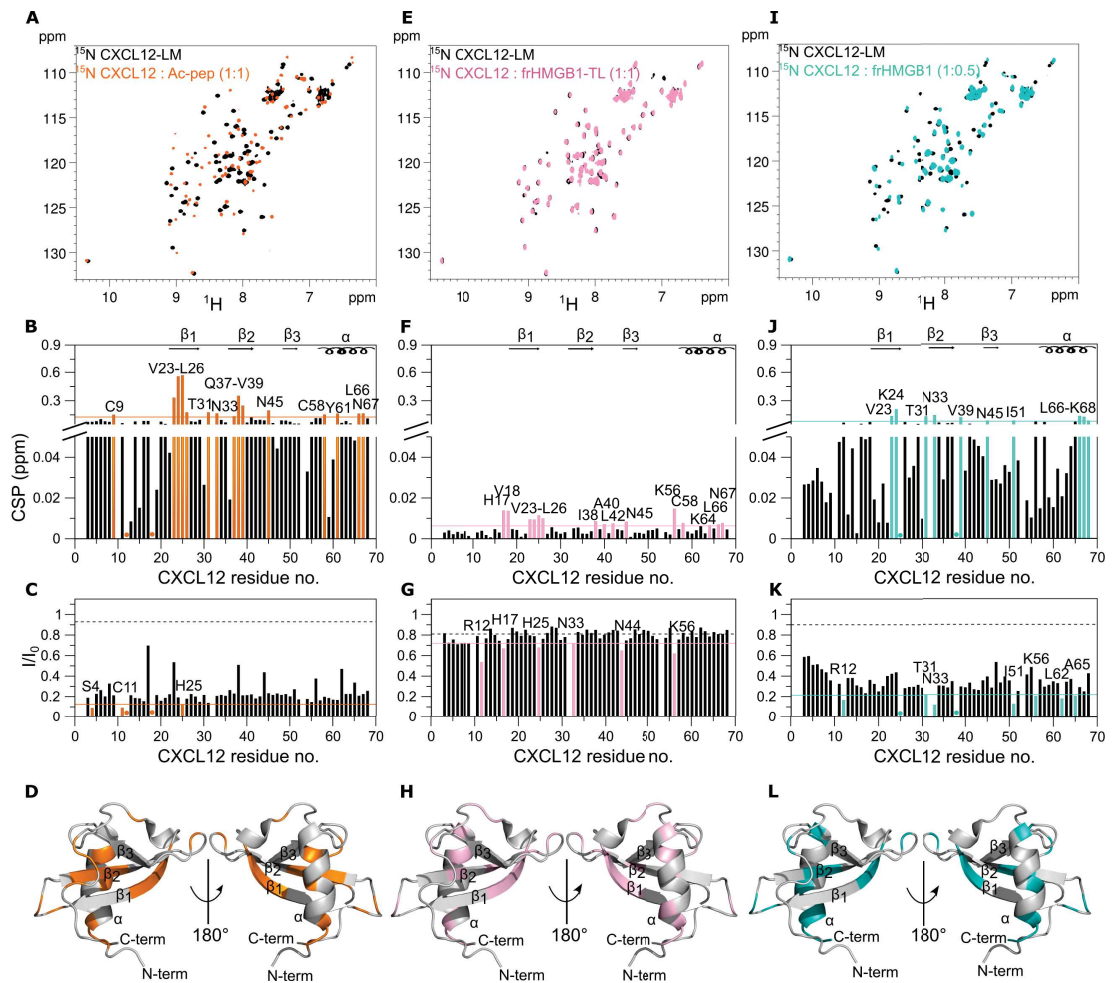
**Figure 2.3:** *The interaction of CXCL12-LM with Ac-pep, HMGB1-TL and HMGB1 is similar to CXCL12. (A, D, G) Superimposition of $^1$-$^{15}$N HSQC spectra of CXCL12-LM free (0.1 mM, black) and CXCL12-LM bound to Ac-pep (orange), HMGB1-TL (salmon), HMGB1 (cyan). Bar plots represent CSP (B, E, H) and $I/I_0$ (C, G, K) of CXCL12-LM upon binding to Ac-pep (B, C), frHMGB1-TL (F, G), frHMGB1 (J, K); highlighted and labelled are CXCL12 residues exhibiting $CSP > AVG+SD_{corr}$ and $I/I_0 < AVG-SD$ beyond the continuous line, dashed black line in bar plots of $I_0$ ratio indicates the peak intensity decrease due to the titration dilution effect. Dots in the CSP plots represent disappearing residues. Interaction surface mapping on the structure of CXCL12, represented as grey cartoon (PDB code: 2n55) upon binding to (D) Ac-pep (orange areas), (H) frHMGB1-TL (salmon areas), (L) frHMGB1 (cyan areas).*

ten times smaller than the ones generated by Ac-pep, but larger as compared to frHMGB1-TL. Moreover, the line broadening effects upon HMGB1 addition were much more pronounced as compared to frHMGB1-TL, suggesting different binding dynamics and affinities for the full-length protein and for its different constructs.

In summary, analysis of signal perturbations of $^{15}$N CXCL12 (or $^{15}$N CXCL12-LM) upon addition of Ac-pep demonstrate the involvement of the acidic IDR of HMGB1 in binding to CXCL12. Moreover, both Ac-pep and frHMGB1-TL target the dimerization surface of CXCL12 suggesting a dynamic interplay between HMG boxes and acidic IDR in binding to CXCL12. Indeed,

the profile of chemical shift perturbations (CSPs) of ^{15}N CXCL12 (or ^{15}N CXCL12-LM) titrated with Ac-pep, frHMGB1-TL and full-length frHMGB1 are similar. The binding effects of Ac-pep on CXCL12 in terms of CSP and $I/I_0$ are more pronounced compared to the ones produced by frHMGB1-TL. Thus, the contribution of the HMG tandem domains to the spectral perturbations of ^{15}N CXCL12 titrated with full-length frHMGB1 are overshadowed by the acidic IDR binding. Collectively, these findings show that the acidic IDR together with the HMG boxes are involved in complex formation with CXCL12. Therefore, both functional domains of HMGB1 need to be included in structural models of the CXCL12•frHMGB1 heterocomplex.

## 2.2.2 Binding between CXCL12 and HMGB1 is governed by fuzzy interactions mediated by the acidic IDR of HMGB1

***Titrations of ^{15}N frHMGB1 and ^{15}N frHMGB1-TL with CXCL12***

The dynamic nature of HMGB1 is governed by multi-valent intramolecular interactions between the acidic IDR and HMG tandem domains (Stott et al., 2010). The emerging conformational equilibria of HMGB1 are modulated through charge interactions affecting the binding between the acidic IDR and HMG boxes. Thus, presence of charged binding partners (e.g. DNA) or increasing salt concentrations perturb the conformational equilibria of HMGB1. Therefore, spectral perturbations (CSPs and $I/I_0$) of ^{15}N HMGB1 in titrations with CXCL12 are more complicated to interpret, as the addition of CXCL12 to ^{15}N frHMGB1 may perturb the intramolecular conformational equilibria of HMGB1 due to intermolecular electrostatic interactions between CXCL12 and acidic IDR. Indeed, reverse titrations of ^{15}N frHMGB1 (and ^{15}N frHMGB1-TL) with CXCL12 confirmed this hypothesis.

HMGB1 amide resonances of spy residues that are reported to interact with the acidic IDR (e.g. T76, W48, I78 on BoxA, and A93, I158, R109 on BoxB) (Knapp et al., 2004b) moved partially towards their NMR frequency in the tailless construct upon addition of CXCL12 (Figure 2.4).
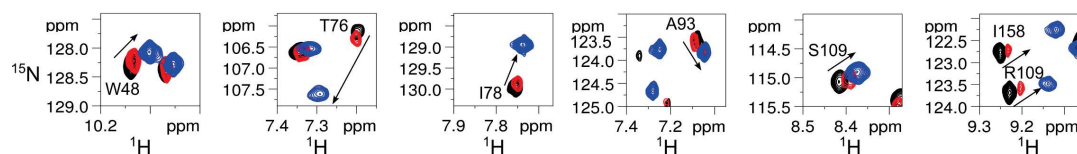


**Figure 2.4:** ***CXCL12 weakens the intra-molecular binding between HMGB1 acidic IDR and boxes.** Spy residues of ^{15}N frHMGB1 free (0.1 mM, black) and bound to CXCL12 added at two equivalents (red), superimposed with the respective residues of frHMGB1-TL (0.1 mM, blue).*

These displacements suggest a weakening of the intramolecular interaction between the acidic IDR and the HMG boxes. The shifts towards HMGB1-TL resonances were relatively small, presumably because CXCL12 only partially competes with frHMGB1 intra-molecular interactions. Competition experiments adding an equimolar amount of Ac-pep to ^{15}N frHMGB1 in complex
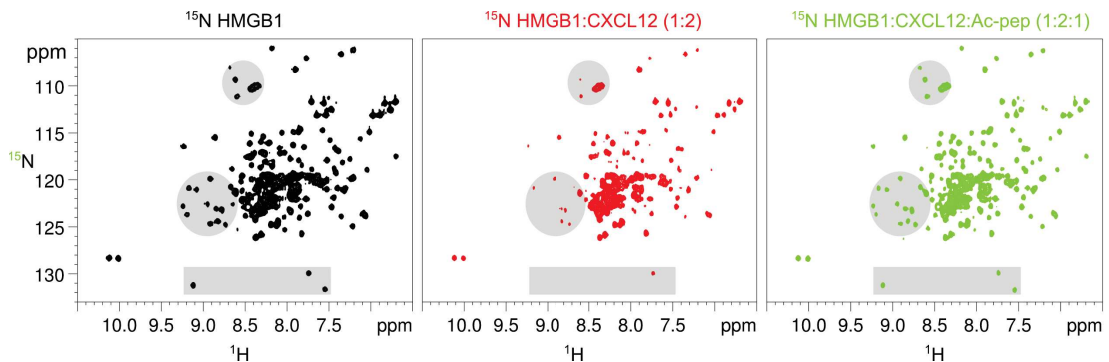
**Figure 2.5:** *The acidic IDR mediates the interaction between CXCL12 and frHMGB1.* *Competition experiment showing HSQC spectra of $^{15}N$ frHMGB1 free (0.1 mM, black), $^{15}N$ frHMGB1:CXCL12 (1:2) (red) and recovered $^{15}N$ frHMGB1 free upon addition of one equivalent of Ac-pep (green).*
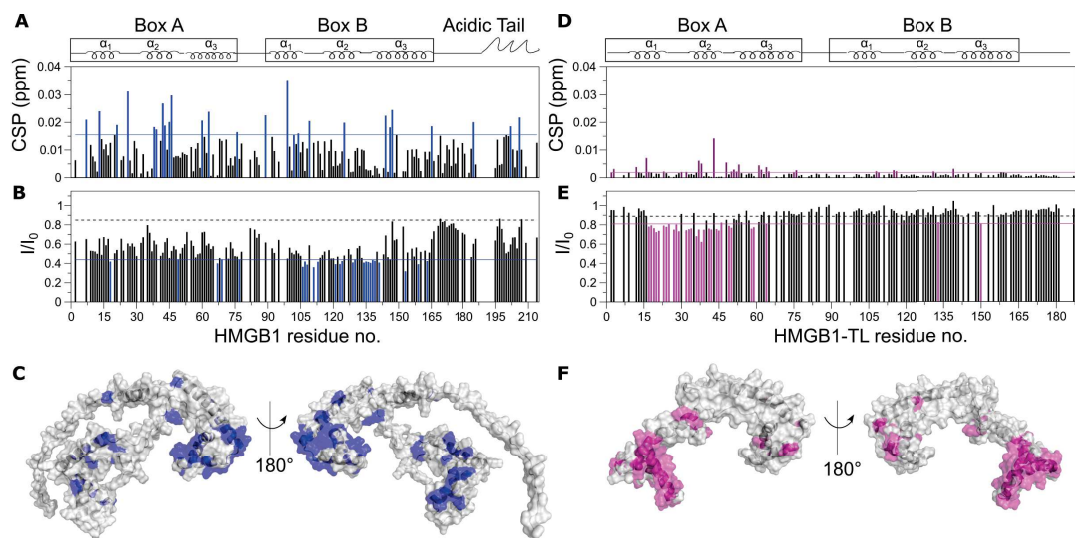


**Figure 2.6:** *CXCL12 binds to fully reduced BoxA with no major involvement of the second domain BoxB.* *Bar plot of (A) CSP and (B) $I/I_0$ of $^{15}N$ frHMGB1 (0.1 mM) titrated with one equivalent of CXCL12. (C) Interaction surface of frHMGB1: residues exhibiting CSP $>$ AVG + SD and $I/I_0 <$ AVG $-$ SD are mapped on the model of HMGB1 (blue on grey surface, Aphafold2 model AF- P63159). Bar plot of (D) CSP and (E) ($I/I_0$) of $^{15}N$ frHMGB1-TL (0.1 mM) titrated with one equivalent of CXCL12. (F) Analogue to frHMGB1 interaction mapping, binding surface of frHMGB1-TL: residues with CSP $>$ AVG + SD and $I/I_0 <$ AVG $-$ SD mapped on the model of HMGB1-TL (magenta on grey surface, PDB code: 2yrq).*

with CXCL12, shown in Figure 2.5, was sufficient to sequester CXCL12 and disrupt the heterocomplex, as $^{15}N$ frHMGB1 resonances reappeared. Hence, this confirms the important contribution of the acidic IDR to heterocomplex formation.

As the CSPs in terms of peak displacement and intensity changes in $^{15}N$ NMR titrations of HMGB1 with CXCL12 are caused by both intra- and inter-molecular interactions, mapping of the spectral perturbations on the HMGB1 structure are difficult to interpret, as they reflect both phenomena (Figure 2.6). Since equimolar concentrations of Ac-pep are sufficient to sequester CXCL12 from HMGB1, we can deduce that the acidic IDR peptide competes with
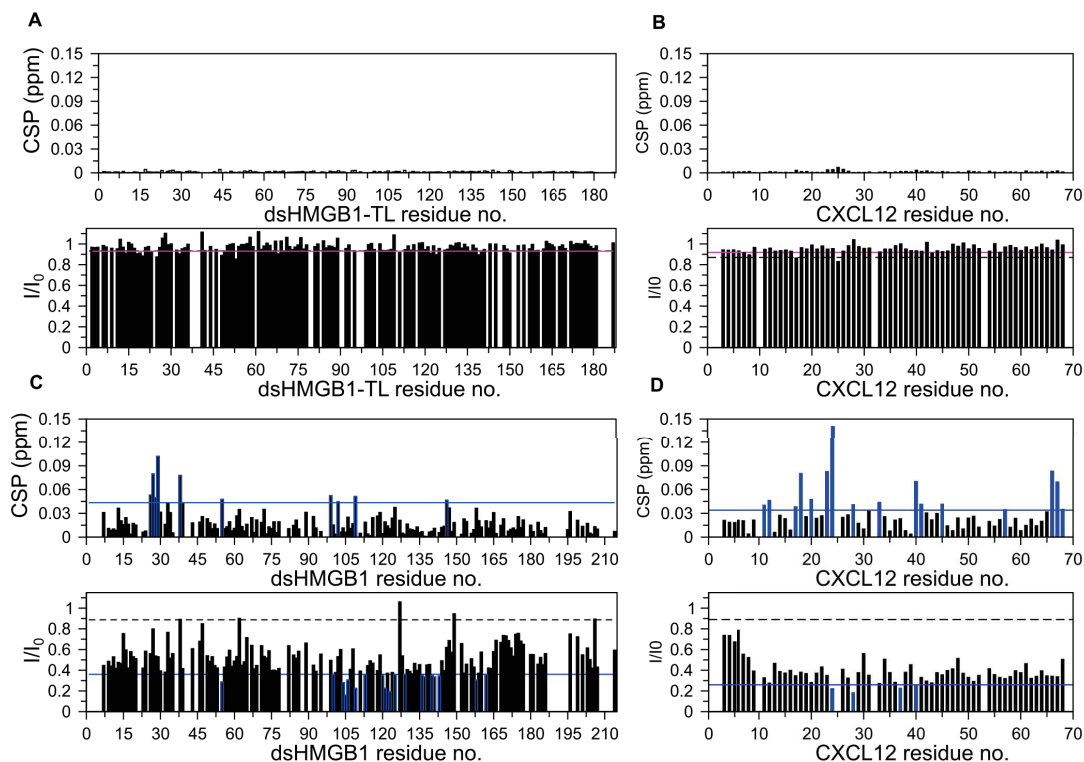
**Figure 2.7:** *CXCL12 interacts with the acidic IDR, but not with oxidized BoxA of dsHMGB1.* *Spectral perturbations in terms of CSP and reduced $I/I_0$ of (A) $^{15}$N dsHMGB1-TL (0.1 mM) titrated with CXCL12 at ratio 1:1 and of (B) $^{15}$N CXCL12 (0.1 mM) tirated with dsHMGB1-TL at ratio 1:1. Spectral perturbations in terms of CSP and reduced $I/I_0$ of (C) $^{15}$N dsHMGB1 (0.1 mM) upon CXCL12 addition at ratio 1:1 and (D) $^{15}$N CXCL12 (0.1 mM) upon addition of dsHMGB1 at equimolar ratio.*

the acidic IDR of HMGB1 for CXCL12 and that the HMG domains weakens the acidic IDR binding to CXCL12. Thus, the observed spectral perturbations of $^{15}$N frHMGB1 upon CXCL12 addition mainly result from the acidic IDR binding to CXCL12 (Figure 2.5). The acidic IDR may thus mask the interactions between CXCL12 and the HMG boxes. Hence, NMR titration experiments were performed with $^{15}$N frHMGB1-TL and CXCL12. The removal of the veiling effect of the acidic IDR resulted in smaller peak displacement and intensity reduction profiles (Figure 2.6 D, E) compared to the ones of the full-length protein (Figure 2.6 A, B). Importantly, the deletion of the acidic IDR brought to light an interaction surface formed by the first HMG box, BoxA, where CXCL12 binds to the first two helices, with no major involvement of BoxB (Figure 2.6 D-F).

In accordance with biological data that demonstrate the ability of CXCL12 to discriminate the thiol and the disulphide form of BoxA of full-length HMGB1, this finding highlights the relevant role of BoxA in the interaction. The preference of CXCL12 for the thiol state of BoxA in frHMGB1 for complex formation (Venereau et al., 2012) is supported by the negligible small CSPs and intensity reduction in NMR titrations between CXCL12 and dsHMGB1-TL (Figure

40

2.7 A, B). Nonetheless, NMR titrations of ^{15}N dsHMGB1 and CXCL12 and the reverse ones produced comparable results with frHMGB1 (Figure 2.7 C, D). This confirms that the major spectral perturbations arise from intra- and intermolecular interactions of the acidic IDR, whose binding to CXCL12 is independent from the redox state of BoxA.

### Spectral perturbation analysis combined with Relaxation and heteronuclear NOE of [15]N Ac-pep_rec free and in complex with CXCL12

The dynamic nature of the interaction of the acidic IDR with CXCL12 was further verified by relaxation experiments of recombinant ^{15}N acidic IDR (Ac-pep_rec) with unlabelled CXCL12. IDRs of proteins or IDPs that retain their structural disorder in complex with other binding partners are referred to as "fuzzy" protein complexes, as it enables them to engage into multiple bound states in a promiscuous fashion (Fuxreiter, 2020). The ^{1}H-^{15}N HSQC spectrum of [15]N Ac-pep_rec showcases common spectral features of IDRs or IDPs, characterized by low peak dispersion of the ^{1}H chemical shift region with many peak overlaps.
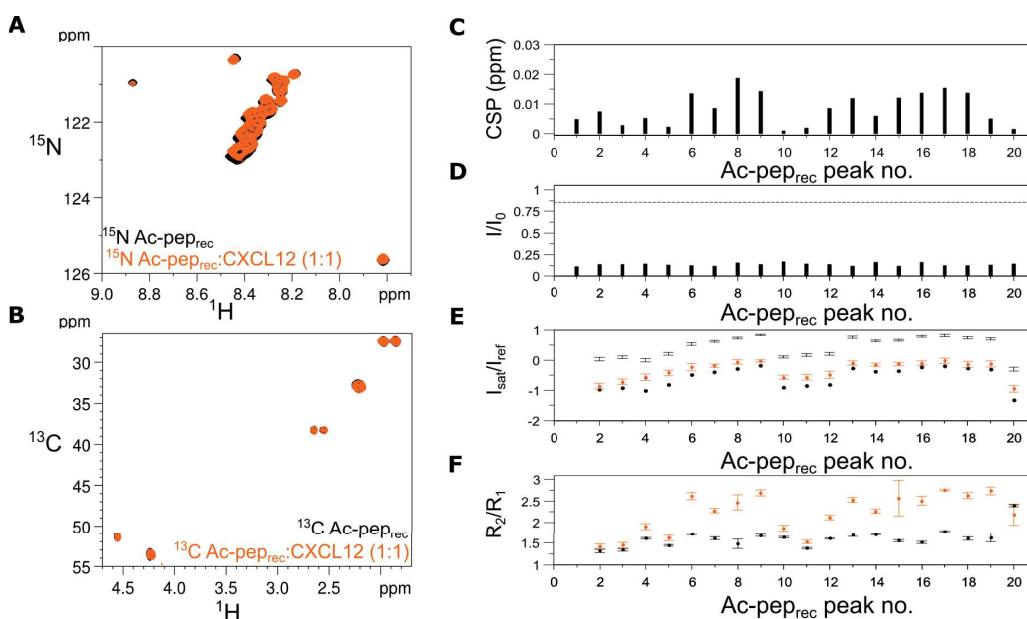


**Figure 2.8:** *[15]N Ac-pep_rec) dynamically interacts with CXCL12. Superposition of (A) ^{1}H-^{15}N HSQC spectra of [15]N Ac-pep_rec without (0.2 mM, black) and with (orange) CXCL12 (1:1), (B) ^{1}H-^{13}C HSQC spectra of ^{15}N/[13]C Ac-pep_rec without (0.2 mM, black) and with (orange) CXCL12 (1:1). Bar graphs showing (C) chemical shift perturbation (CSPs) and (D) peak intensities ratios ($I/I_0$) of [15]N Ac-pep_rec upon addition of CXCL12 (1:1). (E) Signal intensity ratios of heteronuclear NOE with and without proton saturation ($I_{sat}/I_{ref}$), error bars were calculated by error propagation described in methods. (F) Ratios of $R_2$ and $R_1$ relaxation rates of [15]N Ac-pep_rec without (0.2 mM, black) and with CXCL12 (1:1) (orange). Error bars are derived from relaxation data as described in methods.*

Interestingly, the narrow spectral range, indicative for a random-coil structure like the ones of flexible peptides, is maintained in the ^{1}H-^{15}N HSQC spectrum of the [15]N Ac-pep_rec•CXCL12 complex, as evident by the absence of significant chemical shift changes in the superimposed

spectra of $^{15}$N Ac-pep$_{rec}$ and $^{15}$N Ac-pep$_{rec}$•CXCL12 (Figure 2.8 A). This suggests that the acidic IDR does not adopt a secondary structure upon binding to CXCL12. Due to the repetitive D/E regions of the acidic IDR, the $^1$H-$^{13}$C HSQC spectra of $^{13}$C and $^{15}$N labelled Ac-pep$_{rec}$ displayed clustered signals of C$\alpha$ and C$\beta$ atoms of aspartic and glutamic acid residues, whose assignment to specific Aspartic and Glutamic acid residues of Ac-pep$_{rec}$ was not possible (Figure 2.8 B). Minor chemical shift changes were also observed in the $^1$H-$^{13}$C HSQC spectra of $^{15}$N Ac-pep$_{rec}$ titrated with equimolar CXCL12 (Figure 2.8 B). The manifestation of reduced peak dispersion and high signal overlap with minimal chemical shift perturbations is typical for IDRs or IDPs in fuzzy protein complexes, in which their structural disorder is retained in the bound state (Mittag et al., 2008, Borgia et al., 2018). Changes of the motional dynamics of Ac-pep$_{rec}$ upon binding to CXCL12 were probed by $^{15}$N relaxation parameters, in which local motions of the protein backbone were analysed. For the analysis, peaks of $^{15}$N Ac-pep$_{rec}$ were assigned to arbitrary numbers, as specific residue assignment was not possible. The examination of $^{15}$N relaxation parameters (heteronuclear steady state NOE, $R_1$, $R_2$) for free and bound $^{15}$N Ac-pep$_{rec}$ in Figure 2.8 E,F show that the acidic IDR remains mobile in both forms displaying negative heteronuclear NOE values that are indicative for high flexibility in the picosecond to nanosecond timescale. The modest increase in heteronuclear NOE values of the complex indicate a slight rigidification of the acidic tail peptide in the presence of CXCL12. The increase in $R_2/R_1$ values and reduction of peak intensities are consistent with complex formation, which results in slower rotational molecular tumbling in solution. Importantly, the distributed increase in $R_2/R_1$ values for bound $^{15}$N Ac-peprec indicates the presence of multiple CXCL12 binding sites within the acidic IDR. The observed line-broadening-induced signal attenuations of all CXCL12 residues in $^{15}$N CXCL12-Acpep titrations can be ascribed to exchange contributions due to dynamic binding. Collectively, the relaxation experiments provide evidence that the acidic IDR remains disordered in complex with CXCL12 supporting the formation of a fuzzy complex.

Fuzzy interactions arise from binding motifs of IDPs that similarly interact with their binding partner allowing for a dynamic exchange. For this purpose, IDPs or IDRs contain repetitive amino acid sequences with low residue variability, also known as low complexity regions, that bind equally to a broad range of interaction partners due to their unspecific recognition motifs. The D/E repeats of the acidic IDR represent an unspecific, charged binding surface for CXCL12 containing potentially multiple binding sites. To demonstrate this, peptide fragments of the IDR (Ac-pep$_{185-195}$ and Ac-pep$_{204-214}$) were titrated into $^{15}$N CXCL12. As a negative control, a peptide corresponding to the arginine/lysine-rich C-tail of a variant of HMGB1 leading to a human malformation syndrome (Mensah et al., 2023) was used. Both Ac-pep$_{185-195}$ and Ac-pep$_{201-214}$ similarly interacted with the CXCL12 dimerization surface (Figure 2.9 A-F) suggesting multiple CXCL12 binding sites on the acidic IDR. The formation of multiple and interchangeable bound states of acidic IDR and CXCL12 elucidate furthermore the dynamic nature of HMGB1's acidic IDR in complex formation with CXCL12. The titration with the control peptide highlights the electrostatic nature of interaction between CXCL12 and acidic IDR of

HMGB1, as evident by the negligible small spectral perturbations of CXCL12 residues (Figure 2.9 G-I).
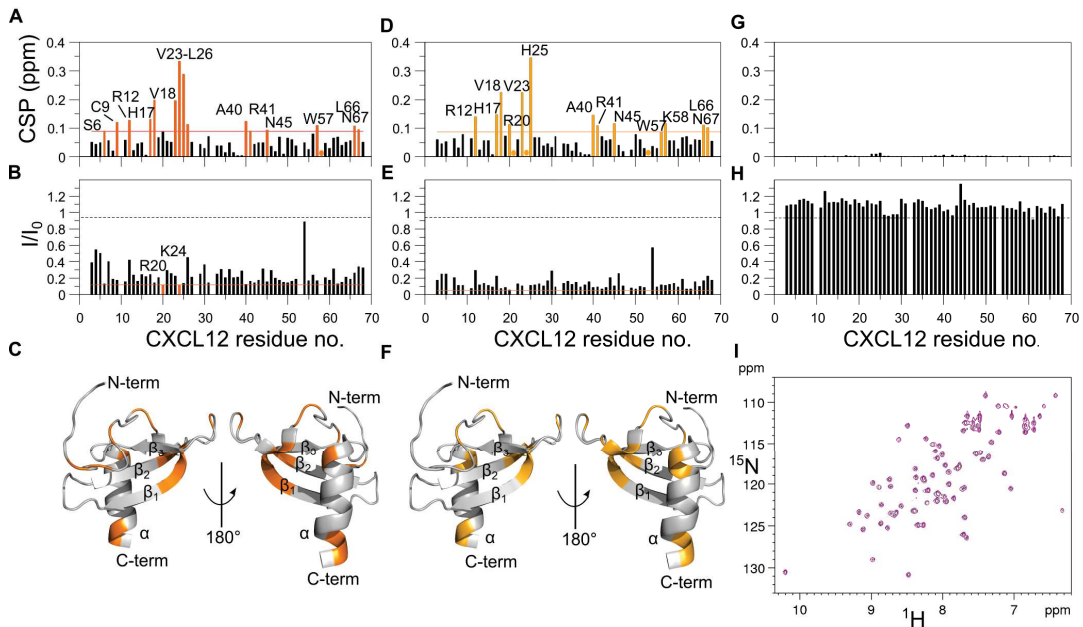


**Figure 2.9:** *The CXCL12-Ac-pep interaction is primarily electrostatic and CXCL12 dimerization region is targeted by multiple internal sites in the acidic IDR.* Bar plots of CSP and intensity ratio $I/I_0$ of $^{15}$N CXCL12 (0.1 mM) titrated with (A, B) Ac-pep$_{185-195}$ segment and with (D, E) Ac-pep$_{204-214}$ segment, respectively. Labelled residues go beyond the continuous lines in bar plots. Dashed lines indicates reduced signal intensities due to dilution effects. Dots in CSP bar plots indicate disappeared residues. (C, F) Interaction surface formed by binding-induced perturbed residues mapped on CXCL12 structure (PDB code: 2kee). (G, H) Histogram of CSP and intensity ratio $I/I_0$ of $^{15}$N CXCL12 titrated with basic K/R enriched IDR peptide of pathogenic HMGB1-mutant. (I) HSQC spectrum of $^{15}$N CXCL12 titrated with basic K/R enriched IDR peptide.

Taken together, the combination of the different NMR titrations and the relaxation data on $^{15}$N Ac-pep$_{rec}$ indicate that CXCL12•frHMGB1 is a fuzzy dynamic heterocomplex, characterized by multivalent inter- and intra-molecular equilibria involving CXCL12, the HMG tandem domains and the acidic IDR as major players within this intricate network of interactions.

## 2.3 Summary

The examination of NMR-based binding studies of the heterophilic interactions between CXCL12 and frHMGB1 and relaxation analysis unravel multivalent intra- and intermolecular interactions involving HMGB1's functional tandem domains, acidic IDR and CXCL12. The dissection approach elucidates the pivotal role of the acidic IDR in binding to CXCL12, as shown by prominent spectral perturbations of $^{15}$N CXCL12 peaks upon addition of Ac-pep. Both minor spectral perturbations in NMR titrations of $^{15}$N Ac-pep$_{rec}$ free and bound to CXCL12 and relaxation analysis showed that the mobility of the acidic IDR is retained in complex with CXCL12,

which defines a fuzzy complex. Interaction mappings of CXCL12 unveil the dimerization sur-face as a shared interaction hub for the acidic IDR and HMG boxes, while reverse titrations of ^{15}N frHMGB1-TL and ^{15}N frHMGB1 reveal frBoxA domain and acidic IDR as the important in-teraction partners of CXCL12 with the acidic IDR presenting multiple binding sites for CXCL12.

Collectively, these findings spot the key elements of dynamic binding between CXCL12 and HMGB1, as observed in fuzzy protein complexes. The heterocomplex is characterized by multivalent inter- and intra-molecular equilibria involving CXCL12, the HMG tandem domain and the acidic IDR as major players within this intricate network of interactions.

# Chapter 3

# Thermodynamics and Affinity of the CXCL12-HMGB1 Interaction

## 3.1 Introduction

CXCL12 is known to exert its chemoattractant function also as a heterocomplex with the reduced form HMGB1 (Schiraldi et al., 2012, Fassi et al., 2019). NMR studies in the previous chapter provide evidence that, besides the redox state of BoxA, inter- and intramolecular interactions of the acidic IDR also play a role in complex formation and in modulating the CXCL12-frHMGB1 interaction. The question arises to which extent the acidic IDR does contribute to the binding to CXCL12 from the thermodynamic point of view. We have therefore applied the same dissection approach used for NMR studies to investigate the thermodynamics of the CXCL12 interaction with HMGB1. To this end, we combined isothermal titration calorimetry (ITC), microscale thermophoresis (MST) and fluorescence measurements to derive the binding affinity between CXCL12 and Ac-pep, HMGB1-TL and HMGB1.

## 3.2 Results

### 3.2.1 The acidic IDR of HMGB1 interacts with CXCL12 via long-range electrostatic interactions

***Binding of CXCL12 to frHMGB1 and constructs thereof by ITC and MST.***

ITC injection of CXCL12 into Ac-pep solution generated spikes with a biphasic profile (Figure 3.1 A), indicative of different binding events with exothermic heat changes ($\approx$ -0.6 $\mu$cal/s). Global fitting of the buffer-subtracted binding isotherm yielded an apparent $K_{D_1}$ of 0.6 $\pm$ 0.1 $\mu$M and $K_{D_2}$ of 0.1 $\pm$ 0.1 $\mu$M (Table 3.1), in agreement with the low micromolar affinity estimated by NMR line-shape analysis. Also the interaction between frHMGB1 and CXCL12 appeared biphasic and exothermic (Figure 3.1 B), though with one order of magnitude reduced amplitude ($\approx$ -0.06 $\mu$cal/s). The fitting of the curve yielded an apparent $K_{D_1}$ = 1.2 $\pm$ 0.4 $\mu$M and a second one, whose nanomolar value should be taken with caution because of the large error in the global fitting (Houtman et al., 2007) (Table 3.1). Importantly, the low micromolar affinities
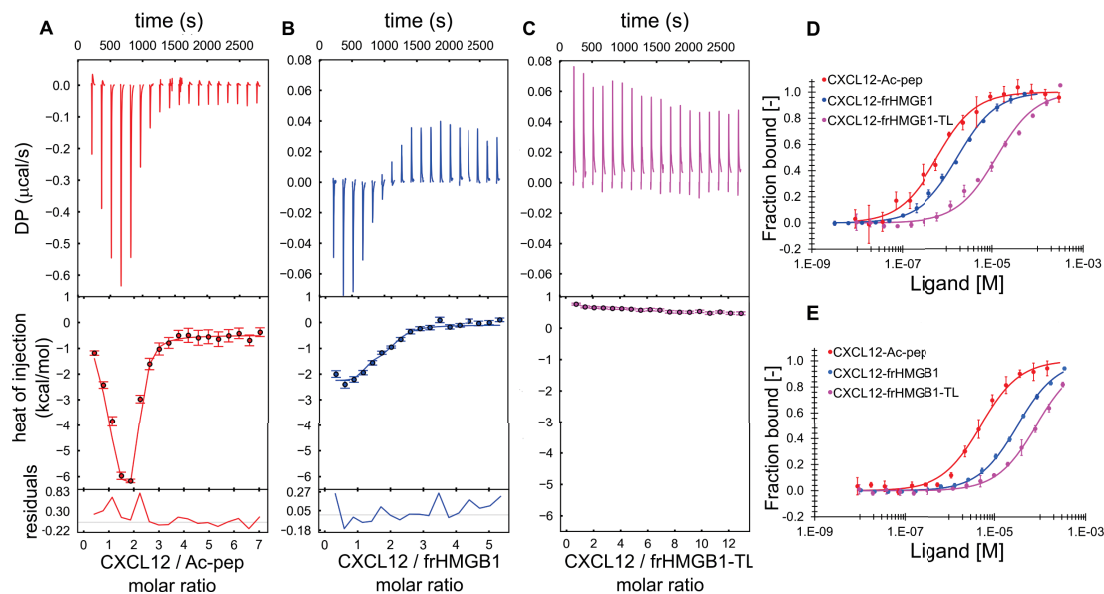
**Figure 3.1:** *The acidic IDR of frHMGB1 interacts with CXCL12 through electrostatic interactions.* *ITC measurements of CXCL12 (600 μM) titrated into (A) Ac-pep (10 μM, red), (B) frHMGB1 (10 μM, blue) and (C) frHMGB1-TL (10 μM, magenta). The upper, middle and lower panels show, respectively, the ITC sequential heat pulses (DP, differential power) for binding, the integrated data corrected for heat of dilution and the residuals. Data in (A, B) were globally fitted. Data in (C) could not be fitted because the heat of reaction was too small to be fitted with a nonlinear least-squares method. Data represents peak integration of ITC signal. One representative curve (n=3 for (A) and n=2 for (B)) for each titration is shown. The error associated with the integrated heat of injection arises from baseline uncertainties and is estimated by the automatic peak integration procedure in NITPIC 2.0.0 (Keller et al., 2012). Normalized variation of fluorescence of 5,6-FAM-labelled Ac-pep upon addition of CXCL12 (red) and normalized variation of MST signal of Red-tris-NTA labelled His-tagged CXCL12 in the presence of frHMGB1 (blue) and of frHMGB1-TL (magenta), with (D) 20 mM NaCl and with (E) 150 mM NaCl. Data are presented as mean values +/- SD of n=3 independent replicates. The thermodynamic parameters and $K_D$ values are summarized in Table 3.1.*

measured by ITC for Ac-pep and frHMGB1 were in good agreement with the ones deriving from fluorescence and MST experiments, respectively (Figure 3.1 D (red and blue), Table 3.2). While the heat of reaction between CXCL12 and frHMGB1-TL was not sufficient to derive any binding parameters (endothermic spikes at baseline level, ≈ 0.05 μcal/s) (Figure 3.1 C), a change of the thermophoretic diffusion properties of fluorescently labelled CXCL12 was detectable in the presence of frHMGB1-TL (Figure 3.3 D and E, magenta curve). Notably, the derived affinity ($K_D$ = 12.5 ± 5.5 μM) was almost one order of magnitude weaker than the one measured with full-length frHMGB1 ($K_D$ = 1.7 ± 0.2 μM), thus confirming the important role of the acidic IDR in heterocomplex formation (Table 3.2).

**Table 3.1: *ITC thermodynamic parameters*** *of the interactions between CXCL12 and Ac-pep, frHMGB1 and frHMGB1-TL in 20 mM TrisHCl, 50 mM NaCl at pH 7.5.*

| | $K_{D_1}$ (µM) | $K_{D_2}$ (µM) | $\delta H_1$ (kcal/mol) | $\delta H_2$ (kcal/mol) |
|---|---|---|---|---|
| Ac-pep[1] | $0.6 \pm 0.1$ | $0.1 \pm 0.1$ | $-10.4 \pm 0.8$ | $1.6 \pm 0.7$ |
| frHMGB1[2] | $1.2 \pm 0.4$ | $7.8 \cdot 10^{-3} \pm 1.5 \cdot 10^{-2}$ | $-1.4 \pm 0.1$ | $-2.1 \pm 0.2$ |
| frHMGB1-TL | n.d. | n.d | n.d. | n.d. |

[1] CXCL12 is the titrant, n=3 independent replicates, error estimates from covariance matrix
[2] CXCL12 is the titrant, n=2 independent replicates, error estimates from covariance matrix
[3] CXCL12 is the titrant, n=2 independent replicates, n.d. not detected

### Short versus long-range electrostatic interactions between the acidic IDR peptide and CXCL12 measured by ITC and MST at increased ionic strength

The recognition process between CXCL12 and HMGB1 might be governed by long-range electrostatic interactions between the acidic IDR of HMGB1 and the basic charged surface of CXCL12 (Figure 3.2 A, B). In fact, upon increase of the ionic strength (150 mM NaCl) the heat of reaction associated to CXCL12 interaction with Ac-pep or frHMGB1 at higher did not yield any spikes above baseline (3.2 C, D), thus confirming the important role of long range electrostatic interaction in the binding. Complementary evidence stems from fluorescence and MST experiments at 150 mM that yielded reduced binding affinities by one order of magnitude with respect to the same measurements performed at 20 mM NaCl (Figure 3.1 E, Table 3.2).
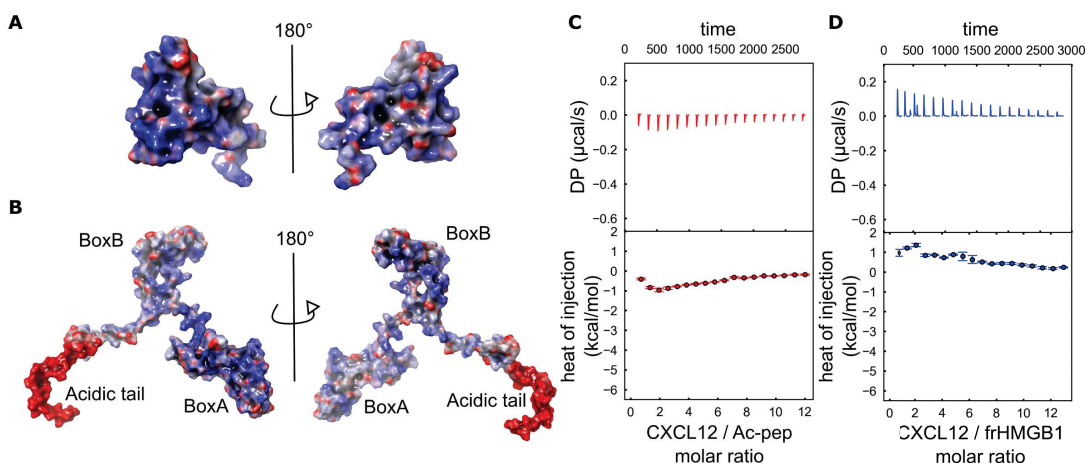


**Figure 3.2: *Electrostatic interactions drive enthalpic changes in CXCL12•frHMGB1 complex formation.*** *Electrostatic surface representation (as calculated by the Poisson Boltzmann Electrostatic Surface routine in Maestro-Schrödinger) of (A) CXCL12 and (B) frHMGB1. The ITC sequential heat pulses (upper panel) and the integrated data corrected for heat of dilution (lower panel) of CXCL12 binding (600 µM) to (C) Ac-pep (10 µM, 20 mM TrisHCl at pH 7.5, 150 mM NaCl) and to (D) frHMGB1 (10 µM, 20 mM TrisHCl at pH 7.5, 150 mM NaCl)*

**Table 3.2: *MST binding affinity parameters*** of the interactions between CXCL12 and Ac-pep, frHMGB1 and frHMGB1-TL in 20 mM $NaH_2PO_4/Na_2HPO_4$, 20 mM NaCl at pH 7.3 and 20 mM $NaH_2PO_4/Na_2HPO_4$, 150 mM NaCl at pH 7.3.

| | Binding parameters derived from MST | |
| --- | --- | --- |
| | $K_D$ (µM)    [NaCl]=20 mM | $K_D$ (µM)    [NaCl]=150 mM |
| Ac-pep[1] | $0.6 \pm 0.1$ | $5.0 \pm 0.6$ |
| frHMGB1[2] | $1.7 \pm 0.2$ | $31.8 \pm 1.4$ |
| frHMGB1-TL[2] | $12.5 \pm 5.5$ | $81.4 \pm 6.8$ |

[1] CXCL12 is the titrant, n=3 independent replicates, values are mean $\pm$ standard deviation

[2] frHMGB1 or frHMGB1-TL is the titrant, n=3 independent replicates, values are mean $\pm$ standard deviation, n.m. not measure

Given the dynamic nature of binding between CXCL12 and HMGB1, the binding mechanism is more complex than the binding models we used for fitting to derive the $K_D$. The entropies obtained in ITC experiments of CXCL12 titrations into Ac-pep and into frHMGB1 were $\delta S_1$ = 5.3 cal/mol·K, $\delta S_2$ = 38 cal/mol·K and $\delta S_1$ = 23 cal/mol·K, $\delta S_2$ = 28 cal/mol·K, respectively. It was not possible to derive the entropic contribution ($\delta S$) of the binding of CXCL12 with frHMGB1-TL from $\delta H$, which could not been determined, and the equilibrium constant K. Importantly, the calculated entropic contributions of CXCL12-binding to Ac-pep and to frHMGB1 should be considered with caution! An adequate way of deriving the entropy of IDRs and IDPs considering also the conformational entropy of IDRs ($\delta S_{conf}$) has been described by (Skriver, Theisen, and Kragelund, 2023). The scope of using ITC was to understand, whether long-range electrostatic interactions may govern the interaction between CXCL12 and frHMGB1, in particular with the acidic IDR given that long-range electrostatic interactions play important roles in the molecular recognition in *fuzzy* complexes (Mukhopadhyay, Ahmed, and Forman-Kay, 2022).

### Binding of CXCL12 to frHMGB1 and dsHMGB1 measured by MST

Although NMR titrations emphasize the redox selectivity of CXCL12 for frHMGB1, they also show that CXCL12, as it binds to the acidic IDR, is also able to interact with the disulphide form of HMGB1. Indeed, MST data reveal that binding between CXCL12 and dsHMGB1 occurs, but with reduced affinity ($37.3 \pm 3.3$µM) with respect to frHMGB1 ($1.7 \pm 0.2$µM), in line with the concept that the oxidized BoxA within the full length protein has a reduced interaction with CXCL12. Figure 3.3 represents the MST binding curves of CXCL12 titrated with frHMGB1 and dsHMGB1, respectively.
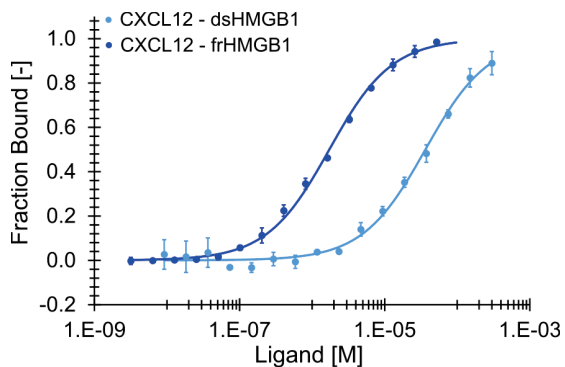
**Figure 3.3:** *Redox-selectivity of CXCL12 is grounded on the different binding affinities to the redox state of BoxA.* MST binding curves of Red-tris-NTA labelled His-tagged CXCL12 titrated with frHMGB1 (blue) and dsHMGB1 (light blue) show a shift of deflection points corresponding to apparent $K_D$ values towards higher ligand concentrations indicating reduced affinity.

## 3.3   Summary

Taken together, ITC, MST, as well as fluorescence measurements support a scenario in which the frHMG tandem domains and the acidic IDR together contribute to binding to CXCL12. The long-range electrostatic interactions between the acidic IDR and CXCL12 represent a driving force for complex formation between CXCL12 and HMGB1, as increasing ionic content in solution shields the heterophilic interactions. The interaction between CXCL12 and HMGB1 is stronger with the reduced state of BoxA compared to the disulphide form, thus supporting the notion that CXCL12 preferentially interacts and exerts its biological function with the fully reduced form of HMGB1.

**Chapter 4**

# CXCL12•HMGB1 Stoichiometry obtained by Analytical Ultracentrifugation

## 4.1 Introduction

Previous studies postulated that HMGB1 and CXCL12 form a 1:2 complex implying that synergism emerges from HMGB1 operating as a cargo of two CXCL12 molecules to activate a pair of CXCR4 receptors (Fassi et al., 2019, Cecchinato et al., 2023). However, this hypothesis has been never validated experimentally. To determine the stoichiometry of the heterocomplex, we used analytical ultracentrifugation (AUC), a label-free technique, that has the capacity to detect weak binding protein complexes by discriminating sizes based on sedimentation velocities.

## 4.2 Results

### 4.2.1 CXCL12 and HMGB1 form a transient equimolar complex

We first attempted to determine the size of the heterocomplex by sodium dodecyl sulphate polyacrylamide gel electrophoresis (SDS PAGE) and size exclusion chromatography (SEC). Both methods, although commonly used to determine the size of protein assemblies, were unable to detect the heterocomplex due to the weak and transient interactions between CXCL12 and HMGB1. We therefore utilized analytical ultracentrifugation that monitors the sedimentation of proteins by UV absorbance or interference measurements. First, the size of the individual proteins were determined by sedimentation velocity AUC (SV-AUC) experiments. The sedimentation coefficients of 1.1 S and 2.3 S that correspond to the derived molecular weights (MW) of 8.7 kDa and 27.1 kDa for CXCL12 and frHMGB1, respectively (Figure 4.1 A, B, 4.1) were in good agreement with the theoretical calculated molecular weights of 9 and 25 kDa. Of note, the MW discrepancy of frHMGB1 can be explained by the fact that the hydrodynamic radius of HMGB1 is larger because of the IDRs occupying a larger space compared to compact globular proteins of equivalent MW (Perez et al., 2014). The determined shape factors, expressed as the quotient of the friction coefficients of the molecule and an ideal sphere ($f/f_0$), of 1.3 of CXCL12 and of 1.4 of frHMGB1 indicate a globular and moderately elongated shape, respectively (Table 4.1). To study the hydrodynamic properties of the heterocomplex, CXCL12
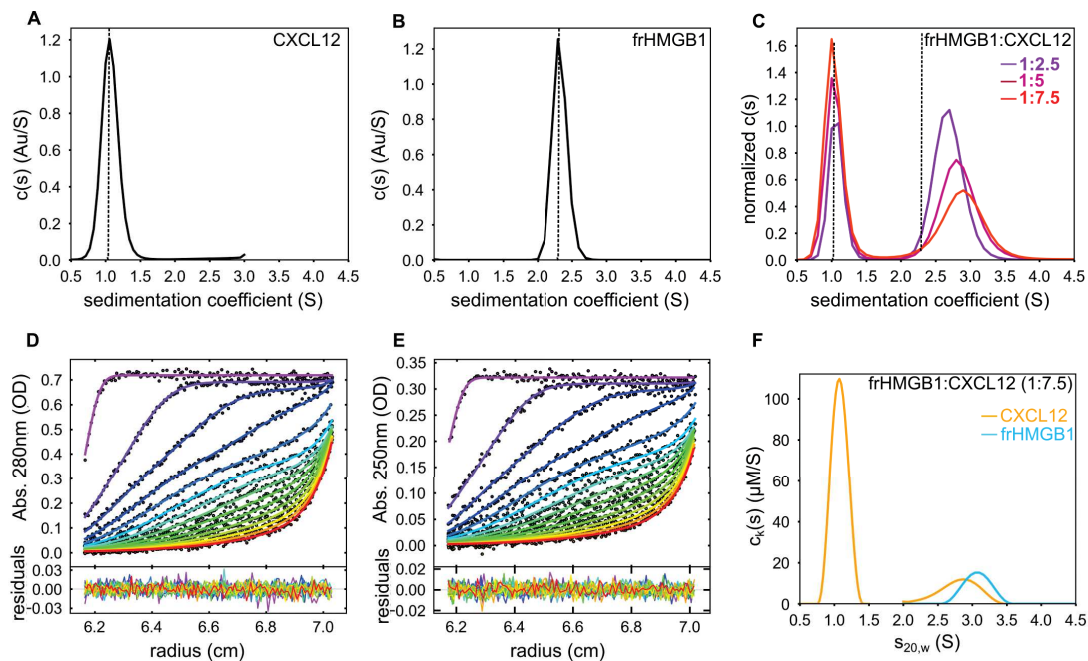
**Figure 4.1: *frHMGB1 and CXCL12 form a transient equimolar heterocomplex.*** *Sedimentation veloc- ity analytical ultracentrifugation (SV-AUC) experiments of free (A) CXCL12 (38 $\mu M$) and (B) frHMGB1 (15 $\mu M$), scanned by absorbance at 280 nm. (C) SV-AUC profiles of frHMGB1-CXCL12 mixtures at ratios with increasing amounts of CXCL12 (colors). The dotted lines indicate the sedimentation coefficients of the free components. (D-E) Multi-signal sedimentation velocity (MS-SV) analysis to determine the stoichiometry of frHMGB1:CXCL12 complex, with 7.7 $\mu M$ frHMGB1 and 43 $\mu M$ CXCL12. The raw sedi- mentation signals of frHMGB1:CXCL12 mixture acquired at different time points with (D) absorbance at 280 nm, and (E) absorbance at 250 nm with the corresponding signal profiles as a function of radius in centimetres. The time-points of the boundaries are indicated in rainbow colors, progressing from purple (early scans) to red (late scans). Only every 3rd scan used in the analysis are shown. Residuals of the fit are shown at the bottom. (F) Decomposition into the component sedimentation coefficient distributions, $c_k(s)$, for CXCL12 (8.5 $\mu M$, yellow line) and frHMGB1 (7.7 $\mu M$ cyan line).*

and HMGB1 were prepared as mixtures at different stoichiometric ratios (Schuck, 2000a). At variance to stable complexes, characterized by distinct SV-AUC curves for the bound and individual components, the frHMGB1•CXCL12 heterocomplex presented only two separable sedimentation distributions: one peak at lower s-values, corresponding to free CXCL12, and one at higher s-values, deriving from the sedimentation of free and bound frHMGB1 (Figure 4.1 C).

At 50 mM NaCl, the latter experienced line-broadening and shifts towards higher s-values (and apparent MWs) with increasing concentrations of CXCL12 (Figure 4.1 C, 4.2). This behaviour is typically observed in highly dynamic complexes, where the reaction boundaries between bound and unbound species cannot be resolved within the signal-to-noise ratio of the exper- iment (Balbo and Schuck, 2005). Hetero-association was also observed at 150 mM NaCl, but less complex was formed, as line-broadening and shifts of the reaction boundary towards higher s-values (and apparent MWs) were smaller compared to the ones observed at 50 mM NaCl (Figure 4.2). This confirms that long-range electrostatic interactions govern complex
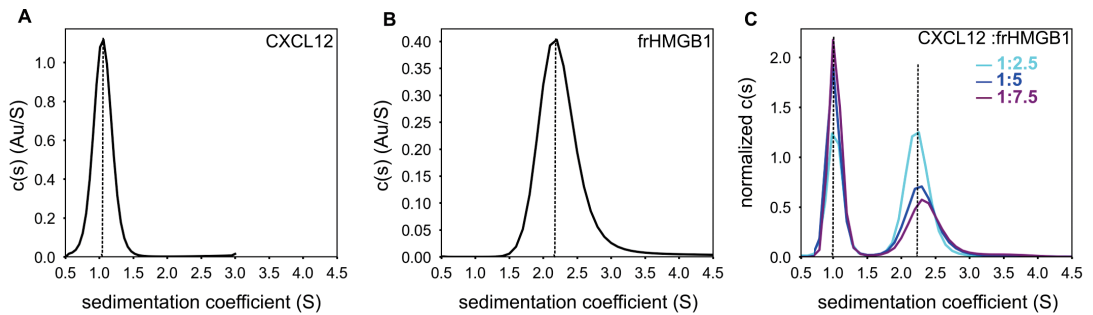
**Figure 4.2:** *The association reaction between CXCL12 and frHMGB1 at 150 mM NaCl concentration.* SV-AUC analysis of (A) CXCL12 (38 µM) and (B) frHMGB1 (15 µM) at 20 mM TrisHCL pH 7.5, 150 mM NaCl, scanned by absorbance at 280 nm and (C) frHMGB1:CXCL12 mixtures with HMGB1 (7.7 µM) with increasing amounts of CXCL12 at 20 mM TrisHCL pH 7.5, 150 mM NaCl (colors).
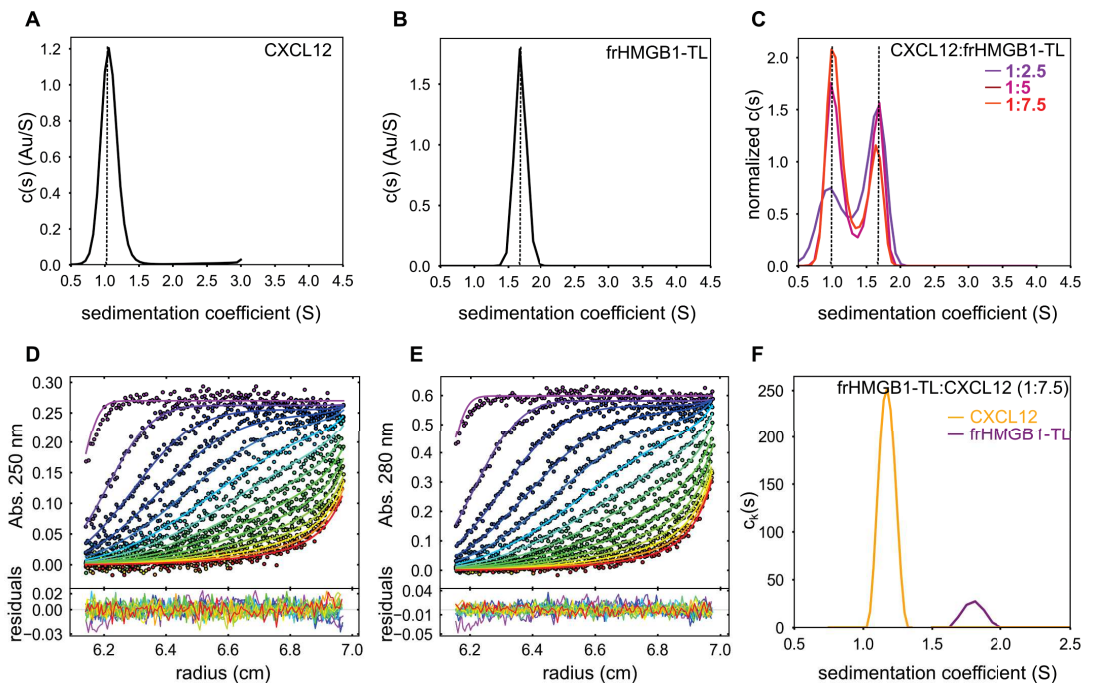


**Figure 4.3:** *The association reaction between CXCL12 and frHMGB1 stabilized by the acidic IDR.* SV-AUC experiments of free (A) CXCL12 (38 µM) and (B) frHMGB1-TL (15 µM) at 20 mM TrisHCL pH 7.5, 50 mM NaCl, scanned by absorbance at 280 nm and (C) SV-AUC profiles of frHMGB1-TL:CXCL12 mixtures with HMGB1-TL (7.7 µM) with increasing amounts of CXCL12 at 20 mM TrisHCL pH 7.5, 50 mM NaCl (colors). The sedimentation signals of frHMGB1-TL:CXCL12 mixture acquired at different time points with (D) absorbance at 280 nm, and (E) absorbance at 250 nm with the corresponding signal profiles as a function of radius in centimetres. The time-points of the boundaries are indicated in rainbow colors, progressing from purple (early scans) to red (late scans). Only every 3rd scan used in the analysis are shown. Residuals of the fit are shown at the bottom. (F) Decomposition into the component sedimentation coefficient distributions, $c_k(s)$, for CXCL12 (0 µM, yellow line) and frHMGB1-TL (5.6 µM, purple line).

formation between CXCL12 and frHMGB1. Notably, without the acidic IDR the association between CXCL12 and HMG tandem domains is too rapid to detect the CXCL12•frHMGB1-TL
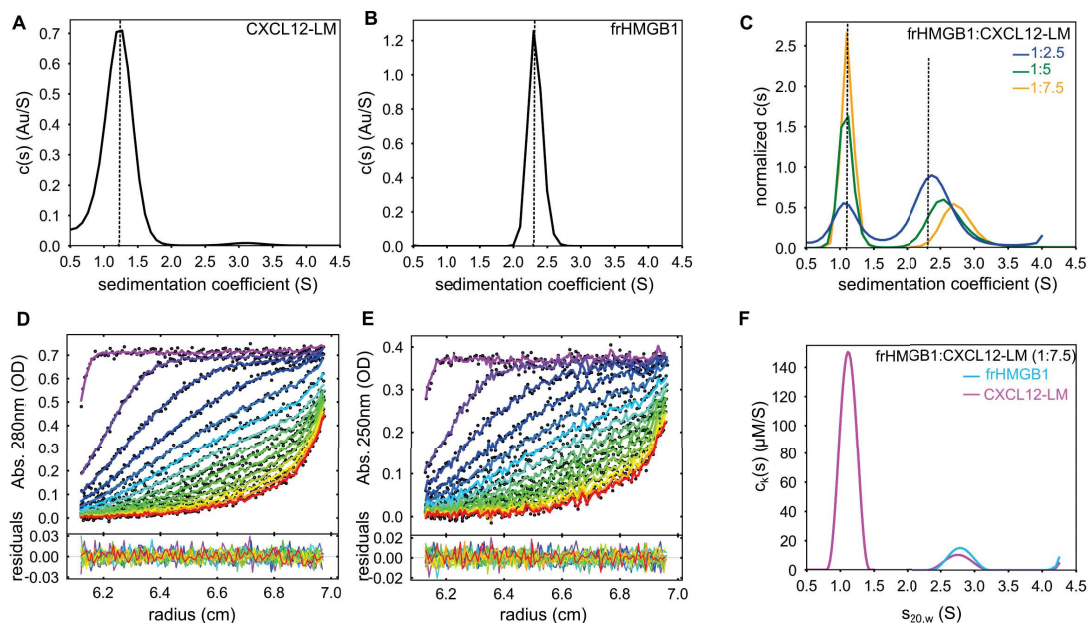
**Figure 4.4:** ***frHMGB1 forms with monomeric CXCL12 mutant a 1:1 heterocomplex.*** *SV-AUC experiments of free (A) CXCL12-LM and (B) frHMGB1, scanned by absorbance at 280nm. (C) SV-AUC profiles of frHMGB1:CXCL12-LM mixtures at ratios with increasing amounts of CXCL12-LM (colors). The dotted lines indicate the sedimentation coefficients of the free components. The c(s) analysis shows that the peak corresponding to frHMGB1 broadens and shifts to a larger s-value in an CXCL12-LM concentration-dependent manner. (D-E) MS-SV analysis reveal a frHMGB1:CXCL12-LM 1:1 complex. The raw sedimentation signals of frHMGB1:CXCL12 mixture acquired at different time points with (D) absorbance at 280 nm, and (E) absorbance at 250 nm with the corresponding signal profiles as a function of radius in centimetres. The time-points of the boundaries are indicated in rainbow colors, progressing from purple (early scans) to red (late scans). Only every 3rd scan used in the analysis are shown. Residuals of the fit are shown at the bottom. (F) Decomposition into the component sedimentation coefficient distributions, $c_k(s)$, for CXCL12 (4.9 $\mu$M, magenta line) and frHMGB1 (5.3 $\mu$M, cyan line).*

**Table 4.1:** ***SV-AUC of CXCL12, CXCL12-LM, frHMGB1 and frHMGB1-TL in 20 mM TrisHCl, 50 mM NaCl at pH 7.5.*** *Parameters were calculated from c(s) model analysis of SV profile of the free components.*

| Parameters | CXCL12 | CXCL12-LM | frHMGB1 | frHMGB1-TL |
|---|---|---|---|---|
| s[1] (S) | 1.1 | 1.2 | 2.3 | 1.7 |
| $f/f_0$[2] | 1.3 | 1.2 | 1.4 | 1.6 |
| MW (kDa) | 8.4 | 8.9 | 27.1 | 21.1 |
| RMSD[3] | 0.0052 | 0.0057 | 0.0051 | 0.0049 |

[1] sedimentation coefficient expressed in Svedberg (S)
[2] frictional ratio, f is the frictional parameter of the particle and $f_0$ is the frictional value of a smooth sphere
[3] root mean square deviation of the fitting of the c(s) model to the experimental sedimentation curves

complex in the sedimentation time scale (Figure 4.3 C, E, Table 4.2). This finding suggests that the acidic IDR also increases the life time of the CXCL12•HMGB1 heterocomplex besides

**Table 4.2:** *MSSV-AUC analysis of CXCL12:frHMGB1, CXCL12-LM:HMGB1, CXCL12:frHMGB1-TL mixtures in 20 mM TrisHCl, 50 mM NaCl at pH 7.5.* Parameters were derived from multi signal sedimentation velocity (MS-SV) model of frHMGB1:CXCL12 (1:7.5), frHMGB1-TL:CXCL12-LM (1:7.5) and frHMGB1-TL:CXCL12 (1:7.5).

| Parameters | frHMGB1:CXCL12 1:7.5 | | frHMGB1:CXCL12-LM 1:7.5 | | frHMGB1-TL:CXCL12 1:7.5 | |
|---|---|---|---|---|---|---|
| | CXCL12 | frHMGB1 | CXCL12-LM | frHMGB1 | CXCL12 | frHMGB1-TL |
| $s_{w,20}$[1] (S) | 2.8 | 3.1 | 2.8 | 2.9 | - | 1.8 |
| $Conc_{mix}$[2] ($\mu$M) | 43.0 | 7.7 | 51.0 | 7.9 | 48.0 | 7.8 |
| $Conc_{comp}$[3] ($\mu$M) | 8.5 | 7.7 | 4.9 | 6.5 | - | 5.3 |
| $RMSD_{280nm}$[4] | | 0.0072 | | 0.0077 | | 0.0079 |
| $RMSD_{250nm}$[5] | | 0.0050 | | 0.0057 | | 0.0058 |
| $D_{norm}$[6] | | 0.08 | | 0.16 | | 0.08 |

[1] sedimentation coefficient normalized to standard solution conditions of water at 20°C
[2] concentration of the components in mixture
[3] calculated concentration of the components in the complex sedimentation distribution
[4] root mean square deviation of the fitting of the MS-SV model to the experimental sedimentation curves
[5] determinant of the extinction coefficient matrix

recruiting CXCL12. Next, to determine the ratio of frHMGB1 and CXCL12 in the complex distribution, multi-signal SV-AUC experiments (MS-SV-AUC) was carried out. The method exploits the different extinction coefficients of frHMGB1 and CXCL12 at minimal (250 nm) and maximal (280 nm) wavelengths to distinguish between the two components in complex (Brautigam, Padrick, and Schuck, 2013, Padrick and Brautigam, 2011). Analysis of MS-SV-AUC suggested that frHMGB1 predominantly forms with CXCL12 a 1:1 heterocomplex, as indicated by the equimolar concentrations of CXCL12 and frHMGB1 derived from the peak area at $\approx 3$ S (Figure 4.1 E, Table 4.2). The equimolar stoichiometry of the CXCL12•frHMGB1 complex was furthermore confirmed by MS-SV-AUC analysis of monomeric variant CXCL12-LM with frHMGB1 (Figure 4.4 E, Table 4.2).

## 4.3 Summary

Previous studies describe the mechanism of synergism of CXCL12•frHMGB1 as a result of two CXCL12 molecules, each delivered by the single boxes of HMGB1, to CXCR4. In contrast to past assumptions, we provided experimental evidence that the heterocomplex forms transiently an equimolar heterocomplex by AUC analysis suggesting a different mechanism for synergism. Moreover, we established that the acidic IDR promotes complex formation via long-range electrostatic interactions and prolongs the heterocomplex life-time that is detectable in the sedimentation time scale. These findings suggest that the acidic IDR plays a fundamental role in complex assembly.

# Chapter 5

# CXCL12•frHMGB1 Size and Shape obtained by Small Angle X-ray Scattering

## 5.1 Introduction

Complementary to AUC, Small-Angle X-ray Scattering (SAXS) provides molecular properties such as size and shape of proteins and protein complexes. Compared to X-ray diffraction, SAXS has the advantage to provide structural information of solution samples containing partially or completely disordered macromolecules. We performed SAXS to derive the size and shape of the heterocomplex and to obtain low-resolution models by utilizing programs that integrate NMR data with SAXS structure determination.

## 5.2 Results

### 5.2.1 Small Angle X-ray scattering (SAXS) analysis supports the dynamic nature of HMGB1-CXCL12 heterocomplex

Primary analysis of the SAXS scattering curves of CXCL12 and frHMGB1 yielded radii of gyration ($R_g$) of 1.52 nm and 2.60 nm, respectively, as well as pair distance distribution plot (P(r)) derived maximum distance ($D_{max}$) values of 4.8 nm and 8.5 nm. These values indicate that both proteins are monomeric and monodisperse in solution (Figure 5.1 A, gold and black curves respectively, Table 5.1). The values obtained for frHMGB1 are in accordance with a previous report (Stott et al., 2010). The normalized Kratky representation of free CXCL12 and HMGB1 displayed upward trends at higher $qR_g$ values (4 and 6, respectively) well in agreement with the presence of flexible regions within a folded core (Figure 5.1 B). While the profile of the P(r) plot of CXCL12 was relatively symmetric compared to the one of frHMGB1 that displayed an asymmetric, elongated shape, tailed off to large distances (Figure 5.1 C, gold and black).

This feature suggests the existence of multiple conformations in solution, and aligns with the presence of flexible regions and intramolecular multivalent fuzzy interactions between the acidic IDR and the basic HMG domains (Stott et al., 2010). Thus, to generate an ensemble of HMGB1 conformers able to account for its intrinsic dynamics and able to fit the experimental scattering curve, the Ensemble Optimization Method (EOM) was utilized (Stott et al.,
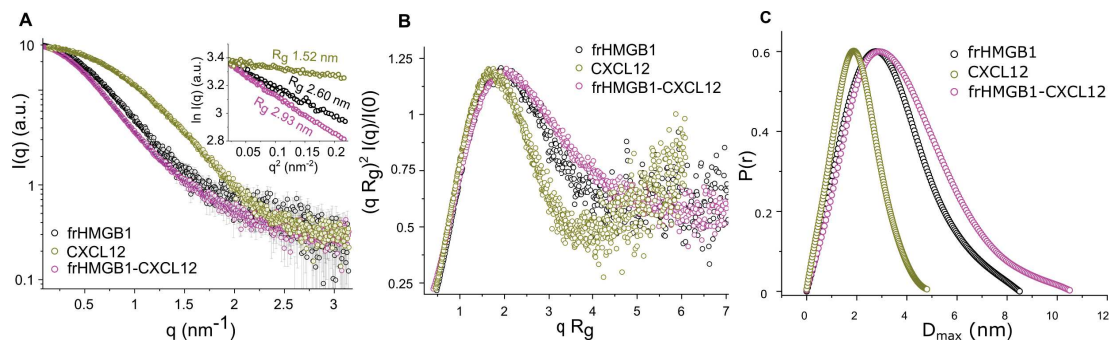
**Figure 5.1:** *SAXS studies of free frHMGB1, CXCL12 and CXCL12•frHMGB1 heterocomplex. (A) I(q) versus q experimental SAXS profiles for CXCL12 (3.9 mg/ml, gold), frHMGB1 (1.95 mg/ml, black) and frHMGB1•CXCL12 complex (magenta). In the inset, the Guinier regions used to estimate the radii of gyration. Increased steepness indicates complex formation with the $R_g$ value of 2.9 nm corresponding to the size of a 1:1 CXCL12•frHMGB1 complex (35.8 kDa). (B) Dimensionless Kratky plot of CXCL12, frHMGB1 and CXCL12•frHMGB1 (gold, black and magenta curve, respectively) indicating flexible and structured regions. (C) Pair distance distribution function (PDF) plotted against the maximal particle distance ($D_{max}$).*

**Table 5.1:** *Experimental SAXS parameters and analysis of CXCL12, frHMGB1 and frHMGB1•CXCL12.*

| Parameters | CXCL12 | frHMGB1 | CXCL12•frHMGB1 |
|---|---|---|---|
| | | Guinier analysis | |
| I(0) (cm$^{-1}$) | 33 | 44 | 83 |
| $R_g$ (nm) | $1.52 \pm 0.01$ | $2.60 \pm 0.02$ | $2.93 \pm 0.02$ |
| q-range (nm$^{-1}$), point range | 0.04-4.0, 11-752 | 0.16-3.0, 13-573 | 0.03-2.8, 7-508 |
| | | P(r) analysis | |
| I(0) (cm$^{-1}$) | 33 | 44 | 83 |
| $R_g$ (nm) | 1.5 | 2.6 | 2.9 |
| $D_{max}$ ($R_{max}$, nm) | 4.8 | 8.5 | 10.5 |
| q-range (nm$^{-1}$) | 0.04-4.0, 11-752 | 0.16-3.0, 13-573 | 0.03-2.8, 7-508 |
| | | Porod analysis | |
| Porod volume (nm$^3$) | 19.4 | 52.7 | 71.7 |
| Estimated MW (kDa) | 9.1 | 26.4 | 35.8 |

[1] Intensity
[2] estimated radius of gyration ($R_g$)
[3] estimated maximal particle distance ($D_{max}$)
[4] estimated Porod volume
[5] estimated Molar Mass

2010) and combined with rigid body modelling (Bernadó et al., 2007) to obtain models of the CXCL12•frHMGB1 heterocomplex. However, due to the transient and dynamic nature of the heterocomplex, the SAXS measurements coupled to size chromatography could not be successfully applied to study the heterocomplex from CXCL12•frHMGB1 sample mixtures.

Instead, a "batch-mode" strategy was used where HMGB1 was incubated with increasing concentrations of CXCL12 and immediately measured and analysed by SAXS. In the SAXS spectrum of a protein complex in batch mode, the relative contribution of the individual components to the overall scattering curve varies depending on their size and scattering intensity (Tuukkanen and Svergun, 2014). Hence, the heterocomplex, which is the largest component (35.8 kDa), was expected to contribute the most to the overall scattering signal and to dominate over the scattering contribution of the smallest component CXCL12 (9.1 kDa). Indeed, in the presence of two equivalents of CXCL12, where more than 96% of frHMGB1 was saturated with CXCL12, a 1:1 complex with an estimated molecular weight of 35.8 kDa was obtained (Table 5.1). At higher CXCL12 concentrations the molecular weight estimation was not accurate and unreliable due to the increasing scattering contribution of unbound CXCL12. Thus, the SAXS analysis of the heterocomplex was performed on the sample comprising two CXCL12 equivalents. The overall increase of the derived SAXS parameters with respect to free HMGB1, were compatible with complex formation ($R_g$ of 3.0 nm and $D_{max}$ of 10.5 nm). The normalized Kratky plot confirmed the dynamic and flexible nature of the complex, containing both folded domains and unstructured segments (Figure 5.1 B, magenta curve).

Next, to model more quantitatively the fuzzy nature of HMGB1•CXCL12 heterocomplex, NMR-guided rigid-body docking (SASREF (Petoukhov and Svergun, 2005) and FoXSdock (Schneidman-Duhovny et al., 2016) was combined to EOM analysis (Bernadó et al., 2007) (details in materials and methods).
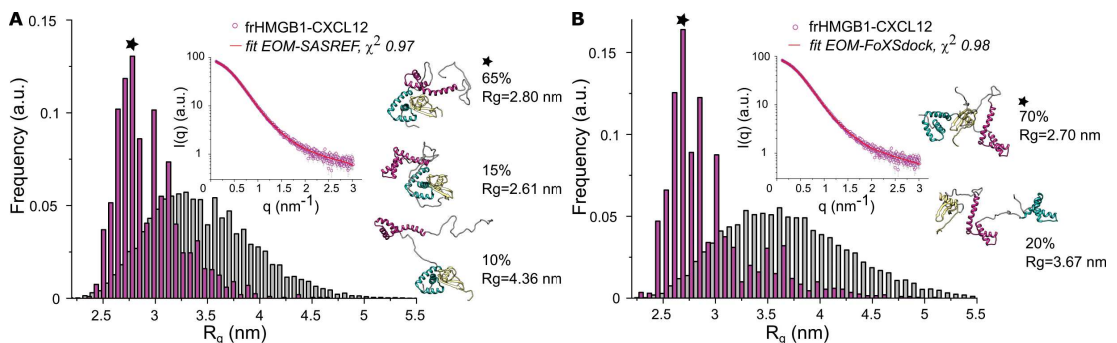


**Figure 5.2: *EOM models that describe the ensemble of CXCL12•frHMGB1 complexes.*** *Analysis of SAXS data by EOM on CXCL12•frHMGB1 models obtained using (A) SASREF and (B) FoXSDock with distributions of the selected ensemble conformers (magenta bars) and the initial pools of structures (grey bars) as a function of $R_g$ in nm. In the insets, I(q) versus q (magenta squares) with the EOM fitting (red lines with the corresponding $\chi^2$ values) for the frHMGB1•CXCL12 complex. Representative structures of the most populated EOM ensembles are shown in cartoon, with BoxA, BoxB, IDR and CXCL12 coloured in cyan, magenta, grey and gold, respectively. For each ensemble, the frequency-weighted size average (the asterisks indicate the most populated fractions) and $R_g$ values are indicated.*

The IDRs of HMGB1 in complex remain flexible generating thereby conformational ensembles of bound HMGB1 that contribute to the overall scattering pattern. EOM derived conformational ensembles of frHMGB1 that best fit the experimental SAXS curve of the CXCL12•frHMGB1 were utilized as starting structure for rigid docking on CXCL12. Since our NMR data indicated that CXCL12 can bind both BoxA and the acidic IDR, two initial docking models were

generated. One was obtained by guiding the interaction between CXCL12 on BoxA with program SASREF (Petoukhov and Svergun, 2005) taking advantage of the experimental CSPs, while for the other binding between CXCL12 and the acidic IDR was modelled with FoXSDock (Schneidman-Duhovny et al., 2016), which is more suitable when no prior information is available about the specific interacting regions within a disordered segment. As a result, two EOM conformational ensembles were obtained reflecting well the experimental SAXS curve (with $\chi^2 < 1$, Figure 5.2 A and B denoted with a star in bar graphs, Table 5.2). In the first ensemble, CXCL12 binds to BoxA of HMGB1, adopting alternatively open or more collapsed conformations (Figure 5.2 A). In the second one, the acidic IDR of frHMGB1 interacts with CXCL12, while the two HMG boxes adopt different reciprocal orientations (Figure 5.2 B). To quantify the flexibility of the CXCL12•frHMGB1 heterocomplex, the size of the ensemble distribution and of the generated pool were determined by the $R_{flex}$ metric. For highly flexible proteins, the $R_{flex}$ is close to 1 or 100% or in case of complete rigidity it assumes a value close to 0. Indeed, the CXCL12•frHMGB1 retains the structural flexibilty of frHMGB1, as the $R_{flex}$ value of the heterocomplex (69.2%) is similar, if not almost identical, to the one of frHMGB1 free 69.4% (Table 5.2). Compared to the original pool containing highly flexible HMGB1 conformers, the conformational space of HMGB1 in complex with CXCL12 appears to be smaller, as indicated by the $R_{\sigma}$ value smaller than 1 of complexes with CXCL12 bound to frBoxA of 0.6 and bound to acidic IDR of 0.7.

**Table 5.2:** *EOM parameters of frHMGB1 and CXCL12•frHMGB1 models.*

| Parameters | frHMGB1 | CXCL12•frHMGB1 | |
| --- | --- | --- | --- |
| Input Struct. | AFmodel P63159 | SASREF: CXCL12-frBoxA | FOXSDOCK: CXCL12-acidic IDR |
| | | 5 | 4 |
| Structures[1] | 6 | 5 | 4 |
| $R_{flex}$ ensemble[2] (%) | 73.1 | 69.4 | 69.2 |
| $R_{\sigma}$ ensemble[3] | 1.2 | 0.6 | 0.7 |
| Avg. $R_g$ (nm)[4] | 2.81 | 2.99 | 2.95 |
| Avg. $D_{max}$ (nm)[5] | 9.07 | 9.19 | 9.88 |

[1] Selected structures from ensemble that best fit the experimental SAXS curve
[2] EOM flexibility parameter derived from the Shannon Theory of entropy as a measure of conformational space
[3] EOM flexibility parameter using the randomized pool as reference
[4] estimated radius of gyration ($R_g$) of ensemble
[5] estimated maximal particle distance ($D_{max}$) of ensemble

Overall, SAXS analysis of $R_g$, $D_{max}$ and Kratky profile as well as EOM metrics support the notion that frHMGB1 and CXCL12 form an equimolar and fuzzy complex.

## 5.3  Summary

We utilized small angle X-ray scattering (SAXS) in combination with NMR-guided rigid body docking to obtain low-resolution models of the CXCL12•frHMGB1 heterocomplex. In accordance with analytical ultracentrifugation data, the derived structural parameters from SAXS indicate the formation of an 1:1 heterocomplex between CXCL12 and frHMGB1 ($R_g$ = 2.9 nm, MW = 35 kDa). Since HMGB1 does not have a unique structure but assumes multiple, interconvertible conformational states, the ensemble optimization method (EOM), developed for SAXS analysis of IDPs and proteins with IDRS, was used to model frHMGB1 in complex with CXCL12. Exploiting the structural information about the binding interface and stoichiometry from NMR and AUC studies, NMR-driven rigid body docking in EOM analysis delivered to major ensembles of the CXCL12•frHMGB1 heterocomplex. In the first CXCL12 molecule binds to frBoxA and in the second CXCL12 interacts with the acidic IDR of HMGB1. Overall, these findings reflect very well the dynamic nature of the CXCL12•frHMGB1 heterocomplex, as they show the heterocomplex as an ensembles of multiple conformational bound states of CXCL12 and frHMGB1.

**Chapter 6**

# Discussion

## 6.1 Chemokine•alarmin heterocomplexes in the chemokine interaction landscape

The intricacy of the chemokine interactome has complicated our biological understanding of the chemokine interaction landscape but also opened many opportunities to study a wide range of modulators of the chemokine interaction network. The mechanism underlying the chemokine biology are multifaceted and governed by a multitude of protein-protein interactions ranging from oligomerization including homo- and hetero-associations of chemokines (Miller and Mayo, 2017, Weber and Koenen, 2006) and their receptors (Allen, Crown, and Handel, 2007), GAG-binding (Proudfoot et al., 2003, Yang et al., 1994, Veldkamp, 2005) as well as interactions with atypical chemokines (Brandhofer et al., 2022). Chemokine-chemokine interactions represent therefore a pharmacological opportunity to manipulate the chemokine interactome to gain therapeutic benefits from potentiating or dampening certain chemokine activities. The advantage of targeting chemokine complexes, rather than chemokine receptors, is that a complete blockade or abrogation of the chemokine receptor activity is likely to be accompanied by side effects. As the chemokine system represents an integral part of the immune system, the consequences of complete receptor inhibition are undesired immunological side effects. The administration of for instance Met-CCL5, a CCL5 variant, blocks the receptors CCR1, CCR3 and CCR5. Despite its beneficial effect in reducing plaque formation and leukocyte infiltration in diet-induced atherosclerosis (Combadière et al., 2008), it compromised immune responses against herpes simplex virus type 2 (HSV2) (Sørensen and Paludan, 2004). The emergence of chemokine heterocomplexes as functional fine-tuners of the chemokine system represents a convenient approach to reduce the risk of immunological side effects by attenuating a particular chemokine–receptor axis during disease with the idea to shift favourably the immune balance, meanwhile leaving physiological functions intact (Weber and Koenen, 2006).

Although structural investigations of heterophilic binding interfaces of chemokine•chemokine and chemokine•receptor complexes provided a better understanding of the molecular basis of

the chemokine interaction landscape, they also raised new questions about chemokine interactions with other ligand classes, such as DAMPs (or alarmins) (Kapurniotu, Gokce, and Bernhagen, 2019). While CC and CXC chemokines are able to form heterocomplexes with binding interfaces similar to those of their homo-dimers and -oligomers, chemokine associations with inflammatory mediators, such as CCL5•HNP1 (Alard et al., 2015) and CXCL12•HMGB1 (Schiraldi et al., 2012) are less studied and therefore quite exotic. Since experimental structures of chemokine•alarmin heteromers are currently unavailable, in-silico derived models were generated to complement experimental findings of their functional activity (Fassi et al., 2019) or to design molecular inhibitors or stabilizers (Wichapong et al., 2016).

In this thesis, we focused on the CXCL12•frHMGB1 heterocomplex, whose functional synergism on the CXCR4 downstream axis has pathological as well as physiological consequences. It promotes tissue regeneration and repair (Bianchi et al., 2017, Tirone et al., 2018), but at the same time favours the inflammatory state of rheumatoid arthritis (Cecchinato et al., 2018). In addition, HMGB1, CXCL12 and CXCR4 assume a protagonistic role in promoting malignant mesothelioma (Mezzapelle et al., 2021). However, our understanding of the molecular interactions underlying the synergistic actions of this chemokine•alarmin complex is limited, as HMGB1 is structurally very different from the chemokine scaffold, with only two structured domains, each formed by three helices, and extensive unstructured segments. So, can HMGB1 be considered as a normal chemokine for our interaction studies? Does it maintain the characteristics of chemokine•chemokine complexes?

## 6.2 Previous structural model of the CXCL12•frHMGB1 heterocomplex

Previous structural studies aimed at getting mechanistic insights into frHMGB1•CXCL12 have focused on the interaction of CXCL12 with the single isolated HMG boxes (Schiraldi et al., 2012, Fassi et al., 2019). In these studies the authors took advantage of NMR CSPs obtained from titrations of CXCL12 with the isolated HMG boxes to produce a 3D model in which each single HMG box bound one CXCL12 molecule (Schiraldi et al., 2012, Fassi et al., 2019). The question arose whether such a simplified approach, in which the HMG boxes are separated and the IDRs (i.e. the acidic C-terminal tail and the linker connecting the HMG boxes) are neglected, can faithfully recapitulate the interaction of CXCL12 with the full-length protein.

The aim of this work was thus to characterize the entire CXCL12•frHMGB1 heterocomplex through integrative structural biology techniques to provide an experimentally validated 3D structural model. The prospect of our findings was to elucidate interaction sites between CXCL12 and frHMGB1 that could be exploited for drug design through pharmacological inhibition, since dampening CXCR4 hyperactivity by targeting the synergically acting heterocomplex seemed to be a promising strategy for treating inflammatory disorder and possibly

also for inflammation-related cancers.

By considering the dynamic features of HMGB1, namely its IDRs, that fulfil essential regulatory activities in the cell nucleus as described below, we expected that they also play an important role in the extracellular environment in binding to CXCL12.

## 6.3 The involvement of HMGB1's acidic IDR in complex formation with CXCL12

The IDRs of HMGB1 include its interdomain linker and acidic C-terminal tail. The acidic C-terminal IDR of HMGB1 modulates interactions with nucleic acids (Wang et al., 2007) and different proteins, such as histones (Cato et al., 2008, Watson, Stott, and Thomas, 2007) and p53 (Rowell et al., 2012). From a structural perspective, the mechanism underlying the nuclear function of HMGB1 is linked to the acidic IDR regulating DNA-binding to the basic charged HMG boxes (Stott et al., 2010). The binding affinity of DNA to HMG boxes is decreased, when the acidic IDR is bound to the tandem domains. This conformational state inhibits the chromatin-protein domain interaction, which is referred to the auto-inhibitory state of HMGB1 (Wang et al., 2021). Conversely in the extracellular milieu, the acidic IDR attracts both positively charged HMG boxes and CXCL12 increasing thereby the binding affinity for heterocomplexation. The acidic IDR is strongly negatively charged composed of only aspartate (D) or glutamate (E) residues. Its polyelectrolyte characteristics are fundamental for HMGB1's nuclear function through the formation of biomolecular condensates via liquid-liquid phase separation (LLPS) (Mensah et al., 2023). Biomolecular condensates are membrane-less organelles composed of higher-order, non-stoichiometric molecular assemblies containing proteins, RNA/DNA and/or small molecules ( Capasso Palmiero et al., 2022, Wan et al., 2018, Li et al., 2012). Biomolecular condensates emerged as important regulators of cellular responses via controlled LLPS behaviour (Banani et al., 2017). LLPS is driven by multivalency or by multiple weak interactions that rapidly form, break and reform (Banani et al., 2017). HMGB1 achieves multivalency through the dynamic exchange between the structured tandem domains and the acidic IDR. Indeed, replacement of the acidic IDR with an arginine-rich basic tail has been recently shown to cause a rare human malformation syndrome, which results from HMGB1 aberrant phase separation behaviour in the nucleolus leading to nucleolar dysfunction (Mensah et al., 2023). In accordance with the functional relevance of HMGB1's acidic IDR, in this work we show that the acidic IDR, whether isolated or in the context of the full-length protein, binds to the CXCL12 homo- and hetero-dimerization surface. Interestingly, the CXCL12 residues involved in the interaction with both Ac-pep and frHMGB1 in part coincide with the ones involved in the interaction with negatively charged heparin oligosaccharides (Veldkamp, 2005, Ziarek et al., 2013b). Importantly, the acidic IDR, because of its repetitive sequence, contains multivalent sites able to interact with CXCL12, as indicated by NMR titrations of $^{15}$N CXCL12 with synthetic peptide fragments of the acidic IDR. In line with

this multivalency, NMR relaxation experiments performed on the $^{15}$N Ac-pep$_{rec}$ show that the acidic IDR maintains its conformational flexibility also when bound to CXCL12. Noteworthy, binding of full-length frHMGB1 to CXCL12 is significantly weaker than to the isolated acidic IDR, indicating competition of the intra-molecular frHMGB1 boxes with CXCL12 for the acidic IDR. Both ITC and MST experiments suggest long range electrostatic interactions between the acidic IDR and the basic surface of CXCL12 as major drivers for binding, as increased ionic strength or deletion of the acidic IDR reduced binding to CXCL12. Long-range electrostatic interactions, though fundamental, are not the unique driving force for complex formation, as both NMR and MST indicate that tailless frHMGB1 (frHMGB1-TL) binds with micromolar affinity to the dimerization surface of CXCL12, albeit less well with respect to the full-length protein. Thus, structured and unstructured frHMGB1 regions potentially recognize the same CXCL12 surface, which behaves as a structural hub for multivalent interactions. Notably, while previous NMR titrations suggested that the isolated HMG-boxes interact similarly with the dimerization surface of CXCL12 (Schiraldi et al., 2012), a preference for BoxA is apparent in the context of the tandem HMG-boxes, with the interaction surface mainly involving the two short helices of the HMG domain. Of note, the targeting of BoxA is in line with the ability of CXCL12 to preferentially recognize the reduced forms of Cys-22 and Cys-44 (Venereau et al., 2012). Moreover, our MST and NMR experiments show that, while dsHMGB1 is still able to bind to CXCL12, most likely via the acidic IDR, its affinity is starkly lower, thus confirming the important contribution of BoxA to the interaction. Privileged binding to BoxA is also in agreement with the equimolar stoichiometry of the heterocomplex suggested by both AUC and SAXS experiments.

## 6.4  Intrinsically disordered protein regions (IDRs) – the neglected modulators of cellular function and their contribution to fuzzy interactions

IDRs within their host proteins are often the major players in the recognition of their partners (Bugge et al., 2020, Uversky, 2019, Arbesú et al., 2018) and they are generally characterized by low complexity sequences, often containing charged residues (Arbesú et al., 2018). In several cases IDRs maintain a significant level of disorder in their bound states, exchanging between multiple conformations and giving rise to so-called fuzzy complexes (Tompa and Fuxreiter, 2008, Ahmed and Forman-Kay, 2022, Waudby et al., 2016). To be specific, each bound-state configuration of a fuzzy protein complex is structurally and functionally relevant and necessary to describe the biological activity of the entire complex (Tompa and Fuxreiter, 2008). While protein-protein interactions were categorized and defined as distinct structural phenomena, being either static or dynamic disordered, nowadays a paradigm-shift towards a continuous spectrum of binding modes involving structural disorder is observed and covered by the umbrella term of fuzziness. In static disorder, a region of a protein might adopt

multiple stable conformations, whereas a protein, or a region of a protein, that constantly fluctuates between a large number of states, can be best described as a conformational ensemble (Tompa and Fuxreiter, 2008). The disorder in that case is dynamic. In fuzzy interactions, the dynamic rearrangement of bound complex states occur in time scales that are faster than the time scales of complex dissociation. Examples of static and dynamic fuzzy complexes are the MEEVD peptide of molecular chaperone Hsp90 in binding to the Tetra-trico-peptide repeat (TPR) domain found in numerous proteins (Cliff et al., 2006) and the SP1 transcription factor in complex with TATA-box-binding protein (TBP) in the TFIID complex (Gill et al., 1994), respectively. The structural plasticity and ability of IDRs allows them to engage in fuzzy interactions rendering them well-suited to favour the formation of biomolecular condensates through LLPS (Fuxreiter, 2020), where specific interactions can be established without a clearly defined bound-state conformation (Ahmed and Forman-Kay, 2022). Moreover, their conformational malleability allows IDRs to engage with various partners and in different cellular conditions, thus broadening the interaction scopes of their host protein (Miskei et al., 2017). Collectively, our data reveal that the frHMGB1•CXCL12 heterocomplex behaves as a typical fuzzy complex (Tompa and Fuxreiter, 2008), whose formation relies on an intricate network of inter- and intramolecular interactions of comparable affinities. As commonly observed in fuzzy binding, at least one of the elements, in this case the acidic IDR, is dynamic, maintains its conformational flexibility in the bound state and is fundamental for the interaction (Mittag et al., 2008, Sharma et al., 2015). In addition, the intrinsic independent rotation of the two HMG-boxes provides an additional dynamic level to the system. Thus, the heterocomplex cannot be described by a unique structure, but is best represented by a heterogeneous ensemble of structures reflecting the different ongoing equilibria. Accordingly, the SAXS data of the heterocomplex are best fit by different plausible docking models obtained by EOM, where CXCL12 binds frHMGB1 in a promiscuous manner, alternatively associating to the manifold conformations of the acidic IDR and the different BoxA orientations.

## 6.5 A new proposed structural model for the fuzzy CXCL12•frHMGB1 heterocomplex

Based on our data, we propose a model (Figure 6.1, top) in which the acidic IDR works as an antenna that recruits CXCL12 through long-range electrostatic interactions. Being intrinsically disordered, the acidic IDR does not present a single binding site to CXCL12 but rather resembles a diffuse binding cloud, in which multiple nearly-identical binding sites are dynamically distributed (Uversky, 2013, Borg et al., 2007), preserving a significant flexibility even in bound states. This behaviour is reminiscent of the mean electrostatic field created by multiple phosphates between the disordered yeast cyclin-dependent kinase (CDK) inhibitor Sic1 and its cognate binding partner, the F-box protein Cdc4 (Mittag et al., 2008). The rapid on-off rate usually associated to long-range electrostatic interactions allows then CXCL12 to interact with

HMG-boxes, in particular with BoxA in its reduced form, partially outcompeting HMGB1's intramolecular contacts. Remarkably, the binding mode of frHMGB1 to CXCL12 radically differs from the usual beta-beta or alpha-beta interactions observed in chemokine heterocomplexes (Miller and Mayo, 2017).
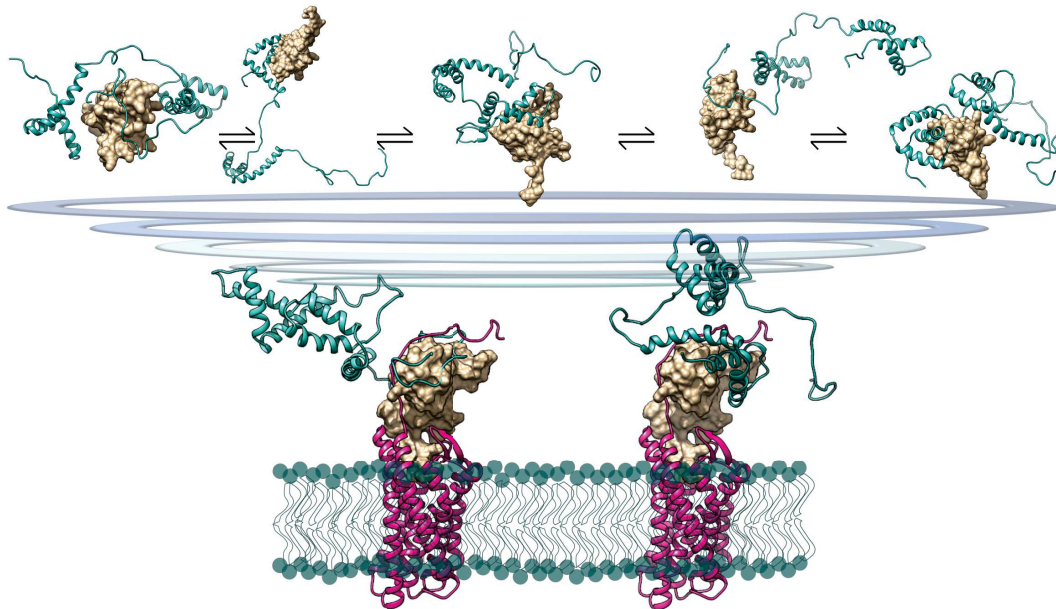


**Figure 6.1:** *New proposed structural model of the CXCL12•frHMGB1 heterocomplex. Combining our integrative structural approach with cell-based interaction studies, we propose a model of a heterogeneous ensemble CXCL12•frHMGB1 complexes.*

## 6.6 Role of the acidic IDR in the ternary complex in the cellular context

The CXCL12•frHMGB1 heterocomplex elicits an amplifying effect on the CXCL12/CXCR4 axis by binding exclusively to CXCR4. The question on how HMGB1 increases the efficiency of CXCL12 in the activation of CXCR4 for enabling enhanced signalling and surface retention requires an atomistic description of the heterocomplex involving the receptor. Our data already indicate that the acidic IDR may not only recruit CXCL12 for complex formation with HMGB1, but also promote the recognition process between CXCL12 and CXCR4 through a ternary complex. Indeed, proximity ligation assays (PLA), used to localize protein complexes in cells, proved the existence of the CXCL12•frHMGB1 complex on CXCR4-overexpressed cells and demonstrated higher CXCL12•frHMGB1 content on CXCR4 upon addition of CXCL12•frHMGB1 compared to the content of heterocomplex detected in titrations with CXCL12•frHMGB1-TL (Mantonico et al., 2024). This implies that CXCL12 bound

to frHMGB1 can accommodate inside the cradle formed by the transmembrane helices of CXCR4, yielding a three-component complex (Figure 6.1), whose existence on the cell surface is supported by PLA experiments. These results are in line with the observation that the HMGB1•CXCL12 heterocomplex acts differentially from CXCL12 alone on the reorganization of the actin cytoskeleton and on β-arrestin recruitment (D'Agostino, Cecchinato, and Uguccioni, 2018). Both actions depend on CXCR4. So far, however, our data do not specify whether a specific subset of the conformations of the HMGB1•CXCL12 heterocomplex preferentially binds to CXCR4. In our cellular context, the acidic IDR facilitates the binding of the frHMGB1•CXCL12 heterocomplex to CXCR4, and Ac-Pep does compete with it, confirming the results obtained by NMR, and implying that the acidic IDR plays a major role in the formation of the CXCR4•frHMGB1•CXCL12 ternary complex as well. The fuzziness of the interactions in the frHMGB1•CXCL12 heterocomplex forces us to reconsider the structure of HMGB1, which itself can be considered fuzzy: in solution HMGB1 populates an ensemble of different micro-states in which the D/E repeats are associated through electrostatic transient interactions with different segments of HMGB1, that in turn are partially screened and only transiently exposed to natural interactors (Wang et al., 2021). Plausibly, the fuzzy conformation of HMGB1 allows interactions with multiple partners (Bianchi, 2009), all of which have micromolar-range apparent affinities. Indeed, HMGB1 often works as a chaperone, by binding one interactor and facilitating its further interaction with another molecule (Agresti et al., 2005, Celona et al., 2011, Agresti and Bianchi, 2003). As such, the mechanism and the conformational heterogeneity through which HMGB1 binds to CXCL12 is in part reminiscent of other chaperones, like small heat shock proteins, that exploit their large IDR to transiently interact with their clients (Clouser et al., 2019).

## 6.7 Conclusion and future perspective for therapeutic targeting of the CXCL12•frHMGB1 complex

In brief, we show here that frHMGB1 and CXCL12 form a bimolecular heterocomplex, which is fuzzy and highly dynamic, and can go on to form a ternary complex with the CXCR4 receptor. These conclusions are in line with the concepts of HMGB1 working as a molecular chaperone and of IDPs/IDRs being typically involved in signaling, regulation, recognition, and control of various cellular pathways (Wright and Dyson, 2015). Finally, recent studies have revealed that inhibiting heterophilic interactions among chemokines interactions can reduce inflammation (Von Hundelshausen et al., 2017). Consequently, targeting these protein-protein interactions is emerging as a valuable strategy for developing selective antagonists to finely modulate specific inflammatory responses. This holds true also for the frHMGB1•CXCL12 heterocomplex, a key regulator of inflammatory cell recruitment via the CXCR4 axis, making it an attractive target for selective anti-inflammatory agents. Indeed, previous research has demonstrated that HMGB1•CXCL12 is druggable exploiting specific pockets within HMGB1 and CXCL12 (De Leo et al., 2019). As the targeting of IDR and IDPs is starting to emerge as

a pharmacological strategy (Tsafou et al., 2018), we anticipate that interfering with the fuzzy interactions within the HMGB1•CXCL12 heterocomplex could represent an additional opportunity to inhibit its detrimental activity in inflammatory conditions.

Our structural studies of the complex CXCL12•frHMGB1 led to the discovery of the first *fuzzy* chemokine heterocomplex. Besides providing a new interaction mode of chemokine heteromers, our work highlights the importance of IDRs of proteins and IDPs in complex with chemokines. Our findings exemplifies a *fuzzy* chemokine heteromer leading to reconsiderations of other CXCL12 as well as other chemokine heterocomplexes in general. One example is the heterodimer of CXCL12 with Galectin-3 (Gal-3), a member of carbohydrate-binding proteins, known as galectins (Eckardt et al., 2020a). Interestingly, Gal-3 is unique among galectins, as it has a relatively long N-terminal tail (NT) attached to the carbohydrate recognition domain (CRD). So far, only the CRD of Gal-3 has been considered in the binding to CXCL12. Given the evidence that the N-terminal domain of Gal-3 is structurally disordered and involved in the biological function of Gal-3 including in the formation of functionally relevant biomolecular condensates (Voss and Wang, 2023), Gal-3 may undergo as well *fuzzy* interactions with CXCL12.

Thus, the chapter of *fuzzy* chemokine heteromers is just the beginning of embracing structurally diverse and dynamic binding partners of chemokines and their role in the chemokine interactome.

# Chapter 7

# Materials and Methods

## 7.1 Protein Production and Peptide Synthesis

### 7.1.1 Expression and Purification of HMGB1 and HMGB1-TL

Recombinant labelled and unlabelled ($^{15}$N/$^{13}$C) HMGB1 (uniprot code P63159, residues 2–215) and HMGB1-TL (uniprot code P63159, residues 2–188) were transformed in pLysS BL21 (DE3) and BL21 (DE3) strains of Escherichia coli, respectively, using the pETM-11 expression vector (EMBL, Heidelberg, DE). Cells were grown at 37°C until the optical density at 600 nm reached 0.8 absorbance units. Gene expression was induced by the addition of isopropyl β-D-1-thiogalactopyranoside (IPTG) to a final concentration of 0.5 mM. After 18 h of incubation at 25°C with shaking, cells were harvested by centrifugation. The cells were resuspended in lysis buffer (20 mM Tris–HCl pH 8.0, 150 mM NaCl, 10 mM imidazole, 2 mM β-mercaptoethanol, 0.2% NP-40, Complete EDTA-free protease inhibitor (Roche), 2 μg/ml DNase, 20 μg/ml RNase, 1mg/ml lysozyme) and lysed by sonication. Cell debris was removed by centrifugation at 11,000 g for 45 min at 4°C. The soluble 6His-tagged proteins were purified from the supernatant by affinity chromatography using Ni$^{2+}$-NTA agarose resin (Qiagen, Hilden, Germany). After several washing steps, proteins were eluted in 20 mM Tris pH 8.0, 150 mM NaCl, 300 mM imidazole pH 8.0, and 2 mM β-mercaptoethanol. The 6His-tag was removed by overnight incubation at 4°C with TEV protease. During incubation, the sample was dialyzed against 20 mM Tris pH 8.0, 150 mM NaCl, 2 mM β-mercaptoethanol. Uncleaved 6His-tagged protein and TEV protease were then removed by repassing the sample over Ni$^{2+}$-NTA resin. frHMGB1 was further purified on a HitrapQ ion-exchange column using buffer A (20 mM Tris pH 8, 25-50 mM NaCl, 2 mM β-mercaptoethanol) and buffer B (20 mM Tris pH 8, 1 M NaCl, 2 mM β-mercaptoethanol) to create a linear gradient of NaCl. frHMGB1 elutes at 500 mM NaCl. frHMGB1-TL was purified by gel filtration on a Superdex-75 column (Amersham Biosciences, Milan, Italy) equilibrated in 20 mM phosphate buffer (pH 7.3), 150 mM NaCl, and 1 mM dithiothreitol (DTT). For MST experiments, the 6His-tag was not removed. Uniformly $^{15}$N labelled samples were prepared using M9 minimal bacterial growth media appropriately supplemented with $^{15}$NH$_4$Cl. dsHMGB1 and dsHMGB1-TL were obtained by extensively dialyzing their fully reduced forms against a buffer devoid of DTT (volume ratio sample:buffer 1:2000), changing the buffer every 2 hours overday, followed by an overnight dialysis. To reach the fully

oxidized state, the samples were incubated at 4°C for 72 hours, before NMR and MST analysis. The oxidation status of HMGB1 constructs was checked by $^1$H-1D NMR monitoring the aliphatic spectral region, which displays distinctive features for the oxidized and reduces forms. Protein concentrations were determined considering molar extinction coefficients at 280 nm of 21,430 M$^{-1}$ cm$^{-1}$ for HMGB1 (and HMGB1-TL).

### 7.1.2 Expression and Purification of Ac-pep$_{rec}$

Recombinant Ac-pep (Ac-pep$_{rec}$) (corresponding to the HMGB1 acidic IDR, 30 aa, uniprot code P63159, residues 186-215) was produced as 6His-SUMO3 tagged fusion protein using the pETM11-SUMO3 expression vector (EMBL, Heidelberg, DE). Cloning was performed by GENEWITZ from Azenta Life Sciences. Expression was carried out in BL21 (DE3) E.coli cells by induction at 30°C for 18 hours with 0.5 mM Isopropyl-$\beta$-D-1-thiogalattopiranoside (IPTG). Cells were harvested by centrifugation (8,000 rpm, 4°C) and lysed by sonication in Lysis Buffer (150 mM NaCl, 20 mM Tris-HCl pH 8.0, 0.2% NP-40, 2 mM $\beta$-mercaptoethanol (BME), Complete EDTA-free protease inhibitor (Roche), 2 $\mu$g/mL DNAse, 20 $\mu$g/mL RNAse). The 6His-SUMO3-tagged protein was purified on a histidine affinity column (Ni-NTA agarose, Quiagen) and eluted with Elution Buffer (150 mM NaCl, 20 mM Tris-HCl pH 8, 2 mM BME, 300 mM imidazole). The 6His-SUMO3 tag was cleaved during overnight dialysis at 4 °C against Dialysis Buffer (20 mM Tris-HCl pH 8, 150 mM NaCl, 2 mM BME, 5% glycerol) by addition of 6His-tagged Small Ubiquitin-Related Modifier (SUMO)-Specific Protease 2 protease (SENP2, homemade). 6His-SUMO3 tag and 6His-SENP2 were then separated from the digested Ac-pep$_{rec}$ by a second purification step on a Ni-NTA column. The peptide (having a serine at the N-terminus, deriving from cloning) was further purified on an HiTrap Q HP anion exchange chromatography column (Cytiva) using buffer A (20 mM Tris-HCl pH 8.0, 50 mM NaCl) and a slow linear gradient (3 ml/min flow, 15 column volumes) of buffer B (20 mM Tris-HCl pH 8, 1 M NaCl). The purified peptide was dialyzed against Milli-Q, lyophilyzed and resuspended into NMR buffer (20 mM NaH$_2$PO$_4$/Na$_2$HPO$_4$ pH 6.3, 20 or 150 mM NaCl). The peptide identity was confirmed by mass spectroscopy. Peptide concentration was determined using the absorbance at 205 nm and the molar extinction coefficient at 205 nm (83,400 M$^{-1}$ cm$^{-1}$). Uniformly labelled $^{15}$N and $^{15}$N/$^{13}$C Ac-pep$_{rec}$ was produced by growing BL21 (DE3) E.coli cells in M9 minimal medium containing $^{15}$NH$_4$Cl, with or without $^{13}$C D-glucose.

Synthetic Ac-pep (corresponding to HMGB1 acidic IDR, 30 aa, uniprot code P63159, residues 186-215, renumbered from 185 to 214) was purchased from Caslo Lyngby, Denmark. Synthetic Ac-pep fragments corresponding to residues 185-195 (Ac-pep185-195) and residues 204-214 (Ac-pep204-214) and the synthetic peptide corresponding to the arginine rich tail present in an aberrant HMGB1 form (Mensah et al., 2023) (R$_{185}$RKMRKMKRMRRRRKMKKMK-MKKKMKKMNK$_{214}$, whereby M$_{210}$-M$_{211}$ where mutated into lysines to avoid possible aggregation problems deriving from four consecutive methionines) were purchased from Davids Biotechnologie GmbH (Germany). Peptide purity (>95%) was confirmed by HPLC and mass

spectrometry. Peptide concentration was estimated from its dry weight. For ITC measurements with Ac-pep, to obtain a more accurate estimation of the concentration by UV a tyrosine $\epsilon_{274nm}$ = 1,405 M$^{-1}$ cm$^{-1}$. For MST experiments 5,6 FAM was added at the peptide N-terminus.

### 7.1.3 Expression and Purification of CXCL12 and CXCL12-LM

Recombinant labelled and unlabelled $^{15}$N/$^{13}$C CXCL12 (uniprot code P48061, residues 23–89, renumbered from 1–68) and CXCL12-LM were transformed into E. coli strain BL21 (DE3) using the expression vector pET30a. The plasmid of CXCL12 was transformed into E.coli BL21(DE3) and cells were grown at 37°C in Luria-Bertani medium. CXCL12 expression was induced by the addition of isopropyl-$\beta$-D-thiolgalactopyranoside (IPTG) at a final concentration of 1 mM when cultures reached an optical density of 2.2 at 600 nm. Induced cultures were grown for an additional 4.5 h at 37°C, harvested by centrifugation at 6,000 g, and stored at -80°C until further processing. The cell pellets were resuspended in 20 ml buffer containing 50 mM TrisHCl (pH 8), 100 mM NaCl, 1 mM EDTA, 5 mM DTT, 0.1 mg DNAse, 0.1 mg RNAse, and 5 mg lysozyme. The resuspended cells were lysed by sonication pulsed 1 s on and 1 s off for 2 min at 60% power. The inclusion bodies were washed twice with buffer containing 50 mM TrisHCl (pH 8), 100 mM NaCl, 1 mM EDTA, and 5 mM DTT, and finally with 50 mM TrisHCl (pH 8), 100 mM NaCl, 1 mM EDTA, 5 mM DTT, and 0.1% Triton X100, followed by solubilization in buffer supplemented with 6 M Guanidinium HCl and 50 mM HEPES pH 6.5 overnight at room temperature. The solubilized fraction was cleared by centrifugation at 17,000 g at 4°C for 30 min and diluted dropwise into refolding buffer containing 50 mM TrisHCl pH 8, 50 mM NaCl, 0.1 mM reduced glutathione, and 0.1 mM oxidized glutathione in a sample:buffer volume ratio of 1:12 and kept overnight at 4°C with stirring. Prior to chromatography, the protein solution was centrifuged at 17,000 g for 30 min. CXCL12 was purified by cation-exchange chromatography using a SP Sepharose resin (SP Sepharose HP, GE Healthcare Bioscience AB, Uppsala, Sweden). The protein was washed with buffer A, supplemented with 50 mM TrisHCl pH 8 and 50 mM NaCl, and eluted with buffer B, containing 50 mM TrisHCl pH 8 and 2 M NaCl. CXCL12 was finally dialysed against the desired experimental buffer.

For the production of CXCL12-LM, site-directed mutagenesis was performed to introduce mutations L55C and I58C in CXCL12 pET30a expression vector by using standard overlap extension methods. The following oligo primers were used:

L55C forward (5'→3'): GGTGTGTATTGATCCGAAATGTAAATGGATTCAGGAATACC

L55C reverse (3'→5'): GGTATTCCTGAATCCATTTACATTTCGGATCAATACACACC

I58C forward (5'→3'): GATCCGAAACTGAAATGGTGTCAGGAATACCTGGAAAAAGC

I58C reverse (3'→5'): GCTTTTTCCAGGTATTCCTGACACCATTTCAGTTTCGGATC

CXCL12-LM was then expressed and purified as described for CXCL12. Uniformly $^{15}$N- and $^{13}$C-$^{15}$N-labelled CXCL12 and CXCL12-LM were expressed by growing E. coli BL21 (DE3)

cells in minimal bacterial medium containing $^{15}NH_4Cl$, with or without $^{13}C$-D-glucose as sole nitrogen and carbon sources. Unlabelled N-terminal-6His-tagged CXCL12 for MST measurements was provided by HMGBiotech (Milan, Italy). Protein concentrations were determined by UV absorbance at 280 nm with molar extinction coefficients of 8,730 and 8,855 $M^{-1}$ $cm^{-1}$ for CXCL12 and CXCL12-LM, respectively.

## 7.2   Nuclear Magnetic Resonance Spectroscopy

NMR experiments were performed at 298 K on a Bruker Avance 600 MHz equipped with inverse triple-resonance cryoprobe and pulsed field gradients (Bruker, Karlsruhe, Germany). Typical sample concentration was 0.1–0.4 mM. Data were processed using Topspin 3.6 (Bruker) and analyzed with CCPNmr Analysis 2.4 (Vranken et al., 2005). The $^{1}H$, $^{13}C$, $^{15}N$ chemical shifts of CXCL12 in the presence of Ac-pep and of CXCL12-LM were obtained from three-dimensional HNCA, CBCA(CO)NH, CBCANH, HNCO experiments.

### 7.2.1   Titrations

Before NMR titrations the samples were typically dyalized against the same buffer 20 mM $NaH_2PO_4/Na_2HPO_4$ pH 6.3, 20 mM NaCl (or 150 mM when explicitly stated), supplied with 0.15 mM 4,4-dimethyl-4-silapentane-1-sulfonic acid (DSS) and $D_2O$ (10% v/v). Of note, HMGB1 upon removal of DTT maintained its thiol form for at least 12 hours. In the case of titrations with synthetic peptides the lyophilized peptides were dissolved directly in the NMR buffer, where necessary the pH was adjusted with 0.1 M NaOH. Titrations were carried out by adding to $^{15}N$ labelled protein samples (typically 0.1 mM) small aliquots of concentrated (15 mM) peptide stock solutions or unlabelled protein (0.6-1 mM). For each titration point (typically 0.5, 1, 1.5, 2 equivalents of ligand) a 2D water-flip-back $^{15}N$-edited HSQC spectrum was acquired with 2048 (160) complex points, apodized by 90° shifted squared (sine) window functions and zero filled to 2048 (512) points for $^{1}H$ ($^{15}N$). The Spectra were assigned by following individual cross-peaks throughout the titration series. For each residue the weighted average of the $^{1}H$ and $^{15}N$ chemical shift perturbation (CSP) was calculated as:

$$CSP = \frac{\sqrt{(\delta\delta H)^2 + (\delta\delta N)^2/25}}{2} \qquad (7.1)$$

, where $\delta\delta^{1}H$ and $\delta\delta^{15}N$ are, respectively, the differences of $^{1}H$ and $^{15}N$ chemical shifts between free and bound protein. The corrected standard deviation ($\sigma_0$) was calculated as described(ref). Because of extensive line broadening due to ligand binding in the intermediate exchange regime on the NMR time scale, we also monitored changes in the intensity ratio $\frac{I}{I_0}$ of the $^{1}H$-$^{15}N$ amide resonances, where $I_0$ and I are the peak intensities in the free and bound protein, respectively. The errors in peak intensities were calculated by error propagation, expressed as:

$$\Delta E_{prop} = \sqrt{\left(\frac{SD_{I_0}^N}{I_0}\right)^2 + \left(\frac{SD_I^N}{I}\right)^2} \tag{7.2}$$

, where $SD^N$ is the standard deviation of mean of the noise intensity values of the corresponding HSQC spectra.

### 7.2.2 Lineshape analysis

2D NMR lineshape analysis was performed using the software TITAN 1.6 (Waudby et al., 2016). Spectra were processed with NMRpipe 10.9 (Delaglio et al., 1995) with a script provided by TITAN 1.6. A series of regions of interest (ROI) containing isolated peaks with CSPs > AVG + SD were selected (V18, V23, K24, H17, A40, H25 and R12 for $^{15}$N CXCL12 and V23, K24, H25 for $^{15}$N CXCL12-LM) (Figure x) and fitted by optimizing the chemical shifts and line widths for the free and the bound state. The program estimates $K_D$, $k_{off}$ (set at 1:1 stoichiometry). Error estimates for the fit parameters were obtained using the bootstrap resampling of residuals procedure implemented in TITAN 1.6.

### 7.2.3 Heteronuclear NOE

The $\{^1H\}$-$^{15}$N NOEs were measured recording HSQC spectra with and without proton saturation in an interleaved fashion using a 6 seconds recycle delay/saturation. Values of $\{^1H\}$-$^{15}$N NOE were obtained by means of the CcpNmr2.4 fitting routine (Vranken et al., 2005) and scripts. The standard deviation of the noise ($SD^N$) of both saturated and unsaturated spectra were used to estimate the uncertainty of $I_{sat}/I_{unsat}$ via error propagation:

$$\Delta Err_{prop} = \sqrt{\left(\frac{SD_{unsat}^N}{I_{unsat}}\right)^2 + \left(\frac{SD_{sat}^N}{I_{sat}}\right)^2} \tag{7.3}$$

### 7.2.4 Relaxation

Measurements of heteronuclear $\{^1H\}$-$^{15}$N Nuclear Overhauser (NOE) enhancement, longitudinal and transversal $^{15}$N relaxation rates ($R_1$, $R_2$) on free $^{15}$N Ac-pep (0.15 mM) and in the presence of CXCL12 (1:1) were performed using standard $^1$H–$^{15}$N HSQC spectra with varying relaxation delays. Duty-cycle heating compensation were used for both $T_1$ and $T_2$ relaxation experiments (Farrow et al., 1994). $T_1$ and $T_2$ decay curves were sampled at 10 and 9 different time points respectively ($T_1$ in ms: 50*, 150, 250*, 450, 650, 900, 1100, 1400, 2000, 3000 and $T_2$ in ms: 12*, 28, 44, 56, 72, 112*, 144, 200, 244; with the stars denoting duplicate delay measurements) collected in random order, with 4 seconds recovery delay. $T_1$ and $T_2$ values were obtained from CcpNmr2.4 fitting routine (Vranken et al., 2005) and internal scripts. Values of $R_1$ and $R_2$ were calculated from $T_1$ and $T_2$ values using the following equation:

$$\frac{R_2}{R_1} = \frac{\langle T_1 \rangle}{\langle T_2 \rangle} \qquad (7.4)$$

Error bars were calculated by error propagation of the standard deviation of the means $\langle T_1 \rangle$ and $\langle T_2 \rangle$ derived from relaxation data with duplicate delays.

$$\Delta Err_{prop} = \sqrt{\left( -\frac{SD_{T_1}}{\langle T_1 \rangle^2} \right)^2 + \left( -\frac{SD_{T_2}}{\langle T_2 \rangle^2} \right)^2} \qquad (7.5)$$

## 7.3   Isothermal Titration Calorimetry

Proteins and peptides were dialyzed in a Slide-A-lyser mini-dialysis unit with a 2,000 MWCO and Biodialyzer with 500 Da MWCO (Harvard Apparatus, US) against 20 mM TrisHCl at pH 7.5, 50 mM NaCl (or 150 mM NaCl when explicitly stated). ITC data were collected on a MicroCal PEAQ-ITC instrument (Malvern). The cell temperature was set to 37°C, the syringe stirring speed to 750 rpm, reference power 10 $\mu$cal/sec. FrHMGB1 (frHMGB1-TL, Ac-pep) and CXCL12 were loaded into the cell and syringe at concentrations of ca. 10 and ca. 600 $\mu$M, respectively. The MicroCal PeakITC software (Malvern) was applied for initial data analysis. For global fitting, thermograms were integrated using NITPIC (Keller et al., 2012) and SED-PHAT (Houtman et al., 2007). Data were fitted with the two non-symmetric sites microscopic K model (Brautigam, 2015b) applying Simplex and Marquardt-Levenberg optimization algorithms, as implemented in SEDPHAT. Error estimates were based on the covariance matrix generated by the Marquardt-Levenberg algorithm.

## 7.4   Microscale Thermophoresis

MST experiments were performed at 24°C on a NanoTemper(R) Monolith NT.115 instrument. Binding between Ac-pep and CXCL12 was monitored titrating CXCL12 (16-points) into 50 nM N-terminal-5,6-FAM-labelled Ac-pep (CASLO ApS, Denmark), using the blue filter, 20% LED power and medium MST power. Binding between frHMGB1, dsHMGB1 or frHMGB1-TL and CXCL12 was monitored titrating the different HMGB1 proteins (16-points) into 50 nM 6His-tagged CXCL12, non-covalently labelled with the NT-647 conjugated tris-NTA (RED-tris-NTA) fluorescence dye, using the red filter, 40% LED power and medium MST power. Before MST titrations the proteins (the ligand and the fluorescently labelled target) were dialyzed against the same buffer, 20 mM $NaH_2PO_4$/$Na_2HPO_4$ pH 7.3, 0.05% TWEEN and 20 mM or 150 mM NaCl. In the case of 5,6-FAM-labelled Ac-pep, the lyophilized peptide was dissolved directly in the MST buffer and the pH adjusted to pH 7.3.

The 16 titration points of each experiment were made through serial dilution of the ligand stock into MST buffer and then addition of a constant amount of fluorescently labelled target (50 nM). Before mixing, both the ligand and the fluorescently labelled target were centrifuged at

15,000 g, 4°C, for 10 minutes. Maximum concentrations of frHMGB1, frHMGB1-TL, dsHMGB1 and CXCL12 ligands in the titrations were 104-343 $\mu$M, 315 $\mu$M, 300 $\mu$M and 287-295 $\mu$M, respectively. Complex samples were incubated for 30 minutes before loading into NanoTemper premium capillaries. Each experiment was repeated three times, data points are the average of the triplicates and the error bars correspond to the standard deviation.

Since CXCL12 addition induced >10% variation in the fluorescence of 5,6-FAM-Ac-Pep, thermophoresis traces could not be used to measure binding affinity, we therefore used the quenching of the 5,6-FAM-Ac-Pep fluorescence upon binding to estimate the $K_D$. Data analyses were carried out using NanoTemper Analysis software and the $K_D$ model fitting (one binding site).

## 7.5 Analytical Ultracentrifugation

### 7.5.1 Sedimentation Velocity (SV)

Sedimentation velocity experiments were performed on an Optima XLI (Beckman Coulter) using an A50 Ti eight-hole rotor and with seven 400 µl samples in standard dual-sector Epon centerpieces equipped with sapphire windows. Absorbance data were acquired at 250 and 280 nm simultaneously with the absorbance scanner in the continuous mode with radial increments of 0.003 cm. Three assembled centrifugation cells containing, respectively, free CXCL12 (38.2 $\mu$M), frHMGB1 (15.6 $\mu$M), frHMGB1-TL (15.6 $\mu$M) and the frHMGB1:CXCL12 mixture at the loading ratios of 1:2.5, 1:5, 1:7.5 (with frHMGB1 or frHMGB1-TL at 7.8 $\mu$M concentration), pH 7.5, 20 mM TrisHCl, 50 mM NaCl (or 150 mM NaCl when explicitly stated), were equilibrated at 20°C under vacuum for approximately 1.5 hr prior starting the experiment. Subsequently, centrifugation was performed at 45,000 rpm with 90 scans. The highest protein concentration was determined by the absorbance for which the linear relationship according to Lambert-Beer Law was still guaranteed (O.D._max = 1.0). The buffer density and viscosity were estimated using SEDNTERP (Philo, 2023). c(s) Model: Sedimentation coefficient distributions at 280 nm of the single proteins were obtained by applying the diffusion-deconvoluted c(s) model, implemented in SEDFIT (Schuck, 2000b). Concentration profiles in terms of absorbance (a(r,t)) were modelled as the sum of Lamm Equation solutions scaled by a continuous distribution c(s) (details in Appendix C).

### 7.5.2 Multi-signal Sedimentation Velocity (MS-SV)

Multisignal sedimentation velocity (MS-SV) analysis (Brautigam, Padrick, and Schuck, 2013) was performed to determine the stoichiometry of the complex formed by frHMGB1 and CXCL12 (or CXCL12-LM). It is important to note that in MS-SV, like in c(s) model, the data are not fitted a priori to a binding stoichiometry model (e.g. 1:1 or 1:2) and no binding model assumption is made. The experimental sedimentation data, whose physical observable is absorbance, are fitted with mathematical equations (the Lamm equations) describing the sedimentation process without assuming any binding stoichiometry. The sedimentation process

is described as a superposition of normalized Lamm equation solutions of ideally sedimenting species at a range of sedimentation coefficients s(1... N), with N indicating the range of molecules size expressed as sedimentation coefficient in Svedberg and using the hydrodynamic scaling law to estimate the corresponding diffusion coefficients. The Lamm equation solutions once superimposed give the number of species, molecular weight and weight averaged shape. More in detail, in MS-SV the standard c(s) approach is modified to deconvolute the contributions of individual species in a component distribution $c_k(s)$ based on equation. As the molar extinction coefficients of frHMGB1 ($\epsilon_{280}$=20872.8 $M^{-1}$ $cm^{-1}$, $\epsilon_{250}$=7987.7 $M^{-1}$ $cm^{-1}$) and CXCL12 ($\epsilon_{280}$=9907.2 $M^{-1}$ $cm^{-1}$, $\epsilon_{250}$=4704.2 $M^{-1}$ $cm^{-1}$) or CXCL12-LM ($\epsilon_{280}$=8413.4 $M^{-1}$ $cm^{-1}$, $\epsilon_{250}$=4840.5 $M^{-1}$ $cm^{-1}$) delivered sufficient spectral discrimination with $D_{norm}$ >0.08 (for frHMGB1:CXCL12) and $D_{norm}$ >0.16 (for frHMGB1:CXCL12-LM), it was possible to use SEDPHAT to perform global multi-signal analysis of the sedimentation boundary associated to the co-sedimenting complex. MS-SV of the frHMGB1:CXCL12 (7.7 $\mu$M:43 $\mu$M) and frHMGB1:CXCL12-LM (6.9 $\mu$M:51 $\mu$M) heterocomplexes were collected at 250 nm and 280 nm and globally fitted using the multi-wavelength discrete/continuous distribution analysis with mass constraints in SEDPHAT (Brautigam, Padrick, and Schuck, 2013). Integration of the resulting $c_k(s)$ distributions revealed the content of each protein component under the peak at a given sedimentation value. Plots of the signal profiles, fits, residuals and the MS-SV results were generated using GUSSI (Brautigam, 2015a).

## 7.6   Small angle X-ray scattering

The experiments were performed at the ESRF bioSAXS beamline BM29, Grenoble, France at a detector distance of 2.869 m. CXCL12 and frHMGB1 were measured in batch mode at 20°C using the sample changer immediately after protein thawing and centrifugation (30 minutes at 16,000 g). 45 $\mu$L of sample solution at three different concentrations (1.95, 3.0 and 3.9 mg/mL per each protein, 20 mM Tris pH 7.5, 50 mM NaCl) were used. To characterize the frHMGB1•CXCL12 complex we tested the following protein molar ratio conditions: 1:1, 1:2, 1:4 and 1:6 (frHMGB1:CXCL12, with frHMGB1 1.95 mg/mL). After incubation and centrifugation, the supernatants were immediately measured in the SAXS beamline. Ten frames of 0.5 s each were collected for each sample (frHMGB1•CXCL12, free components at different protein concentration). Data from the frHMGB1 and CXCL12 dilutions were merged following standard procedures to create an idealized scattering curve, using PRIMUS within ATSAS 3.1.4 (Manalastas-Cantos et al., 2021)). The pair distribution function P(r) was calculated using GNOM (Svergun, 1992). Protein molecular masses were estimated using both Porod volume and scattering mass contrast methods. All the plots were generated using OriginPro (Version 2022, OriginLab Corporation, Northampton, MA, USA).

To model the CXCL12•frHMGB1 heterocomplex, we employed a multistep approach relying on complementary experimental knowledge (NMR and AUC). The SAXS curce of frHMGB1

in the presence of two equivalents of CXCL12 was used, as in this condition frHMGB1 is almost fully saturated and the contribution of free CXCL12 to the scattering signal is negligible (Mantonico et al., 2024). This SAXS curve was used to generate EOM a representative bound frHMGB1 starting structure for subsequent rigid docking on CXCL12 (PDB code: 2kee). In particular, two initial rigid docking models were generated. The first was obtained with SASREF (Petoukhov and Svergun, 2005) combining the solution scattering data and guiding docking of CXCL12 (residues 23–28 and 66–67) on frHMGB1 (residues 15–45), as suggested by NMR experiments. The second model was obtained docking CXCL12 (residues 23–28 and 66–67) onto HMGB1 acidic IDR performing a global search with FoXSDock (Schneidman-Duhovny et al., 2016). Next, to describe the dynamic and fuzzy nature of the heterocomplex, we fixed the protein-protein interaction surfaces obtained with SASREF47 and FoXSDock, and allowed the rest of frHMGB1 to explore a wide range of conformations using the EOM algorithm within ATSAS. Similarly, frHMGB1 alone was modelled using the EOM approach. The $\chi^2$ values of EOM fits over the q range from 0.1 to 3 nm$^{-1}$ of the experimental SAXS curves.

All SAXS data were deposited into SASBDB data bank (CXCL12, SASDB ID: SASDRG9); frHMGB1, SASDB ID: SASDRH9; frHMGB1•CXCL12, SASDB ID: SASDRJ9.

# Appendix A

# Appendix - Theoretical Background: NMR

## A.1 Theoretical Background

### A.1.1 Principle

Biomolecules are composed of atoms that primarily comprise the chemical elements carbon, oxygen, hydrogen, nitrogen, phosphor and sulphur. Each element exist in the form of different isotopes (nuclear species) with a non-zero nuclear spin (I > 0). Depending on the atom type, they create a magnetic dipole moment $\mu$, that is defined as:

$$\mu = \gamma \cdot I \qquad (A.1)$$

where $\gamma$ is the gyromagnetic ratio and I the spin angular momentum.

Once a protein sample is placed into a magnetic field of strength $B_0$, its nuclear spins align with the direction of the static magnetic field. A nuclear spin in general rotates about its own axis (spin property) in addition to its precession about the axis of the applied $B_0$ field. The frequency of this precession is referred to as the Lamor frequency, which is atom-specific and proportional to the strength of the magnetic field. The Lamor frequency $\nu_0$ is defined by:

$$\nu_0 = \gamma B_0 \qquad (A.2)$$

The associated energy proportional to $B_0$ and the magnetic dipole moment $\mu$ is expressed as:

$$E = -\mu \cdot B_0 \qquad (A.3)$$

For an angular momentum of $I = \frac{1}{2}$ , the nuclear spin adopts two different orientations, defined by the quantum mechanical definition of 2I + 1. As a result, two distinct energy levels, known as $\alpha$- and $\beta$-states are created and populated according to the Boltzmann distribution (Figure A.1). However, the small population difference in energy levels ($N(\alpha/\beta) \approx 10^{-4}$), makes NMR relatively insensitive compared to other methods, as the signal intensity is proportional to this difference. NMR requires therefore optimization of the signal-to-noise ratio. The NMR signal is only generated by transverse magnetization that is perpendicular to the
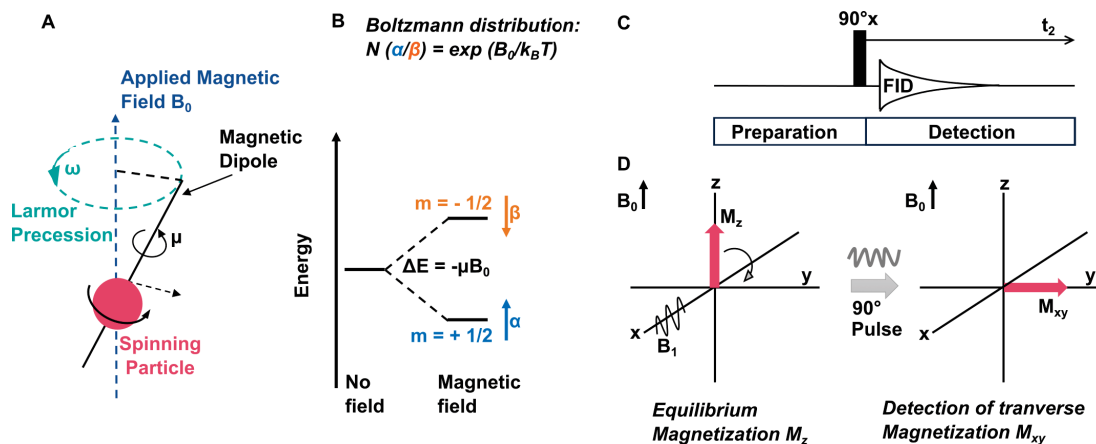
**Figure A.1: *Principle of NMR - the nuclear spin.*** *(A) Movement of a nuclear spin in applied magnetic field. (B) Energy state splitting for 1/2 nuclear spin in a magnetic field. (C) Net magnetization of nuclear spins at equilibrium state ($M_z$) and transverse magnetization ($M_{xy}$) generated after the 90° pulse.*

$B_0$ magnetic field with nuclear spins rotating with precession frequencies that have correlated phases. Thus, to detect transverse magnetization in the x,y-plane, the equilibrium state of the individual nuclear spins, whose precession frequencies are along $B_0$ and have uncorrelated phases, must be disturbed. This involves the application of a radiofrequency (RF) field called $B_1$ along the x- or y-axis perpendicular to the magnetic field $B_0$ that brings the spin precession in the transverse plane and correlates their phases. A typical 1D NMR consists of applying a 90° RF pulse , followed by the detection of the so-called free induction decay (FID) signal (pulse sequence scheme represented in Figure A.1 C). The final spectrum is generated by the Fourier transformation of the FID NMR signal in the time domain to the frequency domain.

### A.1.2    Two-dimensional Heteronuclear Single Quantum Coeherence (HSQC)

Two-dimensional (2D) spectra enable the observation of correlations between spins of the same kind of atoms (homonuclear) or between different atom types (heteronuclear). They are easier to interpret than 1D spectra due to the increased dispersion of NMR frequencies in space. Figure A.2 summarizes the acquisition of a 2D correlation experiment: A 2D spectrum is obtained by recording a set of 1D spectra, in which a delay time, known as evolution time ($t_1$), is systematically incremented (pulse sequence scheme in Figure A.2 A). The signal intensities of the 1D spectra, repeated at different delays, form an amplitude, whose Fourier transformation yields the frequency in the so-called indirect dimension (F1). The final 2D spectrum shows frequencies generated by the delay time in the indirect dimension (F1) against frequencies of the measured 1D spectra in the direct dimension (F2).

The $^1$H-$^{15}$N Heteronuclear Single Quantum Coherence (HSQC) experiment generates a spectrum that correlates the chemical shifts of the amide hydrogen and nitrogen in two dimensions, as shown in the schematic view in Figure A.2 C. The observed NMR-signals correspond to the different amino acids of the protein except for proline, which lacks a $^1$H-$^{15}$N amide couple.
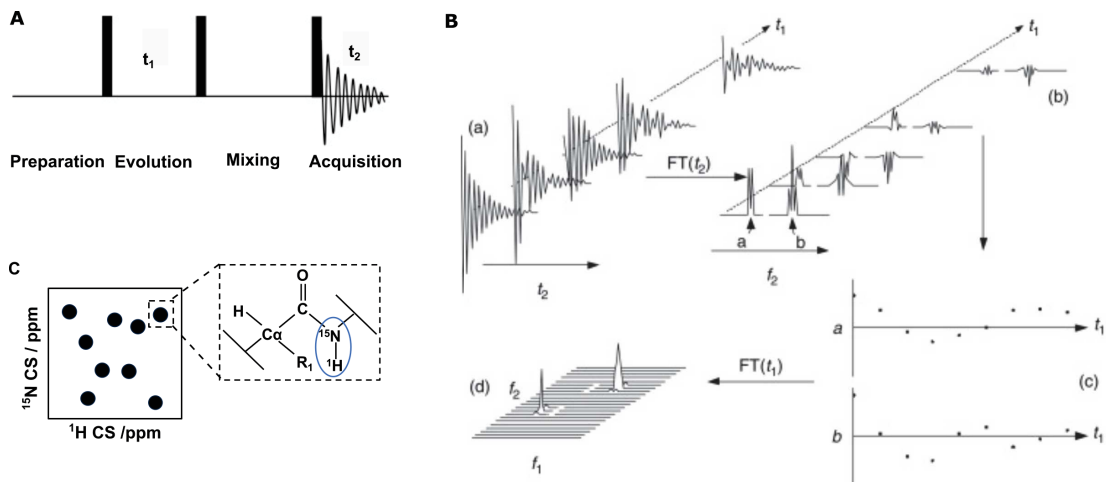
**Figure A.2:** *Schematic representation of the generation of a 2D NMR experiment.* *Figure reused with permission from Elsevier (license no. 5740200034360) from Rinaldi and Monwar, 2017 (A) Pulsse-quence to record a 2D spectrum. (B) Generation of a 2D spectrum. First, 1D spectra are acquired by recording the FID ($t_2$), then Fourier-transformed (FT($t_2$)) to obtain the spectrum in the frequency domain. The 1D spectra acquired at different evolution times differ in the signal intensity maxima that form the amplitude of the indirect dimension ($t_1$). The Fourier transformation of the $t_1$ (F($t_1$)) provides then the frequency of the indirect dimension. (C) A simplified scheme of a 2D $^1$H-$^{15}$N-HSQC spectrum. (D) Chemical shift perturbations related to the exchange rate of protein-ligand binding.*

The $^1$H-$^{15}$N-HSQC spectra can be used as a protein's fingerprint in providing information about its degree of folding, purity and oligomerization. Dispersed signals in the spectrum are indicative for folded proteins, while clustered NMR-peaks limited to the area between amide $^1$H chemical shifts of 8.0 and 8.5 ppm are diagnostic of random-coil like structures indicating disorder. The $^1$H-$^{15}$N-HSQC spectra are useful to monitor binding-induced changes of residue-specific amide frequencies of a $^{15}$N labelled protein during the titration with an unlabelled ligand. The resulting chemical shift perturbations (CSPs) in the form of peak displacement or line-broadening induced signal intensity reduction (intensity ratio of protein bound (I) and protein free ($I_0$)) are manifestations of changes in the electron environment of the nuclear spins due to direct binding or conformational rearrangements. CSPs and reduced $I/I_0$ peaks in the $^1$H-$^{15}$N HSQC spectrum indicate the backbone amide groups of the protein that are involved in ligand-binding or allosteric events and can be thus mapped on the structure of the protein to identify the perturbed regions. The free and bound state of a protein as well as different conformers show distinct HSQC peaks. The exchange rate between these states or between conformers determines the appearance of NMR signals, as shown in Figure A.3. Focusing on ligand-binding effects, the conversion of the protein free to bound upon ligand addition is in the simplest case described by a two-state reaction, where $k_{on}$ and $k_{off}$ are rate constants for the forward and reverse reactions, respectively. The sample contains three species: the protein, the ligand and the protein-ligand complex. The chemical exchange between these species is determined by the concentration of ligand, protein and complex as well as the dissociation constant ($K_D$) and the exchange rate of the reaction, $k_{ex}$, that are related as the following:

$$k_{ex} = k_{on}[L] + k_{off} \tag{A.4}$$

where the rate constants determine the population of the free protein, p(P), and bound protein, p(PL) at equilibrium:

$$p(P) = \frac{k_{off}}{k_{on}[L] + k_{off}} \tag{A.5}$$

and

$$p(PL) = \frac{k_{on}[L]}{k_{on}[L] + k_{off}} \tag{A.6}$$

The chemical exchange can be categorized into three timescales: slow, intermediate or fast depending on the magnitude of $k_{ex}$ relative to the chemical shift timescale of a given nucleus in P and PL. A slow exchange rate is much lower than the difference of the resonance frequencies between free and unbound state ($k_{ex} \ll \delta\omega$). Thus, a slow exchange between the free and bound state on the chemical shift time scale gives rise to two separate resonance peaks corresponding to the respective forms.
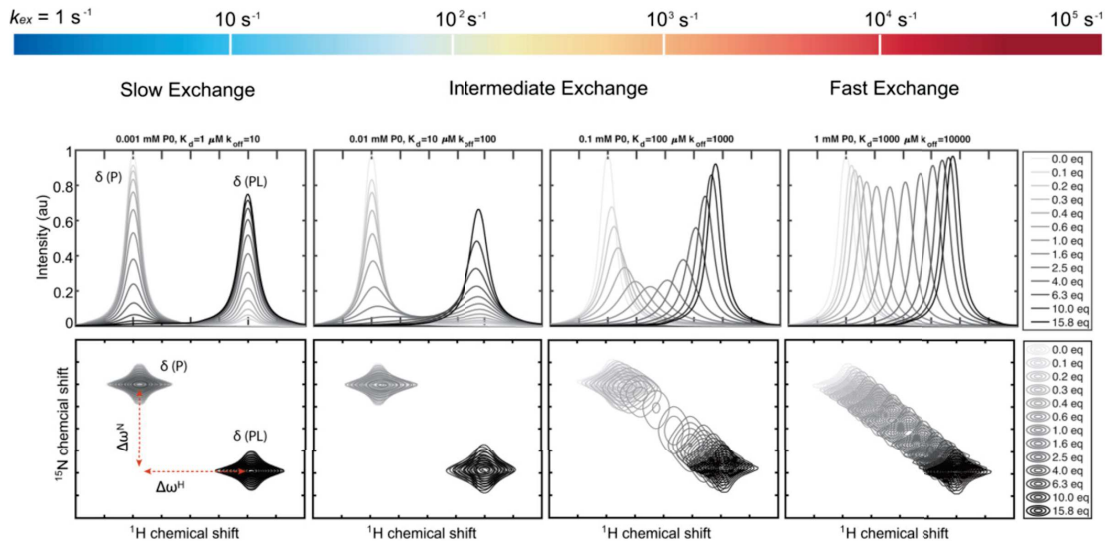


**Figure A.3:** *NMR quantification of binding events at different exchange regimes.* *Figure reused under the terms of the Creative Commons Attribution License from Teilum et al., 2017. Protein with added amounts of ligand ranging from 0 (light grey) to 15.8 (black) molar equivalents of ligand. Changing the exchange rate ($k_{ex}$) from slow to fast (left to right) compared to the difference in resonance between the free and bound states, changes the appearance of the spectra. In the slow exchange regime (left), the quantification will rely on either the peak intensities of the unbound protein or of the protein-ligand complex. In the fast exchange regime (right), the chemical shift of the observed peak will be a weighted average of the population of the two states, and thus, the binding constant can be readily determined from the chemical shift. In this case, quantification is feasible in both dimensions.*

The intermediate exchange regime can either appear as a fast-exchange accompanied with line-broadening or as one resonance with extensive line-broadening, where $k_{ex} \approx \delta\omega$.

At the fast exchange regime, the exchange rate is much greater than the chemical shift time scale ($k_{ex} >> \delta\omega$). A fast chemical exchange leads to a single resonance peak positioned at an average frequency between the two state populations that moves towards the bound state with increasing ligand-binding.

## A.1.3 Relaxation experiments: longitudinal and transverse relaxation rates $R_1$ and $R_2$, and steady state heteronuclear Overhauser effect (HetNOE)

The biological function of a protein can be deduced from both its atomic structure and dynamic behaviour. Solution NMR is a powerful tool to characterize the structure and dynamics of proteins by measuring structural transitions at broad timescales ranging from fast (ps-ns) to slow (μs-s) molecular motions (Figure A.4). Like any other molecules in solution, proteins undergo constantly global motions. They can translate and rotate, but also segments and specific residues can exhibit motions including fast atomic fluctuation, sidechain rotation, and large-scale local structural change.
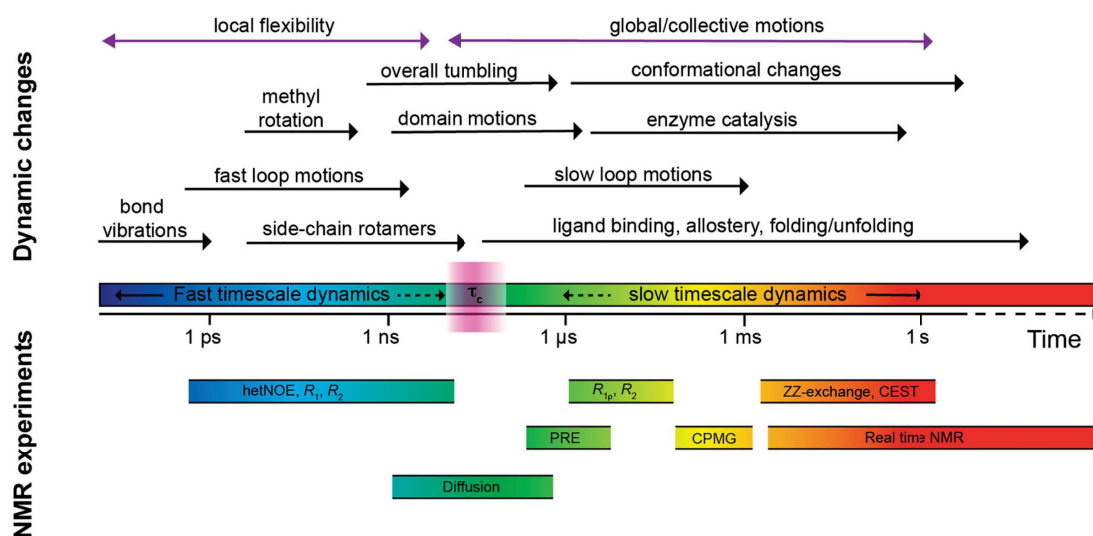


**Figure A.4: *NMR methods to discern protein dynamics at different time scales.*** *Figure reused under the terms of the Creative Commons Attribution license from Kawale and Burmann, 2021.*

The internal dynamics of a protein directly affects the process of nuclear spins returning to their equilibrium state after being perturbed by the RF pulse to generate detectable magnetization. This process is referred to as relaxation. The internal motions of the protein modulate local randomly fluctuating magnetic fields of its nuclear spins, which induce a variety of relaxation mechanisms including dipole-dipole interactions, chemical shift (shielding) anisotropy (CSA), quadrupolar interactions, and cross correlation. Thanks to the direct relationship between internal dynamics and relaxation, it is possible to quantify the internal motions of a protein's backbone and to measure the tumbling time, i.e. the time of a protein to complete a 360°

rotation, by means of $^1H$-$^{15}N$ relaxation experiments. Relaxation experiments consist of a series of 2D $^1H$-$^{15}N$ HSQC experiments recorded at different time delay increments. The acquired $^1H$-$^{15}N$ HSQC spectra display intensity changes of the backbone amide peaks of the protein as a result of relaxation. In most cases, the relationship between peak intensity and relaxation rate is exponential:

$$I(t) = I_0 \exp^{-Rt} \tag{A.7}$$

where I(t) is the peak height at delay time, t, $I_0$ is the initial peak height, and R is the relaxation rate. In other cases, the relaxation time dependence can more complicated (e.g. cross correlated relaxation in methyl groups) or simply derived from a steady-state value (e.g. the heteronuclear NOE). The observed relaxation processes are:

1. The spin-lattice or longitudinal relaxation ($T_1$ relaxation) that corresponds to the time of nuclear spins to re-establish the equilibrium distribution of the $\alpha/\beta$ states

2. The spin-spin or transverse relaxation ($T_2$ relaxation) that describes the time of the decay of transverse magnetization due to dephasing of spin precession frequencies (loss of the coherence).

Typically, three relaxation parameters are determined in $^{15}N$ relaxation experiments, which are the longitudinal relaxation rate $R_1$, the transverse relaxation rate $R_2$, as well as the heteronuclear steady state Nuclear Overhauser effect, $\{^1H\}$-$^{15}N$ HetNOE. To determine the rate of longitudinal and transverse relaxation $R_1$ and $R_2$, inversion recovery measurements of $T_1$ relaxation and spin-echo experiments of $T_2$ relaxation are performed (Figure A.5 B, C). The first applies a $180°$ pulse to invert the spin magnetization along $B_0$, followed by the acquisition at different time points t after the application of a $90°$ pulse. The latter applies $90°$ pulse to create transverse magnetization, that due to coherence loss of spin precession, diminishes, but is recovered by a $180°$ pulse that refocuses the spin precession to detect the FID signal. The $T_1$ curve is represented as a plot of longitudinal magnetization $M_z$ against the time t of acquisition showing a logarithmic profile (Figure A.5 A). The $T_2$ graph represents the transverse magnetization $M_{xy}$ as a function of time and reflects the exponential transverse magnetization decay, as illustrated in Figure A.5 B.

The Nuclear Overhauser Effect or NOE describes the phenomenon of an irradiated nucleus having an effect on another nucleus in close space that consequently manifests an increase or decrease of its signal intensity as a result of mutual interaction. The steady state approach in $\{^1H\}$-$^{15}N$ HetNOE relaxation experiments refers to the measurement of longitudinal polarization of a spin system at thermal equilibrium and under proton $^1H$ irradiation (Noggle, 2012). In general, irradiation of a specific nucleus saturates the population difference between all spin states. As a result, the net-magnetization along B0 is zero. In the $\{^1H\}$-$^{15}N$ HetNOE experiment, two NMR spectra are recorded: one at constant $^1H$-irradiation and another one without the selective $^1H$ irradiation. If there is cross relaxation between $^{15}N$ and $^1H$ nuclear spins, then the intensities of the unirradiated $^{15}N$ spin will be different and a NOE is observed (Figure A.5
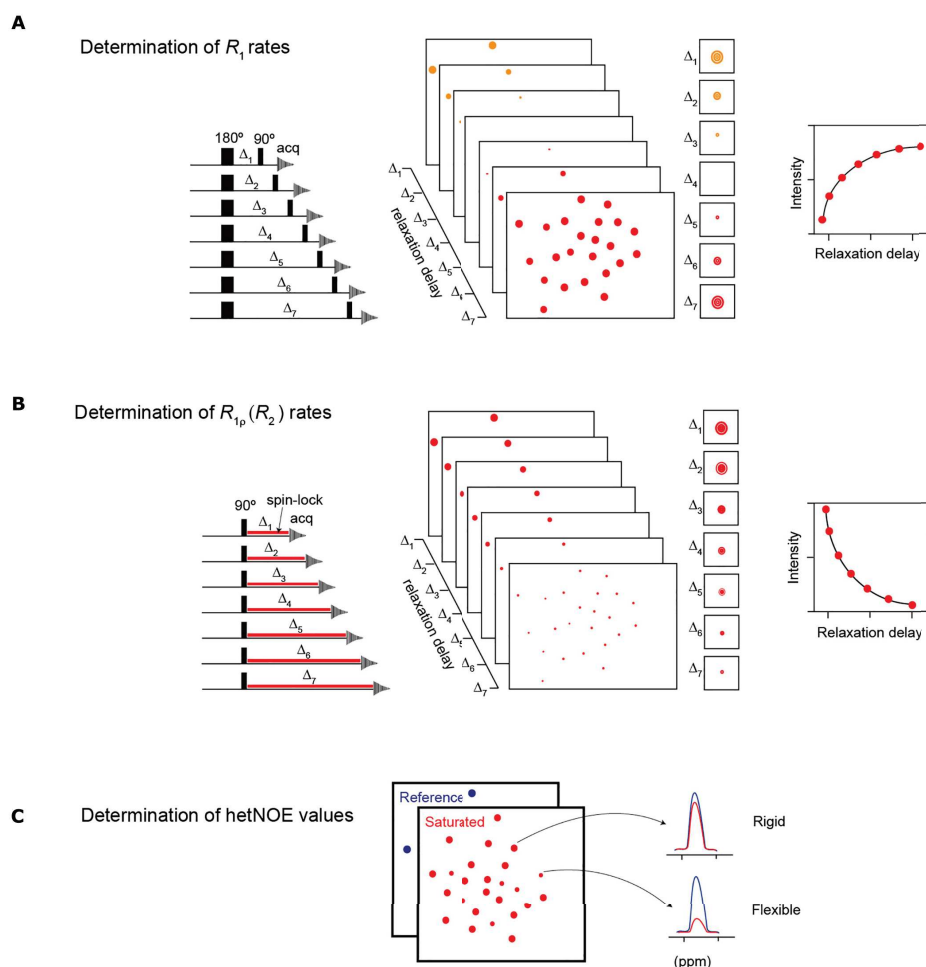
**Figure A.5:** ***Schematic work-flow representation protein backbone dynamics characterization*** *Figure reused under the terms of the Creative Commons Attribution License from source: Kawale and Burmann, 2021.*

C). The NOE in spectrum can be positive or negative depending on the sign of cross correlation rate in the motional time regime. A fast rotation of the protein will result in positive NOE values, while a slow tumbling protein will produce negative NOE values.

Overall, the relaxation parameters $R_1$, $R_2$, and HetNOE values provide insights into the (global) molecular tumbling, local backbone mobility, and local correlation times.

# Appendix B

# Appendix - Theoretical Background: ITC and MST

## B.1  Isothermal Titration Calorimetry (ITC)

ITC is a label-free quantification technique that directly measures the heat exchange during a chemical or biochemical reaction. The method is ideal for investigating ligand binding to biological macromolecules based on energetics (Freire, Mayorga, and Straume, 1990).

The typical set-up (Figure 3.1 A) consists of a calorimetric titration of a reagent, usually the ligand, into another reagent, the macromolecule at constant temperature and pressure. The heat exchange is detected by the created temperature difference between the sample cell, in which the binding reaction occurred, and the reference cell filled with buffer or water. To compensate the temperature difference, depending on the reaction type (exothermic or endothermic) the sample cell is either heated or cooled down to return the system to thermal equilibrium. This is achieved by a power supply that brings the power level to the constant baseline reference value. The ITC raw data consists therefore of power spikes plotted against the time, as shown in Figure 3.1 B. The integration of each spike quantifies the heat exchange per injection and is plotted against the added mole of ligand or against the molar fraction of ligand/macromolecule, represented in Figure 3.1 C. Bindings models are then fitted to the binding isotherm (Figure 3.1 C ) to derive the thermodynamic parameters that include the association and dissociation constant ($K_A$ and $K_D$) as a measure of binding affinity. The association constant ($K_A$) and stoichiometry (n) are respectively extracted from the slope and deflection point of the binding curve. From the thermodynamic perspective, the value of $K_A$ is associated with the free Gibbs energy ($\delta G$) and entropic contribution ($\delta S$) by the following relation:

$$\delta G = -RT \cdot lnK_A \qquad (B.1)$$

with $\delta G$ defined by the reaction enthalpy $\delta H$ and entropy $\delta S$ of the binding:

$$\delta G = \delta H \tilde{\ } T \cdot \delta S \qquad (B.2)$$

where R is the universal gas constant.
The value of $K_D$ and $K_A$ is defined by the concentrations of ligand, protein and complex. Given the relation:
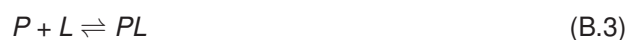
$$P + L \rightleftharpoons PL \tag{B.3}$$

the $K_D$ and $K_A$ are expressed as:

$$K_D = \frac{1}{K_A} = \frac{[P][L]}{[PL]} \tag{B.4}$$

where [P] and [L] are the concentrations of free protein and free ligand and [PL] is the concentration of the protein-ligand complex.

Under constant pressure the heat of reaction $\delta$Q is approximated to be equal to the reaction enthalpy $\delta$H, which represents the height of the hyperbolic shaped binding isotherm. The profile of the binding curve is modulated by the c-value that ideally should describe a hyperbolic curve (Figure 3.1 D, middle). Assuming a one-binding site model, the theoretical c-window for a hyperbolic shape is expressed as:

$$c = n \cdot K_A[titrand] = n \cdot \frac{[titrand]}{K_D} \tag{B.5}$$

where n is the number of ligands that bind the macromolecule that is usually the titrand or analyte. The inspection of the c-value is crucial to evaluate the accuracy of the determined apparent $K_D$ value. The c-value should be between 1 and 1000, ideally between 10 and 100, which corresponds to binding affinity range from $1 \cdot 10^3$ to $1 \cdot 10^7$ M.

The accuracy of the derived thermodynamic parameters strongly relies on the binding model, whose choice represents one of the greatest pitfalls of ITC experiments if chosen wrongly. In this case, independent knowledge from other biophysical techniques or justified assumptions about the binding affinity, symmetry and interactions sites as well as number and composition of complexes must be considered. The most common binding models include: one-site binding site, two equivalent and independent binding sites, n-equivalent and independent sites as well as non-independent (cooperative) binding sites.
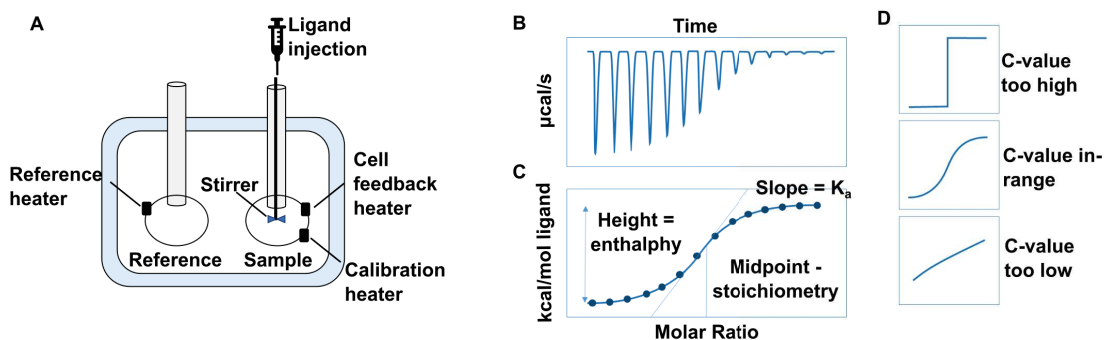
**Figure B.1:** *The experimental set-up of an ITC experiment. Figure adapted according to the Creative Commons (CC BY 4.0) license terms from Simon Caulton (Wikipedia). (A) The ITC instrument. (B) The output of an ITC raw measurement. (C) The derived binding isotherm from heat integration. (D) The c-value range defining the profile of the binding curve.*

### B.1.1   Microscale Thermophoresis (MST)

Microscale thermophoresis complements ITC in the sense that fluorescence emission of thermophoresis (Ludwig, 1856) or fluorescence quenching (Maiti, Haupts, and Webb, 1997) is used as an alternative physical readout to quantify biomolecular interactions. The method allows for the detection of the directed motion of a fluorescent molecule along a local microscopic temperature gradient upon binding to a non-fluorescent ligand.

The core piece of a MST instrument (Figure B.2) is an incorporated IR-Laser that is highly efficient in generating a temperature rise at microscopic scale and very precise in focusing locally the heat on the sample within only a few $\mu$m of capillary. This enables fast MST analysis and quantification of thermophoretic property changes in less than 30 s. In detail, the local heat induced thermophoresis of fluorescent molecules through the temperature gradient. The signal detection of a MST experiment occurs as the following (Figure B.2 B): Constant "intial fluorescence" is measured. After the activation of the IR laser, a rapid change in fluorophore properties due to the temperature change, known as the "T-jump" is observed. Thermophoretic movement of the fluorescently labelled molecule is detected. After deactivation of the IR-Laser, an inverse T-jumps takes place, which then leads to the "backdiffusion" of molecules. The typical binding affinity experiment (Figure B.2 C) consists of detecting the thermophoretic movement of a fluorescent molecule free (black trace, unbound) and in complex with a non-fluorescent ligand upon binding (grey traces, bound). The change in thermophoresis is translated into the change in the normalized fluorescence $\delta F_{norm}$, defined by the ratio of $F_{hot}/F_{cold}$. The plot of the ligand-binding induced change in thermophoresis against ligand concentration leads to a binding curve (Figure B.2 D) which can be fitted to derive the binding constants.

MST is therefore very sensitive to changes in molecular properties such as size, charge, hydration shell or conformation. The advantage of MST measurements is that it requires low

sample quantities, compared to ITC, and does not require surface immobilization for studying molecular interactions.

During a binding titration experiment, the normalized fluorescence changes, according to the following expression:

$$F_{norm} = (1 - x)F(P)_{norm} + x \cdot F(PL)_{norm} \tag{B.6}$$

Where $F(P)_{norm}$ is the contribution of the unbound fluorescent molecule P and $F(PL)_{norm}$ the contribution of the complex PL of the fluorescent molecule P and its interacting titrant ligand L and x the fraction of fluorescent complexes. The normalized fluorescence is defined by the temperature-dependent fluorescent quenching of the dye and the concentration ratio approximated in terms of Soret coefficient, defined as the quotient of the diffusion constant D and thermodiffusion coefficient $D_T$ and thermal distribution. The fraction of bound molecules x can be derived from the measured change in normalized fluorescence $F_{norm}$. The dissociation constant $K_D$ is obtained by fitting the MST binding curve with the quadratic solution for the fraction of bound fluorescent molecules $F_B$, calculated from the law of mass action:

$$F_B = \frac{[PL]}{[P]} = \frac{[P] + [L] + K_D - \sqrt{([P] + [L] + K_D)^2 - 4[PL]}}{2[P]} \tag{B.7}$$

with the concentration of bound molecules [PL] and unbound protein [P] and ligand [L].
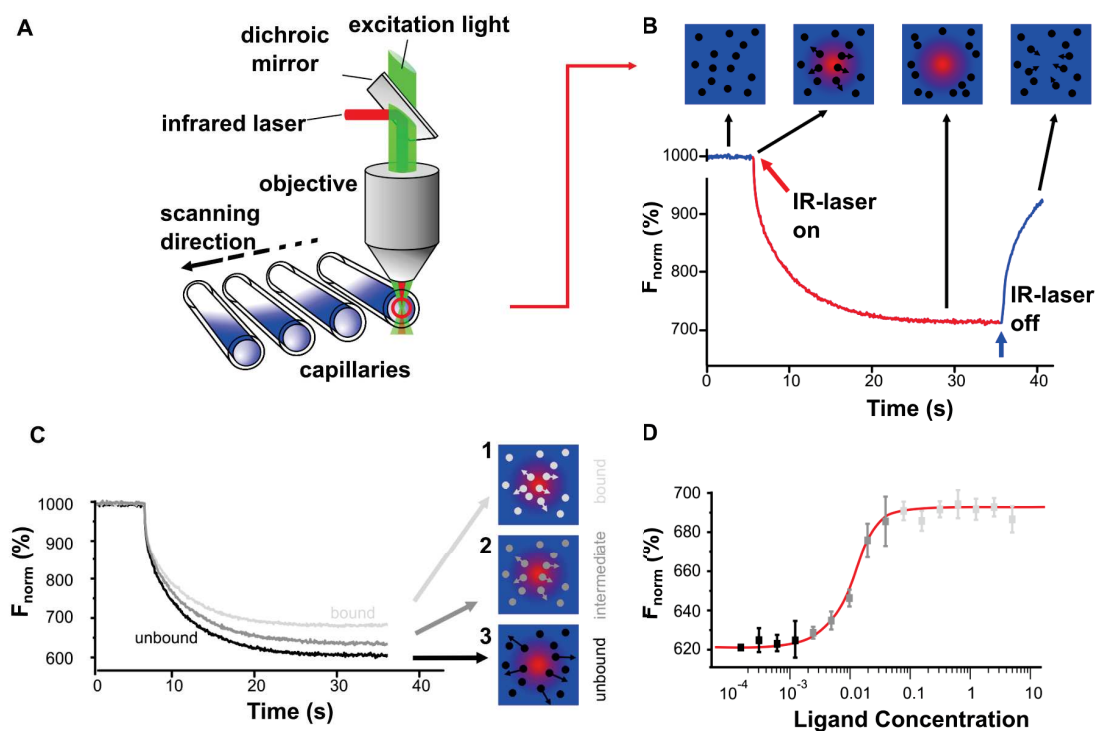
**Figure B.2:** *The MST technology and experimental set-up.* *Figure adapted in accordance with the terms of Creative Commons Attribution license from Jerabek-Willemsen et al., 2014. A scheme representing the MST optics: The fluorescence within the capillary is excited and detected through the same objective. (A) Focused IR-Laser is used to locally heat a defined sample volume. Thermophoresis of fluorescent molecules through the temperature gradient is detected. (B) Signal detection of a MST experiment. (C) The typical binding affinity experiment consists of detecting the thermophoretic movement of a fluorescent molecule free (black trace, unbound) and in complex with a non-fluorescent ligand upon binding (grey traces, bound). (D) Binding constants are derived from fitted the binding curve.*

# Appendix C

# Appendix - Theoretical Background: AUC

## C.1 Theoretical Background

### C.1.1 Principle

Analytical ultracentrifugation (AUC) is an informative technique and broadly applicable for investigating hydrodynamic characteristics and binding properties of compounds, proteins and other molecular species.

The AUC instrument is an ultracentrifuge equipped with an optical device to monitor the sedimentation of particles of different sizes. Sedimentation velocity (SV) and sedimentation equilibrium (SE) are complementary measurements performed at high ( >40,000 rpm) and low (< 40,000 rpm) rotor speeds, respectively to obtain structural and biophysical properties of biomolecules, such as proteins. SV separates proteins based on their size-dependent migration rates in the centrifugal field, while sedimentation equilibrium is a thermodynamic method to determine the binding affinity at equilibrium concentration gradients at lower rotor fields.

The time-evolved sedimentation-diffusion process generates concentration profiles with sigmoid shape that migrate with time towards the bottom of the sample cell (Figure C.1 B). The signature of a protein's sedimentation is the formation of a concentration boundary at specific radial position of the cell, where the centrifugal, frictional and boyant forces are in equilibrium. The position and profile of the sedimentation boundary is therefore size and shape dependent. The sedimentation in a sector-shaped cell can be mathematically expressed by the Lamm equation (Lamm, 1929), which defines the time-evolved radial concentration $\frac{\delta c}{\delta t}$ during sedimentation as:

$$\frac{\delta c}{\delta t} = D \left[ \left( \frac{\delta^2 c}{\delta r^2} \right) + \frac{1}{r} \left( \frac{\delta c}{\delta r} \right) \right] - s\omega^2 \left[ r \left( \frac{\delta c}{\delta r} \right) + 2c \right] \tag{C.1}$$

where c is the solute concentration, t and r are the time and radius, and the parameters D, s, and $\omega$ represent the solute diffusion constant, sedimentation coefficient and the rotor angular velocity, respectively.

The relationship between solvent and physical properties of sedimenting particles is defined by the Svedberg equation. The sedimentation coefficient *s* is mathematically expressed as the
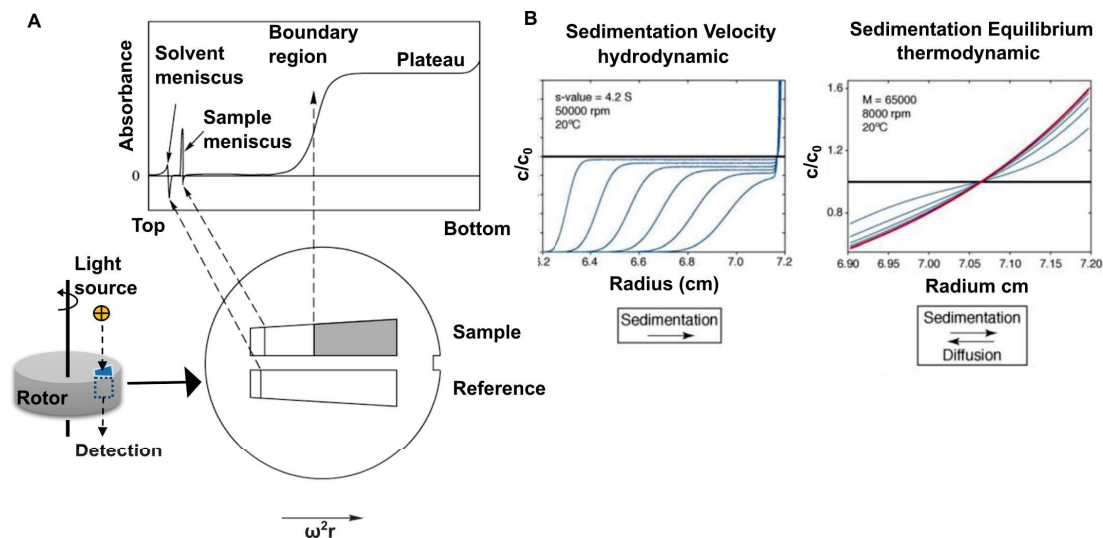
**Figure C.1:** ***AUC and the experimental set-up.*** *Figure-Panel A reproduced from Ralston, 1993. Figure-Panel B reused from "Sedimentation Velocity Analytical Ultracentrifugation ( SV-AUC ) for characterizing protein aggregates and contaminants in therapeutic proteins The elaboration of mathematical relations behind SV-AUC theory" 2014. (A) The schematic representation of an AUC instrument and the sedimentation profile. The concentration profile of (B) sedimentation velocity and (C) sedimentation equilibrium measurement.*

quotient of solute velocity $\nu$ and the centrifugal acceleration, defined by $\omega^2 r$ and is related to the particle and solution properties as the following:

$$s \equiv \frac{\nu}{\omega^2 r} = \frac{M(1 - \bar{\nu}\rho)}{N_A f} \tag{C.2}$$

with M the molecular mass, $\bar{\nu}$ the partial specific volume, $N_A$ the Avogadro constant, f the friction factor and $\rho$ the solvent density.

## C.1.2    The Diffusion Corrected Sedimentation Coefficient Distribution Model - The c(s)-Model

Since the Lamm equation cannot be analytically solved, computational approaches were developed to provide numerical solutions. One approach simulates solutions of the Lamm equation as diffusion-broadened hyperbolic functions that are superimposed and fitted to the experimental sedimentation curves (Stafford III, 1992, Schuck, 1998, Claverie, Dreux, and Cohen, 1975). The measured spectral readout (absorbance or interference or both) of a protein or protein mixture during sedimentation a(r,t) can be mathematically approximated to the superposition of Lamm equation solutions over a range of sedimentation velocities ($s_{min}$, ...$s_{max}$) expressed in units of Svedberg. The so-called Diffusion Corrected Sedimentation Coefficient Distribution model (c(s)-model) (Schuck, 1998, Schuck, 2000b) is given by:

**Figure C.2:** *The continous diffusion corrected c(s) model.* *(A) The formation of the sedimentation boundary: the size and shape of a particle determines the location of the sedimentation boundary, where the centrifugal, frictional and boyant forces are equili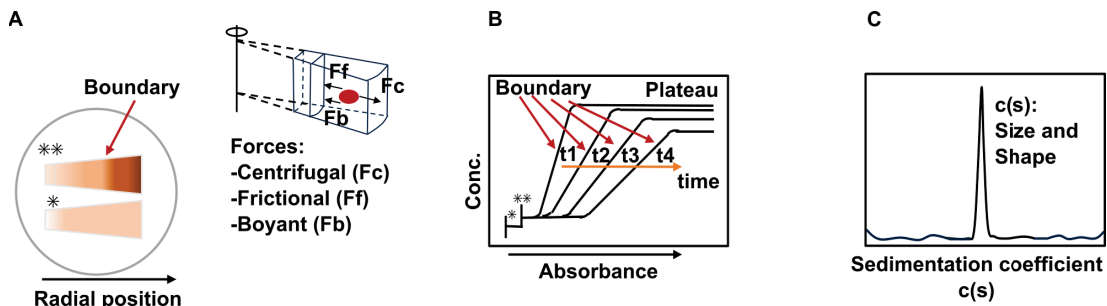brium. (B) The counter-effect of sedimentation is diffusion leading to the depletion of the particle concentration at the cell bottom and consequently to the broadening of the sedimentation boundary over time. (C) Modelling of mathematical functions that fit the sedimentation curves gives rise to the sedimentation coefficient of the species in the sample.*

$$a(r, t) \simeq \int_{S_{min}}^{S_{max}} c(s)\chi\,(s, D(s), r, t)\,ds \tag{C.3}$$

where c(s) corresponds to the sedimentation coefficient and $\chi$(s, D(s), r, t) to the Lamm Equation solution, which depends on the diffusion coefficient D(s), sector-radius r, and time t. The c(s) analysis over a size range of proteins and a fitted frictional ratio provides the sedimentation coefficient c(s) as a measure of the size and shape. The integration of the spectral signal at the c(s) value expressed in Svedberg (1 S = $1 \cdot 10^{-13}$ s) corresponds to the concentration of the sedimented protein of interest. The shape factor is the ratio of the friction by a molecule during sedimentation (f) against the friction constant of an ideal spherical particle ($f_0$). It is used to measure the deviation from a globular particle shape and can be modelled in the same way as the c(s), a method that has been implemented in the c(s, $ff_0$) method (Brown and Schuck, 2006).

## C.1.3 The c(s) and multi-signal $c_k$(s)-model for protein-protein interaction analysis

Centrifugation can be utilized to study interacting species during sedimentation (Balbo and Schuck, 2005). However, reactions undergoing multiple kinetic steps are generally not resolvable in the centrifugal time-scale. Fortunately, many protein-protein interactions (PPI) occur within the kinetics of sedimentation that falls into the range of $10^{-3} - 10^{-5}$ s$^{-1}$. The classification of PPI in that range is convenient to assess fast or slow interactions in the sedimentation time-scale. Slow reacting proteins with low dissociation rates ($k_{off} = 10^{-3} - 10^{-5}$ s$^{-1}$) show distinct c(s)-peaks that directly reflect the sedimentation of each species. The number and value of the sedimentation coefficients correspond to the number and size of the components and formed complexes. In contrast, proteins undergoing association reactions with high dissociation rates ($k_{off} = 10^{-1} - 10^{-2}$ s$^{-1}$) do not form stable complexes throughout sedimentation.
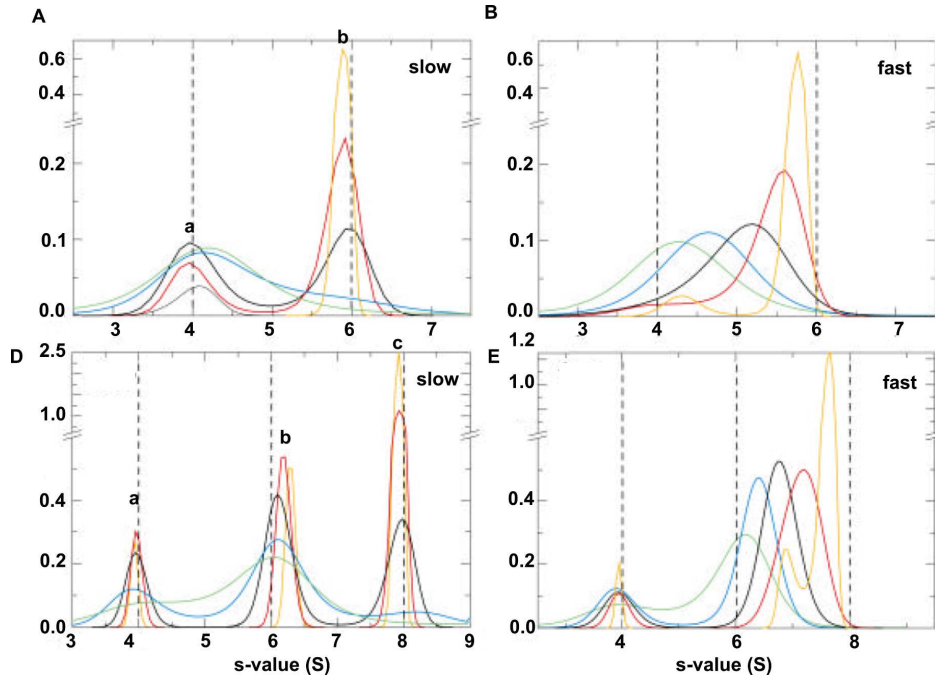
**Figure C.3:** *Homo- and hetero-assoications of proteins studied by sedimentation velocity.* *Figure reused in accordance with the terms of Common Creative license from source Balbo and Schuck, 2005. Represented are c(s) distributions of proteins undergoing slow and fast homo - and hetero-association reactions in the sedimentation time scale. (A) Slow self-association gives rise to two distinct peaks corresponding to the monomeric and dimeric species of the protein. The dimeric species increases with increasing concentration of monomeric species. (B) Fast homo-associations result in unresolved c(s) peaks that moderately resolve with higher amounts monomeric species. Analogue to homo-associations reactions c(s) distributions of (D) slow and (E) fast hetero-association reactions.*

As a result, the sedimentation boundary of the component with the closest molecular weight of the complex co-sediments into a single reaction boundary of the complex (Figure C.3).

In this case, the c(s) value is unreliable to determine the size and stoichiometry of the protein complex. To overcome this problem, multi-signal SV (MS-SV) analysis (Brautigam, Padrick, and Schuck, 2013) has been developed to enable the spectral discrimination of the individual components to determine the concentration ratio in the reaction boundary as complex stoichiometry. This approximation is valid, if the larger protein is completed saturated in complex at a large excess of the smaller binding partner. The mathematical expression is a generalized form of the c(s) model, annotated here as the $c_k(s)$ model. The proportion of the single proteins in complex is calculated by the absorbance at wavelength $\lambda$ ($a\lambda(r, t)$) that is modelled as:

$$a(r, t) \simeq \sum_{k=1}^{K} \epsilon_\lambda^{k_l} \int_{S_{min}}^{S_{max}} c_k(s)\chi\,(s, D(s), r, t)\,ds \tag{C.4}$$

where k represents the individual components of a mixture, l is the path length and $c_k(s)$ is

a continuous distribution for component k. The familiar equation is a generalized form of the c(s) model. Step functions are simulated to fit the experimental sedimentation boundaries of components and complex. Similar to the c(s) model, a distribution plot of spectral signal of each component against the corresponding c(s) is obtained. The integration of both distributions give the concentration of each individual component and the component at the c(s) of the complex.

MS-SV deconvolution is possible when the complex components have sufficiently different spectral properties that is calculated as:

$$D_{norm} = \frac{\|det\epsilon_k^\lambda\|}{\prod k \|\vec{\epsilon_k}\|} \tag{C.5}$$

where det stands for the determinant of the matrix, $\epsilon_k^\lambda$ is the extinction coefficient of component k at a given wavelength.

Using either the extinction coefficient of absorbance at 280 nm with interference parameters or absorbance extinction coefficients at minimum (at 250 nm) and maximum (at 280 nm) wavelength.

MS-SV is also suitable for studying slow-reacting protein in complex in the time scale of sedimentation. The discrepancy between fast and slow interacting proteins allows for functional categorization as well. For instance, rapid associations are essential for signal transduction, cell regulation and the immune responses, while slower kinetics implies additional processes such as conformational rearrangements (Schreiber, 2002). The rate of association of most protein complexes is restricted by diffusion and geometric constraints of the binding sites (diffusion control). Sedimentation velocity experiments are therefore optimal tools to investigate biological relevant kinetics of PPIs.

# Appendix D

# Appendix - Theoretical Background: SAXS

SAXS measures scattered X-ray intensities of a sample as a function of the scattering angle. The technique is performed at the small scattering angles, typically ranging from 0.1 degrees to 5 degrees, to encapsulate nanometre dimensions of proteins, nucleic acids and complexes.

### D.0.1    Instrument and Principle

In a SAXS experiment, a collimated, monochromatic X-ray beam is directed on the sample and scattered and recorded at low angles by a detector. The SAXS instrument consists of an X-ray source, collimators directing the X-ray beam, a sample probe and a detector. In a synchrotron facility the set-up is more complex and includes additional equipment to enhance the X-ray intensity and reduce the beam divergence through an undulator, collimator and focusing mirrors, and contains a monochromator to filter a single wavelength, followed by the mirrors and a shutter before entering the sample. The detector is equipped with a beam stop.

The SAXS profile is a plot of the scattered X-ray intensity against the scattering angle of a macromolecule that provides the hydrodynamic properties of the macromolecule after subtracting undesired scattering from small molecules in the buffer and the surrounding probe materials. The samples need to be monodispersed and pure to neglect the scattering contributions from aggregates and intermolecular correlations in SAXS analysis.

The basis for SAXS is elastic scattering of X-rays on electrons that create waves with constructive and destructive interference depending on the phase superposition. The addition of waves that are in-phase results in waves with higher amplitude, while the summation of out-of-phase waves leads to waves with smaller amplitudes (Figure D.1 B). The scattering amplitude A(q) depends on the scattering or momentum transfer vector $\mathbf{q}$ in the reciprocal space. The momentum transfer $\mathbf{q}$ denotes the change in momentum between the incoming and scattered X-ray that is defined by the difference between the incoming and scattered wave vectors $k_i$ and $k_s$:

$$\mathbf{q} = \mathbf{k}_s - \mathbf{k}_i \tag{D.1}$$

The physical meaning of the $\mathbf{q}$ is that it describes the interaction between the radiation and the sample through photon transfer. The quantity of $\mathbf{q}$ is defined as:
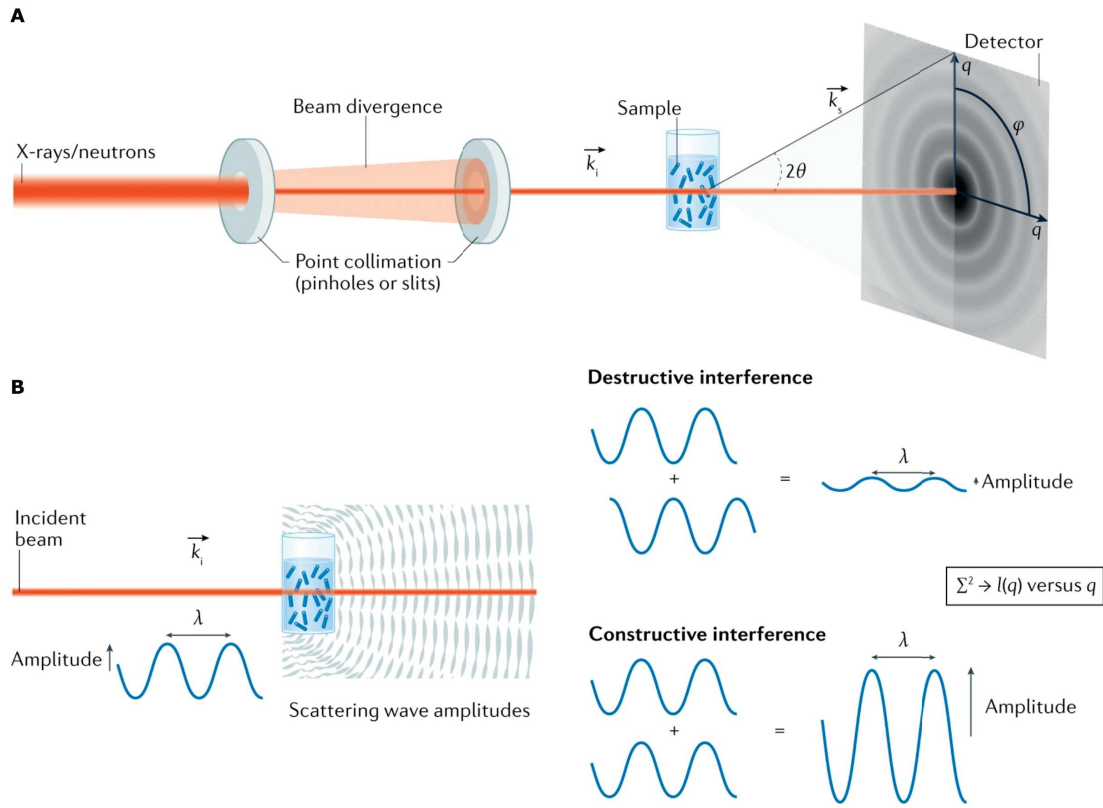
**Figure D.1:** *The experimental set-up of SAXS. Figure reused with permission from Springer (license no. 5742641268761) from Jeffries et al., 2021. (A) Transmission geometry set-up for small angel X-ray (SAXS) or small angle neutron scattering (SANS): A collimated beam is directed to the sample. As it travels through a sample, a small proportion, that interacts with the sample is scattered. The intensity of the scattered radiation is collected by a detector. The typica SAXS curve is a 1D plot of the scattered intensity I(q) against the angular dependence of scattering, expressed as momentum transfer vector, q. (B) Scheme of X-ray interference on sample.*

$$|\mathbf{q}| = q = \frac{4\pi \sin \theta}{\lambda} \tag{D.2}$$

where $\lambda$ is the wavelength of the X-rays and $\theta$ the scattering angle.

The form factor F($\mathbf{q}$) of a molecule represents the particle shape is directly related to the size of the particle (Pérez and Nishino, 2012). It is derived from the equation of the scattering of N electrons (equation D.3), averaged over all orientations (equation D.4). The scattering intensity is determined by the Debye formula (equation D.6, Debye, 1915).

$$F(\mathbf{q}) = \sum_{i=1}^{N} f_i(\mathbf{q}) \exp(i\mathbf{q} \cdot \mathbf{r}_i) \tag{D.3}$$
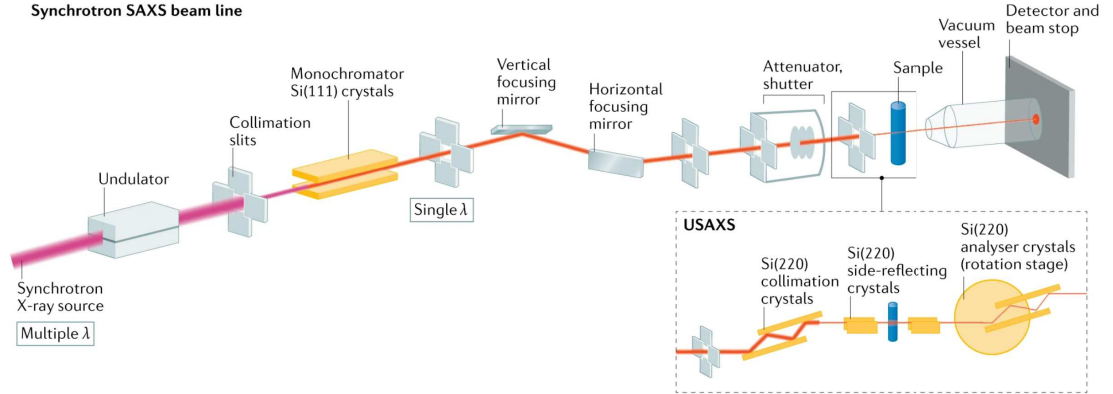
**Figure D.2:** *The experimental set-up of SAXS in synchroton beamlines.* *Figure resued with permission from Spinger (license no. 5742641268761) from Jeffries et al., 2021. Synchrotron X-ray sources consist of accelerated electrons (or positrons) emitting multiple-wavelength X-rays. The undulator gap controls the energy spectrum released into the front end of the instrument. X-rays are directed towards a monochromator, that selects a specific X-ray wavelength. The monochromatic X-ray beam is then shaped by vertical and horizontal focusing mirrors in combination with slits. Additional components include attenuators and shutters that control the X-ray flux and exposure.*

$$\langle F(\mathbf{q}) \rangle = \sum_{i=1}^{N} f_i(q) \frac{\sin(qr_i)}{qr_i} \tag{D.4}$$

$$I(\mathbf{q}) = |F(\mathbf{q})|^2 = \sum_{i=1}^{N} \sum_{j=1}^{N} f_i(q)f_j(q) \exp(i\mathbf{q} \cdot (\mathbf{r}_i - \mathbf{r}_j)) \tag{D.5}$$

$$I(\mathbf{q}) = |F(\mathbf{q})|^2 = \sum_{i=1}^{N} \sum_{j=1}^{N} f_i(q)f_j(q) \frac{\sin(qr_{ij})}{qr_{ij}} \tag{D.6}$$

where the value of $f_i(q)$ is the atomic form factor of atom i with its radius i, $\mathbf{q}$ is the scattering vector and $r_{ij}$ is the distance between atoms i and j, and N is the number of atoms in the molecule.

The scattered intensity from the isolated molecule $I(\mathbf{q})$ is obtained from the squared $F(\mathbf{q})$ in the reciprocal (Fourier) space, where the information about the phase of the scattered X-ray wave is lost. The phase problem is present in all X-ray crystallography methods determining the structure from intensities in the reciprocal space. The exception is Cryo-electron microscopy (EM) that provides real-space images containing both amplitude and phase information. Structure determination by SAXS is performed by fitting the computed theoretical profile $I(\mathbf{q})$ to the experimental profile $I_{exp}(\mathbf{q})$. The Debye formula (Debye, 1915) is used for the computation of SAXS profiles. The accuracy is obtained by minimizing the square root of the $\chi^2$ term $\chi$ over the total number of data points or particles M.

$$\chi = \frac{\sqrt{I_{exp}(\mathbf{q}) - I_{comp}(\mathbf{q})}}{\sigma(\mathbf{q})} \tag{D.7}$$

where c is a scaling factor and $\sigma(\mathbf{q})$ is the experimental error. Different methods of calculating the theoretical intensity distribution will result in different statistical fits.

## D.0.2 SAXS Parameters

Molecular parameters, which include the molecular mass (MM), radius of gyration ($R_g$), the hydrated particle volume ($V_p$) and the maximum particle diameter ($D_{max}$), can be obtained from the SAXS scattering curve. The SAXS profile contains three distinct regions, known as Guinier, Fourier, and Porod (Figure D.3 A-C), from which this information can be extracted. The radius of gyration ($R_g$) is defined as the average of the squared center-of-mass distances in a particle weighted by the electron density. The $R_g$ value can be extracted from the Guinier plot. At the smallest angles, the Guinier equation (Guinier and Fournet, 1955) holds for the scattered intensity $I(\mathbf{q})$:

$$I(\mathbf{q}) = I(0) \exp\left(-\frac{1}{3}R_g^2\mathbf{q}^2\right) \tag{D.8}$$

where I(0) is the intensity of the incoming X-ray and $\mathbf{q}$ the scattering vector.
The values of I(0) and $R_g$ can be extracted from the y-axis intercept and the slope of the linear region of a Guinier plot (ln[I(s)] versus $\mathbf{q}^2$), respectively (Figure D.3 A). The $R_g$ value is determined from the fitting range. This range is limited the experimental set-up including the beam size and the beamstop and is only valid approximation for up to q < 1.3/$R_g$. Of note, the $R_g$ value is greatly affected by aggregation of particles, polydispersity, and improper subtraction of the background or buffer.

The particle size is defined by the $D_{max}$ value, the range of observed electron density distribution within distance r, described by the pair distance distribution function P(r) in the Fourier region. The P(r) function is expressed as:

$$P(r) = \frac{r^2}{2\pi^2} \int_0^{\inf} q^2 I(q) \frac{\sin(qr)}{qr} dq \tag{D.9}$$

It represents the probability of finding pair of scattering elements within the particle at a distance r, described by the autocorrelation function. The P(r) function provides the information regarding the particle shape (Figure D.3), as it is related to the experimental form factor F($\mathbf{q}$) through indirect Fourier transformation. For particles with a similar shape, the P(r) curves are used to determine the general particle shape.
Other useful information about the volume and molecular weight for compact particles provides the Porod graph plotted as $q^4 I(q)$ vs q. The Porod's law describes the asymptotic behaviour intensity decay proportional to $q^{-4}$ at higher angles or large scattering wave vectors $\mathbf{q}$ (Porod, 1951).

The Kratky plot of $q^2 I(q)$ versus q is another useful tool to assess the flexibility and/or the degree of unfolding in samples (Roessle, 2009). Unfolded (highly flexible) proteins display a plateau in the Kratky plot at high q values, while compact, globular proteins have a bell-shaped
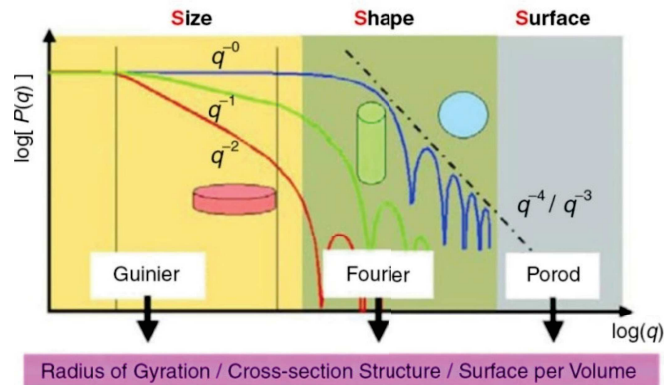
**Figure D.3: *Structural parameters derived from SAXS profile regions.*** *Figure reused in according to Creative Common license terms from Boldon, Laliberte, and Liu, 2015. The Guinier region determines the size regime of a biomolecule. The maximal particle dimension can be obtained from the pair distance distribution function in the Fourier region and the molar mass and molecular weight of compact molecules can be derived from the Porod region.*

(Gaussian) peak. The combination of both indicate partially unfolded proteins or proteins containing IDRs. Dimensionless Kratky plots are normalized by mass and concentration and presented as $(qR_g)^2/I(0)$ versus $qR_g$ (Figure D.4). Dimensionless Kratky plots are useful to compare the content of flexible regions of proteins across different systems.
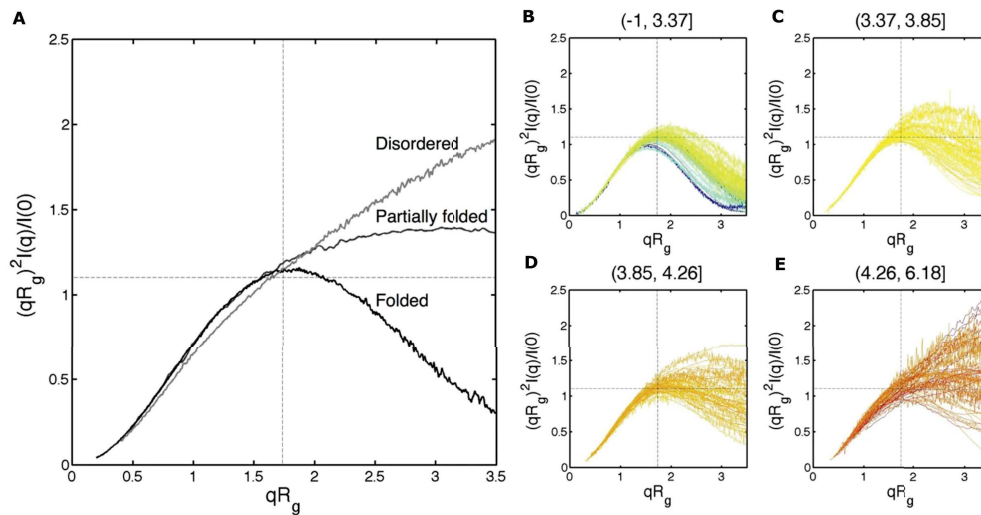


**Figure D.4: *Dimensionless Kratky plots of globular, partially unfolded and entirely disordered proteins.*** *Figure reused according to the terms of Creative Commons Attribution (CC BY 4.0) license from Burger, Arenas, and Stultz, 2016. (A) Disordered spectrum: C-terminal region of the Bromodomain adjacent to zinc finger protein domain (pdb: 2B62); Partially folded spectrum: Splicing factor U2 Auxiliary Factor 65 KD (U2AF65), residues 148–47552; Folded spectrum: Chymotrypsinogen A63. (B–E) Dimensionless Kratky plots of 226 proteins from the BIOISIS33 and SASBDB34 databases organized into quartiles based on their entropy values.*

### D.0.3 Ab initio structure determination

SAXS can be used to obtain low resolution structures of biomolecules. For this purpose, good models are required to compute accurate SAXS curves that best fit the experimental data. There are different approaches on modelling for the structure determination. The most popular approach of *ab initio* methods are bead modelling methods, where dummy-residues represent scattering centres to construct the shape of a particle that fits the experimental SAXS curve. The scattering intensities of the beads are computed using spherical harmonics, which are mathematical functions used to describe the shape and surface of objects. The densely packed beads inside a volume are typically restrained by the $D_{max}$. The *ab initio* methods involves iterative runs with different random seeds yielding a variety of models. The analysis of these models allows one to detect the most reliable features (Volkov and Svergun, 2003). These approaches have also been integrated with NMR chemical shift data to determine particle shape and rationalise the potential binding interface regions of complexes (Tidow et al., 2007).

### D.0.4 Ensemble Optimization Method (EOM)

The Ensemble Optimization Method (EOM) has been developed to obtain structural properties of disordered and highly flexible proteins from SAXS data. The scattering curve of proteins with IDRs or IDPs is a result of the scattering from a large number of their conformers rather than the from a single structure. The strategy of EOM consists of three main steps: First, the generation of a large pool of possible conformations that covers the conformational space of the protein; second the computation of the scattering profile for each conformation and third the selection of a subset of conformations that best fit the experimental SAXS curve. The results are distributions of the low-resolution structural parameters $R_g$ and $D_{max}$ indicative for the particle dimension. Comparing the $R_g$ and $D_{max}$ distributions of the sub-ensemble that best fit the data with the those derived from the initial pool, representing the unresticted conformational space of the protein, delivers a measure of compactness and flexibility (Bernadó et al., 2007). To quantify the degree of flexibility, the size of the EOM distribution that determines the conformational space is calculated by using entropy as a measure from the Shannon Theory (Shannon and Weaver, 1949). The flexibility parameter $R_{flex}$:

$$R_{flex} = -S \tag{D.10}$$

with the Shannon entropy S:

$$S = -\sum_{i=1}^{n} p(x_i) \log_b \left( p(x_i) \right) \tag{D.11}$$

where ■denotes the sum over the possible events, p is the probability of a specific event $x_i$. The logarithm depends on the basis (b).

Under the assumption that disordered regions move randomly in solution, a broad Gaussian-like distribution reflects higher entropy (S tends to -1) with greater uncertainty. Consequently, the distribution size of the ensemble reflects the experimental SAXS data S is expected to be close to the entropy calculated for the randomized pool. Conversely, a narrow distribution represents limited flexibility providing low uncertainty, with S tending to 0. Here, the randomized pool and the experimental representative ensemble population differ. In cases of maximal flexibility or complete rigidity, S is either equal to -1 or 0, respectively. While the $R_{flex}$ metric quantifies the difference between flexible and rigid systems, the additional metric $R_\sigma$ indicates the variance of the ensemble distribution with respect to the original pool, providing values close to 1.0 when the ensemble distribution describes a fully flexible system and largely reproduces the conformational space of the pool. $R_\sigma$ is calculated as:

$$R_\sigma = \frac{\sigma_s}{\sigma_p} \tag{D.12}$$

where where $\sigma_s$ and $\sigma_p$ are the standard deviations for the distributions of the selected ensemble and of the pool, respectively.

In addition to $R_{flex}$ and $R_\sigma$, distributions are also compared using a set of standard descriptors: standard deviation, average absolute deviation, kurtosis, skewness and geometric average (Tria et al., 2015). Figure D.5 illustrates EOM ensemble distributions with different flexibility metrics.
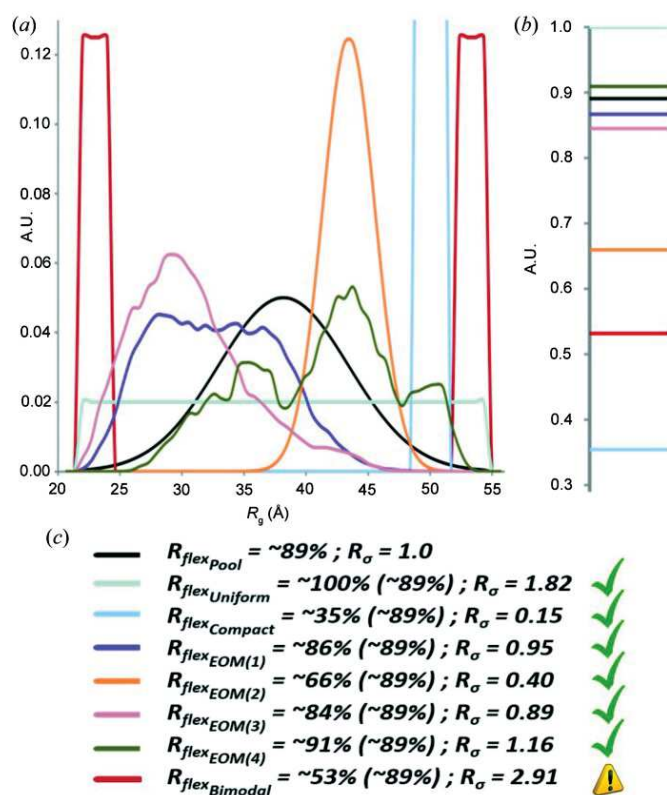
**Figure D.5:** *EOM distributions of molecules displaying maximal flexibility (100%) to rigidity (35%).*
*Figure reused according to the Common Creative license terms from Tria et al., 2015.*

# Bibliography

Abedini, Fatemeh et al. (2012). "Cationized dextran nanoparticle-encapsulated CXCR4-siRNA enhanced correlation between CXCR4 expression and serum alkaline phosphatase in a mouse model of colorectal cancer." In: *International journal of nanomedicine* 7, pp. 4159–68. ISSN: 1178-2013. DOI: 10.2147/IJN.S29823. URL: http://www.ncbi.nlm.nih.gov/pubmed/22888250http://www.pubmedcentral.nih.gov/articlerender.fcgi?artid=PMC3415322.

Agresti, Alessandra and Marco E Bianchi (2003). "HMGB proteins and gene expression". In: *Current opinion in genetics & development* 13.2, pp. 170–178.

Agresti, Alessandra et al. (2005). "GR and HMGB1 interact only within chromatin and influence each other's residence time". In: *Molecular cell* 18.1, pp. 109–121.

Ahmed, Rashik and Julie D Forman-Kay (2022). "NMR insights into dynamic, multivalent interactions of intrinsically disordered regions: from discrete complexes to condensates". In: *Essays in Biochemistry* 66.7, pp. 863–873.

Alard, Jean-Eric et al. (2015). "Recruitment of classical monocytes can be inhibited by disturbing heteromers of neutrophil HNP1 and platelet CCL5". In: *Science translational medicine* 7.317, 317ra196–317ra196.

Allavena, Paola et al. (2011). "Chemokines in cancer related inflammation". In: *Experimental Cell Research* 317.5, pp. 664–673. ISSN: 00144827. DOI: 10.1016/j.yexcr.2010.11.013. URL: https://linkinghub.elsevier.com/retrieve/pii/S0014482710005422.

Allen, Samantha J, Susan E Crown, and Tracy M Handel (2007). "Chemokine: receptor structure, interactions, and antagonism". In: *Annu. Rev. Immunol.* 25, pp. 787–820.

Arbesú, Miguel et al. (2018). "Intramolecular fuzzy interactions involving intrinsically disordered domains". In: *Frontiers in molecular biosciences* 5, p. 39.

Bachelerie, Francoise et al. (2014a). "International Union of Basic and Clinical Pharmacology. LXXXIX. Update on the Extended Family of Chemokine Receptors and Introducing a New Nomenclature for Atypical Chemokine Receptors". In: *Pharmacological Reviews* 66.1. Ed. by Eliot H. Ohlstein, pp. 1–79. ISSN: 0031-6997. DOI: 10.1124/pr.113.007724. URL: http://pharmrev.aspetjournals.org/lookup/doi/10.1124/pr.113.007724.

— (2014b). "International Union of Basic and Clinical Pharmacology. LXXXIX. Update on the Extended Family of Chemokine Receptors and Introducing a New Nomenclature for Atypical Chemokine Receptors". In: *Pharmacological Reviews* 66.1. Ed. by Eliot H. Ohlstein, pp. 1–79. ISSN: 0031-6997. DOI: 10.1124/pr.113.007724. URL: http://pharmrev.aspetjournals.org/lookup/doi/10.1124/pr.113.007724.

Baggiolini, Marco (1998). "Chemokines and leukocyte traffic". In: *Nature* 392.6676, pp. 565–568. ISSN: 0028-0836. DOI: 10.1038/33340. URL: https://www.nature.com/articles/33340.

Balbo, Andrea and Peter Schuck (2005). "Analytical Ultracentrifugation in the Study of Protein Self- association and Heterogeneous Protein-Protein Interactions". In: URL: https://api.semanticscholar.org/CorpusID:30783714.

Balkwill, Fran (2003). "Chemokine biology in cancer". In: *Seminars in Immunology* 15.1, pp. 49–55. ISSN: 10445323. DOI: 10.1016/S1044-5323(02)00127-6. URL: https://linkinghub.elsevier.com/retrieve/pii/S1044532302001276.

Banani, Salman F et al. (2017). "Biomolecular condensates: organizers of cellular biochemistry". In: *Nature reviews Molecular cell biology* 18.5, pp. 285–298.

Bao, Shunshun et al. (2023). "CXC chemokine receptor 4 (CXCR4) blockade in cancer treatment". In: *Journal of Cancer Research and Clinical Oncology* 149.10, pp. 7945–7968. ISSN: 0171-5216. DOI: 10.1007/s00432-022-04444-w. URL: https://link.springer.com/10.1007/s00432-022-04444-w.

Baryshnikova, Olga K and Brian D Sykes (2006). "Backbone dynamics of SDF-1alpha determined by NMR: interpretation in the presence of monomer-dimer equilibrium." In: *Protein science : a publication of the Protein Society* 15.11, pp. 2568–78. ISSN: 0961-8368. DOI: 10.1110/ps.062255806. URL: http://www.ncbi.nlm.nih.gov/pubmed/17075134http://www.pubmedcentral.nih.gov/articlerender.fcgi?artid=PMC2242403.

Beider, Katia et al. (2011). "CXCR4 antagonist 4F-benzoyl-TN14003 inhibits leukemia and multiple myeloma tumor growth." In: *Experimental hematology* 39.3, pp. 282–92. ISSN: 1873-2399. DOI: 10.1016/j.exphem.2010.11.010. URL: http://www.ncbi.nlm.nih.gov/pubmed/21138752.

Bendall, Linda J et al. (2005). "Defective p38 mitogen-activated protein kinase signaling impairs chemotaxic but not proliferative responses to stromal-derived factor-1alpha in acute lymphoblastic leukemia." In: *Cancer research* 65.8, pp. 3290–8. ISSN: 0008-5472. DOI: 10.1158/0008-5472.CAN-04-3402. URL: http://www.ncbi.nlm.nih.gov/pubmed/15833862.

Berger, Edward A., Philip M. Murphy, and Joshua M. Farber (1999). "CHEMOKINE RECEPTORS AS HIV-1 CORECEPTORS: Roles in Viral Entry, Tropism, and Disease". In: *Annual Review of Immunology* 17.1, pp. 657–700. ISSN: 0732-0582. DOI: 10.1146/annurev.immunol.17.1.657. URL: https://www.annualreviews.org/doi/10.1146/annurev.immunol.17.1.657.

Bernadó, Pau et al. (2007). "Structural characterization of flexible proteins using small-angle X-ray scattering." In: *Journal of the American Chemical Society* 129.17, pp. 5656–64. ISSN: 0002-7863. DOI: 10.1021/ja069124n. URL: http://www.ncbi.nlm.nih.gov/pubmed/17411046.

Bianchi, Marco E (2009). "HMGB1 loves company". In: *Journal of leukocyte biology* 86.3, pp. 573–576.

Bianchi, Marco E. et al. (2017). "High-mobility group box 1 protein orchestrates responses to tissue damage via inflammation, innate and adaptive immunity, and tissue repair". In:

*Immunological Reviews* 280.1, pp. 74–82. ISSN: 01052896. DOI: 10.1111/imr.12601. URL: http://doi.wiley.com/10.1111/imr.12601.

Blanchet, Xavier, Christian Weber, and Philipp von Hundelshausen (2023). "Chemokine Heteromers and Their Impact on Cellular Function—A Conceptual Framework". In: *International Journal of Molecular Sciences* 24.13, p. 10925.

Blanchet, Xavier et al. (2012). "Touch of Chemokines". In: *Frontiers in Immunology* 3. ISSN: 1664-3224. DOI: 10.3389/fimmu.2012.00175. URL: http://journal.frontiersin.org/article/10.3389/fimmu.2012.00175/abstract.

Blanpain, Cedric et al. (1999). "CCR5 binds multiple CC-chemokines: MCP-3 acts as a natural antagonist". In: *Blood, The Journal of the American Society of Hematology* 94.6, pp. 1899–1905.

Boldon, Lauren, Fallon Laliberte, and Li Liu (Feb. 2015). "Review of the fundamental theories behind small angle X-ray scattering, molecular dynamics simulations, and relevant integrated application". In: *Nano reviews* 6, p. 25661. DOI: 10.3402/nano.v6.25661.

Borg, Mikael et al. (2007). "Polyelectrostatic interactions of disordered ligands suggest a physical basis for ultrasensitivity". In: *Proceedings of the National Academy of Sciences* 104.23, pp. 9650–9655.

Borgia, Alessandro et al. (2018). "Extreme disorder in an ultrahigh-affinity protein complex." In: *Nature* 555.7694, pp. 61–66. ISSN: 1476-4687. DOI: 10.1038/nature25762. URL: http://www.ncbi.nlm.nih.gov/pubmed/29466338http://www.pubmedcentral.nih.gov/articlerender.fcgi?artid=PMC6264893.

Brandhofer, Markus et al. (2022). "Heterocomplexes between the atypical chemokine MIF and the CXC-motif chemokine CXCL4L1 regulate inflammation and thrombus formation." In: *Cellular and molecular life sciences : CMLS* 79.10, p. 512. ISSN: 1420-9071. DOI: 10.1007/s00018-022-04539-0. URL: http://www.ncbi.nlm.nih.gov/pubmed/36094626http://www.pubmedcentral.nih.gov/articlerender.fcgi?artid=PMC9468113.

Brautigam, Chad A (2015a). "Calculations and publication-quality illustrations for analytical ultracentrifugation data". In: *Methods in enzymology*. Vol. 562. Elsevier, pp. 109–133.

— (2015b). "Fitting two- and three-site binding models to isothermal titration calorimetric data." In: *Methods (San Diego, Calif.)* 76, pp. 124–136. ISSN: 1095-9130. DOI: 10.1016/j.ymeth.2014.11.018. URL: http://www.ncbi.nlm.nih.gov/pubmed/25484338http://www.pubmedcentral.nih.gov/articlerender.fcgi?artid=PMC4591754.

Brautigam, Chad A, Shae B Padrick, and Peter Schuck (2013). "Multi-signal sedimentation velocity analysis with mass conservation for determining the stoichiometry of protein complexes." In: *PloS one* 8.5, e62694. ISSN: 1932-6203. DOI: 10.1371/journal.pone.0062694. URL: http://www.ncbi.nlm.nih.gov/pubmed/23696787http://www.pubmedcentral.nih.gov/articlerender.fcgi?artid=PMC3656001.

Brelot, A et al. (2000). "Identification of residues of CXCR4 critical for human immunodeficiency virus coreceptor and chemokine receptor activities." In: *The Journal of biological chemistry* 275.31, pp. 23736–44. ISSN: 0021-9258. DOI: 10.1074/jbc.M000776200. URL: http://www.ncbi.nlm.nih.gov/pubmed/10825158.

Brown, Aaron J. et al. (2017a). "Platelet-Derived Chemokine CXCL7 Dimer Preferentially Exists in the Glycosaminoglycan-Bound Form: Implications for Neutrophil–Platelet Crosstalk". In: *Frontiers in Immunology* 8. ISSN: 1664-3224. DOI: 10.3389/fimmu.2017.01248. URL: http://journal.frontiersin.org/article/10.3389/fimmu.2017.01248/full.

— (2017b). "Platelet-Derived Chemokine CXCL7 Dimer Preferentially Exists in the Glycosaminoglycan-Bound Form: Implications for Neutrophil–Platelet Crosstalk". In: *Frontiers in Immunology* 8. ISSN: 1664-3224. DOI: 10.3389/fimmu.2017.01248. URL: http://journal.frontiersin.org/article/10.3389/fimmu.2017.01248/full.

Brown, Patrick H and Peter Schuck (2006). "Macromolecular size-and-shape distributions by sedimentation velocity analytical ultracentrifugation". In: *Biophysical journal* 90.12, pp. 4651–4661.

Bugge, Katrine et al. (2020). "Interactions by disorder–a matter of context". In: *Frontiers in Molecular Biosciences* 7, p. 110.

Burger, Virginia, Daniel Arenas, and Collin Stultz (June 2016). "A Structure-free Method for Quantifying Conformational Flexibility in proteins". In: *Scientific Reports* 6, p. 29040. DOI: 10.1038/srep29040.

Capasso Palmiero, Umberto et al. (2022). "Programmable zwitterionic droplets as biomolecular sorters and model of membraneless organelles". In: *Advanced Materials* 34.4, p. 2104837.

Carbone, Michele and Haining Yang (2012). "Molecular Pathways: Targeting Mechanisms of Asbestos and Erionite Carcinogenesis in Mesothelioma". In: *Clinical Cancer Research* 18.3, pp. 598–604. ISSN: 1078-0432. DOI: 10.1158/1078-0432.CCR-11-2259. URL: http://clincancerres.aacrjournals.org/cgi/doi/10.1158/1078-0432.CCR-11-2259.

Carbone, Michele et al. (2012). "Malignant mesothelioma: Facts, Myths, and Hypotheses". In: *Journal of Cellular Physiology* 227.1, pp. 44–58. ISSN: 00219541. DOI: 10.1002/jcp.22724. URL: http://doi.wiley.com/10.1002/jcp.22724.

Cato, Laura et al. (2008). "The interaction of HMGB1 and linker histones occurs through their acidic and basic tails". In: *Journal of molecular biology* 384.5, pp. 1262–1272.

Cecchinato, Valentina et al. (2016a). "Chemokine interaction with synergy-inducing molecules: fine tuning modulation of cell trafficking". In: *Journal of Leukocyte Biology* 99.6, pp. 851–855. ISSN: 0741-5400. DOI: 10.1189/jlb.1MR1015-457R. URL: https://academic.oup.com/jleukbio/article/99/6/851/6936283.

— (2016b). "Chemokine interaction with synergy-inducing molecules: fine tuning modulation of cell trafficking". In: *Journal of Leukocyte Biology* 99.6, pp. 851–855. ISSN: 0741-5400. DOI: 10.1189/jlb.1MR1015-457R. URL: https://academic.oup.com/jleukbio/article/99/6/851/6936283.

Cecchinato, Valentina et al. (2018). "Redox-Mediated Mechanisms Fuel Monocyte Responses to CXCL12/HMGB1 in Active Rheumatoid Arthritis". In: *Frontiers in Immunology* 9. ISSN: 1664-3224. DOI: 10.3389/fimmu.2018.02118. URL: https://www.frontiersin.org/article/10.3389/fimmu.2018.02118/full.

Cecchinato, Valentina et al. (2023). "The chemokine landscape: one system multiple shades". In: *Frontiers in Immunology* 14. ISSN: 1664-3224. DOI: 10.3389/fimmu.2023.1176619. URL: https://www.frontiersin.org/articles/10.3389/fimmu.2023.1176619/full.

Celona, Barbara et al. (2011). "Substantial histone reduction modulates genomewide nucleosomal occupancy and global transcriptional output". In: *PLoS biology* 9.6, e1001086.

Chang, Chun-Chun et al. (2020). "Internal water channel formation in CXCR4 is crucial for Gi-protein coupling upon activation by CXCL12". In: *Communications Chemistry* 3.1, p. 133. ISSN: 2399-3669. DOI: 10.1038/s42004-020-00383-0. URL: https://www.nature.com/articles/s42004-020-00383-0.

Charo, Israel F. and Richard M. Ransohoff (2006a). "The Many Roles of Chemokines and Chemokine Receptors in Inflammation". In: *New England Journal of Medicine* 354.6, pp. 610–621. ISSN: 0028-4793. DOI: 10.1056/NEJMra052723. URL: http://www.nejm.org/doi/abs/10.1056/NEJMra052723.

— (2006b). "The Many Roles of Chemokines and Chemokine Receptors in Inflammation". In: *New England Journal of Medicine* 354.6, pp. 610–621. ISSN: 0028-4793. DOI: 10.1056/NEJMra052723. URL: http://www.nejm.org/doi/abs/10.1056/NEJMra052723.

Chatterjee, Samit, Babak Behnam Azad, and Sridhar Nimmagadda (2014). "The Intricate Role of CXCR4 in Cancer". In: *Advances in Cancer Research*, pp. 31–82. DOI: 10.1016/B978-0-12-411638-2.00002-1. URL: https://linkinghub.elsevier.com/retrieve/pii/B9780124116382000021.

Chen, Mu Jung and Kevin H. Mayo (1991). "Human platelet factor 4 subunit association/dissociation thermodynamics and kinetics". In: *Biochemistry* 30.26, pp. 6402–6411. ISSN: 0006-2960. DOI: 10.1021/bi00240a009. URL: https://pubs.acs.org/doi/abs/10.1021/bi00240a009.

Chen, Yunching et al. (2015). "CXCR4 inhibition in tumor microenvironment facilitates anti-programmed death receptor-1 immunotherapy in sorafenib-treated hepatocellular carcinoma in mice". In: *Hepatology* 61.5, pp. 1591–1602. ISSN: 02709139. DOI: 10.1002/hep.27665. URL: http://doi.wiley.com/10.1002/hep.27665.

Cho, Byung-Sik, Hee-Je Kim, and Marina Konopleva (2017). "Targeting the CXCL12/CXCR4 axis in acute myeloid leukemia: from bench to bedside". In: *The Korean Journal of Internal Medicine* 32.2, pp. 248–257. ISSN: 1226-3303. DOI: 10.3904/kjim.2016.244. URL: http://kjim.org/journal/view.php?doi=10.3904/kjim.2016.244.

Choi, Hyong Woo et al. (2015). "Aspirin's Active Metabolite Salicylic Acid Targets High Mobility Group Box 1 to Modulate Inflammatory Responses". In: *Molecular Medicine* 21.1, pp. 526–535. ISSN: 1076-1551. DOI: 10.2119/molmed.2015.00148. URL: https://molmed.biomedcentral.com/articles/10.2119/molmed.2015.00148.

Chopra, Martin and Stefan K Bohlander (2019). "The cell of origin and the leukemia stem cell in acute myeloid leukemia." In: *Genes, chromosomes & cancer* 58.12, pp. 850–858. ISSN: 1098-2264. DOI: 10.1002/gcc.22805. URL: http://www.ncbi.nlm.nih.gov/pubmed/31471945.

Chou, Chuan-Chu et al. (2002). "Pharmacological characterization of the chemokine receptor, hCCR1 in a stable transfectant and differentiated HL-60 cells: antagonism of hCCR1 activation by MIP-1$\beta$". In: *British journal of pharmacology* 137.5, pp. 663–675.

Christopherson, Kent W, Giao Hangoc, and Hal E Broxmeyer (2002). "Cell surface peptidase CD26/dipeptidylpeptidase IV regulates CXCL12/stromal cell-derived factor-1 alpha-mediated chemotaxis of human cord blood CD34+ progenitor cells." In: *Journal of immunology (Baltimore, Md. : 1950)* 169.12, pp. 7000–8. ISSN: 0022-1767. DOI: 10.4049/jimmunol.169.12.7000. URL: http://www.ncbi.nlm.nih.gov/pubmed/12471135.

Clark-Lewis, I. et al. (1991). "Structure-activity relationships of interleukin-8 determined using chemically synthesized analogs. Critical role of NH2-terminal residues and evidence for uncoupling of neutrophil chemotaxis, exocytosis, and receptor binding activities." In: *Journal of Biological Chemistry* 266.34, pp. 23128–23134. ISSN: 00219258. DOI: 10.1016/S0021-9258(18)54472-0. URL: https://linkinghub.elsevier.com/retrieve/pii/S0021925818544720.

Claverie, Jean-Michel, Henri Dreux, and René Cohen (1975). "Sedimentation of generalized systems of interacting particles. I. Solution of systems of complete Lamm equations". In: *Biopolymers: Original Research on Biomolecules* 14.8, pp. 1685–1700.

Cliff, Matthew J et al. (2006). "Conformational diversity in the TPR domain-mediated interaction of protein phosphatase 5 with Hsp90". In: *Structure* 14.3, pp. 415–426.

Clore, G. Marius and Angela M. Gronenborn (1995). "Three-dimensional structures of $\alpha$ and $\beta$ chemokines". In: *The FASEB Journal* 9.1, pp. 57–62. ISSN: 0892-6638. DOI: 10.1096/fasebj.9.1.7821760. URL: https://onlinelibrary.wiley.com/doi/10.1096/fasebj.9.1.7821760.

Clouser, Amanda F et al. (2019). "Interplay of disordered and ordered regions of a human small heat shock protein yields an ensemble of 'quasi-ordered'states". In: *Elife* 8, e50259.

Cocchi, Florenza et al. (1996). "The V3 domain of the HIV–1 gp120 envelope glycoprotein is critical for chemokine–mediated blockade of infection". In: *Nature Medicine* 2.11, pp. 1244–1247. ISSN: 1078-8956. DOI: 10.1038/nm1196-1244. URL: https://www.nature.com/articles/nm1196-1244.

Combadière, Christophe et al. (2008). "Combined inhibition of CCL2, CX3CR1, and CCR5 abrogates Ly6Chi and Ly6Clo monocytosis and almost abolishes atherosclerosis in hypercholesterolemic mice". In: *Circulation* 117.13, pp. 1649–1657.

Cormier, E G et al. (2001). "Mapping the determinants of the CCR5 amino-terminal sulfopeptide interaction with soluble human immunodeficiency virus type 1 gp120-CD4 complexes." In: *Journal of virology* 75.12, pp. 5541–9. ISSN: 0022-538X. DOI: 10.1128/JVI.75.12.5541-5549.2001. URL: http://www.ncbi.nlm.nih.gov/pubmed/11356961http://www.pubmedcentral.nih.gov/articlerender.fcgi?artid=PMC114266.

Crijns, Helena, Vincent Vanheule, and Paul Proost (2020). "Targeting Chemokine—Glycosaminoglycan Interactions to Inhibit Inflammation". In: *Frontiers in Immunology* 11. ISSN: 1664-3224. DOI: 10.3389/fimmu.2020.00483. URL: https://www.frontiersin.org/articles/10.3389/fimmu.2020.00483.

Crump, M P et al. (1997). "Solution structure and basis for functional activity of stromal cell-derived factor-1; dissociation of CXCR4 activation from binding and inhibition of HIV-1." In: *The EMBO journal* 16.23, pp. 6996–7007. ISSN: 0261-4189. DOI: 10.1093/emboj/16.23.6996. URL: http://www.ncbi.nlm.nih.gov/pubmed/9384579http://www.pubmedcentral.nih.gov/articlerender.fcgi?artid=PMC1170303.

Crusz, Shanthini M. and Frances R. Balkwill (2015). "Inflammation and cancer: advances and new agents". In: *Nature Reviews Clinical Oncology* 12.10, pp. 584–596. ISSN: 1759-4774. DOI: 10.1038/nrclinonc.2015.105. URL: http://www.nature.com/articles/nrclinonc.2015.105.

Currie, Stuart et al. (Dec. 2012). "Understanding MRI: Basic MR physics for physicians". In: *Postgraduate medical journal* 89. DOI: 10.1136/postgradmedj-2012-131342.

D'Agostino, Gianluca, Valentina Cecchinato, and Mariagrazia Uguccioni (2018). "Chemokine Heterocomplexes and Cancer: A Novel Chapter to Be Written in Tumor Immunity". In: *Frontiers in Immunology* 9. ISSN: 1664-3224. DOI: 10.3389/fimmu.2018.02185. URL: https://www.frontiersin.org/article/10.3389/fimmu.2018.02185/full.

D'Agostino, Gianluca et al. (2020). "$\beta$-Arrestin1 and $\beta$-Arrestin2 Are Required to Support the Activity of the CXCL12/HMGB1 Heterocomplex on CXCR4." In: *Frontiers in immunology* 11, p. 550824. ISSN: 1664-3224. DOI: 10.3389/fimmu.2020.550824. URL: http://www.ncbi.nlm.nih.gov/pubmed/33072091http://www.pubmedcentral.nih.gov/articlerender.fcgi?artid=PMC7533569.

De Buck, Mieke et al. (2017). "COOH-terminal SAA1 peptides fail to induce chemokines but synergize with CXCL8 and CCL3 to recruit leukocytes via FPR2". In: *Blood*, blood–2017–06–788554. ISSN: 0006-4971. DOI: 10.1182/blood-2017-06-788554. URL: http://www.bloodjournal.org/lookup/doi/10.1182/blood-2017-06-788554.

De Leo, Federica et al. (2019). "Diflunisal targets the HMGB1/CXCL12 heterocomplex and blocks immune cell recruitment - SM". In: *bioRxiv*, p. 563890. DOI: 10.1101/563890. URL: http://biorxiv.org/content/early/2019/03/01/563890.abstract.

De Leo, Federica et al. (2020). "Discovery of 5,5'-Methylenedi-2,3-Cresotic Acid as a Potent Inhibitor of the Chemotactic Activity of the HMGB1·CXCL12 Heterocomplex Using Virtual Screening and NMR Validation". In: *Frontiers in Chemistry* 8. ISSN: 2296-2646. DOI: 10.3389/fchem.2020.598710. URL: https://www.frontiersin.org/articles/10.3389/fchem.2020.598710/full.

De Leo, Federica et al. (2022). "Pamoic acid is an inhibitor of HMGB1·CXCL12 elicited chemotaxis and reduces inflammation in murine models of Pseudomonas aeruginosa pneumonia." In: *Molecular medicine (Cambridge, Mass.)* 28.1, p. 108. ISSN: 1528-3658. DOI: 10.1186/s10020-022-00535-z. URL: http://www.ncbi.nlm.nih.gov/pubmed/36071400http://www.pubmedcentral.nih.gov/articlerender.fcgi?artid=PMC9449960.

Dealwis, C et al. (1998a). "Crystal structure of chemically synthesized [N33A] stromal cell-derived factor 1alpha, a potent ligand for the HIV-1 "fusin" coreceptor." In: *Proceedings of the National Academy of Sciences of the United States of America* 95.12, pp. 6941–6. ISSN: 0027-8424. DOI: 10.1073/pnas.95.12.6941. URL: http://www.ncbi.nlm.nih.gov/

pubmed/9618518http://www.pubmedcentral.nih.gov/articlerender.fcgi?artid=
PMC22694.

Dealwis, C et al. (1998b). "Crystal structure of chemically synthesized [N33A] stromal cell-
derived factor 1alpha, a potent ligand for the HIV-1 "fusin" coreceptor." In: *Proceedings
of the National Academy of Sciences of the United States of America* 95.12, pp. 6941–6.
ISSN: 0027-8424. DOI: 10.1073/pnas.95.12.6941. URL: http://www.ncbi.nlm.nih.gov/
pubmed/9618518http://www.pubmedcentral.nih.gov/articlerender.fcgi?artid=
PMC22694.

Debye, Peter (1915). "Zerstreuung von röntgenstrahlen". In: *Annalen der Physik* 351.6, pp. 809–
823.

Del Prete, Annalisa et al. (2017). "Leukocyte trafficking in tumor microenvironment". In: *Current
Opinion in Pharmacology* 35, pp. 40–47. ISSN: 14714892. DOI: 10.1016/j.coph.2017.
05.004. URL: https://linkinghub.elsevier.com/retrieve/pii/S1471489217300280.

Delaglio, F et al. (1995). "NMRPipe: a multidimensional spectral processing system based
on UNIX pipes." In: *Journal of biomolecular NMR* 6.3, pp. 277–93. ISSN: 0925-2738. DOI:
10.1007/BF00197809. URL: http://www.ncbi.nlm.nih.gov/pubmed/8520220.

Doranz, B J et al. (1999). "Identification of CXCR4 domains that support coreceptor and
chemokine receptor functions." In: *Journal of virology* 73.4, pp. 2752–61. ISSN: 0022-538X.
DOI: 10.1128/JVI.73.4.2752-2761.1999. URL: http://www.ncbi.nlm.nih.gov/pubmed/
10074122http://www.pubmedcentral.nih.gov/articlerender.fcgi?artid=PMC104032.

Drury, Luke J. et al. (2011a). "Monomeric and dimeric CXCL12 inhibit metastasis through dis-
tinct CXCR4 interactions and signaling pathways". In: *Proceedings of the National Academy
of Sciences* 108.43, pp. 17655–17660. ISSN: 0027-8424. DOI: 10.1073/pnas.1101133108.
URL: https://pnas.org/doi/full/10.1073/pnas.1101133108.

— (2011b). "Monomeric and dimeric CXCL12 inhibit metastasis through distinct CXCR4 in-
teractions and signaling pathways". In: *Proceedings of the National Academy of Sciences*
108.43, pp. 17655–17660. ISSN: 0027-8424. DOI: 10.1073/pnas.1101133108. URL: https:
//pnas.org/doi/full/10.1073/pnas.1101133108.

Duan, Hongyang et al. (2017a). "Peptide-binding induced inhibition of chemokine CXCL12".
In: *RSC Advances* 7.34, pp. 21298–21307. ISSN: 2046-2069. DOI: 10.1039/C7RA01735A.
URL: http://xlink.rsc.org/?DOI=C7RA01735A.

— (2017b). "Peptide-binding induced inhibition of chemokine CXCL12". In: *RSC Advances*
7.34, pp. 21298–21307. ISSN: 2046-2069. DOI: 10.1039/C7RA01735A. URL: http://xlink.
rsc.org/?DOI=C7RA01735A.

Eckardt, Veit et al. (2020a). "Chemokines and galectins form heterodimers to modulate in-
flammation". In: *EMBO reports* 21.4, e47852. DOI: https://doi.org/10.15252/embr.
201947852. eprint: https://www.embopress.org/doi/pdf/10.15252/embr.201947852.
URL: https://www.embopress.org/doi/abs/10.15252/embr.201947852.

Eckardt, Veit et al. (2020b). "Chemokines and galectins form heterodimers to modulate inflam-
mation". In: *EMBO reports* 21.4, e47852.

Engl, Tobias et al. (2006). "CXCR4 chemokine receptor mediates prostate tumor cell adhesion through alpha5 and beta3 integrins." In: *Neoplasia (New York, N.Y.)* 8.4, pp. 290–301. ISSN: 1476-5586. DOI: 10.1593/neo.05694. URL: http://www.ncbi.nlm.nih.gov/pubmed/16756721http://www.pubmedcentral.nih.gov/articlerender.fcgi?artid=PMC1600676.

Farrow, N A et al. (1994). "Backbone dynamics of a free and phosphopeptide-complexed Src homology 2 domain studied by 15N NMR relaxation." In: *Biochemistry* 33.19, pp. 5984–6003. ISSN: 0006-2960. DOI: 10.1021/bi00185a040. URL: http://www.ncbi.nlm.nih.gov/pubmed/7514039.

Farzan, Michael et al. (2002). "The role of post-translational modifications of the CXCR4 amino terminus in stromal-derived factor 1α association and HIV-1 entry". In: *Journal of Biological Chemistry* 277.33, pp. 29484–29489.

Fassi, Enrico M.A. et al. (2019). "Oxidation State Dependent Conformational Changes of HMGB1 Regulate the Formation of the CXCL12/HMGB1 Heterocomplex". In: *Computational and Structural Biotechnology Journal* 17, pp. 886–894. ISSN: 20010370. DOI: 10.1016/j.csbj.2019.06.020. URL: https://linkinghub.elsevier.com/retrieve/pii/S2001037019301035.

Fennell, Dean A. et al. (2008a). *Advances in the systemic therapy of malignant pleural mesothelioma*. DOI: 10.1038/ncpcardio1089.

— (2008b). *Advances in the systemic therapy of malignant pleural mesothelioma*. DOI: 10.1038/ncpcardio1089.

Fennell DGaudino GO'Byrne K (2008). "Advances in the systemic therapy of malignant pleural mesothelioma". In: *Nature Clinical Practice Cardiovascular Medicine* 5.3, pp. 136–137. ISSN: 1743-4297. DOI: 10.1038/ncpcardio1089. URL: http://www.nature.com/articles/ncpcardio1089.

Ferrari, S et al. (1994). "The mouse gene coding for high mobility group 1 protein (HMG1)." In: *The Journal of biological chemistry* 269.46, pp. 28803–8. ISSN: 0021-9258. URL: http://www.ncbi.nlm.nih.gov/pubmed/7961836.

Flomenberg, N. (2005). "The use of AMD3100 plus G-CSF for autologous hematopoietic progenitor cell mobilization is superior to G-CSF alone". In: *Blood* 106.5, pp. 1867–1874. ISSN: 0006-4971. DOI: 10.1182/blood-2005-02-0468. URL: http://www.bloodjournal.org/cgi/doi/10.1182/blood-2005-02-0468.

Freire, Ernesto, Obdulio L Mayorga, and Martin Straume (1990). "Isothermal titration calorimetry". In: *Analytical chemistry* 62.18, 950A–959A.

Fulkerson, Patricia C et al. (2004). "Negative regulation of eosinophil recruitment to the lung by the chemokine monokine induced by IFN-γ (Mig, CXCL9)". In: *Proceedings of the National Academy of Sciences* 101.7, pp. 1987–1992.

Fuxreiter, Monika (2020). "Fuzzy protein theory for disordered proteins". In: *Biochemical Society Transactions* 48.6, pp. 2557–2564. ISSN: 0300-5127. DOI: 10.1042/BST20200239. URL: https://portlandpress.com/biochemsoctrans/article/48/6/2557/226928/Fuzzy-protein-theory-for-disordered-proteins.

Galluzzi, Lorenzo et al. (2017). "Immunogenic cell death in cancer and infectious disease". In: *Nature Reviews Immunology* 17.2, pp. 97–111.

Ganju, R K et al. (1998). "The alpha-chemokine, stromal cell-derived factor-1alpha, binds to the transmembrane G-protein-coupled CXCR-4 receptor and activates multiple signal transduction pathways." In: *The Journal of biological chemistry* 273.36, pp. 23169–75. ISSN: 0021-9258. DOI: 10.1074/jbc.273.36.23169. URL: http://www.ncbi.nlm.nih.gov/pubmed/9722546.

Gether, Ulrik (2000). "Uncovering Molecular Mechanisms Involved in Activation of G Protein-Coupled Receptors". In: *Endocrine Reviews* 21.1, pp. 90–113. ISSN: 0163-769X. DOI: 10.1210/edrv.21.1.0390. URL: https://academic.oup.com/edrv/article/21/1/90/2423934.

Gill, Grace et al. (1994). "A glutamine-rich hydrophobic patch in transcription factor Sp1 contacts the dTAFII110 component of the Drosophila TFIID complex and mediates transcriptional activation." In: *Proceedings of the National Academy of Sciences* 91.1, pp. 192–196.

Goldsmith, Z G and D N Dhanasekaran (2007). "G protein regulation of MAPK networks." In: *Oncogene* 26.22, pp. 3122–42. ISSN: 0950-9232. DOI: 10.1038/sj.onc.1210407. URL: http://www.ncbi.nlm.nih.gov/pubmed/17496911.

Gong, Jiang-Hong et al. (1997). "An antagonist of monocyte chemoattractant protein 1 (MCP-1) inhibits arthritis in the MRL-lpr mouse model". In: *The Journal of experimental medicine* 186.1, pp. 131–137.

Gong, Wei et al. (2009). "Amino acid residues 201-205 in C-terminal acidic tail region plays a crucial role in antibacterial activity of HMGB1". In: *Journal of Biomedical Science* 16.1, p. 83. ISSN: 1423-0127. DOI: 10.1186/1423-0127-16-83. URL: https://jbiomedsci.biomedcentral.com/articles/10.1186/1423-0127-16-83.

Gouwy, Mieke et al. (2012). "Possible mechanisms involved in chemokine synergy fine tuning the inflammatory response". In: *Immunology Letters* 145.1-2, pp. 10–14. ISSN: 01652478. DOI: 10.1016/j.imlet.2012.04.005. URL: https://linkinghub.elsevier.com/retrieve/pii/S0165247812001083.

Guinier, A and G Fournet (1955). *Small Angle Scattering of X-rays. New York: John Willey and Sons.*

Guo, F et al. (2016). "CXCL12/CXCR4: a symbiotic bridge linking cancer cells and their stromal neighbors in oncogenic communication networks". In: *Oncogene* 35.7, pp. 816–826. ISSN: 0950-9232. DOI: 10.1038/onc.2015.139. URL: https://www.nature.com/articles/onc2015139.

Guo, Hua et al. (2017). "Targeting the CXCR4/CXCL12 axis with the peptide antagonist E5 to inhibit breast tumor progression". In: *Signal Transduction and Targeted Therapy* 2.1, p. 17033. ISSN: 2059-3635. DOI: 10.1038/sigtrans.2017.33. URL: https://www.nature.com/articles/sigtrans201733.

Hachet-Haas, Muriel et al. (2008). "Small Neutralizing Molecules to Inhibit Actions of the Chemokine CXCL12". In: *Journal of Biological Chemistry* 283.34, pp. 23189–23199. ISSN:

00219258. DOI: 10.1074/jbc.M803947200. URL: https://linkinghub.elsevier.com/retrieve/pii/S0021925819493757.

Haider, Sajjad, Assem Barakat, and Zaheer Ul-Haq (2020). "Discovery of Potential Chemical Probe as Inhibitors of CXCL12 Using Ligand-Based Virtual Screening and Molecular Dynamic Simulation". In: *Molecules* 25.20, p. 4829. ISSN: 1420-3049. DOI: 10.3390/molecules25204829. URL: https://www.mdpi.com/1420-3049/25/20/4829.

Hersh, Taylor A et al. (2018). "A role for the CXCR4-CXCL12 axis in the little skate, Leucoraja erinacea". In: *American Journal of Physiology-Regulatory, Integrative and Comparative Physiology* 315.2, R218–R229.

Hitchinson, Ben et al. (2018). "Biased antagonism of CXCR4 avoids antagonist tolerance". In: *Science Signaling* 11.552, eaat2214. ISSN: 1945-0877. DOI: 10.1126/scisignal.aat2214. URL: http://stke.sciencemag.org/lookup/doi/10.1126/scisignal.aat2214.

Honczarenko, Marek et al. (2002). "CCR5-binding chemokines modulate CXCL12 (SDF-1)–induced responses of progenitor B cells in human bone marrow through heterologous desensitization of the CXCR4 chemokine receptor". In: *Blood, The Journal of the American Society of Hematology* 100.7, pp. 2321–2329.

Hoover, David M. et al. (2002). "The Structure of Human Macrophage Inflammatory Protein-3$\alpha$/CCL20". In: *Journal of Biological Chemistry* 277.40, pp. 37647–37654. ISSN: 00219258. DOI: 10.1074/jbc.M203907200. URL: https://linkinghub.elsevier.com/retrieve/pii/S0021925818364913.

Houtman, Jon C D et al. (2007). "Studying multisite binary and ternary protein interactions by global analysis of isothermal titration calorimetry data in SEDPHAT: application to adaptor protein complexes in cell signaling." In: *Protein science : a publication of the Protein Society* 16.1, pp. 30–42. ISSN: 0961-8368. DOI: 10.1110/ps.062558507. URL: http://www.ncbi.nlm.nih.gov/pubmed/17192587http://www.pubmedcentral.nih.gov/articlerender.fcgi?artid=PMC1794685.

Hundelshausen, Philipp von et al. (2021). "The marriage of chemokines and galectins as functional heterodimers". In: *Cellular and Molecular Life Sciences* 78.24, pp. 8073–8095. ISSN: 1420-682X. DOI: 10.1007/s00018-021-04010-6. URL: https://link.springer.com/10.1007/s00018-021-04010-6.

J. Ziarek, Joshua et al. (2013). "Fragment-Based Optimization of Small Molecule CXCL12 Inhibitors for Antagonizing the CXCL12/CXCR4 Interaction". In: *Current Topics in Medicinal Chemistry* 12.24, pp. 2727–2740. ISSN: 15680266. DOI: 10.2174/1568026611212240003. URL: http://www.eurekaselect.com/openurl/content.php?genre=article&issn=1568-0266&volume=12&issue=24&spage=2727.

Janko, Christina et al. (2014). "Redox modulation of HMGB1-related signaling." In: *Antioxidants & redox signaling* 20.7, pp. 1075–85. ISSN: 1557-7716. DOI: 10.1089/ars.2013.5179. URL: http://www.ncbi.nlm.nih.gov/pubmed/23373897http://www.pubmedcentral.nih.gov/articlerender.fcgi?artid=PMC3928832.

Jansma, Ariane L. et al. (2010). "NMR Analysis of the Structure, Dynamics, and Unique Oligomerization Properties of the Chemokine CCL27". In: *Journal of Biological Chemistry*

285.19, pp. 14424–14437. ISSN: 00219258. DOI: 10.1074/jbc.M109.091108. URL: https://linkinghub.elsevier.com/retrieve/pii/S0021925820548898.

Jeffries, Cy M. et al. (2021). "Small-angle X-ray and neutron scattering". In: *Nature Reviews Methods Primers* 1.1, p. 70. ISSN: 2662-8449. DOI: 10.1038/s43586-021-00064-9. URL: https://www.nature.com/articles/s43586-021-00064-9.

Jerabek-Willemsen, Moran et al. (2014). "MicroScale Thermophoresis: Interaction analysis and beyond". In: *Journal of Molecular Structure* 1077. Fluorescence studies of biomolecular association processes., pp. 101–113. ISSN: 0022-2860. DOI: https://doi.org/10.1016/j.molstruc.2014.03.009. URL: https://www.sciencedirect.com/science/article/pii/S0022286014002750.

Juarez, Julius, Linda Bendall, and Ken Bradstock (2004). "Chemokines and their receptors as therapeutic targets: the role of the SDF-1/CXCR4 axis." In: *Current pharmaceutical design* 10.11, pp. 1245–59. ISSN: 1381-6128. DOI: 10.2174/1381612043452640. URL: http://www.ncbi.nlm.nih.gov/pubmed/15078139.

Jube, Sandro et al. (2012). "Cancer Cell Secretion of the DAMP Protein HMGB1 Supports Progression in Malignant Mesothelioma". In: *Cancer Research* 72.13, pp. 3290–3301. ISSN: 0008-5472. DOI: 10.1158/0008-5472.CAN-11-3481. URL: http://cancerres.aacrjournals.org/cgi/doi/10.1158/0008-5472.CAN-11-3481.

Kaffashi, Kimia, Didier Dréau, and Irina V. Nesmelova (2023). "Heterodimers Are an Integral Component of Chemokine Signaling Repertoire". In: *International Journal of Molecular Sciences* 24.14, p. 11639. ISSN: 1422-0067. DOI: 10.3390/ijms241411639. URL: https://www.mdpi.com/1422-0067/24/14/11639.

Kapurniotu, Aphrodite and Jürgen Bernhagen (2023). "Lasso-grafted designer cytokines". In: *Nature Biomedical Engineering* 7.2, pp. 89–91.

Kapurniotu, Aphrodite, Ozgun Gokce, and Jürgen Bernhagen (2019). "The multitasking potential of alarmins and atypical chemokines". In: *Frontiers in medicine* 6, p. 3.

Karpova, Darja et al. (2017). "Continuous blockade of CXCR4 results in dramatic mobilization and expansion of hematopoietic stem and progenitor cells." In: *Blood* 129.21, pp. 2939–2949. ISSN: 1528-0020. DOI: 10.1182/blood-2016-10-746909. URL: http://www.ncbi.nlm.nih.gov/pubmed/28400375http://www.pubmedcentral.nih.gov/articlerender.fcgi?artid=PMC5445573.

Kawaguchi, Nanako, Ting-Ting Zhang, and Toshio Nakanishi (2019). "Involvement of CXCR4 in Normal and Abnormal Development". In: *Cells* 8.2, p. 185. ISSN: 2073-4409. DOI: 10.3390/cells8020185. URL: http://www.mdpi.com/2073-4409/8/2/185.

Kawale, Ashish A. and Bjoern M. Burmann (2021). "Characterization of backbone dynamics using solution NMR spectroscopy to discern the functional plasticity of structurally analogous proteins". In: *STAR Protocols* 2.4, p. 100919. ISSN: 2666-1667. DOI: https://doi.org/10.1016/j.xpro.2021.100919. URL: https://www.sciencedirect.com/science/article/pii/S2666166721006250.

Kawatkar, Sameer P et al. (2011). "Computational analysis of the structural mechanism of inhibition of chemokine receptor CXCR4 by small molecule antagonists." In: *Experimental*

*biology and medicine (Maywood, N.J.)* 236.7, pp. 844–50. ISSN: 1535-3699. DOI: `10.1258/ ebm.2011.010345`. URL: `http://www.ncbi.nlm.nih.gov/pubmed/21697335http: //www.pubmedcentral.nih.gov/articlerender.fcgi?artid=PMC3900290`.

Keller, Sandro et al. (2012). "High-precision isothermal titration calorimetry with automated peak-shape analysis." In: *Analytical chemistry* 84.11, pp. 5066–73. ISSN: 1520-6882. DOI: `10.1021/ac3007522`. URL: `http://www.ncbi.nlm.nih.gov/pubmed/22530732http: //www.pubmedcentral.nih.gov/articlerender.fcgi?artid=PMC3389189`.

Kioi, Mitomu et al. (2010). "Inhibition of vasculogenesis, but not angiogenesis, prevents the recurrence of glioblastoma after irradiation in mice". In: *Journal of Clinical Investigation* 120.3, pp. 694–705. ISSN: 0021-9738. DOI: `10.1172/JCI40283`. URL: `http://www.jci. org/articles/view/40283`.

Knapp, Stefan et al. (2004a). "The Long Acidic Tail of High Mobility Group Box 1 (HMGB1) Protein Forms an Extended and Flexible Structure That Interacts with Specific Residues within and between the HMG Boxes". In: *Biochemistry* 43.38, pp. 11992–11997. ISSN: 0006-2960. DOI: `10.1021/bi049364k`. URL: `https://pubs.acs.org/doi/10.1021/ bi049364k`.

— (2004b). "The Long Acidic Tail of High Mobility Group Box 1 (HMGB1) Protein Forms an Extended and Flexible Structure That Interacts with Specific Residues within and between the HMG Boxes †". In: *Biochemistry* 43.38, pp. 11992–11997. ISSN: 0006-2960. DOI: `10. 1021/bi049364k`. URL: `https://pubs.acs.org/doi/10.1021/bi049364k`.

Kobilka, Brian K (2007). "G protein coupled receptor structure and activation." In: *Biochimica et biophysica acta* 1768.4, pp. 794–807. ISSN: 0006-3002. DOI: `10.1016/j.bbamem. 2006.10.021`. URL: `http://www.ncbi.nlm.nih.gov/pubmed/17188232http://www. pubmedcentral.nih.gov/articlerender.fcgi?artid=PMC1876727`.

Koenen, Rory R et al. (2009). "Disrupting functional interactions between platelet chemokines inhibits atherosclerosis in hyperlipidemic mice". In: *Nature Medicine* 15.1, pp. 97–103. ISSN: 1078-8956. DOI: `10.1038/nm.1898`. URL: `https://www.nature.com/articles/nm.1898`.

Kofuku, Yutaka et al. (2009a). "Structural basis of the interaction between chemokine stromal cell-derived factor-1/CXCL12 and its G-protein-coupled receptor CXCR4." In: *The Journal of biological chemistry* 284.50, pp. 35240–50. ISSN: 1083-351X. DOI: `10.1074/jbc. M109.024851`. URL: `http://www.ncbi.nlm.nih.gov/pubmed/19837984http://www. pubmedcentral.nih.gov/articlerender.fcgi?artid=PMC2787383`.

— (2009b). "Structural Basis of the Interaction between Chemokine Stromal Cell-derived Factor-1/CXCL12 and Its G-protein-coupled Receptor CXCR4". In: *Journal of Biological Chemistry* 284.50, pp. 35240–35250. ISSN: 0021-9258. DOI: `10.1074/jbc.M109.024851`. URL: `http: //www.jbc.org/lookup/doi/10.1074/jbc.M109.024851`.

— (2009c). "Structural Basis of the Interaction between Chemokine Stromal Cell-derived Factor-1/CXCL12 and Its G-protein-coupled Receptor CXCR4". In: *Journal of Biological Chemistry* 284.50, pp. 35240–35250. ISSN: 00219258. DOI: `10.1074/jbc.M109.024851`. URL: `https: //linkinghub.elsevier.com/retrieve/pii/S0021925820376444`.

Kontos, Christos et al. (2020). "Designed CXCR4 mimic acts as a soluble chemokine receptor that blocks atherogenic inflammation by agonist-specific targeting". In: *Nature Communications* 11.1, p. 5981. ISSN: 2041-1723. DOI: 10.1038/s41467-020-19764-z. URL: https://www.nature.com/articles/s41467-020-19764-z.

Krug, Anne et al. (2002). "Cutting edge: IFN-producing cells respond to CXCR3 ligands in the presence of CXCL12 and secrete inflammatory chemokines upon activation". In: *The Journal of Immunology* 169.11, pp. 6079–6083.

Kuhne, Michelle R et al. (2013). "BMS-936564/MDX-1338: a fully human anti-CXCR4 antibody induces apoptosis in vitro and shows antitumor activity in vivo in hematologic malignancies." In: *Clinical cancer research : an official journal of the American Association for Cancer Research* 19.2, pp. 357–66. ISSN: 1557-3265. DOI: 10.1158/1078-0432.CCR-12-2333. URL: http://www.ncbi.nlm.nih.gov/pubmed/23213054.

Kuscher, Katrin et al. (2009). "Synergy-inducing chemokines enhance CCR2 ligand activities on monocytes". In: *European journal of immunology* 39.4, pp. 1118–1128.

Lai, Wing Yee and Anja Mueller (2021). "Latest update on chemokine receptors as therapeutic targets." In: *Biochemical Society transactions* 49.3, pp. 1385–1395. ISSN: 1470-8752. DOI: 10.1042/BST20201114. URL: http://www.ncbi.nlm.nih.gov/pubmed/34060588http://www.pubmedcentral.nih.gov/articlerender.fcgi?artid=PMC8286821.

Lamm, Ole (1929). *Die differentialgleichung der ultrazentrifugierung.* Almqvist & Wiksell.

Lee, Geoffrey et al. (2018a). "Fully reduced HMGB1 accelerates the regeneration of multiple tissues by transitioning stem cells to G Alert". In: *Proceedings of the National Academy of Sciences* 115.19, E4463–E4472. ISSN: 0027-8424. DOI: 10.1073/pnas.1802893115. URL: http://www.pnas.org/lookup/doi/10.1073/pnas.1802893115.

— (2018b). "Fully reduced HMGB1 accelerates the regeneration of multiple tissues by transitioning stem cells to G Alert". In: *Proceedings of the National Academy of Sciences* 115.19. ISSN: 0027-8424. DOI: 10.1073/pnas.1802893115. URL: https://pnas.org/doi/full/10.1073/pnas.1802893115.

Li, Binghao et al. (2018). "AMD3100 Augments the Efficacy of Mesothelin-Targeted, Immune-Activating VIC-008 in Mesothelioma by Modulating Intratumoral Immunosuppression". In: *Cancer Immunology Research* 6.5, pp. 539–551. ISSN: 2326-6066. DOI: 10.1158/2326-6066.CIR-17-0530. URL: https://aacrjournals.org/cancerimmunolres/article/6/5/539/466761/AMD3100-Augments-the-Efficacy-of-Mesothelin.

Li, Jianhua et al. (2003). "Structural basis for the proinflammatory cytokine activity of high mobility group box 1." In: *Molecular medicine (Cambridge, Mass.)* 9.1-2, pp. 37–45. ISSN: 1076-1551. URL: http://www.ncbi.nlm.nih.gov/pubmed/12765338http://www.pubmedcentral.nih.gov/articlerender.fcgi?artid=PMC1430376.

Li, Jianhua et al. (2004). "Recombinant HMGB1 with cytokine-stimulating activity". In: *Journal of Immunological Methods* 289.1-2, pp. 211–223. ISSN: 00221759. DOI: 10.1016/j.jim.2004.04.019. URL: https://linkinghub.elsevier.com/retrieve/pii/S0022175904001577.

Li, Li et al. (2015). "Heparin inhibits the inflammatory response induced by LPS and HMGB1 by blocking the binding of HMGB1 to the surface of macrophages." In: *Cytokine* 72.1, pp. 36–42. ISSN: 1096-0023. DOI: 10.1016/j.cyto.2014.12.010. URL: http://www.ncbi.nlm.nih.gov/pubmed/25562836.

Li, Pilong et al. (2012). "Phase transitions in the assembly of multivalent signalling proteins". In: *Nature* 483.7389, pp. 336–340.

LIAO, YU-XIN et al. (2015). "AMD3100 reduces CXCR4-mediated survival and metastasis of osteosarcoma by inhibiting JNK and Akt, but not p38 or Erk1/2, pathways in in vitro and mouse experiments". In: *Oncology Reports* 34.1, pp. 33–42. ISSN: 1021-335X. DOI: 10.3892/or.2015.3992. URL: https://www.spandidos-publications.com/10.3892/or.2015.3992.

Ling, Yan et al. (2011). "Heparin changes the conformation of high-mobility group protein 1 and decreases its affinity toward receptor for advanced glycation endproducts in vitro." In: *International immunopharmacology* 11.2, pp. 187–93. ISSN: 1878-1705. DOI: 10.1016/j.intimp.2010.11.014. URL: http://www.ncbi.nlm.nih.gov/pubmed/21095260.

Liu, Yezhou et al. (2023). "Cryo-EM structure of monomeric CXCL12-bound CXCR4 in active state". In: *bioRxiv*. DOI: 10.1101/2023.12.21.572776. eprint: https://www.biorxiv.org/content/early/2023/12/23/2023.12.21.572776.full.pdf. URL: https://www.biorxiv.org/content/early/2023/12/23/2023.12.21.572776.

Loetscher, Pius et al. (2001). "The ligands of CXC chemokine receptor 3, I-TAC, Mig, and IP10, are natural antagonists for CCR3". In: *Journal of Biological Chemistry* 276.5, pp. 2986–2991.

Lortat-Jacob, Hugues, Aurélien Grosdidier, and Anne Imberty (2002). "Structural diversity of heparan sulfate binding domains in chemokines". In: *Proceedings of the National Academy of Sciences* 99.3, pp. 1229–1234. ISSN: 0027-8424. DOI: 10.1073/pnas.032497699. URL: https://pnas.org/doi/full/10.1073/pnas.032497699.

Lounsbury, Nicole (2020). "Advances in CXCR7 Modulators". In: *Pharmaceuticals* 13.2. ISSN: 1424-8247. DOI: 10.3390/ph13020033. URL: https://www.mdpi.com/1424-8247/13/2/33.

Lubkowski, Jacek et al. (1997). "The structure of MCP-1 in two crystal forms provides a rare example of variable quaternary interactions". In: *Nature Structural & Molecular Biology* 4.1, pp. 64–69. ISSN: 1545-9993. DOI: 10.1038/nsb0197-64. URL: https://www.nature.com/doifinder/10.1038/nsb0197-64.

Ludwig, Carl (1856). "Difusion awischen ungleich erwärmten Orten gleich zusammengesetzter Lösungen". In: *Sitz Math Naturwiss Classe Kaiserichen Akad Wiss* 20, p. 539.

Luker, Kathryn E., Mudit Gupta, and Gary D. Luker (2009). "Bioluminescent CXCL12 fusion protein for cellular studies of CXCR4 and CXCR7". In: *BioTechniques*. ISSN: 07366205. DOI: 10.2144/000113126.

Luker, Kathryn E. and Gary D. Luker (2014). "Split Gaussia luciferase for imaging ligand-receptor binding". In: *Methods in Molecular Biology*. ISSN: 10643745. DOI: 10.1007/978-1-62703-718-1_5.

Luker, Kathryn E. et al. (2012). "In vivo imaging of ligand receptor binding with Gaussia luciferase complementation". In: *Nature Medicine*. ISSN: 10788956. DOI: 10.1038/nm.2590.

Maiti, Sudipta, Ulrich Haupts, and Watt Webb (Nov. 1997). "Fluorescence Correlation Spectroscopy: Diagnostics for Sparse Molecules". In: *Proceedings of the National Academy of Sciences of the United States of America* 94, pp. 11753–7. DOI: 10.1073/pnas.94.22.11753.

Manalastas-Cantos, Karen et al. (2021). "ATSAS 3.0: expanded functionality and new tools for small-angle scattering data analysis". In: *Journal of applied crystallography* 54.1, pp. 343–355.

Mantonico, Malisa Vittoria et al. (2023). "The acidic intrinsically disordered region of the inflammatory mediator HMGB1 mediates fuzzy interactions with chemokine CXCL12". In: *bioRxiv*, p. 2023.06.06.543836. DOI: 10.1101/2023.06.06.543836. URL: http://biorxiv.org/content/early/2023/06/07/2023.06.06.543836.abstract.

Mantonico, Malisa Vittoria et al. (2024). "The acidic intrinsically disordered region of the inflammatory mediator HMGB1 mediates fuzzy interactions with CXCL12". In: *Nature Communications* 15.1, p. 1201.

Mantovani, Alberto et al. (2008). "Cancer-related inflammation". In: *Nature* 454.7203, pp. 436–444. ISSN: 0028-0836. DOI: 10.1038/nature07205. URL: https://www.nature.com/articles/nature07205.

Märkl, Florian et al. (2022). "Utilizing chemokines in cancer immunotherapy". In: *Trends in Cancer* 8.8, pp. 670–682. ISSN: 24058033. DOI: 10.1016/j.trecan.2022.04.001. URL: https://linkinghub.elsevier.com/retrieve/pii/S2405803322000875.

Marshall, Garland R and Flavio Ballante (2017). "Limiting Assumptions in the Design of Peptidomimetics." In: *Drug development research* 78.6, pp. 245–267. ISSN: 1098-2299. DOI: 10.1002/ddr.21406. URL: http://www.ncbi.nlm.nih.gov/pubmed/28875546.

Mayo, Kevin H. (1991). "Low-affinity platelet factor 4 proton NMR derived aggregate equilibria indicate a physiologic preference for monomers over dimers and tetramers". In: *Biochemistry* 30.4, pp. 925–934. ISSN: 0006-2960. DOI: 10.1021/bi00218a007. URL: https://pubs.acs.org/doi/abs/10.1021/bi00218a007.

Mellado, M et al. (2001). "Receptor dimerization: a key step in chemokine signaling." In: *Cellular and molecular biology (Noisy-le-Grand, France)* 47.4, pp. 575–82. ISSN: 0145-5680. URL: http://www.ncbi.nlm.nih.gov/pubmed/11502066.

Mensah, Martin A et al. (2023). "Aberrant phase separation and nucleolar dysfunction in rare genetic diseases." In: *Nature* 614.7948, pp. 564–571. ISSN: 1476-4687. DOI: 10.1038/s41586-022-05682-1. URL: http://www.ncbi.nlm.nih.gov/pubmed/36755093http://www.pubmedcentral.nih.gov/articlerender.fcgi?artid=PMC9931588.

Meunier, S. et al. (1997). "Determination of the Three-Dimensional Structure of CC Chemokine Monocyte Chemoattractant Protein 3 by 1 H Two-Dimensional NMR Spectroscopy". In: *Biochemistry* 36.15, pp. 4412–4422. ISSN: 0006-2960. DOI: 10.1021/bi9627929. URL: https://pubs.acs.org/doi/10.1021/bi9627929.

Mezzapelle, Rosanna et al. (2016). "Human malignant mesothelioma is recapitulated in immunocompetent BALB/c mice injected with murine AB cells". In: *Scientific Reports* 6.1, p. 22850. ISSN: 2045-2322. DOI: 10.1038/srep22850. URL: http://www.nature.com/articles/srep22850.

Mezzapelle, Rosanna et al. (2021). "CXCR4 engagement triggers CD47 internalization and antitumor immunization in a mouse model of mesothelioma". In: *EMBO Molecular Medicine* 13.6, e12344.

Miller, Michelle and Kevin Mayo (2017). "Chemokines from a Structural Perspective". In: *International Journal of Molecular Sciences* 18.10, p. 2088. ISSN: 1422-0067. DOI: 10.3390/ijms18102088. URL: http://www.mdpi.com/1422-0067/18/10/2088.

Miskei, Marton et al. (2017). "Fuzziness enables context dependence of protein interactions". In: *Febs Letters* 591.17, pp. 2682–2695.

Mittag, Tanja et al. (2008). "Dynamic equilibrium engagement of a polyvalent ligand with a single-site receptor." In: *Proceedings of the National Academy of Sciences of the United States of America* 105.46, pp. 17772–7. ISSN: 1091-6490. DOI: 10.1073/pnas.0809222105. URL: http://www.ncbi.nlm.nih.gov/pubmed/19008353http://www.pubmedcentral.nih.gov/articlerender.fcgi?artid=PMC2582940.

Mollica, Luca et al. (2007). "Glycyrrhizin binds to high-mobility group box 1 protein and inhibits its cytokine activities." In: *Chemistry & biology* 14.4, pp. 431–41. ISSN: 1074-5521. DOI: 10.1016/j.chembiol.2007.03.007. URL: http://www.ncbi.nlm.nih.gov/pubmed/17462578.

Mukhopadhyay, Samrat, Rashik Ahmed, and Julie D. Forman-Kay (Dec. 2022). "NMR insights into dynamic, multivalent interactions of intrinsically disordered regions: from discrete complexes to condensates". In: *Essays in Biochemistry* 66.7, pp. 863–873. ISSN: 0071-1365. DOI: 10.1042/EBC20220056. eprint: https://portlandpress.com/essaysbiochem/article-pdf/66/7/863/940849/ebc-2022-0056c.pdf. URL: https://doi.org/10.1042/EBC20220056.

Murphy, James W. et al. (2007). "Structural and Functional Basis of CXCL12 (Stromal Cell-derived Factor-1$\alpha$) Binding to Heparin". In: *Journal of Biological Chemistry* 282.13, pp. 10018–10027. ISSN: 00219258. DOI: 10.1074/jbc.M608796200. URL: https://linkinghub.elsevier.com/retrieve/pii/S0021925819336579.

Murphy, James W. et al. (2010). "Heterologous quaternary structure of CXCL12 and its relationship to the CC chemokine family". In: *Proteins: Structure, Function, and Bioinformatics* 78.5, pp. 1331–1337. ISSN: 08873585. DOI: 10.1002/prot.22666. URL: https://onlinelibrary.wiley.com/doi/10.1002/prot.22666.

Murphy, P M et al. (2000). "International union of pharmacology. XXII. Nomenclature for chemokine receptors." In: *Pharmacological reviews* 52.1, pp. 145–76. ISSN: 0031-6997. URL: http://www.ncbi.nlm.nih.gov/pubmed/10699158.

Nagasawa, Takashi et al. (1996). "Defects of B-cell lymphopoiesis and bone-marrow myelopoiesis in mice lacking the CXC chemokine PBSF/SDF-1". In: *Nature* 382.6592, pp. 635–638. ISSN: 0028-0836. DOI: 10.1038/382635a0. URL: https://www.nature.com/articles/382635a0.

Najima, Yuho et al. (2005). "High Mobility Group Protein-B1 Interacts with Sterol Regulatory Element-binding Proteins to Enhance Their DNA Binding". In: *Journal of Biological Chemistry* 280.30, pp. 27523–27532. ISSN: 00219258. DOI: 10.1074/jbc.M414549200. URL: https://linkinghub.elsevier.com/retrieve/pii/S0021925820566003.

Nguyen, Khanh TP et al. (2022). "A new obligate CXCL4–CXCL12 heterodimer for studying chemokine heterodimer activities and mechanisms". In: *Scientific Reports* 12.1, p. 17204.

Nibbs, Robert JB et al. (2000). "CC chemokine receptor 3 antagonism by the $\beta$-chemokine macrophage inflammatory protein 4, a property strongly enhanced by an amino-terminal alanine-methionine swap". In: *The Journal of Immunology* 164.3, pp. 1488–1497.

Noggle, Joseph (2012). *The nuclear Overhauser effect*. Elsevier.

Nyman, May and Lauren McQuade (June 2015). "Small Angle X-ray Scattering of Group V Polyoxometalates". In: pp. 151–170. ISBN: 978-1-63482-656-3.

Ochieng, Josiah et al. (1994). "Galectin-3 is a novel substrate for human matrix metalloproteinases-2 and-9". In: *Biochemistry* 33.47, pp. 14109–14114.

Ogilvie, Patricia et al. (2001). "Eotaxin is a natural antagonist for CCR2 and an agonist for CCR5". In: *Blood, The Journal of the American Society of Hematology* 97.7, pp. 1920–1924.

Ohnishi, Y et al. (2000). "Crystal structure of recombinant native SDF-1alpha with additional mutagenesis studies: an attempt at a more comprehensive interpretation of accumulated structure-activity relationship data." In: *Journal of interferon & cytokine research : the official journal of the International Society for Interferon and Cytokine Research* 20.8, pp. 691–700. ISSN: 1079-9907. DOI: 10.1089/10799900050116390. URL: http://www.ncbi.nlm.nih.gov/pubmed/10954912.

Padrick, Shae B and Chad A Brautigam (2011). "Evaluating the stoichiometry of macromolecular complexes using multisignal sedimentation velocity." In: *Methods (San Diego, Calif.)* 54.1, pp. 39–55. ISSN: 1095-9130. DOI: 10.1016/j.ymeth.2011.01.002. URL: http://www.ncbi.nlm.nih.gov/pubmed/21256217http://www.pubmedcentral.nih.gov/articlerender.fcgi?artid=PMC3147156.

Paoletti, Samantha et al. (2005). "A rich chemokine environment strongly enhances leukocyte migration and activities". In: *Blood* 105.9, pp. 3405–3412. ISSN: 0006-4971. DOI: 10.1182/blood-2004-04-1648. URL: https://ashpublications.org/blood/article/105/9/3405/21242/A-rich-chemokine-environment-strongly-enhances.

Papadopoulos, Jason S and Richa Agarwala (2007). "COBALT: constraint-based alignment tool for multiple protein sequences." In: *Bioinformatics (Oxford, England)* 23.9, pp. 1073–9. ISSN: 1367-4811. DOI: 10.1093/bioinformatics/btm076. URL: http://www.ncbi.nlm.nih.gov/pubmed/17332019.

Pérez, Javier and Yoshinori Nishino (2012). "Advances in X-ray scattering: from solution SAXS to achievements with coherent beams." In: *Current opinion in structural biology* 22.5, pp. 670–8. ISSN: 1879-033X. DOI: 10.1016/j.sbi.2012.07.014. URL: http://www.ncbi.nlm.nih.gov/pubmed/22954648.

Perez, Romel B et al. (2014). "Alanine and proline content modulate global sensitivity to discrete perturbations in disordered proteins." In: *Proteins* 82.12, pp. 3373–84. ISSN: 1097-0134. DOI: 10.1002/prot.24692. URL: http://www.ncbi.nlm.nih.gov/pubmed/25244701http://www.pubmedcentral.nih.gov/articlerender.fcgi?artid=PMC4237723.

Petkovic, Vibor et al. (2004a). "Eotaxin-3/CCL26 is a natural antagonist for CC chemokine receptors 1 and 5: a human chemokine with a regulatory role". In: *Journal of Biological Chemistry* 279.22, pp. 23357–23363.

— (2004b). "I-TAC/CXCL11 is a natural antagonist for CCR5". In: *Journal of leukocyte biology* 76.3, pp. 701–708.

Petoukhov, Maxim V and Dmitri I Svergun (2005). "Global rigid body modeling of macromolecular complexes against small-angle scattering data." In: *Biophysical journal* 89.2, pp. 1237–50. ISSN: 0006-3495. DOI: 10.1529/biophysj.105.064154. URL: http://www.ncbi.nlm.nih.gov/pubmed/15923225http://www.pubmedcentral.nih.gov/articlerender.fcgi?artid=PMC1366608.

Philo, John S (2023). "SEDNTERP: a calculation and database utility to aid interpretation of analytical ultracentrifugation and light scattering data". In: *European Biophysics Journal*, pp. 1–34.

Pillozzi, Serena et al. (2018a). "Peptides and small molecules blocking the CXCR4/CXCL12 axis overcome bone marrow-induced chemoresistance in acute leukemias". In: *Oncology Reports*. ISSN: 1021-335X. DOI: 10.3892/or.2018.6808. URL: http://www.spandidos-publications.com/10.3892/or.2018.6808.

— (2018b). "Peptides and small molecules blocking the CXCR4/CXCL12 axis overcome bone marrow-induced chemoresistance in acute leukemias". In: *Oncology Reports*. ISSN: 1021-335X. DOI: 10.3892/or.2018.6808. URL: http://www.spandidos-publications.com/10.3892/or.2018.6808.

Polnarev, Alexander G. and Ilia Musco (2007). "Curvature profiles as initial conditions for primordial black hole formation". In: *Classical and Quantum Gravity* 24.6, pp. 1405–1431. ISSN: 0264-9381. DOI: 10.1088/0264-9381/24/6/003. URL: http://stacks.iop.org/0264-9381/24/i=6/a=003?key=crossref.9685e12c48ee8d84f52f582f3f987948.

Porod, G (1951). "The x-ray small-angle scattering of close-packed colloid systems". In: *Kolloid Z* 124, p. 32.

Premack, Brett A. and Thomas J. Schall (1996). "Chemokine receptors: Gateways to inflammation and infection". In: *Nature Medicine* 2.11, pp. 1174–1178. ISSN: 1078-8956. DOI: 10.1038/nm1196-1174. URL: https://www.nature.com/articles/nm1196-1174.

Princen, Katrien et al. (2003). "Evaluation of SDF-1/CXCR4-induced Ca2+ signaling by fluorometric imaging plate reader (FLIPR) and flow cytometry". In: *Cytometry* 51A.1, pp. 35–45. ISSN: 0196-4763. DOI: 10.1002/cyto.a.10008. URL: http://doi.wiley.com/10.1002/cyto.a.10008.

Proost, P et al. (1999). "Truncation of macrophage-derived chemokine by CD26/ dipeptidyl-peptidase IV beyond its predicted cleavage site affects chemotactic activity and CC chemokine receptor 4 interaction." In: *The Journal of biological chemistry* 274.7, pp. 3988–93. ISSN:

0021-9258. DOI: 10.1074/jbc.274.7.3988. URL: http://www.ncbi.nlm.nih.gov/pubmed/9933589.

Proudfoot, Amanda E. I. and Mariagrazia Uguccioni (2016). "Modulation of Chemokine Responses: Synergy and Cooperativity". In: *Frontiers in Immunology* 7. ISSN: 1664-3224. DOI: 10.3389/fimmu.2016.00183. URL: http://journal.frontiersin.org/Article/10.3389/fimmu.2016.00183/abstract.

Proudfoot, Amanda E. I. et al. (2003). "Glycosaminoglycan binding and oligomerization are essential for the in vivo activity of certain chemokines". In: *Proceedings of the National Academy of Sciences* 100.4, pp. 1885–1890. ISSN: 0027-8424. DOI: 10.1073/pnas.0334864100. URL: https://pnas.org/doi/full/10.1073/pnas.0334864100.

Rajagopal, Sudarshan et al. (2010a). "Beta-arrestin- but not G protein-mediated signaling by the "decoy" receptor CXCR7." In: *Proceedings of the National Academy of Sciences of the United States of America* 107.2, pp. 628–32. ISSN: 1091-6490. DOI: 10.1073/pnas.0912852107. URL: http://www.ncbi.nlm.nih.gov/pubmed/20018651http://www.pubmedcentral.nih.gov/articlerender.fcgi?artid=PMC2818968.

— (2010b). "Beta-arrestin- but not G protein-mediated signaling by the "decoy" receptor CXCR7." In: *Proceedings of the National Academy of Sciences of the United States of America* 107.2, pp. 628–32. ISSN: 1091-6490. DOI: 10.1073/pnas.0912852107. URL: http://www.ncbi.nlm.nih.gov/pubmed/20018651http://www.pubmedcentral.nih.gov/articlerender.fcgi?artid=PMC2818968.

Rajagopalan, Lavanya and Krishna Rajarathnam (2006). "Structural Basis of Chemokine Receptor Function—A Model for Binding Affinity and Ligand Selectivity". In: *Bioscience Reports* 26.5, pp. 325–339. ISSN: 0144-8463. DOI: 10.1007/s10540-006-9025-9. URL: https://portlandpress.com/bioscirep/article/26/5/325/55295/Structural-Basis-of-Chemokine-Receptor-Function-A.

Ralston, G.B. (1993). *Introduction to Analytical Ultracentrifugation*. Beckman. URL: https://books.google.it/books?id=RhrFZwEACAAJ.

Ratajczak, M Z et al. (2006). "The pleiotropic effects of the SDF-1–CXCR4 axis in organogenesis, regeneration and tumorigenesis". In: *Leukemia* 20.11, pp. 1915–1924. ISSN: 0887-6924. DOI: 10.1038/sj.leu.2404357. URL: https://www.nature.com/articles/2404357.

Ray, Paramita et al. (2012a). "Secreted CXCL12 (SDF-1) forms dimers under physiological conditions". In: *Biochemical Journal* 442.2, pp. 433–442. ISSN: 0264-6021. DOI: 10.1042/BJ20111341. URL: https://portlandpress.com/biochemj/article/442/2/433/45975/Secreted-CXCL12-SDF-1-forms-dimers-under.

Ray, Paramita et al. (2012b). "Secreted CXCL12 (SDF-1) forms dimers under physiological conditions." In: *The Biochemical journal* 442.2, pp. 433–42. ISSN: 1470-8728. DOI: 10.1042/BJ20111341. URL: http://www.ncbi.nlm.nih.gov/pubmed/22142194http://www.pubmedcentral.nih.gov/articlerender.fcgi?artid=PMC4419379.

Rinaldi, Peter L. and Masud Monwar (2017). "Two-Dimensional NMR". In: *Encyclopedia of Spectroscopy and Spectrometry (Third Edition)*. Ed. by John C. Lindon, George E. Tranter,

and David W. Koppenaal. Third Edition. Oxford: Academic Press, pp. 475–487. ISBN: 978-0-12-803224-4. DOI: https://doi.org/10.1016/B978-0-12-803224-4.00087-X. URL: https://www.sciencedirect.com/science/article/pii/B978012803224400087X.

Robert, Xavier and Patrice Gouet (Apr. 2014). "Deciphering key features in protein structures with the new ENDscript server". In: *Nucleic Acids Research* 42.W1, W320–W324. ISSN: 0305-1048. DOI: 10.1093/nar/gku316. eprint: https://academic.oup.com/nar/article-pdf/42/W1/W320/17422987/gku316.pdf. URL: https://doi.org/10.1093/nar/gku316.

Roessle, Manfred (2009). "Basics of X-ray Scattering". In: *EMBO course*.

Rollins, Barrett J. (2006). "Inflammatory chemokines in cancer growth and progression". In: *European Journal of Cancer* 42.6, pp. 760–767. ISSN: 09598049. DOI: 10.1016/j.ejca.2006.01.002. URL: https://linkinghub.elsevier.com/retrieve/pii/S0959804906000384.

Rowell, John P et al. (2012). "HMGB1-facilitated p53 DNA binding occurs via HMG-Box/p53 transactivation domain interaction, regulated by the acidic tail". In: *Structure* 20.12, pp. 2014–2024.

Sakai, Katsuya, Shunsuke Aoki, and Kunio Matsumoto (2015). "Hepatocyte growth factor and Met in drug discovery". In: *The journal of biochemistry* 157.5, pp. 271–284.

Sakai, Katsuya et al. (2023). "Designing receptor agonists with enhanced pharmacokinetics by grafting macrocyclic peptides into fragment crystallizable regions". In: *Nature Biomedical Engineering* 7.2, pp. 164–176.

Santagata, Sara et al. (2021). "CXCR4 and CXCR7 Signaling Pathways: A Focus on the Cross-Talk Between Cancer Cells and Tumor Microenvironment." In: *Frontiers in oncology* 11, p. 591386. ISSN: 2234-943X. DOI: 10.3389/fonc.2021.591386. URL: http://www.ncbi.nlm.nih.gov/pubmed/33937018http://www.pubmedcentral.nih.gov/articlerender.fcgi?artid=PMC8082172.

Saotome, Kei et al. (2024). "Structural insights into CXCR4 modulation and oligomerization". In: *bioRxiv*. DOI: 10.1101/2024.02.09.579708. eprint: https://www.biorxiv.org/content/early/2024/02/10/2024.02.09.579708.full.pdf. URL: https://www.biorxiv.org/content/early/2024/02/10/2024.02.09.579708.

Sass, H. J. et al. (2000). "Solution NMR of proteins within polyacrylamide gels: Diffusional properties and residual alignment by mechanical stress or embedding of oriented purple membranes". In: *Journal of Biomolecular NMR*. ISSN: 09252738. DOI: 10.1023/A:1026703605147.

Sawant, Kirti V. et al. (2016). "Chemokine CXCL1 mediated neutrophil recruitment: Role of glycosaminoglycan interactions". In: *Scientific Reports* 6.1, p. 33123. ISSN: 2045-2322. DOI: 10.1038/srep33123. URL: https://www.nature.com/articles/srep33123.

Scala, Stefania (2015). "Molecular Pathways: Targeting the CXCR4-CXCL12 Axis–Untapped Potential in the Tumor Microenvironment". In: *Clinical Cancer Research* 21.19, pp. 4278–4285. ISSN: 1078-0432. DOI: 10.1158/1078-0432.CCR-14-0914. URL: http://clincancerres.aacrjournals.org/cgi/doi/10.1158/1078-0432.CCR-14-0914.

Schiraldi, Milena et al. (2012). "HMGB1 promotes recruitment of inflammatory cells to damaged tissues by forming a complex with CXCL12 and signaling via CXCR4". In: *The Journal of Experimental Medicine* 209.3, pp. 551–563. ISSN: 0022-1007. DOI: 10.1084/jem.20111739. URL: http://www.jem.org/lookup/doi/10.1084/jem.20111739.

Schnablegger, Heimo and Yashveer Singh (2017). *The SAXS guide: getting acquainted with the principles*. Anton Paar GmbH.

Schneidman-Duhovny, Dina et al. (2016). "FoXS, FoXSDock and MultiFoXS: Single-state and multi-state structural modeling of proteins and their complexes based on SAXS profiles." In: *Nucleic acids research* 44.W1, W424–9. ISSN: 1362-4962. DOI: 10.1093/nar/gkw389. URL: http://www.ncbi.nlm.nih.gov/pubmed/27151198http://www.pubmedcentral.nih.gov/articlerender.fcgi?artid=PMC4987932.

Schreiber, Gideon (2002). "Kinetic studies of protein–protein interactions". In: *Current Opinion in Structural Biology* 12.1, pp. 41–47. ISSN: 0959-440X. DOI: https://doi.org/10.1016/S0959-440X(02)00287-7. URL: https://www.sciencedirect.com/science/article/pii/S0959440X02002877.

Schuck, P (2000a). "Size-distribution analysis of macromolecules by sedimentation velocity ultracentrifugation and lamm equation modeling." In: *Biophysical journal* 78.3, pp. 1606–19. ISSN: 0006-3495. DOI: 10.1016/S0006-3495(00)76713-0. URL: http://www.ncbi.nlm.nih.gov/pubmed/10692345http://www.pubmedcentral.nih.gov/articlerender.fcgi?artid=PMC1300758.

Schuck, Peter (1998). "Sedimentation analysis of noninteracting and self-associating solutes using numerical solutions to the Lamm equation". In: *Biophysical Journal* 75.3, pp. 1503–1512.

— (2000b). "Size-distribution analysis of macromolecules by sedimentation velocity ultracentrifugation and lamm equation modeling". In: *Biophysical journal* 78.3, pp. 1606–1619.

Sebastiani, Silvia et al. (2005). "CCL22-induced responses are powerfully enhanced by synergy inducing chemokines via CCR4: evidence for the involvement of first $\beta$-strand of chemokine". In: *European journal of immunology* 35.3, pp. 746–756.

"Sedimentation Velocity Analytical Ultracentrifugation ( SV-AUC ) for characterizing protein aggregates and contaminants in therapeutic proteins The elaboration of mathematical relations behind SV-AUC theory" (2014). In: URL: https://api.semanticscholar.org/CorpusID:8780347.

Sgrignani, Jacopo et al. (2021). "Systematic Development of Peptide Inhibitors Targeting the CXCL12/HMGB1 Interaction." In: *Journal of medicinal chemistry* 64.18, pp. 13439–13450. ISSN: 1520-4804. DOI: 10.1021/acs.jmedchem.1c00852. URL: http://www.ncbi.nlm.nih.gov/pubmed/34510899.

Shannon, C.E. and W. Weaver (1949). *The Mathematical Theory of Communication*. Illini books Bd. 1. University of Illinois Press. ISBN: 9780252725487. URL: https://books.google.it/books?id=dk0n_eGcqsUC.

Sharma, Rashmi et al. (2015). "Fuzzy complexes: Specific binding without complete folding". In: *FEBS Letters* 589.19, Part A. Dynamics, flexibility, and intrinsic disorder in protein assemblies, pp. 2533–2542. ISSN: 0014-5793. DOI: https://doi.org/10.1016/j.febslet.2015.07.022. URL: https://www.sciencedirect.com/science/article/pii/S001457931500647X.

Shi, Yi, David J. Riese, and Jianzhong Shen (2020). "The Role of the CXCL12/CXCR4/CXCR7 Chemokine Axis in Cancer". In: *Frontiers in Pharmacology* 11. ISSN: 1663-9812. DOI: 10.3389/fphar.2020.574667. URL: https://www.frontiersin.org/articles/10.3389/fphar.2020.574667/full.

Silva, Ana Catarina and JM Sousa Lobo (2020). "Cytokines and growth factors". In: *Current Applications of Pharmaceutical Biotechnology*, pp. 87–113.

Sison, Edward Allan R et al. (2014). "Plerixafor as a chemosensitizing agent in pediatric acute lymphoblastic leukemia: efficacy and potential mechanisms of resistance to CXCR4 inhibition." In: *Oncotarget* 5.19, pp. 8947–58. ISSN: 1949-2553. DOI: 10.18632/oncotarget.2407. URL: http://www.ncbi.nlm.nih.gov/pubmed/25333254http://www.pubmedcentral.nih.gov/articlerender.fcgi?artid=PMC4253409.

Skriver, Karen, Frederik Friis Theisen, and Birthe B. Kragelund (2023). "Conformational entropy in molecular recognition of intrinsically disordered proteins". In: *Current Opinion in Structural Biology* 83, p. 102697. ISSN: 0959-440X. DOI: https://doi.org/10.1016/j.sbi.2023.102697. URL: https://www.sciencedirect.com/science/article/pii/S0959440X23001719.

Smith, Emmanuel W. et al. (2014). "Structural Analysis of a Novel Small Molecule Ligand Bound to the CXCL12 Chemokine". In: *Journal of Medicinal Chemistry* 57.22, pp. 9693–9699. ISSN: 0022-2623. DOI: 10.1021/jm501194p. URL: https://pubs.acs.org/doi/10.1021/jm501194p.

Smith, Emmanuel W. et al. (2016). "Structure-Based Identification of Novel Ligands Targeting Multiple Sites within a Chemokine–G-Protein-Coupled-Receptor Interface". In: *Journal of Medicinal Chemistry* 59.9, pp. 4342–4351. ISSN: 0022-2623. DOI: 10.1021/acs.jmedchem.5b02042. URL: http://pubs.acs.org/doi/10.1021/acs.jmedchem.5b02042.

Sørensen, LN and SR Paludan (2004). "Blocking CC chemokine receptor (CCR) 1 and CCR5 during herpes simplex virus type 2 infection in vivo impairs host defence and perturbs the cytokine response". In: *Scandinavian journal of immunology* 59.3, pp. 321–333.

Stafford III, Walter F (1992). "Boundary analysis in sedimentation transport experiments: a procedure for obtaining sedimentation coefficient distributions using the time derivative of the concentration profile". In: *Analytical biochemistry* 203.2, pp. 295–301.

Stephens, Bryan S. et al. (2020a). "Functional anatomy of the full length CXCR4-CXCL12 complex systematically dissected by quantitative model-guided mutagenesis". In: *bioRxiv*. DOI: 10.1101/2020.01.21.913772.

— (2020b). "Functional anatomy of the full-length CXCR4-CXCL12 complex systematically dissected by quantitative model-guided mutagenesis". In: *Science Signaling* 13.640. ISSN:

1945-0877. DOI: 10.1126/scisignal.aay5024. URL: https://www.science.org/doi/10.1126/scisignal.aay5024.

Stott, Katherine et al. (2010). "Tail-mediated collapse of HMGB1 is dynamic and occurs via differential binding of the acidic tail to the A and B domains." In: *Journal of molecular biology* 403.5, pp. 706–22. ISSN: 1089-8638. DOI: 10.1016/j.jmb.2010.07.045. URL: http://www.ncbi.nlm.nih.gov/pubmed/20691192.

Su, Liping et al. (2005). "Differential expression of CXCR4 is associated with the metastatic potential of human non-small cell lung cancer cells." In: *Clinical cancer research : an official journal of the American Association for Cancer Research* 11.23, pp. 8273–80. ISSN: 1078-0432. DOI: 10.1158/1078-0432.CCR-05-0537. URL: http://www.ncbi.nlm.nih.gov/pubmed/16322285.

Sun, Xueqing et al. (2010). "CXCL12 / CXCR4 / CXCR7 chemokine axis and cancer progression." In: *Cancer metastasis reviews* 29.4, pp. 709–22. ISSN: 1573-7233. DOI: 10.1007/s10555-010-9256-x. URL: http://www.ncbi.nlm.nih.gov/pubmed/20839032http://www.pubmedcentral.nih.gov/articlerender.fcgi?artid=PMC3175097.

Svergun, DI (1992). "Determination of the regularization parameter in indirect-transform methods using perceptual criteria". In: *Journal of applied crystallography* 25.4, pp. 495–503.

Tachibana, K et al. (1998). "The chemokine receptor CXCR4 is essential for vascularization of the gastrointestinal tract." In: *Nature* 393.6685, pp. 591–4. ISSN: 0028-0836. DOI: 10.1038/31261. URL: http://www.ncbi.nlm.nih.gov/pubmed/9634237.

Takekoshi, Tomonori et al. (2012). "A locked, dimeric CXCL12 variant effectively inhibits pulmonary metastasis of CXCR4-expressing melanoma cells due to enhanced serum stability." In: *Molecular cancer therapeutics* 11.11, pp. 2516–25. ISSN: 1538-8514. DOI: 10.1158/1535-7163.MCT-12-0494. URL: http://www.ncbi.nlm.nih.gov/pubmed/22869557http://www.pubmedcentral.nih.gov/articlerender.fcgi?artid=PMC3496366.

Tamamis, Phanourios and Christodoulos A Floudas (2014). "Elucidating a key component of cancer metastasis: CXCL12 (SDF-1$\alpha$) binding to CXCR4." In: *Journal of chemical information and modeling* 54.4, pp. 1174–88. ISSN: 1549-960X. DOI: 10.1021/ci500069y. URL: http://www.ncbi.nlm.nih.gov/pubmed/24660779http://www.pubmedcentral.nih.gov/articlerender.fcgi?artid=PMC4004218.

Tamamura, Hirokazu et al. (2003). "T140 analogs as CXCR4 antagonists identified as anti-metastatic agents in the treatment of breast cancer." In: *FEBS letters* 550.1-3, pp. 79–83. ISSN: 0014-5793. DOI: 10.1016/s0014-5793(03)00824-x. URL: http://www.ncbi.nlm.nih.gov/pubmed/12935890.

Tang, Daolin et al. (2010). "High-mobility group box 1 and cancer". In: *Biochimica et Biophysica Acta (BBA) - Gene Regulatory Mechanisms* 1799.1-2, pp. 131–140. ISSN: 18749399. DOI: 10.1016/j.bbagrm.2009.11.014. URL: https://linkinghub.elsevier.com/retrieve/pii/S1874939909001606.

Tang, Daolin et al. (2023). "The multifunctional protein HMGB1: 50 years of discovery". In: *Nature Reviews Immunology* 23.12, pp. 824–841. ISSN: 1474-1733. DOI: 10.1038/s41577-023-00894-6. URL: https://www.nature.com/articles/s41577-023-00894-6.

Tashiro, K et al. (1993). "Signal sequence trap: a cloning strategy for secreted proteins and type I membrane proteins." In: *Science (New York, N.Y.)* 261.5121, pp. 600–3. ISSN: 0036-8075. DOI: 10.1126/science.8342023. URL: http://www.ncbi.nlm.nih.gov/pubmed/8342023.

Teilum, Kaare et al. (2017). "(S) Pinning down protein interactions by NMR". In: *Protein Science* 26.3, pp. 436–451.

Thomas, Jean O and Andrew A Travers (2001). "HMG1 and 2, and related 'architectural' DNA-binding proteins". In: *Trends in Biochemical Sciences* 26.3, pp. 167–174. ISSN: 09680004. DOI: 10.1016/S0968-0004(01)01801-1. URL: https://linkinghub.elsevier.com/retrieve/pii/S0968000401018011.

Tidow, Henning et al. (2007). "Quaternary structures of tumor suppressor p53 and a specific p53–DNA complex". In: *Proceedings of the National Academy of Sciences* 104.30, pp. 12324–12329.

Tirone, Mario et al. (2018). "High mobility group box 1 orchestrates tissue regeneration via CXCR4". In: *Journal of Experimental Medicine* 215.1, pp. 303–318. ISSN: 0022-1007. DOI: 10.1084/jem.20160217. URL: https://rupress.org/jem/article/215/1/303/42473/High-mobility-group-box-1-orchestrates-tissue.

Tiveron, Marie-Catherine and Harold Cremer (2008). "CXCL12/CXCR4 signalling in neuronal cell migration." In: *Current opinion in neurobiology* 18.3, pp. 237–44. ISSN: 0959-4388. DOI: 10.1016/j.conb.2008.06.004. URL: http://www.ncbi.nlm.nih.gov/pubmed/18644448.

Tompa, Peter and Monika Fuxreiter (2008). "Fuzzy complexes: polymorphism and structural disorder in protein-protein interactions." In: *Trends in biochemical sciences* 33.1, pp. 2–8. ISSN: 0968-0004. DOI: 10.1016/j.tibs.2007.10.003. URL: http://www.ncbi.nlm.nih.gov/pubmed/18054235.

Tria, Giancarlo et al. (2015). "Advanced ensemble modelling of flexible macromolecules using X-ray solution scattering". In: *IUCrJ* 2.2, pp. 207–217. ISSN: 2052-2525. DOI: 10.1107/S205225251500202X. URL: https://scripts.iucr.org/cgi-bin/paper?S205225251500202X.

Tsafou, K et al. (2018). "Targeting intrinsically disordered transcription factors: changing the paradigm". In: *Journal of molecular biology* 430.16, pp. 2321–2341.

Tuukkanen, Anne T and Dmitri I Svergun (2014). "Weak protein-ligand interactions studied by small-angle X-ray scattering." In: *The FEBS journal* 281.8, pp. 1974–87. ISSN: 1742-4658. DOI: 10.1111/febs.12772. URL: http://www.ncbi.nlm.nih.gov/pubmed/24588935.

Ueda, Tetsuya et al. (2004). "Acidic C-tail of HMGB1 is required for its target binding to nucleosome linker DNA and transcription stimulation." In: *Biochemistry* 43.30, pp. 9901–8. ISSN: 0006-2960. DOI: 10.1021/bi035975l. URL: http://www.ncbi.nlm.nih.gov/pubmed/15274644.

Ueshima, Shuhei, Kyosuke Nagata, and Mitsuru Okuwaki (2017). "Internal Associations of the Acidic Region of Upstream Binding Factor Control Its Nucleolar Localization." In: *Molecular and cellular biology* 37.22. ISSN: 1098-5549. DOI: 10.1128/MCB.00218-17. URL: http://www.ncbi.nlm.nih.gov/pubmed/28874518http://www.pubmedcentral.nih.gov/articlerender.fcgi?artid=PMC5660467.

Uversky, Vladimir N (2013). "A decade and a half of protein intrinsic disorder: biology still waits for physics". In: *Protein Science* 22.6, pp. 693–724.

— (2019). "Intrinsically disordered proteins and their "mysterious"(meta) physics". In: *Frontiers in Physics* 7, p. 10.

Vanbervliet, Béatrice et al. (2003). "The inducible CXCR3 ligands control plasmacytoid dendritic cell responsiveness to the constitutive chemokine stromal cell–derived factor 1 (SDF-1)/CXCL12". In: *The Journal of experimental medicine* 198.5, pp. 823–830.

Veldkamp, C. T. (2005). "The monomer-dimer equilibrium of stromal cell-derived factor-1 (CXCL 12) is altered by pH, phosphate, sulfate, and heparin". In: *Protein Science* 14.4, pp. 1071–1081. ISSN: 0961-8368. DOI: 10.1110/ps.041219505. URL: http://doi.wiley.com/10.1110/ps.041219505.

Veldkamp, Christopher T et al. (2006). "Recognition of a CXCR4 sulfotyrosine by the chemokine stromal cell-derived factor-1alpha (SDF-1alpha/CXCL12)." In: *Journal of molecular biology* 359.5, pp. 1400–9. ISSN: 0022-2836. DOI: 10.1016/j.jmb.2006.04.052. URL: http://www.ncbi.nlm.nih.gov/pubmed/16725153http://www.pubmedcentral.nih.gov/articlerender.fcgi?artid=PMC2670582.

Veldkamp, Christopher T. et al. (2007). "On-column refolding of recombinant chemokines for NMR studies and biological assays". In: *Protein Expression and Purification*. ISSN: 10465928. DOI: 10.1016/j.pep.2006.09.009.

Veldkamp, Christopher T. et al. (2008). "Structural Basis of CXCR4 Sulfotyrosine Recognition by the Chemokine SDF-1/CXCL12". In: *Science Signaling* 1.37, ra4–ra4. ISSN: 1937-9145. DOI: 10.1126/scisignal.1160755. URL: http://stke.sciencemag.org/cgi/doi/10.1126/scisignal.1160755.

Veldkamp, Christopher T et al. (2010). "Targeting SDF-1/CXCL12 with a ligand that prevents activation of CXCR4 through structure-based drug design". In: *Journal of the American Chemical Society* 132.21, pp. 7242–7243.

Veldkamp, Christopher T. et al. (2016). "Production of Recombinant Chemokines and Validation of Refolding". In: *Methods in Enzymology*. Vol. 570. Academic Press Inc., pp. 539–565. DOI: 10.1016/bs.mie.2015.09.031.

Vénéreau, Emilie, Chiara Ceriotti, and Marco Emilio Bianchi (2015). "DAMPs from Cell Death to New Life". In: *Frontiers in Immunology* 6. ISSN: 1664-3224. DOI: 10.3389/fimmu.2015.00422. URL: http://journal.frontiersin.org/Article/10.3389/fimmu.2015.00422/abstract.

Venereau, Emilie et al. (2012). "Mutually exclusive redox forms of HMGB1 promote cell recruitment or proinflammatory cytokine release". In: *Journal of Experimental Medicine* 209.9, pp. 1519–1528. ISSN: 1540-9538. DOI: 10.1084/jem.20120189. URL: https://rupress.org/jem/article/209/9/1519/41247/Mutually-exclusive-redox-forms-of-HMGB1-promote.

Venereau, Emilie et al. (2013a). "HMGB1 and leukocyte migration during trauma and sterile inflammation". In: *Molecular Immunology* 55.1, pp. 76–82. ISSN: 01615890. DOI: 10.1016/

j.molimm.2012.10.037. URL: https://linkinghub.elsevier.com/retrieve/pii/S0161589012004518.

— (2013b). "HMGB1 and leukocyte migration during trauma and sterile inflammation". In: *Molecular Immunology* 55.1, pp. 76–82. ISSN: 01615890. DOI: 10.1016/j.molimm.2012.10.037. URL: https://linkinghub.elsevier.com/retrieve/pii/S0161589012004518.

Venetz, Daniel et al. (2010). "Perivascular expression of CXCL9 and CXCL12 in primary central nervous system lymphoma: T-cell infiltration and positioning of malignant B cells". In: *International Journal of Cancer* 127.10, pp. 2300–2312. ISSN: 00207136. DOI: 10.1002/ijc.25236. URL: https://onlinelibrary.wiley.com/doi/10.1002/ijc.25236.

Vlahakis, Stacey R et al. (2002). "G protein-coupled chemokine receptors induce both survival and apoptotic signaling pathways." In: *Journal of immunology (Baltimore, Md. : 1950)* 169.10, pp. 5546–54. ISSN: 0022-1767. DOI: 10.4049/jimmunol.169.10.5546. URL: http://www.ncbi.nlm.nih.gov/pubmed/12421931.

Volkov, Vladimir V and Dmitri I Svergun (2003). "Uniqueness of ab initio shape determination in small-angle scattering". In: *Journal of applied crystallography* 36.3, pp. 860–864.

Von Hundelshausen, Philipp et al. (2005). "Heterophilic interactions of platelet factor 4 and RANTES promote monocyte arrest on endothelium". In: *Blood* 105.3, pp. 924–930.

Von Hundelshausen, Philipp et al. (2017). "Chemokine interactome mapping enables tailored intervention in acute and chronic inflammation". In: *Science translational medicine* 9.384, eaah6650.

Voss, Patricia G. and John L. Wang (2023). "Liquid-liquid phase separation: Galectin-3 in nuclear speckles and ribonucleoprotein complexes". In: *Experimental Cell Research* 427.1, p. 113571. ISSN: 0014-4827. DOI: https://doi.org/10.1016/j.yexcr.2023.113571. URL: https://www.sciencedirect.com/science/article/pii/S0014482723001180.

Vranken, Wim F et al. (2005). "The CCPN data model for NMR spectroscopy: development of a software pipeline." In: *Proteins* 59.4, pp. 687–96. ISSN: 1097-0134. DOI: 10.1002/prot.20449. URL: http://www.ncbi.nlm.nih.gov/pubmed/15815974.

Wagner, Patrick L et al. (2009). "CXCL12 and CXCR4 in adenocarcinoma of the lung: association with metastasis and survival." In: *The Journal of thoracic and cardiovascular surgery* 137.3, pp. 615–21. ISSN: 1097-685X. DOI: 10.1016/j.jtcvs.2008.07.039. URL: http://www.ncbi.nlm.nih.gov/pubmed/19258077.

Wan, Gang et al. (2018). "Spatiotemporal regulation of liquid-like condensates in epigenetic inheritance". In: *Nature* 557.7707, pp. 679–683.

Wang, Jingzhe et al. (2020). "CXCR4 antagonist AMD3100 (plerixafor): From an impurity to a therapeutic agent". In: *Pharmacological Research* 159, p. 105010. ISSN: 10436618. DOI: 10.1016/j.phrs.2020.105010. URL: https://linkinghub.elsevier.com/retrieve/pii/S1043661820313189.

Wang, Lunqing et al. (2014). "High-level C-X-C chemokine receptor type 4 expression correlates with brain-specific metastasis following complete resection of non-small cell lung cancer." In: *Oncology letters* 7.6, pp. 1871–1876. ISSN: 1792-1074. DOI: 10.3892/ol.

2014.1979. URL: http://www.ncbi.nlm.nih.gov/pubmed/24932250http://www.pubmedcentral.nih.gov/articlerender.fcgi?artid=PMC4049707.

Wang, Qiyu et al. (2007). "The HMGB1 acidic tail regulates HMGB1 DNA binding specificity by a unique mechanism." In: *Biochemical and biophysical research communications* 360.1, pp. 14–9. ISSN: 0006-291X. DOI: 10.1016/j.bbrc.2007.05.130. URL: http://www.ncbi.nlm.nih.gov/pubmed/17585880.

Wang, Xi et al. (2021). "Dynamic Autoinhibition of the HMGB1 Protein via Electrostatic Fuzzy Interactions of Intrinsically Disordered Regions". In: *Journal of Molecular Biology* 433.18, p. 167122. ISSN: 00222836. DOI: 10.1016/j.jmb.2021.167122. URL: https://linkinghub.elsevier.com/retrieve/pii/S0022283621003466.

Watson, Matthew, Katherine Stott, and Jean O. Thomas (2007). "Mapping Intramolecular Interactions between Domains in HMGB1 using a Tail-truncation Approach". In: *Journal of Molecular Biology*. ISSN: 00222836. DOI: 10.1016/j.jmb.2007.09.075.

Waudby, Christopher A et al. (2016). "Two-Dimensional NMR Lineshape Analysis." In: *Scientific reports* 6, p. 24826. ISSN: 2045-2322. DOI: 10.1038/srep24826. URL: http://www.ncbi.nlm.nih.gov/pubmed/27109776http://www.pubmedcentral.nih.gov/articlerender.fcgi?artid=PMC4843008.

Weber, Christian and Rory R Koenen (2006). "Fine-tuning leukocyte responses: towards a chemokine 'interactome'". In: *Trends in immunology* 27.6, pp. 268–273.

Weis, William I and Brian K Kobilka (2008). "Structural insights into G-protein-coupled receptor activation." In: *Current opinion in structural biology* 18.6, pp. 734–40. ISSN: 1879-033X. DOI: 10.1016/j.sbi.2008.09.010. URL: http://www.ncbi.nlm.nih.gov/pubmed/18957321http://www.pubmedcentral.nih.gov/articlerender.fcgi?artid=PMC4019673.

Wichapong, Kanin et al. (2016). "Structure-based design of peptidic inhibitors of the interaction between CC chemokine ligand 5 (CCL5) and human neutrophil peptides 1 (HNP1)". In: *Journal of medicinal chemistry* 59.9, pp. 4289–4301.

Wiebe, Matthew S, Tamara K Nowling, and Angie Rizzino (2003). "Identification of novel domains within Sox-2 and Sox-11 involved in autoinhibition of DNA binding and partnership specificity." In: *The Journal of biological chemistry* 278.20, pp. 17901–11. ISSN: 0021-9258. DOI: 10.1074/jbc.M212211200. URL: http://www.ncbi.nlm.nih.gov/pubmed/12637543.

Wishart, David S. et al. (1995). "1H, 13C and 15N random coil NMR chemical shifts of the common amino acids. I. Investigations of nearest-neighbor effects". In: *Journal of Biomolecular NMR* 5.1, pp. 67–81. ISSN: 0925-2738. DOI: 10.1007/BF00227471. URL: http://link.springer.com/10.1007/BF00227471.

Wisler, James W et al. (2014). "Recent developments in biased agonism". In: *Current Opinion in Cell Biology* 27, pp. 18–24. ISSN: 09550674. DOI: 10.1016/j.ceb.2013.10.008. URL: https://linkinghub.elsevier.com/retrieve/pii/S0955067413001610.

Wright, Peter E and H Jane Dyson (2015). "Intrinsically disordered proteins in cellular signalling and regulation". In: *Nature reviews Molecular cell biology* 16.1, pp. 18–29.

Wu, Yang et al. (2016). "CXC motif chemokine receptor 4 gene polymorphism and cancer risk". In: *Medicine* 95.49, e5317. ISSN: 0025-7974. DOI: 10.1097/MD.0000000000005317. URL: http://insights.ovid.com/crossref?an=00005792-201612060-00007.

Xu, Ding et al. (2011). "Heparan sulfate is essential for high mobility group protein 1 (HMGB1) signaling by the receptor for advanced glycation end products (RAGE)". In: *Journal of Biological Chemistry* 286.48, pp. 41736–41744.

Xu, Lei et al. (2013). "Structural basis of the interactions between CXCR4 and CXCL12/SDF-1 revealed by theoretical approaches". In: *Molecular BioSystems* 9.8, p. 2107. ISSN: 1742-206X. DOI: 10.1039/c3mb70120d. URL: http://xlink.rsc.org/?DOI=c3mb70120d.

Xue, Li-Jun et al. (2017). "Inhibition of CXCL12/CXCR4 axis as a potential targeted therapy of advanced gastric carcinoma." In: *Cancer medicine* 6.6, pp. 1424–1436. ISSN: 2045-7634. DOI: 10.1002/cam4.1085. URL: http://www.ncbi.nlm.nih.gov/pubmed/28544785http://www.pubmedcentral.nih.gov/articlerender.fcgi?artid=PMC5463074.

Yang, Y et al. (1994). "Subunit association and structural analysis of platelet basic protein and related proteins investigated by 1H NMR spectroscopy and circular dichroism." In: *The Journal of biological chemistry* 269.31, pp. 20110–8. ISSN: 0021-9258. URL: http://www.ncbi.nlm.nih.gov/pubmed/8051099.

Yu, Lan et al. (2006a). "Identification and expression of novel isoforms of human stromal cell-derived factor 1". In: *Gene* 374, pp. 174–179.

— (2006b). "Identification and expression of novel isoforms of human stromal cell-derived factor 1." In: *Gene* 374, pp. 174–9. ISSN: 0378-1119. DOI: 10.1016/j.gene.2006.02.001. URL: http://www.ncbi.nlm.nih.gov/pubmed/16626895.

Yu, Man et al. (2006c). "HMGB1 signals through toll-like receptor (TLR) 4 and TLR2". In: *Shock* 26.2, pp. 174–179.

Zernecke, Alma and Christian Weber (2014). "Chemokines in Atherosclerosis". In: *Arteriosclerosis, Thrombosis, and Vascular Biology* 34.4, pp. 742–750. ISSN: 1079-5642. DOI: 10.1161/ATVBAHA.113.301655. URL: https://www.ahajournals.org/doi/10.1161/ATVBAHA.113.301655.

Zetterström, Cecilia K et al. (2002). "High Mobility Group Box Chromosomal Protein 1 (HMGB1) Is an Antibacterial Factor Produced by the Human Adenoid". In: *Pediatric Research* 52.2, pp. 148–154. ISSN: 0031-3998. DOI: 10.1203/00006450-200208000-00004. URL: https://www.nature.com/doifinder/10.1203/00006450-200208000-00004.

Zhao, Ruogang et al. (2022). "Recent Advances in CXCL12/CXCR4 Antagonists and Nano-Based Drug Delivery Systems for Cancer Therapy". In: *Pharmaceutics* 14.8, p. 1541. ISSN: 1999-4923. DOI: 10.3390/pharmaceutics14081541. URL: https://www.mdpi.com/1999-4923/14/8/1541.

Zhou, N et al. (2001). "Structural and functional characterization of human CXCR4 as a chemokine receptor and HIV-1 co-receptor by mutagenesis and molecular modeling studies." In: *The Journal of biological chemistry* 276.46, pp. 42826–33. ISSN: 0021-9258. DOI: 10.1074/jbc.M106582200. URL: http://www.ncbi.nlm.nih.gov/pubmed/11551942.

— (2006b). "Identification and expression of novel isoforms of human stromal cell-derived factor 1." In: *Gene* 374, pp. 174–9. ISSN: 0378-1119. DOI: 10.1016/j.gene.2006.02.001. URL: http://www.ncbi.nlm.nih.gov/pubmed/16626895.

Zernecke, Alma and Christian Weber (2014). "Chemokines in Atherosclerosis". In: *Arteriosclerosis, Thrombosis, and Vascular Biology* 34.4, pp. 742–750. ISSN: 1079-5642. DOI: 10.1161/ATVBAHA.113.301655. URL: https://www.ahajournals.org/doi/10.1161/ATVBAHA.113.301655.

Zetterström, Cecilia K et al. (2002). "High Mobility Group Box Chromosomal Protein 1 (HMGB1) Is an Antibacterial Factor Produced by the Human Adenoid". In: *Pediatric Research* 52.2, pp. 148–154. ISSN: 0031-3998. DOI: 10.1203/00006450-200208000-00004. URL: https://www.nature.com/doifinder/10.1203/00006450-200208000-00004.

Zhao, Ruogang et al. (2022). "Recent Advances in CXCL12/CXCR4 Antagonists and Nano-Based Drug Delivery Systems for Cancer Therapy". In: *Pharmaceutics* 14.8, p. 1541. ISSN: 1999-4923. DOI: 10.3390/pharmaceutics14081541. URL: https://www.mdpi.com/1999-4923/14/8/1541.

Zhou, N et al. (2001). "Structural and functional characterization of human CXCR4 as a chemokine receptor and HIV-1 co-receptor by mutagenesis and molecular modeling studies." In: *The Journal of biological chemistry* 276.46, pp. 42826–33. ISSN: 0021-9258. DOI: 10.1074/jbc.M106582200. URL: http://www.ncbi.nlm.nih.gov/pubmed/11551942.

Ziarek, Joshua J. et al. (2013a). "Heparin Oligosaccharides Inhibit Chemokine (CXC Motif) Ligand 12 (CXCL12) Cardioprotection by Binding Orthogonal to the Dimerization Interface, Promoting Oligomerization, and Competing with the Chemokine (CXC Motif) Receptor 4 (CXCR4) N Terminus". In: *Journal of Biological Chemistry* 288.1, pp. 737–746. ISSN: 00219258. DOI: 10.1074/jbc.M112.394064. URL: https://linkinghub.elsevier.com/retrieve/pii/S0021925820653789.

Ziarek, Joshua J. et al. (2013b). "Sulfopeptide Probes of the CXCR4/CXCL12 Interface Reveal Oligomer-Specific Contacts and Chemokine Allostery". In: *ACS Chemical Biology* 8.9, pp. 1955–1963. ISSN: 1554-8929. DOI: 10.1021/cb400274z. URL: https://pubs.acs.org/doi/10.1021/cb400274z.

Ziarek, Joshua J. et al. (2017a). "Structural basis for chemokine recognition by a G protein–coupled receptor and implications for receptor activation". In: *Science Signaling* 10.471. ISSN: 1945-0877. DOI: 10.1126/scisignal.aah5756. URL: https://www.science.org/doi/10.1126/scisignal.aah5756.

— (2017b). "Structural basis for chemokine recognition by a G protein–coupled receptor and implications for receptor activation". In: *Science Signaling* 10.471. ISSN: 1945-0877. DOI: 10.1126/scisignal.aah5756. URL: https://www.science.org/doi/10.1126/scisignal.aah5756.

— (2017c). "Structural basis for chemokine recognition by a G protein–coupled receptor and implications for receptor activation". In: *Science Signaling* 10.471. ISSN: 1945-0877. DOI: 10.1126/scisignal.aah5756. URL: https://www.science.org/doi/10.1126/scisignal.aah5756.